Health Canada Santé Canada

MECS # 21-106094-31

Le 25 mars 2021

Destinataires : Ministères provinciaux et territoriaux de la Santé

Objet : Achat et utilisation de masques faciaux contenant du graphène nanoformé

La présente vise à vous informer d'un risque émergent potentiel concernant des masques faciaux qui sont recouverts de matériaux de graphène nanoformé, et à vous mettre en garde contre l'utilisation de ces instruments dans les réseaux de soins de santé, les écoles et les garderies de votre province ou territoire.

Les masques faciaux qui comportent des allégations de propriétés antivirales ou qui font usage de matériaux antiviraux, notamment ceux qui sont recouverts de graphène nanoformé, sont considérés comme des instruments médicaux de classe I aux termes du *Règlement sur les instruments médicaux* (RIM), et en vertu de la *Loi sur les aliments et drogues* (Loi).

Santé Canada a procédé à une évaluation préliminaire des risques qui a révélé un potentiel de toxicité pulmonaire précoce liée à l'inhalation de graphène nanoformé. À ce jour, Santé Canada n'a pas reçu de données permettant d'appuyer l'innocuité et l'efficacité des masques faciaux contenant du graphène nanoformé.

Par conséquent, compte tenu de l'absence de données probantes fournies par les fabricants pour appuyer l'utilisation sécuritaire et efficace des masques recouverts de graphène nanoformé, Santé Canada juge inacceptables les risques liés à ces instruments médicaux.

Pour atténuer ce risque, Santé Canada :

1) a communiqué avec les distributeurs, les importateurs et les fabricants connus de ces instruments médicaux pour les informer que ces instruments contreviennent à la Loi;
2) a demandé aux entreprises qui ont vendu ces instruments d'en cesser immédiatement la vente et de lancer un rappel pour demander que les instruments concernés soient retournés;
3) a préparé une mise en garde afin d'informer la population canadienne des risques potentiels liés à l'utilisation de masques faciaux contenant des matériaux de graphène nanoformé;
4) a entrepris un examen de l'innocuité concernant l'utilisation de matériaux de graphène nanoformé dans les masques faciaux et demandé que les fabricants fournissent des renseignements supplémentaires à l'appui de cette évaluation.

Nous sommes conscients que ces instruments sont peut-être distribués et utilisés dans

votre province ou votre territoire. Pour le moment, Santé Canada vous recommande de cesser l'achat et l'utilisation de masques faciaux contenant du graphène nanoformé. C'est pourquoi nous demandons votre collaboration afin de nous assurer que les réseaux de soins de santé, les écoles et les garderies de votre territoire de compétence sont au courant des préoccupations de Santé Canada quant aux risques potentiels pour la santé des Canadiens.

N'hésitez pas à communiquer avec moi si vous avez des questions.

Nous vous remercions de l'attention que vous porterez à cette question.

Sincères salutations,

Chad Sheehy
Directeur p.i., Programme de conformité des instruments médicaux
Direction générale des opérations réglementaires et de l'application de la loi
Santé Canada
Chad.sheehy@canada.ca

c. c. David Boudreau
Directeur générale
Direction des instruments médicaux
Direction générale des produits de santé et des aliments
Santé Canada

Nicolas Ribes Turgeon

De: Olivier Richer
Envoyé: 26 mars 2021 12:31
À: Maude Lafantaisie; Mariève Pelletier; Claire Labrie (CIUSSSCN); Chantal Sauvageau; Stéphane Perron
Cc: Stéphane Caron; Marie-Pascale Sassine
Objet: RE: Avis de Santé Canada masque

Bonjour,

Il n'y a pas d'articles sur ce sujet dans nos différents tableaux Google Sheet.

Meilleures salutations,

Olivier Richer, M.P.A., Audiologiste (#OOAQ 2982)
Institut national de santé publique du Québec
Direction des risques biologiques et de la santé au travail
Services cliniques de dépistage
945, rue Wolfe, bureau B5-42
Québec (Québec) G1V 5B3
Téléphone : (418) 650-5115 poste 5545
Courriel : olivier.richer@inspq.qc.ca

De : Maude Lafantaisie
Envoyé : 26 mars 2021 12:24
À : Mariève Pelletier <marieve.pelletier@inspq.qc.ca>; Claire Labrie (CIUSSSCN) <claire.labrie.ciussscn@ssss.gouv.qc.ca>; Chantal Sauvageau <chantal.sauvageau@inspq.qc.ca>; Stéphane Perron <stephane.perron@inspq.qc.ca>; Olivier Richer <olivier.richer@inspq.qc.ca>
Cc : Stéphane Caron <stephane.caron@inspq.qc.ca>; Marie-Pascale Sassine <marie-pascale.sassine@inspq.qc.ca>
Objet : Re: Avis de Santé Canada masque

Bonjour,

Voici les articles que j'ai trouvé à partir d'Inoreader sur le graphène et les masques:
https://pubmed.ncbi.nlm.nih.gov/33259195/
https://pubmed.ncbi.nlm.nih.gov/33250970/
https://www.medrxiv.org/content/10.1101/2020.09.16.20194316v2
https://pubs.acs.org/doi/10.1021/acsnano.0c02250
https://pubmed.ncbi.nlm.nih.gov/33619412/
https://www.sciencedirect.com/science/article/pii/S2667056920300110?via%3Dihub

Cependant, nous n'avons retenu aucun de ces articles dans notre veille.

Maude

De : Mariève Pelletier <marieve.pelletier@inspq.qc.ca>
Envoyé : 26 mars 2021 12:03
À : Claire Labrie (CIUSSSCN) <claire.labrie.ciussscn@ssss.gouv.qc.ca>; Chantal Sauvageau <chantal.sauvageau@inspq.qc.ca>; Stéphane Perron <stephane.perron@inspq.qc.ca>; Olivier Richer

<olivier.richer@inspq.qc.ca>; Maude Lafantaisie <maude.lafantaisie@inspq.qc.ca>
Cc : Stéphane Caron <stephane.caron@inspq.qc.ca>; Marie-Pascale Sassine <marie-pascale.sassine@inspq.qc.ca>
Objet : TR: Avis de Santé Canada masque

Bonjour vous tous,
Nous avons reçu la demande suivante de Richard Massé.
Je pense qu'il est important que vous soyez informés et pour certains sollicités à savoir si vous avez vu de la littérature à ce sujet.
Ma d3emande s'adresse surtout au groupe hygiène et à Maude et Olivier.

Merci de nous revenir avec des éléments de réponses si vous en avez.

Marième

De : Patricia Hudson
Envoyé : 26 mars 2021 11:39
À : Marie-Pascale Sassine <marie-pascale.sassine@inspq.qc.ca>; Stéphane Caron <stephane.caron@inspq.qc.ca>; Marième Pelletier <marieve.pelletier@inspq.qc.ca>
Objet : TR: Avis de Santé Canada

Merci de donner suite en répondant directement à Richard et me mettant en copie. SVP me revenir avec un échéancier de réponse.

Patricia Hudson, M.D., FRCPC
Directrice scientifique
Institut national de santé publique du Québec
Direction des risques biologiques et de la santé au travail
courriel : patricia.hudson@inspq.qc.ca

Adresse physique : 190, boulevard Crémazie, 2.36, Montréal (Québec) H2P 1E2
Téléphone : 514 864-1600, poste 3201

Adresse postale : 945, rue Wolfe, C5-21, Québec (Québec) G1V 5B3
Adjointe de direction : 418 650-5115, poste 5200

INSPQ Centre d'expertise et de référence en santé publique INSPQ
www.inspq.qc.ca

De : Richard Massé <richard.masse@msss.gouv.qc.ca>
Envoyé : 26 mars 2021 11:34
À : Jocelyne Sauvé <jocelyne.sauve@inspq.qc.ca>; Patricia Hudson <patricia.hudson@inspq.qc.ca>
Cc : Horacio Arruda <horacio.arruda@msss.gouv.qc.ca>; Yves Jalbert <Yves.Jalbert@msss.gouv.qc.ca>; Cynthia Beaudoin MSSS <cynthia.beaudoin@msss.gouv.qc.ca>; DGSP-Média <dgsp-media@msss.gouv.qc.ca>
Objet : TR: Avis de Santé Canada

Bonjour,
Nous avons autorisé le retrait ce jour de ces masques par le réseau de l'éducation. Ne savons pas si a été beaucoup utilisé.
Est-ce possible d'avoir un avis rapide si nous devons faire qq chose pour les personnes ayant pu les utiliser. Quel type d'information, s'il y a lieu. Ou rien du tout??
Merci beaucoup,
Richard

Richard Massé MD, MSc, FRCPC
Conseiller médical stratégique
Cabinet du directeur national de santé publique
et sous-ministre
Ministère de la Santé et des Services sociaux
Édifice Catherine-De Longpré
1075, Chemin Ste-Foy, 12ième étage
Québec (Québec) G1S 2M1

De : Guillaume Lavoie (MSSS) <guillaume.lavoie@msss.gouv.qc.ca>
Envoyé : 26 mars 2021 11:04
À : Richard Massé <richard.masse@msss.gouv.qc.ca>
Cc : Anne-Marie Langlois <anne.marie.langlois@msss.gouv.qc.ca>; Anne-Sophie Desmeules <anne-sophie.desmeules@msss.gouv.qc.ca>; Julie Rousseau (MSSS) <julie.rousseau@msss.gouv.qc.ca>; Marie Pinard <marie.pinard@msss.gouv.qc.ca>; Renée Levaque <renee.levaque@msss.gouv.qc.ca>; Horacio Arruda <horacio.arruda@msss.gouv.qc.ca>; Marie-Ève Bédard <marie-eve.bedard@msss.gouv.qc.ca>; Karen Bouffard <karen.bouffard@msss.gouv.qc.ca>; Yves Jalbert <Yves.Jalbert@msss.gouv.qc.ca>
Objet : TR: Avis de Santé Canada

Bonjour Dr Massé,

La directrice des communications, Mme Johanne Pelletier, vient de me téléphoner pour me faire part de cet avis de Santé Canada concernant les masques faciaux contenant du graphène nanoformé.

Des vérifications seront faites auprès de M. Luc Desbiens, à savoir si ce type de masques auraient pu circuler dans notre réseau, **mais il est confirmé que ce type de masque a circulé et a été utilisé dans le réseau de l'Éducation.**

Mme Pelletier souhaite que vous demeuriez disponible pour éventuellement sortir dans les médias avec Mme Anne-Marie Lepage, du MEQ.

L'intérêt est d'avoir un avis médical sur l'impact de ces masques :

- Est-ce que le fait qu'un enfant ait porté ce masque peut avoir causé des dommages sur sa santé?
    - Est-ce que c'est le cas par exemple sur une longue période, mais pas sur une plus courte?

Bref, vous voyez le topo.

J'attends donc votre retour, et je vais vous tenir au courant de la suite des choses en ce qui a trait aux communications.

Merci et bonne journée,

Guillaume Lavoie
Adjoint au sous-ministre adjoint
Direction générale de la santé publique
Ministère de la Santé et des Services sociaux
Édifice Catherine-De Longpré
1075, chemin Sainte-Foy, 12e étage
Québec (Québec) G1S 2M1
[redacted]

De : Johanne Pelletier (MCE) <johanne.pelletier.mce@msss.gouv.qc.ca>
Envoyé : 26 mars 2021 10:49
À : Guillaume Lavoie (MSSS) <guillaume.lavoie@msss.gouv.qc.ca>
Objet : TR: Avis de Santé Canada

pour info

Johanne Pelletier | Directrice

Direction des communications
Ministère de la Santé et des Services sociaux

Édifice Catherine-De Longpré
1075, chemin Sainte-Foy, 4e étage
Québec (Québec) G1S 2M1

418 266-8906
www.msss.gouv.qc.ca

De : Audin, Thierry <Thierry.Audin@mce.gouv.qc.ca>
Envoyé : 26 mars 2021 09:55
À : Johanne Pelletier (MCE) <johanne.pelletier.mce@msss.gouv.qc.ca>; Karine White <Karine.White@msss.gouv.qc.ca>; Nathalie Lévesque (MCE) <nathalie.levesque.mce@msss.gouv.qc.ca>; Nathalie Foster <Nathalie.Foster@education.gouv.qc.ca>; Terry McKinnon <Terry.Mckinnon@economie.gouv.qc.ca>
Cc : Lavoie, Antoine <Antoine.Lavoie@mce.gouv.qc.ca>
Objet : Avis de Santé Canada

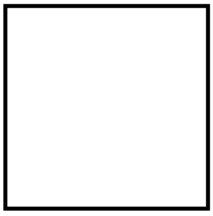

Bonjour,
Serait-il possible que nous nous parlions le plus rapidement possible de cet avis de Santé Canada diffusé en soirée hier ?
Merci.
Bonne journée.
Thierry Audin

De : Mariève Pelletier
A : Ciprian Mihai Cirtiu
Objet : Urgent_Besoin avis NANO_Avis de Santé Canada
Date : 26 mars 2021 14:49:00
Pièces jointes : ~WRD0001.jpg
GrapheneMaskPTnotice_Final - FR.pdf
Importance : Haute

Bonjour Ciprian, P-Y Tremblay m'a donné ton nom pour nous aider peut-être dans une réponse rapide a

Nous avons reçu une demande de réponse rapide suite à l'avis de Santé Canada concernant les risques à la santé des masques contenant du **graphène nanoformé**.

La demande vient de Richard Massé à la DGSP.

Le hic c'est que ce type de masques aurait été distribué dans les écoles et portés par des enfants. Voir message ci-dessous.
Dr Massé a besoin de savoir s'il y a des risques à la santé pour des enfants qui ont portés ce masque et ce même sur une courte période (exemple, en continu durant 7 ou 14 jours) et même beaucoup plus dans certains cas.

Tu peux me joindre si tu as besoin de plus d'info. Nous avons commencé à sortir des articles sur le sujet.

Mariève Pelletier, Ph.D
Coordonnatrice scientifique du GT-SAT COVID
Conseillère scientifique spécialisée
Unité de santé au travail
Institut national de santé publique du Québec
(418) 650-5115, poste 5223

De : Marième Pelletier
A : Axelle Marchand; Jean-Bernard Gamache
Cc : Pierre-Yves Tremblay; Stéphane Perron; Marie-Pascale Sassine; Stéphane Caron
Objet : RE: Avis de Santé Canada
Date : 26 mars 2021 15:37:00
Pièces jointes : image001.jpg

Bonjour Axelle,
Merci de ton retour. Je viens de discuter avec P-Y et avec Ciprian.
J'ai reçu plusieurs réponses à court terme qui nous permettra je crois de faire un premier jet de répondre et surtout d'identifier les éléments supplémentaires que nous devons aller chercher comme information. Possible que l'on sollicite ton expertise dans un deuxième temps lorsqu'on aura un peu plus d'information sur les masques en question. Merci de ton soutien.

Marième Pelletier, Ph.D
Coordonnatrice scientifique du GT-SAT COVID
Conseillère scientifique spécialisée
Unité de santé au travail
Institut national de santé publique du Québec
(418) 650-5115, poste 5223

De : Axelle Marchand
Envoyé : 26 mars 2021 15:14
À : Marième Pelletier <marieve.pelletier@inspq.qc.ca>; Jean-Bernard Gamache <Jean-Bernard.Gamache@inspq.qc.ca>
Cc : Pierre-Yves Tremblay <pierre-yves.tremblay@inspq.qc.ca>; Stéphane Perron <stephane.perron@inspq.qc.ca>; Marie-Pascale Sassine <marie-pascale.sassine@inspq.qc.ca>; Stéphane Caron <stephane.caron@inspq.qc.ca>
Objet : RE: Avis de Santé Canada

Bonjour,

Est-ce que la réponse vise à commenter la toxicité des nanoparticules de graphène ? Personnellement, je crois que l'essentiel de la question est de savoir si des nanoparticules de graphène pourraient avoir été inhalées (ces nanoparticules ne sont pas nécessairement émises lors du port du masque). Je ne suis pas particulièrement qualifiée pour répondre à cette question, mais je suis disponible pour vous assister au besoin.

Axelle Marchand, M. Sc.
Conseillère scientifique
Unité Évaluation et soutien à la gestion des risques
Direction de la santé environnementale et de la toxicologie
Institut national de santé publique du Québec
190, boulevard Crémazie Est, Montréal (Québec) H2P 1E2
514 266-4090

Éric Bédard

De: Ciprian Mihai Cirtiu
Envoyé: 25 juin 2021 11:10
À: Jean-Bernard Gamache
Objet: TR: avis SC (Sophie)

De : Stéphane Caron
Envoyé : 29 mars 2021 10:29
À : Pierre-Yves Tremblay <pierre-yves.tremblay@inspq.qc.ca>; Ciprian Mihai Cirtiu <ciprian-mihai.cirtiu@inspq.qc.ca>
Objet : TR: avis SC (Sophie)

PVI

Stéphane Caron
Médecin-conseil
Santé au travail, DRBST
418 650-5115 poste 5231
stephane.caron@inspq.qc.ca

INSPQ Fhqwuh#g*h{shuwlvh#hw#gh#u‡i‡uhqfh#hq#vdqw‡#sxeoltxh##
<78/#dyhqxh#Zroih/#Tx‡ehf#Tx‡ehf,#J4Y#8E6#
zzz1lqvst1tf1fd#

De : Claire Labrie (CIUSSSCN) <claire.labrie.ciussscn@ssss.gouv.qc.ca>
Envoyé : 29 mars 2021 07:46
À : Mariève Pelletier <marieve.pelletier@inspq.qc.ca>
Cc : Marie-Pascale Sassine <marie-pascale.sassine@inspq.qc.ca>; Stéphane Caron <stephane.caron@inspq.qc.ca>; Stéphane Perron <stephane.perron@inspq.qc.ca>; Maude Lafantaisie <maude.lafantaisie@inspq.qc.ca>
Objet : TR : avis SC (Sophie)

Bonjour,

Voici la réponse du REPTOX…

Claire Labrie

Hygiéniste du travail
Direction de santé publique de la Capitale-Nationale-Santé au travail
CIUSSS de la Capitale-Nationale
Téléphone : 418 666-7000, poste 10233

claire.labrie.ciussscn@ssss.gouv.qc.ca

De : Répertoire Toxicologique <reptox@cnesst.gouv.qc.ca>
Envoyé : 26 mars 2021 17:55
À : Claire Labrie (CIUSSSCN) <claire.labrie.ciussscn@ssss.gouv.qc.ca>
Objet : RE: avis SC (Sophie)

Bonjour,

Comme convenu au téléphone, voici les liens vers des documents contenant des informations, pour des travailleurs adultes, en cas de libération du produit :

- NIOSH, Occupational Exposure to Carbon Nanotubes and Nanofibers : https://www.cdc.gov/niosh/docs/2013-145/pdfs/2013-145.pdf
- IRSST, Rapport R-840 - **Nanomatériaux Guide de bonnes pratiques favorisant la gestion des risques en milieu de travail** : R-840.pdf (irsst.qc.ca)
- CNESST, Répertoire toxicologique – Fiche complète pour le noir de charbon : Fiche complète pour Noir de carbone - CNESST (gouv.qc.ca)

Si nous trouvons d'autres documents, nous vous les ferons parvenir.

Bonne fin de journée

Sophie CHARRON M.Sc.
Conseillère experte en prévention-inspection
Direction générale de la gouvernance et du conseil stratégique en prévention
Commission des normes, de l'équité, de la santé et de la sécurité du travail
1199, rue De Bleury, 3e étage
Montréal (Québec) H3B 3J1
514 906-3080, 2556
1 888 330 6374, 2556

Votre porte d'entrée unique pour les services en matière de travail
cnesst.gouv.qc.ca

De : Claire Labrie (CIUSSSCN) <claire.labrie.ciussscn@ssss.gouv.qc.ca>
Envoyé : 26 mars 2021 15:03

À : Répertoire Toxicologique <reptox@cnesst.gouv.qc.ca>
Objet : avis SC (Sophie)

Claire Labrie

Hygiéniste du travail
Direction de santé publique de la Capitale-Nationale-Santé au travail
CIUSSS de la Capitale-Nationale
Téléphone : 418 666-7000, poste 10233

claire.labrie.ciussscn@ssss.gouv.qc.ca

Éric Bédard

De: Claire Labrie (CIUSSSCN)
Envoyé: 29 mars 2021 11:22
À: Mariève Pelletier
Cc: Stéphane Caron; Stéphane Perron; Marie-Pascale Sassine; Maude Lafantaisie
Objet: TR : Toxicité du graphène nanoformé
Pièces jointes: Toxicology of Graphene-Based Nanomaterials.pdf; Toxicity Studies on Graphene-Based Nanomaterials.pdf; Occupational exposure to graphene based.pdf

Voici d'autres documents envoyés par le REPTOX.

Claire Labrie
Hygiéniste du travail
Direction de santé publique de la Capitale-Nationale-Santé au travail
CIUSSS de la Capitale-Nationale
Téléphone : 418 666-7000, poste 10233
claire.labrie.ciussscn@ssss.gouv.qc.ca

De : Linda Berchiche <linda.berchiche@cnesst.gouv.qc.ca>
Envoyé : 29 mars 2021 11:11
À : Claire Labrie (CIUSSSCN) <claire.labrie.ciussscn@ssss.gouv.qc.ca>
Cc : Sophie Charron <sophie.charron@cnesst.gouv.qc.ca>
Objet : Toxicité du graphène nanoformé

Bonjour Madame Labrie,

Ma collègue Sophie Charron m'a demandé de vous envoyer, si j'en dispose, des documents sur la toxicité du graphène nanoformé.
Je vous envoie les documents les plus récents que j'ai en ma possession en espérant qu'ils vont vous aider dans vos réflexions.

Bonne Journée!

Linda BERCHICHE , M.Sc., M.Env.
Conseillère en prévention-inspection
DGPIP - Direction de l'hygiène du travail
Commission des normes, de l’équité, de la santé et de la sécurité du travail
1199, rue De Bleury, 3e étage
Montréal (Québec) H3B 3J1
514 906-3080, 2296

Votre porte d'entrée unique pour les services en matière de travail
cnesst.gouv.qc.ca

Nanoscale

REVIEW

View Article Online
View Journal | View Issue

Cite this: *Nanoscale*, 2018, **10**, 15894

Occupational exposure to graphene based nanomaterials: risk assessment

Marco Pelin, [a] Silvio Sosa, [a] Maurizio Prato *[b,c,d] and Aurelia Tubaro *[a]

Graphene-based materials (GBMs) are a family of novel materials including graphene, few layer graphene (FLG), graphene oxide (GO), reduced graphene oxide (rGO) and graphene nanoplatelets (GNP). Currently, the risk posed by them to human health is associated mainly with the occupational exposure during their industrial and small-scale production or waste discharge. The most significant occupational exposure routes are inhalation, oral, cutaneous and ocular, inhalation being the majorly involved and most studied one. This manuscript presents a critical up-to-date review of the available *in vivo* toxicity data of the most significant GBMs, after using these exposure routes. The few *in vivo* inhalation toxicity studies (limited to 5-days of repeated exposure and only one to 5 days per week for 4 weeks) indicate inflammatory/fibrotic effects at the pulmonary level, not always reversible after 14/90 days. More limited *in vivo* data are available for the oral and ocular exposure routes, whereas the studies on cutaneous toxicity are at the initial stage. A long persistence of GBMs in rodents is recorded, while contradictory genotoxic data are reported. Data gap identification is also provided. Based on the available data, the occupational exposure limit cannot be determined. More experimental toxicity studies according to specific guidelines (tentatively validated for nanomaterials) and more information on the actual occupational exposure level to GBMs are needed. Furthermore, ADME (Absorption, Distribution, Metabolism, Excretion), genotoxicity, developmental and reproductive toxicity data related to the occupational exposure to GBMs have to be implemented. In addition, sub-chronic and/or chronic studies are still needed to completely exclude other toxic effects and/or carcinogenicity.

Received 18th June 2018,
Accepted 12th July 2018

DOI: 10.1039/c8nr04950e

rsc.li/nanoscale

1. Introduction

In recent years, the development of carbon-based nanomaterials (CBNs) and nanotechnology has constantly increased, offering a wide range of novel opportunities and solutions in different areas of research and application, which involve the environment, manufacturing technology and health care. As a consequence, an emerging area of concern in toxicology is represented by the manufactured nanomaterials.[1]

One of the last discovered CBNs is graphene, consisting of two-dimensional, single atom thick sheets of planar sp^2 bound carbons arranged in a honeycomb-like structure, with a high surface area on both sides of the planar axis.[2] Furthermore, different graphene-based materials (GBMs) have been obtained by oxidation and/or functionalization of graphene, and characterized by a variable lateral size, thickness, surface area, shape, carbon-to-oxygen ratio and possible surface functionalization.[3–6] GBMs are promising tools for a broad range of possible applications in electronics, energy technology, sensors and biomedicine.[6,7] However, GBMs are surrounded by a plethora of unanswered questions regarding their safety. Although their potential toxicity has already been highlighted, limited toxicity studies on GBMs are available and the risk posed by them to human health remains largely unexplored. In fact, despite more than 19 000 scientific publications on GBMs are available since their discovery by Novoselov *et al.*,[8] only about 250 of them reported toxicity data and about 70 (0.4% of total publications) included *in vivo* toxicity findings on laboratory animals (Fig. 1), the key component of the hazard identification process.

The main risk to human health posed by GBMs appears to be associated with the occupational exposure to these materials, their applications being still at the experimental stage.[5] During their industrial or small-scale production and waste discharge, humans can be exposed to GBMs mainly by inhalation, cutaneous and ocular routes, the respiratory tract, the skin and the eyes being in direct contact with the work

[a]*Department of Life Sciences, University of Trieste, 34127 Trieste, Italy. E mail: tubaro@units.it, ssosa@units.it, mpelin@units.it; Tel: +39 040 5588835*
[b]*Department of Chemical and Pharmaceutical Sciences, University of Trieste, 34127 Trieste, Italy. E mail: prato@units.it; Tel: +39 040 5583598*
[c]*CIC BiomaGUNE, Parque Tecnológico de San Sebastián, Paseo Miramón, 182, 20009 San Sebastián, Guipúzcoa, Spain*
[d]*Basque Foundation for Science, Ikerbasque, Bilbao 48013, Spain*

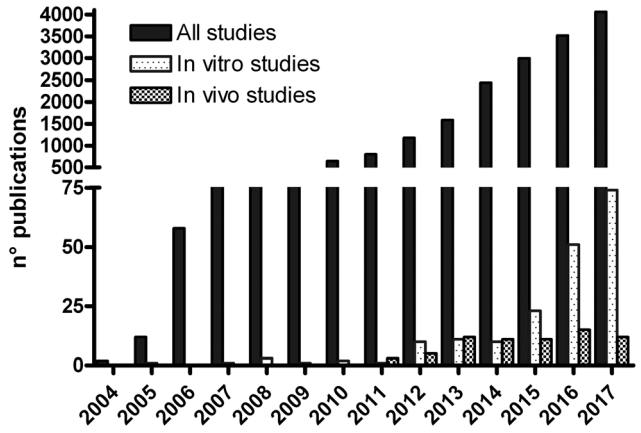

Fig. 1 Number of publications reporting toxicity studies of GBMs com pared with the total number of publications on graphene, for each year (source: http://www.pubmed.com; keywords: graphene, *in vivo* toxicity or *in vitro* toxicity).

environment. Ingestion can also occur by accidental oral intake and/or by secondary swallowing of inhaled GBMs.

In the occupational hazard assessment, various types of data are used, including human data, data from laboratory animal studies, data from *in vitro* studies and non-testing data that can be derived from the physicochemical properties of a substance. For GBMs, human data, case reports and medical surveys of workers are not available so far. Thus, on the basis of the occupational exposure routes, we carried out a critical review of the literature on GBM toxicity provided by laboratory animal studies, together with monitoring data in the work environment. *In vivo* toxicity studies were focused on few layer graphene (FLG), graphene oxide (GO), reduced graphene oxide (rGO) and graphene nanoplatelets (GNP), which are considered as starting materials for further functionalization and of interest for industrial production.

2. Methods of literature review

A systematic review of the literature on GBM toxicity in laboratory mammals and monitoring data in occupational settings was performed with no time restriction, according to the Preferred Reporting Items for Systematic Reviews and Meta-Analyses (PRISMA) guidelines.[9] The electronic databases (PubMed, Scopus and ToxLine) were used as data sources, using the term "graphene".

Inclusion criteria were: (1) *in vivo* studies on FLG, GO, rGO and GNP in laboratory mammals after exposure routes mimicking possible occupational exposure in humans; (2) monitoring data in the work environment; (3) full text articles; (4) English language. Exclusion criteria included editorials, not related abstracts and studies carried out on functionalized and/or composite forms of graphene (*i.e.* polymer- or polysaccharide-conjugated graphene). For each study, information including the physicochemical properties of the administered GBMs, dosage and routes of exposure as well as outcomes was extracted independently.

3 *In vivo* toxicity studies related to occupational exposure

As shown in Fig. 2, very few and incomplete data related to GBM toxic effects after the main occupational exposure routes are available, so far.

Respiratory exposure

The majority of *in vivo* toxicity studies were carried out to assess the effects at the respiratory level after exposure to GBMs by inhalation, intratracheal instillation or pharyngeal aspiration. Studies in rodents after acute exposure to GBMs by intratracheal instillation or pharyngeal aspiration revealed rela-

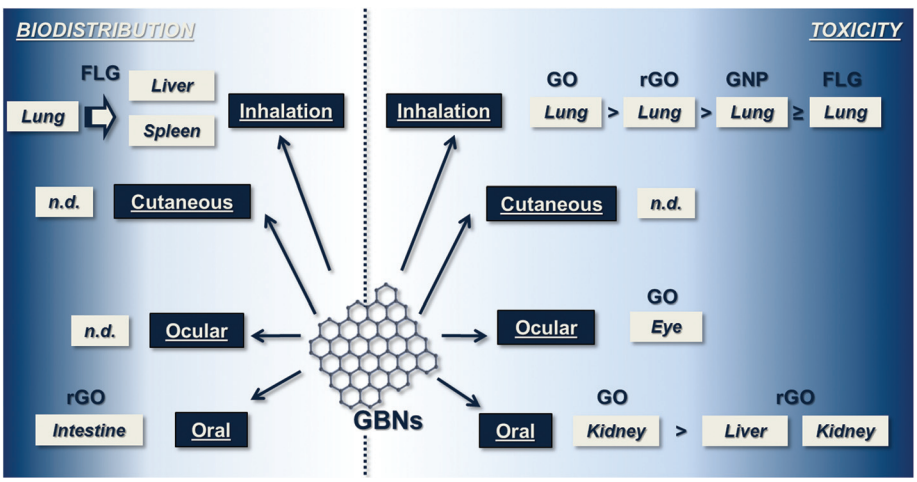

Fig. 2 Summary of the existing knowledge on GBM toxicity in animal models. As signs of toxicity, data of inflammation, granuloma formation, fibrosis and necrosis reported in the revised literature were considered. Data are divided between the main occupational exposure routes. Pictures report the organs in which the main toxic effects (on the right) and biodistribution (on left) of the main GBMs (FLG, GO, rGO, GNP) were found.

Table 1 Physicochemical properties of GBMs evaluated in the *in vivo* studies after other respiratory exposure (intratracheal exposure and pharyngeal aspiration)

	Lateral size (nm)	Thickness		Surface area	Chemical composition	Impurity	Density	Aggregation	*In vivo* exposure route	Ref.
		nm	Layers							
FLG	60 590	0.97 3.94	4 6	n/a	C 89% O 6% N 3.6% H 1.4%	n/a	n/a	Aggregated	it	14
	n/a	1.2 5.0	n/a	40 000 nm^2	n/a	n/a	n/a	Aggregated	it	11
	5000 30 000	n/a	10	100 $m^2 g^{-1}$	n/a	n/a	2 g cm^{-3}	Aggregated	pa	12
GO	2000 3000	2	2 3	338 441 $m^2 g^{-1}$	n/a	n/a	n/a	n/a	it	19
	n/a	0.5 2.0	n/a	200 000 nm^2	n/a	n/a	n/a	n/a	it	11
	100 150	n/a	n/a	n/a	n/a	n/a	n/a	Aggregated	pa	18
	2000 3000	n/a	2 3	n/a	n/a	Inorganic impurities (<1.5%)	n/a	n/a	it	16
rGO	100 150	n/a	n/a	n/a	n/a	n/a	n/a	Aggregated	pa	18
	1000 2000	n/a	2 3	411 $m^2 g^{-1}$	n/a	Inorganic impurities (<1.5%)	n/a	n/a	it	16
GNP	2000	3 4	n/a	735 $m^2 g^{-1}$	n/a	n/a	n/a	n/a	it	13
	2000 20 000	8 25	28 84	106 747 $m^2 g^{-1}$	n/a	n/a	n/a	Aggregated	pa	15
	<2000	<5 nm	<4	>700 $m^2 g^{-1}$	n/a	n/a	n/a	n/a	it	17

it intratracheal exposure; pa pharyngeal aspiration. n/a data not available.

tively severe lung inflammation, as reported in a recent review.[10] Among the investigated GBMs, on evaluating inflammatory cells and/or inflammatory markers in the broncho-alveolar lavage fluid as indices of lung inflammation, GO appeared to be the most toxic one compared to rGO, GNP or FLG, which appeared to be the least toxic GBM at the pulmonary level.[10–17] In contrast, in a very recent comparative study in male C57BL/6 mice (8 weeks-old), pharyngeal aspiration of GO induced lower toxic effects than rGO.[18] However, it should be noted that the physicochemical properties of the tested materials are not always completely reported in these studies (Table 1), making a direct comparison of the effects of GBMs difficult. For instance, chemical composition is not always reported for GO and/or rGO, giving no information on the oxidation state of these materials. Similarly, thickness, surface area and chemical composition data are missing in the majority of the studies.

The studies after intratracheal instillation also suggest that the level of graphene dispersion seems to affect its lung toxicity: highly dispersed graphene induced modest acute lung inflammation without fibrosis in male C57BL/6 mice (8–12 week-old) and its toxicity appeared to be lower than that of aggregated graphene, which lodged in the airways and induced local fibrosis.[11] Furthermore, graphene appears to be accumulated mainly in the lungs, as recorded for ^{14}C-FLG (5 μg per mouse) in male ICR mice (4 weeks-old): 47% of the dose was still detected in the lungs after 4 weeks and the remaining was distributed in the liver and spleen.[14] Similarly, after intratracheal instillation, GNP (2.5–5.0 mg kg^{-1}) was retained in the lungs of male ICR mice (6 weeks-old) for up to 28 days.[13] Very recently, a reproductive toxicity study was carried out in male NMRI mice (age/weight not specified) after the intratracheal instillation of commercial GO once a week for 7 consecutive weeks (18 μg per mouse per instillation; cumulative dose: 126 μg per mouse). The increased neutrophil number in the broncho-alveolar lavage fluid suggested pulmonary inflammation.[19]

In conclusion, these few studies after intratracheal instillation suggest the lung as the target organ and the storage depot of GBMs, with the following toxicity rank: FLG < GNP < rGO < GO. Different pieces of evidence of lung inflammation and fibrosis were observed both after acute exposure and after one exposure per week for 7 consecutive weeks. Moreover, a long persistence of ^{14}C-FLG and GNP in the lungs was observed.

However, intratracheal instillation or pharyngeal aspiration involves a non-physiological delivery of GBMs, which may lead to a less homogeneous distribution of materials as well as higher local concentrations and toxic effects than those occurring by occupational inhalation exposure.[10] For these reasons, inhalation exposure by head–nose or only-nose delivery systems, mimicking the usual human exposure scenario, is more suitable for the hazard identification and characterization.

Currently, only five *in vivo* studies after inhalation exposure to FLG, GO or GNP are reported. Each study was carried out in rats exposed to an atmosphere containing particles with an aerodynamic diameter small enough to reach the broncho-alveolar region (Table 2). The first study was carried out in male Wistar rats (7 weeks-old) head–nose exposed for 5 days (6 h per day) to FLG containing 3D-graphite impurities. The atmosphere contained a mean concentration ranging from 0.54 to 10.1 mg m^{-3} with calculated particle depositions using apparent and agglomerate densities of 0.26 and 0.29 mg per lung. Three and 24 days after the last treatment, the broncho-

Table 2 Physicochemical properties of GBMs evaluated in the *in vivo* studies after inhalation exposure (head nose or only nose exposure)

	Lateral size (nm)	Thickness nm	Thickness Layers	Surface area	Chemical composition	Impurity	Density	Aggregation	Test atmosphere (μm)	Ref.
FLG	<10 000	9	n/a	131 $m^2 g^{-1}$	C 84.1% O 8.8% S 5.4% Na 0.6% Si 0.4%	3D graphite; sulfur impurity	0.02 g mL^{-1}	~40 μm, crumpled napkin	MMAD≤0.4; particle size 0.473 0977	20
	550	8	n/a	100 $m^2 g^{-1}$	C 76.8% O 10.4% Na 10.5% P 2.4%	n/a	n/a	n/a	MMAD 0.567; particle size 0.010 0.130	21
GO	10 120	n/a	n/a	n/a	C 56.8% O 20.2% K 11.3% Na 8.3% Cl 3.4%	n/a	0.46 3.76 mg m^{-3}	n/a	Equivalent hydrodynamic diameter 0.15 0.25	23
	500 5000	1	1 2	8.46 $m^2 g^{-1}$	C 42 45% O 35 40%	n/a	1.7 g mL^{-1}	Stacked platelet structure	MMAD 0.203; particle size 0.265 34	24
GNP	<2000	0.35 0.38	20 30	750 $m^2 g^{-1}$	C 96% O 4%	n/a	0.2 g mL^{-1}	n/a	MMAD 0.123; particle size 0.265 34	22

n/a data not available.

alveolar lavage fluid of rats exposed to 3.05 or 10.1 mg FLG per cm^2 showed cytological, cytokine and enzyme activity changes related to acute/sub-acute inflammation. In parallel, a dose-dependent accumulation of single macrophages or small aggregates of alveolar macrophages loaded with black particles (recognized as graphene) were found in the lungs of all FLG-treated rats (mainly in the lumen of alveoli; only a few in the alveolar wall, alveolar ducts and terminal bronchioles). In addition, lung microgranulomas were also observed after the recovery period of 24 days, without any alteration of the lung parenchyma. For this study, the authors declared to have followed the Organization for Economic Co-operation and Development (OECD) test guideline (TG) 412, which indicates a 4-week exposure period (5 days per week; 6 h day^{-1}). However, the rats were exposed to FLG only for 1 week (5 days; 6 h day^{-1}).[20]

In another study, male Sprague-Dawley rats (6 weeks-old) were nose-only exposed for 5 days (6 h day^{-1}) to commercial FLG. The mean atmosphere FLG concentrations were 0.68 or 3.86 mg m^{-3}, corresponding to deposited doses of 3.6 or 20.3 μg per rat per day, respectively. The exposure to FLG did not change the body weight or organ weight of the rats, also during the recovery period of 28 days. No significant difference was observed in the blood levels of lactate dehydrogenase, protein and albumin between the FLG-treated rats and controls. Histopathological analysis showed FLG ingestion by alveolar macrophages.[21]

In a study on GNP, male Sprague-Dawley rats (6 weeks-old) were nose-only exposed for 4 weeks (6 h day^{-1}, 5 days per week) to commercial GNP and monitored up to 90 days after exposure, according to the OECD TG 412. In the test atmosphere, the mass concentration of GNP particles ranged from 0.12 to 1.88 mg m^{-3}, corresponding to daily deposited doses of 0.6–9.9 μg per rat. Particles of the inhaled GNP were observed in alveolar macrophages up to 90 days post-exposure, with translocation also to lung lymph nodes. However, they did not induce any lung pathology, inflammation, change in blood biochemical parameters or genotoxic effects at the pulmonary level, evaluated using the comet assay. The authors reported a No-Observed-Adverse-Effect-Level (NOAEL) >1.88 mg m^{-3}.[22]

Minor signs of toxicity were recorded for GO: male Sprague-Dawley rats (6 weeks-old) nose-only exposed for 6 h to GO showed alveolar macrophages with ingested GO, also during the recovery period of 14 days.[23] These results are in line with a very recent inhalation study in which male Sprague-Dawley rats (6 weeks-old) were nose-only exposed for 5 days (6 h day^{-1}) to a GO having different physicochemical properties (Table 2) and monitored up to 21 days after exposure. The delivered mass concentrations of GO ranged from 0.76 to 9.78 mg m^{-3}, corresponding to 3.25×10^3–9.97×10^3 particles per cm^3. No significant effects were observed in the hematological analysis or in the broncho-alveolar lavage fluid inflammatory markers and cell number, both at the end of the exposure and during the recovery period. However, alveolar macrophages with ingested GO were observed, although a gradual clearance was noted during the 21-day recovery period.[24]

Overall, the authors of three of five studies reported various levels of lung inflammation in Wistar or Sprague-Dawley rats after inhalation exposure to FLG, GNP or GO, not always reversible at the last observation time (ranging from 14 to 90 days). Although a NOAEL >1.88 mg m^{-3} of GNP was defined, based

Table 3 Physicochemical properties of GBMs evaluated in the *in vivo* studies after oral exposure

	Lateral size (nm)	Thickness		Surface area	Chemical composition	Impurity	Density	Aggregation	Ref.
		nm	Layers						
GO	40	n/a	n/a	n/a	n/a	n/a	n/a	Agglomerated	25
	200	1.8	2	n/a	C/O ratio 2.11	n/a	n/a	n/a	27
rGO	88	n/a	n/a	n/a	n/a	n/a	n/a	n/a	26
	472	n/a	n/a	n/a	n/a	n/a	n/a	n/a	

n/a data not available.

on the lack of inflammation and other lung pathologies, blood biochemical parameter changes and genotoxic effects, the presence of GNP in macrophages and in lung lymph nodes was recorded up to 90 days after inhalation exposure.[22] Furthermore, it has to be underlined that inhalation exposure to GBMs was limited to 6 h or 1 week (5 days per week; 6 h day^{-1}) and only in one study it was extended to 4 weeks (5 days per week; 6 h day^{-1}), although the validated guidelines indicate 4 weeks or 13 weeks of exposure (5 days per week; 6 h day^{-1}). No sub-chronic and chronic toxicity tests are available to evaluate other toxic effects and/or carcinogenicity, so far.

Oral exposure

Considering the exposure by ingestion, *in vivo* studies after oral administration are limited to GO and rGO, whose physicochemical properties are reported in Table 3. Male Sprague-Dawley rats (8–10 weeks-old) daily exposed by gavage to GO (10–40 mg per kg per day) for 5 days showed dose-dependent tissues signs of nephrotoxicity, tentatively mediated by oxidative stress.[25] In contrast, no alteration of kidney and liver functions or hematochemical parameters was recorded in male C57BL/6 mice (6–8 weeks-old) after daily oral exposure by gavage, for 5 days, to 60 mg kg^{-1} of small or large sized rGO. On evaluating the mouse behavior, only a short-term decrease in locomotor activity and impaired neuromuscular coordination were initially observed, without effects on anxiety-like, exploratory, spatial learning and memory behaviors or tissue changes in the hippocampus and neuroglia cells in the brain. Moreover, after daily oral exposure by gavage, for 5 days, to 60 mg kg^{-1} of ^{125}I-rGO, radioactivity was detected throughout the whole body after one day from the last exposure: in descending order in the kidney, stomach, liver, lung, and blood, indicating a considerable absorption of rGO. The majority of radioactivity decreased 15 or 60 days after the treatment.[26]

A perinatal study on GO (0.05 and 0.5 mg ml^{-1} in drinking water, from day 1 to 21 after parturition) was carried out in female ICR mice (age/weight not specified) during the lactation period to verify the developmental effects on offspring. Significant perinatal toxic effects were observed and ascribed to the decreased maternal water consumption containing GO during lactation and the reduced milk production.[27]

In conclusion, after 5-day repeated oral exposure to ^{125}I-rGO, the persistence of radioactivity significantly decreased after 15 or 60 days. A significant absorption was recorded in mice after 1 day from the last exposure, the kidney being the most involved organ.[26] These data seem to be in agreement with the nephrotoxicity recorded in rats orally exposed to GO for 5 days.[25] A reduced milk production, tentatively consequent to a decreased maternal mouse consumption of GO-containing water, induced significant perinatal effects. However, these studies, limited to GO and rGO, provide insufficient data for the GBMs' hazard identification and characterization associated with oral exposure.

Cutaneous exposure

Regarding cutaneous toxicity, except for few *in vitro* studies showing the ability of FLG and GO to penetrate human primary keratinocytes and to exert low cytotoxic effects toward human HaCaT keratinocytes and CRL-2522 fibroblasts,[28–31] no data are currently available on GBM effects at the skin level, one of the main barriers between the human body and the environment.

The lack of these data hinders the characterization of GBMs' effects at the skin level.

Ocular exposure

Concerning ocular toxicity, only two studies, limited to GO, were carried out. An acute eye irritation test in New Zealand white female rabbits (6 months-old), carried out according to the OECD TG 405, showed that dripping of GO on the conjunctival sac (10 μg per eye) did not cause local reactions. In contrast, after daily exposure of female Sprague-Dawley rats (3 weeks-old) to the same GO (25–200 ng per eye per day, for 5 days), reversible mild corneal opacity, conjunctival redness and corneal epithelium damage were noted at 100 and 200 ng per eye, which were mitigated by a topical treatment with reduced glutathione as an antioxidant agent.[32] Another study in Japanese white rabbits (2–3 kg body weight, gender not specified) showed that single intravitreal injection of GO (100–300 ng per eye), which mimics a physical injury rather than exposure by eye contact, induced negligible effects on eyeball appearance, intraocular pressure, eyesight and electroretinogram up to 49 days, when histological analysis revealed no retinal alteration and a very small amount of residual GO.[33] However, the physicochemical characterization of the tested materials is incomplete (Table 4).

Table 4 Physicochemical properties of GBMs evaluated in the *in vivo* studies after ocular exposure

		Thickness							
	Lateral size (nm)	nm	Layers	Surface area	Chemical composition	Impurity	Density	Aggregation	Ref.
GO	120	<1.2	1	n/a	n/a	n/a	n/a	n/a	32
	n/a	1	1	n/a	n/a	n/a	n/a	n/a	33

n/a data not available.

Although these findings indicate only minor ocular effects, they are not sufficient to draw any conclusion on GBMs' effects at the ocular level.

Overall, some of these toxicity data suggest potential adverse effects for some materials, but general conclusions on GBMs' effects cannot be drawn due to the limited solid available toxicity studies on laboratory animals. Consequently, these toxicological data are not sufficient as a starting point also to derive an occupational exposure limit (OEL) for GBMs in working places. Further toxicological studies, tentatively according to validated guidelines, have to be carried out to identify and characterize the hazard posed by GBMs. These studies should consider also other toxic effects, including genotoxicity and carcinogenicity as well as developmental and reproductive toxicity. In fact, although Kim *et al.* did not record genotoxic effects in the lung tissues of rats repeatedly exposed by inhalation to GNP (5 days, 6 h day^{-1}),[22] other *in vivo* studies after different exposure routes showed the genotoxic potential for some GBMs. In fact, El-Yamany *et al.*[34] observed genotoxicity (DNA damage in the lung cells and chromosomal aberrations in the bone marrow) in male albino mice (strain not specified; 25 g) after the repeated intraperitoneal injection of GO (10–500 μg kg^{-1}, once a week, the number of weeks not specified). A genotoxic effect (micronucleated polychromic erythrocytes) was also recorded after 5 days of repeated intravenous injections of GO to Kunming mice (25–30 g; gender not specified).[35] Thus, the occurrence of genotoxic effects after long-term occupational exposure to GO or other GBMs cannot be excluded.

Concerning the developmental and reproductive toxicity, only two studies after oral and intratracheal exposure, respectively, are available. Perinatal toxicity in offspring after oral daily exposure (day 1–21 post parturition) of lactating mice to GO by drinking water (0.05 and 0.5 mg ml^{-1}) was investigated, recording a significant retardation of the body weight, body length and tail length gain in the filial mice after exposure to 0.5 mg GO ml^{-1} (~0.8 mg per mouse per day). Moreover, a delayed development of offspring and a decreased length of the intestinal villi were recorded during the lactation period. These effects could be ascribed to the reduced milk production due to the decreased GO-containing water consumption by maternal mice.[27] In contrast, no reproductive toxicity in male mice was recorded after intratracheal instillation of GO, once a week for 7 consecutive weeks (18 μg per mouse per instillation; cumulative dose: 126 μg per mouse). No significant changes in epididymal sperm parameters, daily sperm production or testosterone levels were found after GO exposure, suggesting no reproductive toxicity in male mice.[19]

4. Occupational human exposure

Besides the potential hazard of GBMs, a crucial point of establishing OELs is the accurate and uniform evaluation of the human exposure in working places. Very limited data are currently available on airborne GBM concentrations in occupational settings, whose level depends on the production method and the measures aimed to reduce the exposure. For GNP, the airborne concentration during the collection of products from the discharge vessel was measured at 2.27 and 0.017 mg m^{-3}.[36] This concentration range is comparable to that not inducing signs of toxicity after 5 days of repeated nose-only exposure of rats to GNP (0.12–1.88 mg m^{-3})[22] and even lower than that of GO (0.76–9.78 mg m^{-3}).[24] Very recently, experimental data, mimicking graphene production using chemical vapor deposition (CVD) in a working place, demonstrate no measurable risk of exposure to airborne graphene in the studied site and only a transient increase in graphene presence during the cleaning of the reactors.[16] In another study, the exposure to graphene was monitored in two working places, one using graphite exfoliation and CVD, and the other growing graphene on a copper plate using CVD, which is then transferred to a polyethylene terephthalate sheet. The peak particle number concentration was lower than 40 000 cm^{-3}, with elemental carbon concentrations mostly below the detection limit, tentatively indicating a very low presence of graphene or of any other particles and very limited exposure.[37] In another study, occupational exposure to GBMs by workers during the large-scale production of graphene was assessed. After 8 h average exposure, the particle concentration in air ranged from 909 to 6438 particles per cm^3, equivalent to 0.38–3.86 μg cm^{-3}.[38] Comparable results were recently recorded for graphene within a study proposing a multi-metric approach based on the harmonized and tiered OECD methodology, in a research and development laboratory.[39] All these concentrations are far lower than the inhalation exposure levels to GBMs provoking toxicity in animals, as assessed by inhalation studies (see above).

5. Data gap identification

During this literature survey, some gaps in knowledge to assess the safety of GBMs for human health, ranging from

incomplete and not homogeneous physicochemical information of the studied materials to the actual human exposure, were identified.[6] In particular, despite the use of standardized preparation procedures, GBMs with different physicochemical properties (*i.e.* lateral size, surface area, shape, aggregation, *etc.*) can be obtained. These differences are known to affect the toxicological properties of a GBM: for instance, the same material can induce different effects if tested as dispersed particles or as agglomerates, aggregates or agglomerated aggregates. Nevertheless, the physicochemical characterization of the investigated GBM is not reported through standardized parameters in all the toxicological studies (Tables 1–4). Therefore, a correct comparison of the effects recorded for the same type of GBM is not always allowed. Furthermore, some basic information on animals and experimental conditions, which can impair the value of the *in vivo* toxicological results (*i.e.* gender, age/weight, strain of animals, dark–light cycle, environmental temperature, *etc.*), are missing in some studies. It has to be underlined that besides the environmental conditions of the animal house, which could provoke hormonal variations affecting a toxic response, also the intrinsic animal characteristics (*i.e.* gender, strain, age, *etc.*) can affect the toxic response.

These gaps can be overcome using validated guidelines for nanomaterials, if available (*i.e.* OECD TG 412 and 413, for inhalation exposure). Nevertheless, it has to be considered that the results obtained following validated guidelines for chemicals cannot always be directly applied to nanomaterials and, consequently, the toxicological evaluation has to be extrapolated with particular care.

Particular attention has to be paid to the exposure routes, focusing on the most suitable animal models mimicking real-life human exposure in occupational settings. For instance, studies after respiratory exposure should be carried out using head–nose or only-nose exposures models, avoiding non-physiological routes (*i.e.* intratracheal instillation or pharyngeal aspiration).

Further information on the Absorption, Distribution, Metabolism and Excretion (ADME) is also needed. In fact, only two animal studies on GBMs' ADME related to occupational exposure are available: they are limited to respiratory or oral exposure to FLG, GNP or rGO.[13,14,26] Other studies reporting ADME data were carried out after exposure routes not associated with an occupational scenario. In particular, after repeated intraperitoneal injection (8 injections in 4 weeks) in female Wistar/cmdb outbred rats (6 weeks-old), GO (4 mg kg^{-1}) was accumulated as large agglomerates (up to 10 mm) along the injection site, as medium dots (around 2 mm) along the mesentery and as small dots (<1 μm) in the connective and fatty tissues of the liver serosa.[40] After an acute intravenous injection of small or large ^{125}I-GO (1 mg kg^{-1}) in male ICR mice (age/weight not specified), a different distribution of the two materials was observed: small GO mainly accumulated in the liver, with few particles in the lungs and spleen, whereas the lungs became the main storage depot for large GO.[41]

Considering genotoxicity, few contradictory studies in rodents are reported: only one after respiratory exposure to GNP[22] and two by intravenous or intraperitoneal injection of GO.[34,35]

Developmental toxicity should also be more deeply investigated, considering that oral administration of GO to maternal mice during lactation was shown to cause growth retardation in offspring.[27] GO was shown to also induce malformations in the embryos of the aquatic vertebrate zebrafish, an alternative model to assess developmental toxicity, incubated in a medium containing GO at concentrations above 1 μg ml^{-1}.[42] Similarly, zebrafish embryos exposed to FLG (1–50 μg l^{-1}) up to 96 hours showed significant mortality, delayed hatching, morphological defects, yolk sac edema and pericardial edema.[43] Moreover, a single intravenous injection of small rGO or large rGO nanosheets (6.25 or 12.5 mg kg^{-1}) to ICR female mice (6–8 weeks-old) caused maternal death or abortion during the late gestational stage,[44] not giving any developmental toxicity indication due to the high administered doses.

In addition, reproductive toxicity data after the usual occupational exposure routes should be implemented, although no adverse effects were observed after repeated intratracheal instillations (one exposure per week for 7 consecutive weeks) of GO in NMRI male mice.[19] Similarly, no reproductive adverse effects were observed in ICR male mice after single intravenous (6.25–25 mg kg^{-1}) or 5 days of intraperitoneal injection (up to 60 mg kg^{-1} day^{-1}) of small GO or large GO.[45] No effects were recorded after the intravenous injection of small rGO or large rGO to ICR male and female 6–8 week-old mice (6.25–25.0 mg kg^{-1}).[44] No histopathological changes were recorded in the testes of BALB/c mice (6–8 weeks-old) after the intravenous injection of GO (200 μg per mouse)[46] or FLG (20 mg kg^{-1}) to Swiss albino mice (4–5 weeks-old).[47] In contrast, the repeated intraperitoneal injection of GO (0.4, 2.0 and 10.0 mg kg^{-1} day^{-1}, 7 or 15 repeated doses on alternate days for 15 or 30 days) to male Wistar rats (10–12 weeks-old) resulted in some adverse effects on the sperms: oxidative stress in the testes and, at the highest dose, also reduced sperm motility, total sperm count, morphological sperm abnormalities and tissues alterations in the testes. Anyway, structure and function alterations in the testes showed a significant recovery within 30 days of recovery period, while the fertility of male rats was not affected after the GO treatment.[48] The physicochemical properties of the materials tested in these studies are reported in Table 5.

Furthermore, more data should be acquired on the possible impact of GBMs on the immune system. In fact, GBM accumulation in the macrophages and lung inflammation frequently recorded in rodents after airway exposure to these materials envisage an impact on the immune system. Moreover, several *in vitro* studies showed significant effects of GBMs on immune cells.[49–54] Thus, *in vivo* studies should be carried out to elucidate the effects of GBMs on the immune system, also considering the use of these materials as biomedical tools.

Particular attention has to be paid to the potential carcinogenic effects of these materials, due to (i) their long persist-

Table 5 Physicochemical properties of GBMs evaluated in the *in vivo* studies after other exposure routes

	Lateral size (nm)	Thickness		Surface area	Chemical composition	Impurity	Density	Aggregation	*In vivo* exposure route	Ref.
		nm	Layers							
FLG	160	0.8	2 4	n/a	n/a	n/a	n/a	n/a	iv	47
GO	8 25	n/a	n/a	540 650 $m^2 g^{-1}$	n/a	n/a	n/a	n/a	ip	40
	100 500	0.9	1	n/a	n/a	n/a	n/a	n/a	iv	41
	1000 5000			n/a	n/a	n/a	n/a	n/a		
	156.4	0.7 1.5	1 2	n/a	n/a	n/a	n/a	n/a	iv	35
	300 1000	1	n/a	n/a	n/a	n/a	n/a	Stable[a]	iv	46
	55	<4	n/a	n/a	n/a	n/a	n/a	n/a	iv/ip	45
	238		n/a	n/a	n/a	n/a	n/a	n/a		
	n/a	n/a	n/a	n/a	n/a	n/a	n/a	n/a	ip	34
	5000 10 000	0.8 2	3 6	>350 $m^2 g^{-1}$	C 77.5% O 16.0% S 0.4% H 1.2% N 4.9%	n/a	0.121 g mL^{-1}	n/a	ip	48
rGO	68	n/a	1 5	n/a	n/a	n/a	n/a	n/a	iv	44
	659	n/a		n/a	n/a	n/a	n/a	n/a		

iv intravenous exposure; ip intraperitoneal exposure. n/a data not available. [a] The authors report that the GO suspension was stable for at least 1 month at room temperature.

ence in the animal body recorded in the available ADME studies using radiolabeled materials;[14,26,41] (ii) the inflammatory/fibrotic effects, observed in the lungs after acute intratracheal instillation or 5 days of repeated inhalation exposure, and the deposition in the lung macrophages, which appeared to be not reversible within 14/90 days recovery.[11,13,14,20–24] On the basis of the current available data, carcinogenic effects induced by GBMs cannot be excluded, considering that related materials (some types of multiwalled carbon nanotubes) are classified by the International Agency for Research on Cancer (IARC) within the 2B group (possibly carcinogenic to humans). However, it should be clear that long, aggregated multiwalled carbon nanotubes have a completely different shape as well as mechanical properties, in comparison with graphene. Thus, considering the potential future market of GBMs, information on the potential carcinogenicity of these materials should be gathered for proper risk management to protect human health and environment, in compliance with specific regulations, such as the REACH (Registration, Evaluation, Authorisation and restriction of Chemicals) in the European Union. Subchronic and chronic studies following validated guidelines, suitable for regulatory purposes, are also necessary for the hazard identification and characterization of GBMs.

More data are also required for the occupational exposure assessment of GBMs through environmental monitoring studies carried out at the breathing area of the workers as well as by cutaneous dosimetry on the workers' skin or clothes. Moreover, it has to be kept in mind that the exposure can be complex, involving more than one exposure route. Further exposure monitoring data should include the measurement of GBMs and/or toxicity biomarkers in workers exposed to these materials, until other human data (*i.e.* case reports, epidemiological studies *etc.*) are not available.[55]

All this information is important to define the OELs for GBMs, which could be further adjusted when workers health surveillance and/or other human data will be available.

6. Conclusions

The risk to human health posed by GBMs is associated mainly with an occupational scenario, during their industrial or small-scale production and waste discharge, which can occur mainly by inhalation, ingestion, cutaneous and ocular exposure. The inhalation toxicity data in laboratory animals, especially those obtained by toxicological studies, partially following the OECD guidelines, suggest that acute, 5 days and/or 4 weeks of repeated inhalation exposure to the tested GBMs (FLG, GO and GNP) might induce lung inflammatory/fibrotic reactions. However, these data are not sufficient to determine OELs since the relevant studies have been limited to a maximum of 5 days or 4 weeks of repeated exposure, so far. Anyway, based on the available data, airborne levels of GBMs in occupational settings seem to be lower than those inducing signs of toxicity in animal studies. Nevertheless, it is noteworthy that chronic and/or carcinogenicity studies are not yet available.

On the other hand, no conclusions can be drawn for the oral, cutaneous and ocular exposure for which very scanty data, limited to GO or rGO are available, so far.

Thus, more data for the hazard identification and characterization should be acquired by robust sub-chronic and chronic toxicological studies, following the official guidelines for regulatory purposes. If available, validated guidelines specific for nanomaterials have to be used, since those validated for chemicals cannot always be applied to nano-

materials: in this case, the toxicological evaluation has to be extrapolated with particular care. In parallel, environmental monitoring to assess the actual occupational exposure to GBMs should be carried out in working places, in association with workers' health surveillance. Once occupational exposure to GBMs and their impact on human health are clarified, we believe that identification of high-quality and safe GBMs, produced by the optimized standard procedures, will provide benefits to different industrial sectors and healthcare fields, in compliance with defined regulations, thus improving the possible negative public perception on nanotechnology.

Conflicts of interest

There are no conflicts to declare.

Acknowledgements

This study was supported by the European Union H2020 Program under grant agreement no. 696656-Graphene Flagship Core1.

References

1 C. Klaassen, *Casarett & Doull's Toxicology: the basic science of poisons*, McGraw-Hill, Health Professions Division, New York, 2013.
2 A. K. Geim and K. S. Novoselov, *Nat. Mater.*, 2007, **6**, 183–191.
3 A. Bianco, *Angew. Chem., Int. Ed.*, 2013, **52**, 4986–4997.
4 P. Wick, A. E. Louw-Gaume, M. Kucki, H. F. Krug, K. Kostarelos, B. Fadeel, K. A. Dawson, A. Salvati, E. Vázquez, L. Ballerini, M. Tretiach, F. Benfenati, E. Flahaut, L. Gauthier, M. Prato and A. Bianco, *Angew. Chem., Int. Ed.*, 2014, **53**, 7714–7718.
5 M. V. D. Z. Park, E. A. J. Bleeker, W. Brand, F. R. Cassee, M. van Elk, I. Gosens, W. H. de Jong, J. A. J. Meesters, W. J. G. M. Peijnenburg, J. T. K. Quik, R. J. Vandebriel and A. J. A. M. Sips, *ACS Nano*, 2017, **11**, 9574–9593.
6 G. Reina, J. M. Gonzalez-Dominguez, A. Criado, E. Vázquez, A. Bianco and M. Prato, *Chem. Soc. Rev.*, 2017, **46**, 4400–4416.
7 X. Guo and N. Mei, *J. Food Drug Anal.*, 2014, **22**, 105–115.
8 K. S. Novoselov, A. K. Geim, S. V. Morozov, D. Jiang, Y. Zhang, S. V. Dubonos, I. V. Grigorieva and A. A. Firsov, *Science*, 2004, **306**, 666–669.
9 D. Moher, A. Liberati, J. Tetzlaff, D. G. Altman and The PRISMA Group, *Ann. Intern. Med.*, 2009, **151**, 264–269.
10 M. Ema, M. Gamo and K. Honda, *Regul. Toxicol. Pharmacol.*, 2017, **85**, 7–24.
11 M. C. Duch, G. R. Budinger, Y. T. Liang, S. Soberanes, D. Urich, S. E. Chiarella, L. A. Campochiaro, A. Gonzalez, N. S. Chandel, M. C. Hersam and G. M. Mutlu, *Nano Lett.*, 2011, **11**, 5201–5207.
12 A. Schinwald, F. Murphy, A. Askounis, V. Koutsos, K. Sefiane, K. Donaldson and C. J. Campbell, *Nanotoxicology*, 2014, **8**, 824–832.
13 E. J. Park, G. H. Lee, B. S. Han, B. S. Lee, S. Lee, M. H. Cho, J. H. Kim and D. W. Kim, *Arch. Toxicol.*, 2015, **89**, 1557–1568.
14 L. Mao, M. Hu, B. Pan, Y. Xie and E. J. Petersen, *Part. Fibre Toxicol.*, 2016, **13**, 7.
15 J. R. Roberts, R. R. Mercer, A. B. Stefaniak, M. S. Seehra, U. K. Geddam, I. S. Chaudhuri, A. Kyrlidis, V. K. Kodali, T. Sager, A. Kenyon, S. A. Bilgesu, T. Eye, J. F. Scabilloni, S. S. Leonard, N. R. Fix, D. Schwegler-Berry, B. Y. Farris, M. G. Wolfarth, D. W. Porter, V. Castranova and A. Erdely, *Part. Fibre Toxicol.*, 2016, **13**, 34.
16 S. Bengtson, K. B. Knudsen, Z. O. Kyjovska, T. Berthing, V. Skaug, M. Levin, I. K. Koponen, A. Shivayogimath, T. J. Booth, B. Alonso, A. Pesquera, A. Zurutuza, B. L. Thomsen, J. T. Troelsen, N. R. Jacobsen and U. Vogel, *PLoS One*, 2017, **12**, e0178355.
17 J. K. Lee, A. Y. Jeong, J. Bae, J. H. Seok, J. Y. Yang, H. S. Roh, J. Jeong, Y. Han, J. Jeong and W. S. Cho, *Arch. Toxicol.*, 2017, **91**, 667–676.
18 R. Li, L. M. Guiney, C. H. Chang, N. D. Mansukhani, Z. Ji, X. Wang, Y. P. Liao, W. Jiang, B. Sun, M. C. Hersam, A. E. Nel and T. Xia, *ACS Nano*, 2018, **12**, 1390–1402.
19 A. Skovmand, A. Jacobsen Lauvås, P. Christensen, U. Vogel, K. Sørig Hougaard and S. Goericke-Pesch, *Part. Fibre Toxicol.*, 2018, **15**, 10.
20 L. Ma-Hock, V. Strauss, S. Treumann, K. Küttler, W. Wohlleben, T. Hofmann, S. Gröters, K. Wiench, B. van Ravenzwaay and R. Landsiedel, *Part. Fibre Toxicol.*, 2013, **10**, 23.
21 J. H. Shin, S. G. Han, J. K. Kim, B. W. Kim, J. H. Hwang, J. S. Lee, J. H. Lee, J. E. Baek, T. G. Kim, K. S. Kim, H. S. Lee, N. W. Song, K. Ahn and I. J. Yu, *Nanotoxicology*, 2015, **9**, 1023–1031.
22 J. K. Kim, J. H. Shin, J. S. Lee, J. H. Hwang, J. H. Lee, J. E. Baek, T. G. Kim, B. W. Kim, J. S. Kim, G. H. Lee, K. Ahn, S. G. Han, D. Bello and I. J. Yu, *Nanotoxicology*, 2016, **10**, 891–901.
23 S. G. Han, J. K. Kim, J. H. Shin, J. H. Hwang, J. S. Lee, T. G. Kim, J. H. Lee, G. H. Lee, K. S. Kim, H. S. Lee, N. W. Song, K. Ahn and I. J. Yu, *BioMed Res. Int.*, 2015, **2015**, 376756.
24 Y. H. Kim, M. S. Jo, J. K. Kim, J. H. Shin, J. E. Baek, H. S. Park, H. J. An, J. S. Lee, B. W. Kim, H. P. Kim, K. H. Ahn, K. Jeon, S. M. Oh, J. H. Lee, T. Workman, E. M. Faustman and I. J. Yu, *Nanotoxicology*, 2018, **1**, 1–15.
25 A. K. Patlolla, J. Randolph, S. A. Kumari and P. B. Tchounwou, *Int. J. Environ. Res. Public Health*, 2016, **13**, 380.
26 D. Zhang, Z. Zhang, Y. Liu, M. Chu, C. Yang, W. Li, Y. Shao, Y. Yue and R. Xu, *Biomaterials*, 2015, **68**, 100–113.
27 C. Fu, T. Liu, L. Li, H. Liu, Q. Liang and X. Meng, *Biomaterials*, 2015, **40**, 23–31.
28 K. H. Liao, Y. S. Lin, C. W. Macosko and C. L. Haynes, *ACS Appl. Mater. Interfaces*, 2011, **3**, 2607–2615.

29 Y. Li, H. Yuan, A. von dem Bussche, M. Creighton, R. H. Hurt, A. B. Kane and H. Gao, *Proc. Natl. Acad. Sci. U. S. A.*, 2013, **110**, 12295–12300.
30 M. Pelin, L. Fusco, V. León, C. Martín, A. Criado, S. Sosa, E. Vázquez, A. Tubaro and M. Prato, *Sci. Rep.*, 2017, **7**, 40572.
31 M. Pelin, L. Fusco, C. Martín, S. Sosa, J. Frontiñan-Rubio, J. M. Gonzalez-Dominguez, M. Duran, E. Vázquez, M. Prato and A. Tubaro, *Nanoscale*, 2018, **10**, 11820–11830.
32 W. Wu, L. Yan, Q. Wu, Y. Li, Q. Li, S. Chen, Y. Yang, Z. Gu, H. Xu and Z. Q. Yin, *Nanotoxicology*, 2016, **10**, 1329–1340.
33 L. Yan, Y. Wang, X. Xu, C. Zeng, J. Hou, M. Lin, J. Xu, F. Sun, X. Huang, L. Dai, F. Lu and Y. Liu, *Chem. Res. Toxicol.*, 2012, **25**, 1265–1270.
34 N. A. El-Yamany, F. F. Mohamed, T. A. Salaheldin, A. A. Tohamy, W. N. Abd El-Mohsen and A. S. Amin, *Exp. Toxicol. Pathol.*, 2017, **69**, 383–392.
35 Y. Liu, Y. Luo, J. Wu, Y. Wang, X. Yang, R. Yang, B. Wang, J. Yang and N. Zhang, *Sci. Rep.*, 2013, **3**, 3469.
36 W. A. Heitbrink, L. M. Lo and K. H. Dunn, *J. Occup. Environ. Hyg.*, 2015, **12**, 16–28.
37 J. H. Lee, H. H. Han, J. H. Kim, B. Kim, D. Bello, J. K. Kim, G. H. Lee, E. K. Sohn, K. Lee, K. Ahn, E. M. Faustman and I. J. Yu, *Inhalation Toxicol.*, 2016, **28**, 281–291.
38 A. Spinazzè, A. Cattaneo, D. Campagnolo, V. Bollati, P. A. Bertazzi and D. M. Cavallo, *Aerosol Sci. Technol.*, 2016, **50**, 812–821.
39 F. Boccuni, R. Ferrante, F. Tombolini, D. Lega, A. Antonini, A. Alvino, P. Pingue, F. Beltram, L. Sorba, V. Piazza, M. Gemmi, A. Porcari and S. Iavicoli, *Int. J. Mol. Sci.*, 2018, **19**, E349.
40 N. Kurantowicz, B. Strojny, E. Sawosz, S. Jaworski, M. Kutwin, M. Grodzik, M. Wierzbicki, L. Lipińska, K. Mitura and A. Chwalibog, *Nanoscale Res. Lett.*, 2015, **10**, 398.
41 J. H. Liu, S. T. Yang, H. Wang, Y. Chang, A. Cao and Y. Liu, *Nanomedicine*, 2012, **7**, 1801–1812.
42 Y. Chen, X. Hu, J. Sun and Q. Zhou, *Nanotoxicology*, 2016, **10**, 42–52.
43 B. Manjunatha, S. H. Park, K. Kim, R. R. Kundapur and S. J. Lee, *Environ. Sci. Pollut. Res. Int.*, 2018, **25**, 12821–12829.
44 S. Xu, Z. Zhang and M. Chu, *Biomaterials*, 2015, **54**, 188–200.
45 S. Liang, S. Xu, D. Zhang, J. He and M. Chu, *Nanotoxicology*, 2015, **9**, 92–105.
46 G. Qu, X. Wang, Q. Liu, R. Liu, N. Yin, J. Ma, L. Chen, J. He, S. Liu and G. Jiang, *J. Environ. Sci.*, 2013, **25**, 873–881.
47 A. Sasidharan, S. Swaroop, C. K. Koduri, C. Madathil Girish, P. Chandran, L. Panchakarla, V. H. Somasundaram, G. S. Gowd, S. Nair and M. Koyakutty, *Carbon*, 2015, **95**, 511–524.
48 N. K. Nirmal, K. K. Awasthi and P. J. John, *Basic Clin. Pharmacol. Toxicol.*, 2017, **121**, 202–210.
49 M. Orecchioni, C. Ménard-Moyon, L. G. Delogu and A. Bianco, *Adv. Drug Delivery Rev.*, 2016, **105**, 163–175.
50 M. Orecchioni, D. A. Jasim, M. Pescatori, R. Manetti, C. Fozza, F. Sgarrella, D. Bedognetti, A. Bianco, K. Kostarelos and L. G. Delogu, *Adv. Healthcare Mater.*, 2016, **5**, 276–287.
51 M. Orecchioni, D. Bedognetti, F. Sgarrella, F. M. Marincola, A. Bianco and L. G. Delogu, *J. Transl. Med.*, 2014, **12**, 138.
52 S. P. Mukherjee, K. Kostarelos and B. Fadeel, *Adv. Healthcare Mater.*, 2018, **7**, 1700815.
53 S. P. Mukherjee, M. Bottini and B. Fadeel, *Front. Immunol.*, 2017, **8**, 673.
54 J. Yan, L. Chen, C. C. Huang, S. C. Lung, L. Yang, W. C. Wang, P. H. Lin, G. Suo and C. H. Lin, *Colloids Surf., B*, 2017, **153**, 300–309.
55 E. Nielsen, G. Østergaard and J. C. Larsen, *Toxicological risk assessment of chemicals. A practical guide*, Informa Healthcare, New York, 2008.

molecules

MDPI

Review

Toxicity Studies on Graphene-Based Nanomaterials in Aquatic Organisms: Current Understanding

Nemi Malhotra [1], Oliver B. Villaflores [2], Gilbert Audira [3,4], Petrus Siregar [4], Jiann-Shing Lee [5,*], Tzong-Rong Ger [1,6,*] and Chung-Der Hsiao [3,4,6,*]

1 Department of Biomedical Engineering, Chung Yuan Christian University, Chung-Li 320314, Taiwan; nemi.malhotra@gmail.com
2 Department of Biochemistry, Faculty of Pharmacy and Research Center for Natural and Applied Sciences, University of Santo Tomas, Manila 1015, Philippines; obvillaflores@ust.edu.ph
3 Department of Chemistry, Chung Yuan Christian University, Chung-Li 320314, Taiwan; gilbertaudira@yahoo.com
4 Department of Bioscience Technology, Chung Yuan Christian University, Chung-Li 320314, Taiwan; siregar.petrus27@gmail.com
5 Department of Applied Physics, National Pingtung University, Pingtung 900391, Taiwan
6 Center for Nanotechnology, Chung Yuan Christian University, Chung-Li 320314, Taiwan
* Correspondence: jslee@mail.nptu.edu.tw (J.-S.L.); sunbow@cycu.edu.tw (T.-R.G.); cdhsiao@cycu.edu.tw (C.-D.H.)

Academic Editor: Seyyed alireza Mirkhani
Received: 24 July 2020; Accepted: 7 August 2020; Published: 9 August 2020

Abstract: Graphene and its oxide are nanomaterials considered currently to be very promising because of their great potential applications in various industries. The exceptional physiochemical properties of graphene, particularly thermal conductivity, electron mobility, high surface area, and mechanical strength, promise development of novel or enhanced technologies in industries. The diverse applications of graphene and graphene oxide (GO) include energy storage, sensors, generators, light processing, electronics, and targeted drug delivery. However, the extensive use and exposure to graphene and GO might pose a great threat to living organisms and ultimately to human health. The toxicity data of graphene and GO is still insufficient to point out its side effects to different living organisms. Their accumulation in the aquatic environment might create complex problems in aquatic food chains and aquatic habitats leading to debilitating health effects in humans. The potential toxic effects of graphene and GO are not fully understood. However, they have been reported to cause agglomeration, long-term persistence, and toxic effects penetrating cell membrane and interacting with cellular components. In this review paper, we have primarily focused on the toxic effects of graphene and GO caused on aquatic invertebrates and fish (cell line and organisms). Here, we aim to point out the current understanding and knowledge gaps of graphene and GO toxicity.

Keywords: graphene; graphene oxide; fish; invertebrates; toxicity

1. Introduction

Graphene is an allotrope of carbon [1]. It is defined as single layer of carbon sheet with a hexagonal packed lattice structure with sp^2 hybridized carbon atoms tightly packed in a 2D honeycomb lattice, which provides large surface area on both sides of the planar axis [2]. The unmodified basal plane sites of graphene comprise free surface π electrons that are hydrophobic [3]. However, the hydrophobicity of the graphene is strongly thickness-dependent, with single-layer graphene being significantly more hydrophilic than its thicker counterparts [4]. The ideal graphene is a single-layer carbon atom held together by covalent bonds. It is difficult to isolate a single layer of graphene, hence graphene is also

categorized as few-layer graphene (2–5 nm), multilayer graphene (2–10 nm), and graphite nanoplates (2D graphite materials, thickness > 100 nm) [5,6].

It is the strongest and thinnest known material known to man [7]. Graphene consists of unique properties such as thermal conductivity [8,9], impermeability to gases, stiffness, high Young's modulus [9], good optical transparency [10], high carrier mobility at room temperature, excellent mechanical strength, large surface area, and outstanding electrocatalytic activity [1,2,7,11,12]. These unique and appealing properties of graphene make it potential candidate for biomedical application, including absorption of enzymes [13,14], electrochemical devices [15,16], energy storage [17,18], drug delivery [19], biosensors [20,21], photovoltaic devices [22,23], supercapacitors [24,25], photocatalysis [26,27], and fuel cells [1,2,19,28,29] (Figure 1).

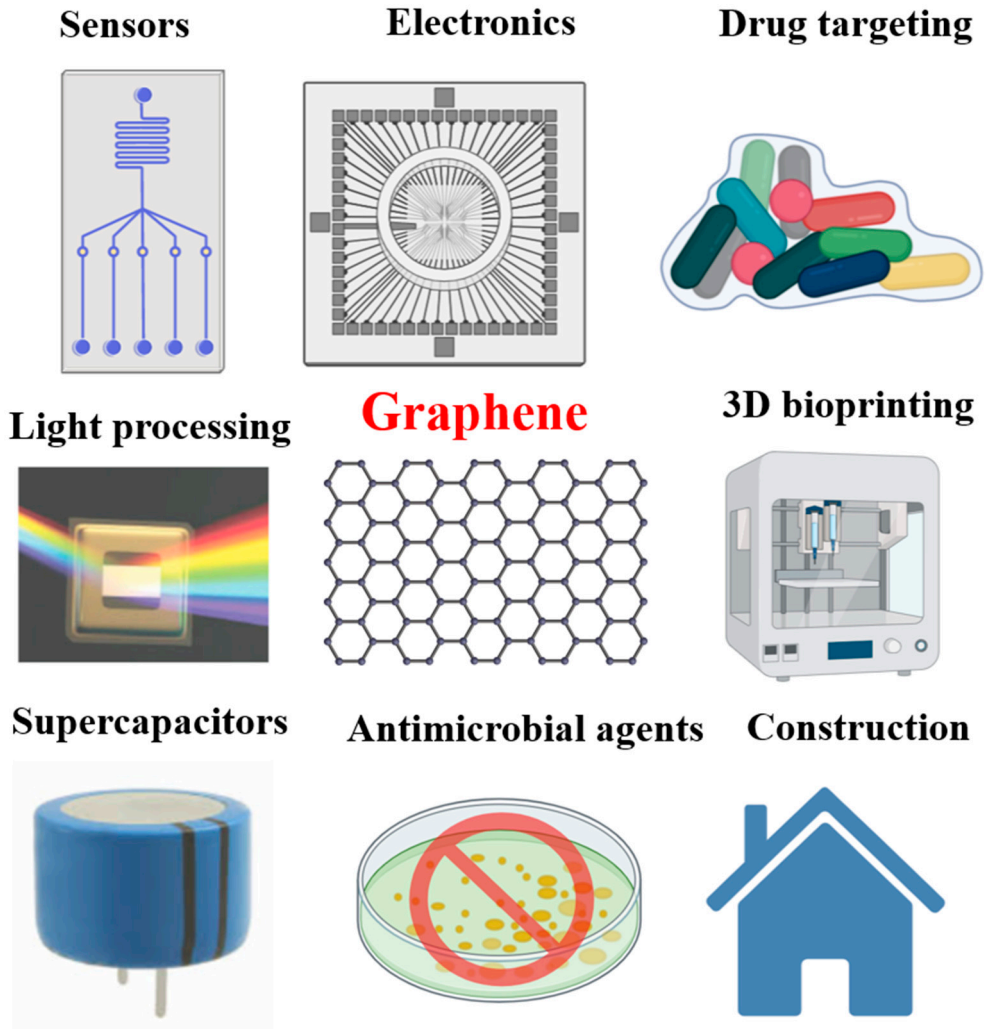

Figure 1. Potential application of graphene-based nanomaterials in industrial and biomedical fields. The graphene-based nanomaterials are widely applied for producing sensor, electronic, drug targeting, 3D bioprinting, construction, antimicrobial agents, supercapacitor, and light processing.

These advantages of graphene make it desirable for the development of graphene composites through the incorporation of different functional materials. Graphene-based composites have been achieved successfully with organic crystals [30,31], inorganic nanostructure [32–35], biomaterials [21,36], polymers [37–39], and carbon nanotubes [40–42].

On the other hand, graphene oxide (GO) is an intermediate product obtained during the synthesis of reduced GO (rGO) [43–45]. It is also a two-dimensional (2D) carbon material and is viewed as the oxidized form of graphene, with oxygen functional groups decorating the basal plane of carbon

layer [46]. It can be regarded as a result of chemical exfoliation and oxidizing of layered crystalline graphite [47]. Owing to the presence of the oxygen functional groups, GO nanosheets are hydrophilic in nature. They can be dispersed in aqueous solution [46] but are not dispersive in organic solvents. These attractive properties of GO make it suitable for biomedical applications such as gene delivery, drug delivery, scaffolds for mammalian cell culture, and substrates for antibacterial agents [48,49].

At this increasing phase of commercial production, the presence of graphene is evident in the environment at a significant level [50,51]. Irrespective of particular forms of graphene, a large number of studies have demonstrated that graphene affects a wide range of living organisms, including prokaryotes, bacteria, viruses, plants, micro and macroinvertebrates, mammals, human cells, and whole animals in vivo [52]. Further, graphene also interacts with physiological components of aquatic environment such as inorganic ions, colloidal particles, surface active molecules, and natural organic matter (NOM), which are known to modify graphene surface [6]. Thus, the interaction with the surrounding media and biota with graphene has demonstrated its transformation and degradation for possible bioremediation of graphene and its oxides [53]. In particular, Indranil Chowdhury et al. (2013) suggested that GO aggregation and stability in aqueous environment follows a colloidal theory [54]. GO contain many oxygen-containing groups, it is dispersible in water, and can be transported in water through physical process or food chain. As a result, it might accumulate in the ecosystem, posing threat for aquatic organisms and eventually to human health [55–57]. Recently, in vivo studies have revealed bio-distribution and persistence of GO in living organisms [58–60]. The hydrophobic lattice of graphene tends to undergo layer-by-layer aggregation in water due to hydrophobic forces, whereas GO with carboxyl, hydroxyl, and epoxy groups on the surface forms stable suspensions [54]. Many investigations have assessed the effects and mechanisms related to the transport and intake of nanoparticles in aquatic invertebrate and fish model at different growth stages to address the eco-toxicity [61–63]. Many biomarkers of environment toxicity notably the density of cellular and subcellular components of blood, lysosomal membrane stability, apoptosis, micronucleation, cellular damages, and cytotoxic responses have been established. Moreover, behavioral shifts and histopathological analyses are suggested as effective parameters of toxicity screening in model invertebrates [64]. On the other hand, fish is an important species in the aquatic food chain. Fish is potentially exposed to released nanoparticles to the environment via the food chain or by direct absorption/adsorption from aquatic medium [65]. The fish model includes sensitive early life-stage bioassays, sensitivity to dissolved chemicals and materials, low rearing cost, and homology with the human genome. The emphasis on fish model as an adjunct to conventional rodent models is gaining acceptability in toxicological research of environment contaminants, especially the ones having direct impact on aquatic systems [66]. Hence, results from thorough analyses of graphene-exposed fish might lead to some constructive outcome for future developments in research.

In this present review, we will analyze the biocompatibility and toxicology of graphene and GO in order to evaluate the safety limits needed for the implementation of upcoming researches. We will also try to draw attention towards knowledge gaps to attain valuable insights on the fate and risks presented by graphene and GO on fish in the aquatic environment. Furthermore, we will discuss the key physiological factors involved in influencing the toxicity of graphene and GO in fish in the surrounding water medium, degradation pathways, and the exposure and administration pathways. We believe that the critical study in this field will lead to collection of current information leading to the production of better modified materials emerging in healthcare, diagnostic, and therapeutics.

2. Graphene Chemistry

Graphene is inert in chemistry because of the immense delocalized π electron system [67]. The graphene in its pure form is hydrophobic and has very less solubility in most of the solvents. The chemistry of graphene is primarily focused on to analyze the solubilization of graphene, and various methods have been developed to attain its well-organized chemical modification. To increase the solubility of graphene, wet chemistry techniques have been devised that are also used for graphite

and carbon nanotubes [45,68]. The graphene sheet can readily be functionalized via non-covalent p-p stacking or covalent C-C coupling reactions. In particular, covalent chemistry provides a strong pathway to tailor physical properties of pristine graphene. The carbon atoms present in graphene are chemically accessible. The derivation of graphene with different organic moieties makes graphene solubility flexible to be adjusted to different solvents required for the processing of composite films [69–71]. Furthermore, functional groups used for modification can broaden the properties of graphene through formation of donor-receptor complex with graphene. Based on the properties of graphene and its derivatives, significant movement in mechanical, thermal, electrical, and viscous properties of graphene-polymer composites can be achieved [72]. The aggregation and dispersion behavior of graphene thus can be altered by solution chemistry. GO demonstrates different dispersion performance in comparison to pristine graphene and reduced graphene [6]. Therefore, keeping the high variability of graphene in mind is important to understand the interaction, adsorption, transformation, and toxicity criteria of graphene.

3. Exposure, Accumulation, and Bio-Distribution of Graphene in Invertebrates

Invertebrates are important organisms utilized for environmental toxicological studies. They have a relatively short life span, fast reproduction, and high sensitivity towards pollutants. They are also cost-effective and contribute quick results. These organisms are regarded as convenient test species for ecotoxicity studies of new chemicals and nanoparticles [73]. The invertebrates enter the food chain at intermediate levels and are considered vehicles for recycling pollutants deposited in sediments. They feed on bacteria, plants, algae, and other invertebrates. These also become prey for larger organisms including fish and birds, which in turn represent a good portion of the human diet. Therefore, the fate of contaminants, bioconcentration, bioaccumulation, and biomagnification should be regarded as important platforms in understanding the toxicity produced, if there is any, over other species [74–76]. In a short-term study of 72 h on the eastern oyster (*Crassostrea virginica*), both 1 and 10 mg/L GO exhibited a dose-dependent elevated lipid peroxidation. No significant changes in glutathione S-transferase (GST) levels were observed, but a reduction in the total protein levels was found in tissues of the digestive glands at both concentrations (1 and 10 mg/L) of the GO. Overall, the study indicated that short-term GO exposures can induce oxidative stress, epithelial inflammation and adversely affected the overall health of *Crassostrea virginica* [77]. In a similar long-term study of 14 days on *Crassostrea virginica*, elevated lipid peroxidation and changes in glutathione-s-transferase (GST) were observed in tissues of gills and digestive gland exposed at 2.5 and 5 mg/L. Reactive oxygen species (ROS) induced oxidative damage. Therefore, the study suggested that detoxification enzyme such as GST are thought to be involved in stress signaling, leading to harmful effects on cellular health [78].

Further in a study by De Marchi et al., different concentrations of GO (0.01, 0.10, and 1.00 mg/L) toxicity were tested over *Diopatra neapolitana* (a polychaete species) for 28 days. The analysis of physiological (regenerative capacity) and biochemical (energy reserve, metabolic activity, and oxidative stress-related biomarkers) depicted negative effects of GO on regenerative capacity of *Diopatra neapolitana*, the organisms exposed to higher concentrations of GO took long periods to complete regeneration. GO also altered the energy-related responses, such as glycogen content with high polychaetes, which might have resulted from decreased metabolism. The research work concluded that cellular damage happened despite higher activities of antioxidant and biotransformation enzymes in *Diopatra neapolitana* exposed to GO [79]. In another study by Zhang and co-workers, acute and chronic toxicity tests were performed on *Daphnia magna* with and without the presence of humic acid (HA). The GO induced significant toxicity to *Daphnia magna* with a median lethal concentration of 48 h LC50 equal to 84.2 mg/L and 21-day LC50 as 3.3 mg/L. The HA mitigated the acute and chronic toxicity in *Daphnia magna*, as in the presence of HA, the decreased toxicity of GO was attributed to alleviation of oxidative damage by HA [80]. Furthermore, assessment of the accumulation and elimination of graphene after 24 h exposure to 250 µg/L of graphene in *Daphnia magna* was done by Guo and colleagues. Their results demonstrated the accumulation of graphene at 1% of organism's dry mass. During the

time for depuration, these organisms bore roughly constant body burdens after 24 h regardless of initial graphene concentration, whereas, after addition of an algae and humic acid, the depuration resulted in significant release of accumulated graphene but leaving some graphene in the organism. The study concluded that the remaining graphene in *Daphnia magna* might possess a risk to be passed on to neonates and thus require further risk assessment and relevant evaluation [81]. In another study by Souza et al., the toxicity of GO was further tested on freshwater flea *Ceriodaphnia dubia* in acute and chronic assay. The mean effective concentration (EC50) estimated during acute exposure was 1.25 mg/L, whereas chronic exposure of GO resulted in significant decrease in number of neonates, feeding rates, and ROS generation. Their research group concluded that in the presence of GO, there was a shift in the available energy for self-maintenance instead of feeding and reproduction activities [82]. Moreover, de Melo and co-investigators reported that when toxicity of GO was ascertained in presence and absence of trace elements (Cd, and Zn) in shrimp *Palaemon pandaliformis*, results suggested that GO did not cause acute toxicity at concentration up to 5.0 mg/L after 96 h exposure. However, GO in association with Cd and Zn increased toxicity of the trace elements as suggested by 96 h LC50 of Cd associated with GO 1.7 times less than the 96 h LC50 of Cd alone and 96 h LC50 of Zn associated with GO 1.8 times less than 96 h LC50 of Zn alone. Likewise, co-exposure of GO with trace elements impaired the routine metabolism of *Palaemon pandaliformis*. The study recommended that more researches and evaluation of data need to be done to understand the toxicity criteria of GO in aquatic organisms or aquatic bodies [83].

4. Exposure of Graphene to Fish Cell, In Vitro

In determining the cytotoxicity of environmental pollutants, cell lines derived from fish are considered very suitable experimental model. Testing the toxicity of nanomaterials is more complex than other chemical compounds. In nanomaterials, various physiochemical properties such as size, shape, surface area, and surface modification need to be considered prior to experimentation. Other factors including agglomeration, aggregation, sedimentation, dissolution, concentration need to be studied as well their fate in the test systems. If these aspects of nanomaterials are not investigated prior to experimentation, they might interfere with the results and misleading conclusions can be drawn. A study by Lamel et al. was done by exposing topminnow fish hepatoma cell line PLHC-1 cells to a single layer GO and carboxyl graphene (CXYG) (16 µg/mL GO or CXYG) suspensions with an aryl hydrocarbon receptor (AhR). Their results demonstrated pre- and co-exposure of cells to GO and CXYG nanoplatelets induced cytochrome P450 1A (cyp1A) expression, suggesting that graphene nanoplatelets increased the effective concentration of AhR agonists by facilitating passive diffusion into cells by damaging the plasma membrane or transporting them over the plasma membrane via a Trojan horse-like mechanism. Based on their results, it was found that there is an existence of combination effects between nanomaterials and environment pollutants [84]. In a similar study, when nanoplatelets GO and CXYG were assessed in PLHC-1 cells (GO: 0.125–16 g/mL; CXYG: 0.25–32 g/mL) for 72 h, oxidative stress was induced. Graphene nanoplatelets penetrated the plasma membrane and accumulated in cytosol, and these nanoplatelets interacted with the mitochondria and nuclear membrane further. The PLHC-1 also demonstrated reduction in the mitochondrial membrane potential and increase in ROS at 16 g/mL [85].

In another study, bluegill sunfish (BF-2 cells) were exposed to GO at concentrations of 0, 10, 20, 40, 60, 80, and 100 µg/mL for 24 h. Two biological assays (3-(4,5-dimethylthiazol-2-yl)-2,5-diphenyl tetrazolium bromide) MTT assay and neutral red uptake (NR) resulted in cytotoxicity and oxidative stress in BF-2 cells. The tested biomarkers of oxidative stress such as lipid peroxidation, superoxide dismutase, catalase, reactive oxygen species, and 8-hydroxy-2′-deoxyguanosine levels increased, and glutathione level was decreased in BF-2 after treatment with GO. The GO induced a dose- and time-dependent cytotoxicity on BF-2 cells [86]. In addition, using two different fish cell lines PLHC-1 and carp leukocytes (CLC), the toxicity and intracellular fate of graphene oxide (GO) were evaluated at a concentration range of 0–200 µg/mL for 24 and 72 h. The results depicted that GO had low cytotoxicity and is present

in the vesicles as well as free in the cytoplasm of both cell types as revealed by transmission electron microscopy (TEM) [87].

5. Exposure, Accumulation, and Bio-Distribution of Graphene in Fish Embryo and Larvae

A reliable way of nanomaterials administration to an aquatic organism is oral and direct injection [88]. For direct injection, the vaccines/or any compound of interest are required to be prepared with oil/water formulations that may cause adverse effects. On the other hand, graphene nanomaterials are administered in fish using either by microinjection or by continuous exposure [89]. After careful selection, viable and fertilized eggs were either microinjected with graphene nanomaterials in nanoliter volumes within 4 hpf (hour post-fertilization) or continuously exposed in a medium containing graphene nanomaterials from 2 hpf until 72–168 hpf with change of medium once every 12–24 h interval [90–93]. The aggregation and stability of graphene nanomaterial can alter its physiochemical dimensions such as size and effective surface area, which may modulate toxicity to aquatic animals including fish [88]. The zebrafish embryos are covered by transparent acellular membrane called chorion, which acts as primary barrier that prevents the entry of exogenous materials including graphene nanomaterials from external environment in embryo's body [65,94]. The route of graphene exposure, accumulation, and bio-distribution has been investigated previously. In a study to test the toxicity of GO and multi-walled carbon nanotubes (MWNTs), the results showed that GO has moderate toxicity to organisms as it inhibited growth and caused slight hatching delay among zebrafish embryos at 50 mg/L but did not depict significant increase on apoptosis in the embryo, whereas MWNTs' toxicity demonstrated strong inhibition of cell proliferation and serious morphological defects in developing embryos even at lower dose of 25 mg/L. This particular work suggested that the distinctive toxicity of GO and MWNTs can be attributed to the different models of interaction between nanomaterials and organisms, which might arise from different geometric structure of nanomaterials [95]. In a similar study, when toxicity of GO, MWCNTs, and reduced graphene oxide (rGO) were tested on zebrafish embryos at a concentration of 1, 5, 10, 50, and 100 mg/L for 96 h, results revealed the inhibition of hatching of zebrafish embryos. The heart rate of the embryos treated with GO was significantly ($p < 0.05$) decreased at 100 mg/L at 48 hpf. Furthermore, rGO and MWCNTs decreased the length of hatched larvae at 96 hpf but no mortality and morphological malformation were observed, which further requires more results and analysis at various concentrations at different time periods [96].

Further in a different study, when the zebrafish embryos were exposed to a concentration of 1–100 μg/L to analyze the developmental toxicity, the results yielded impaired DNA modification, protein carbonylation, and excessive generation of ROS. The work also highlighted nonmonotonic response of zebrafish developmental toxicity to GO at μg/L to mg/L levels. On further analysis, transcriptomics revealed deficiencies in the collagen and matrix metalloproteinase (MMP) related genes, which in turn affected the skeletal and cardiac development of zebrafish. Moreover, to contribute to the results of developmental toxicity, metabolomics assay showed inhibition in amino acid metabolism and disturbance in the ratio of unsaturated fatty acids (UFAs) to saturated fatty acids (SFAs). The work, therefore, demonstrated developmental toxicity on the basis of involved molecular mechanism at trace concentration equal to 10 μg/L [60].

In an interesting study of Hu et al. with parent and offspring zebrafish when GO nanosheets were administered to parental zebrafish at a concentration of 0.01–1 μg/L, GO translocated from water to the brain of parent fish and the offspring with major loss of claudin5a (a core component of neuroepithelial barrier system). However, GO did not induce neurotoxicity in the parent fish and significant neurotoxicity occurred in the offspring, exhibiting loss of dopaminergic neurons and reduction in acetylcholinesterase (AChE) activity. Moreover, endoplasmic reticulum damage, autophagy promotion, ubiquitin down-regulation, and increase in β-galactosidase activities were observed, attributing to the failures in the carbohydrate and fatty acid metabolisms. Their work suggested that more researches and data compilation for the toxicity of GO on fish offspring at environmentally relevant

concentration are required to do reliable analysis and to establish conclusions [97]. Similarly, in another study when the toxicity and molecular mechanism of GO were investigated in larvae and adult zebrafish at 0, 0.25, 0.5, and 1 mg/L for 72 h, results demonstrated that hepatotoxic phenotype has significantly decreased liver area and a dose-dependent decrease in the number of hepatocytes. Moreover, the number of macrophages and neutrophils in zebrafish embryos was reduced, but the expressions of pro-inflammatory cytokines were increased after GO treatment. The thorough analyses revealed down-regulation of lipid metabolism genes and up-regulation of immune genes. Moreover, GO induced NF-κB p65 into the nucleus and increased the protein levels of NF-κB p65, JAK2, STAT3, and Bcl2 in adult zebrafish liver. Overall, the elaborative study and results demonstrated GO-induced hepatic dysfunction mainly through the ROS and PPAR-α-mediated innate immune signaling in zebrafish [98].

In a study by Clemente and co-workers, zebrafish embryos were analyzed after 5 and 7 days of GO exposure at 100 mg/L and humic acid (HA) at 20 mg/L either individually or together. Regardless of the presence of HA, the larvae exposed to GO for 5 days demonstrated increase in the locomotor activity, reduction in yolk sac size, total length, and inhibition of AChE activity. The larvae exposed to GO for 7 days did not show any significant differences in the locomotor activity, but the RT-PCR gene expression analysis depicted an increase in AChE expression. The work suggested that HA is associated with toxicity risk modulation by GO and some compensatory homeostatic mechanisms might be involved in the effects observed in zebrafish [99]. In a similar study when GO and HA were exposed to zebrafish embryos at 0–100 mg/L, significant hatching delay and cardiac edema were observed. The interaction of GO with chorion induced damage to chorion protuberances, excessive generation of $^{\cdot}OH$, and changes in the secondary structure of protein, which, in contrast, were relieved by HA. On the other hand, humic acid reduced interactions between GO and chorion mitigating chorion damage by regulating the morphology, structure, and surface negative charges of GO, indicating a feasible antidotal mechanism for GO in presence of HA [100].

In another study, zebrafish embryos were treated with GO at 0, 0.01, 0.1, 1, and 100 mg/L for 24, 48, and 96 hpf. Results revealed that the GO adhered to and enveloped the chorion of zebrafish embryos via the hydroxyl group interactions and it blocked the pore canals of the chorionic membrane causing hypoxia and hatching delay. Furthermore, GO penetrated the chorion of embryo via endocytosis, damaged the mitochondria, and primarily translocated to the eye, heart, and yolk sac regions involved in circulatory system of zebrafish. In these organs, GO induced excessive generation of reactive oxygen species, thus increasing oxidative stress, DNA damage, and apoptosis. The work highlighted specific adverse effects of GO on embryogenesis and emphasized the potential ecological and health risks of GO [101]. Furthermore, when GO exposure was done to zebrafish embryos at 5, 10, 50, or 100 mg/L for 6 days and up-regulation in *synapsin IIa* expression at 5 mg/L with down-regulation of *dat* expression were observed, showing potential compensatory mechanism. At 10 mg/L GO exposure, increase in heart rate, absolute turn angle, brain cell damage, and decrease in dopamine levels were observed. However, no changes were observed on higher concentrations of GO exposure, which is attributed to GO agglomeration. The work concluded that the results of the toxic effects of GO were not dose-dependent and are pre-eminent at lower concentrations, and hence more studies are required to gather relevant data and analysis [102]. In the next study, dose-dependency effects of three different sized GO particles (50–200 nm, <500 nm, and >500 nm) on zebrafish during the very early developmental stages (4–124 h post-fertilization) were performed. The GO nanoparticles accumulated in the eyes, the heart, the yolk sac, and the blood vessels of the fish larvae. This was also exhibited on observed endpoints of delay in hatching time, shortened body length, modification in heart rate and blood flow, response in photoperiod stimulation, enhanced activities of superoxide dismutase, AChE, caspase-3, and induction of apoptosis-related genes expression. Specifically, oxidative stress and induction of apoptosis in all three different sized GO particles predicted a potential risk of GO on marine organisms [103]. The group of Li reported that when corannulene (non-planar PAH) and graphene (planar PAH) were exposed to zebrafish larvae at 1, 10, and 50 μg/mL, minimal developmental toxicity

and significant decrease in locomotion/increase in sleep caused by corannulene with no significant locomotion alterations at 50 μg/mL graphene were observed. Corannulene increased sleep and reduced locomotor activity and the expression of *hcrt* and *hcrtr* mRNA, while graphene did not obviously disturb the sleep behavior and gene expression patterns [60].

6. Exposure, Accumulation, and Bio-Distribution of Graphene in Adult Fish

Acute toxicity, oxidative stress, and immune-toxicity of GO were analyzed at 1, 5, 10, or 50 mg/L for 14 days were done in a study using the zebrafish adult model. Histological analysis of the liver and intestine showed cellular alterations including vacuolation, loose arrangement of cells, histolysis, and disintegration of cell boundaries. Malondialdehyde (MDA) level and superoxide dismutase (SOD) and catalase (CAT) activities were increased and glutathione was decreased in the liver after treatment with GO. Moreover, levels of tumor necrosis factor alpha (TNF-α), interleukin-1B, and interleukin-6 depicted induction in immune response. Hence, the work suggested GO exposure in aquatic system caused oxidative stress and immune toxicity in adult zebrafish [104]. Moreover, the adult zebrafish was exposed to carbon-14-labeled few-layer graphene (FLG) to analyze the effect of size on graphene uptake, depuration, and bio-distribution as reported by Lu et al. in their research article. After 48 h exposure to larger FLG (L-FLG) at 250 μg/L, the amount of graphene in the organism was close to 48 mg/kg fish dry mass, which was more than 170-fold greater than the body burden of those exposed to the same concentration of smaller FLG (S-FLG). The L-FLG mainly accumulated in the gut of adult zebrafish, and S-FLG was observed in both the gut and the liver after exposure with or without NOM. Strikingly, the S-FLG was able to pass through the intestinal wall and enter the intestinal epithelial cells and blood. The work suggested further tests to contribute concrete results [105]. In another study, zebrafish were fed diets with three graphene family materials (GFMs) monolayer graphene powder (GR), graphene oxide nanosheet (GO), and reduced graphene oxide powder (rGO) for 21 days. Later, gut bacterial communities were analyzed and depicted alteration in intestinal morphology and oxidative stress. Results showed that GFMs led to different inflammatory responses and significantly altered the relative composition of the gut bacterial species by increasing the relative abundance of *Fusobacteria* and the genus *Cetobacterium* and *Lactobacillus* and decreasing the abundance of Firmicutes and the genus *Pseudomonas*; GR caused marked shifts in the diversity of the gut microbiota. The GFMs also altered the intestinal morphology and antioxidant enzyme activities by inducing more vacuolation and generating more goblet cells [106].

The effects of GO were observed on the antioxidant metabolism of zebrafish; after 48 h exposure, SOD activity was significantly increased in 20 mg/L, CAT activity in 2, 10, and 20 mg/L, and lipid peroxidation (LPO) had an increase in 2 mg/L, whereas glutathione peroxidase (GPx) was inhibited at 20 mg/L. Later after 168 h recovery in clean water, SOD remained elevated in 20 mg/L, CAT activity remained unchanged and GPx activity was inhibited at 2, 10, and 20 mg/L, and LPO decreased in 2 mg/L. The study suggested that GO exposure disrupted antioxidant metabolism of adult zebrafish in which it was not restored even after 168 h recovery period in clean water [107]. The toxic effects of GO when evaluated on *Anabas testudineus* (the climbing perch) revealed accumulation of cellular lipid peroxides specifically in the mitochondria. Activity of SOD, CAT, and, GST was augmented in contrast to lowered level of reduced glutathione titer. The results also indicated oxidative stress in cell and mitochondria in fish after exposure to GO, thus suggesting compilation of more data for comparison of results and establishments [108]. In a separate study with graphene nanoparticles, fish were exposed in 10, 20 mg/L concentrations for 10 days. Results of statistical analysis showed significant decrement at $p \leq 0.05$ for RBC (0.770 cells/μL × 10^6) in T1 and 0.850 cells/μL × 10^6 in T2 compared with negative control (1.410 cells/μL × 10^6). There was no significant decrease $p > 0.05$ of each PCV in T1 and T2 (31 and 27%), respectively, compared with control negative (35%) and hemoglobin (10.30 and 9 mg/dL) in T1 and T2, respectively, compared with negative control (11.65 mg/dL), while the addition of graphene nanoparticles did not affect the number of WBC in T1 and T2 (15.1 and 19.1 cells/μL × 10^3), respectively, compared with negative control (15.6 cells/μL × 10^3) [109]. The summary of graphene

and GO-related toxicity in aquatic animals have been compiled in Table 1 and depicted in Figure 2 in the following section.

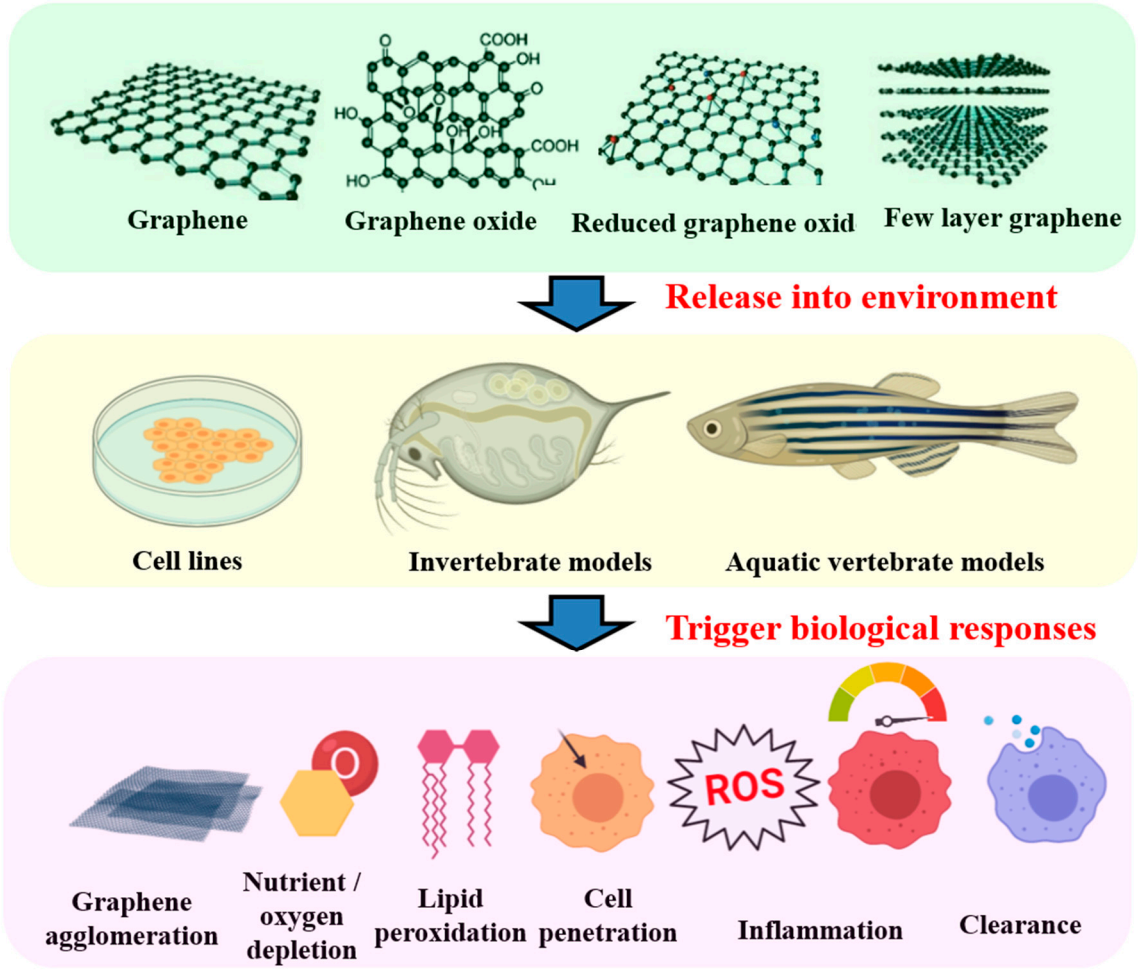

Figure 2. Current understanding of the potential toxicity induced by graphene-based nanomaterials graphene, graphene oxide, reduced graphene, and few-layer graphene are listed in the top panel (green color) in fish cells, invertebrates, embryo, and adult aquatic organisms. The common-used in vitro and in vivo aquatic animal models are listed in the middle panel (yellow color). The potential cytotoxicity induced by graphene-based nanomaterials is summarized in the bottom panel (pink color).

Table 1. Summary of graphene and graphene oxide (GO) toxicity in aquatic animals.

Animal	Route of Graphene Exposure	Adverse Outcome	Dosage Concentration and Time	Ref.
		Tested in invertebrate species		
Crassostrea virginica	Waterborne exposure	Short-term GO exposures can induce oxidative stress, epithelial inflammation, and adversely affect overall *Crassostrea virginica* health.	1 and 10 mg/L 72 h static renewal.	[77]
Crassostrea virginica	Waterborne exposure	Elevated lipid peroxidation and changes in glutathione-s-transferase (GST) activities were observed in gills and digestive gland tissues of the GO-exposed oysters. Oxidative damage, stress signaling leading to adverse effects on cellular health.	2.5 and 5 mg/L 14 days	[78]
Diopatra neapolitana	Waterborne exposure	GO induced negative effects on the regenerative capacity, altered energy-related responses, especially glycogen content, and decrease in metabolism, cellular damage in *Diopatra neapolitana*.	0.01, 0.10 and 1.00 mg/L 28 days	[79]
Daphnia magna	Waterborne exposure	GO induced significant toxicity to *Daphnia magna*. 21 days LC50 chronic toxicity 3.3 mg L^{-1}. In the presence of HA, the decreased toxicity of GO was attributed to the alleviation of oxidative damage by HA.	50.0, 65.0, 84.5, 110.0 and 143.0 mg/L 21 days	[80]
Daphnia magna	Waterborne exposure	^{14}C-labeled graphene accumulated 1% of the organism dry mass. Excretion of graphene at constant phase in depuration. Addition of algae and humic acid to water during the depuration period resulted in release of a significant fraction (~90%) of the accumulated graphene, some remained in the organism. Accumulated graphene in adult *Daphnia* was likely transferred to the neonates.	250, 100, 50 and 25 µg/L 48 h Depuration 24 h	[81]
Ceriodaphnia dubia	Waterborne exposure	GO induced lethality, reproduction inhibition, ROS generation, reduction on feeding rates and accumulation on gut tract. There was a shift in the available energy for self-maintenance rather than feeding or reproduction activities.	Acute exposure: 0.1; 0.2; 0.4; 0.8; 1.6 and 3.2 mg/ L, 48 h Chronic exposure: 0.05; 0.1; 0.2; 0.4 and 0.8 mg/ L 7 days	[82]

Table 1. *Cont.*

Animal	Route of Graphene Exposure	Adverse Outcome	Dosage Concentration and Time	Ref.
Palaemon pandaliformis	Waterborne exposure	GO did not present acute ecotoxicity at concentrations up to 5.0 mg/L. The 96 h LC50 of Cd associated with GO was 1.7 times less than the 96 h LC50 of Cd alone and the 96 h LC50 of Zn associated with GO was 1.8 times less than the 96 h LC50 of Zn alone. The co-exposure of GO with trace elements impaired the routine metabolism of *Palaemon pandaliformis*.	GO - 0.1; 1.0; 2.5 and 5.0 mg/L 96 h Co-exposure of GO 1.0 mg/L with trace elements Cd 1.0 mg/L and Zn 1.0 mg/L	[83]
Cyprinus carpio L.	Waterborne exposure	Significant decrease in RBC count. No significant effect on WBC, PCV, and Hb.	0, 10, 20 mg/L, 10 days	[109]
		Tested in fish cell lines		
PLHC-1	Co-exposure - increasing concentration of AhR agonist alone or in presence of GO and CXYG. Pre and post exposure – increasing concentration of BKF and α-MEM, to α-MEM + 4 mg/mL CXYG or to α-MEM + 16 mg/mL CXYG for another 24 h	GO and CXYG had potentiating effect on PAH- and PCB-induced Cyp1A expression at both the transcriptional and the enzymatic levels. It suggested surface chemistry of GO and CXYG did not had influence on the direct or indirect interaction with the selected AhR agonists. The obtained results suggest that a preceding and/or simultaneous exposure to GO or CXYG nanoplatelets may modify the toxicokinetics of aromatic environmental pollutants such as PAHs and PCBs.	GO and carboxyl graphene (CXYG) at 16 µg/mL, AhR agonist.	[84]
PLHC-1	α-MEM medium	PLHC-1 cells demonstrated significantly reduced mitochondrial membrane potential (MMP) and increased ROS levels at 16 µg/mL GO and CXYG (72 h), but barely any decrease in cell viability. The observation of intracellular graphene accumulations not enclosed by membranes suggests that GO and CXYG internalization in fish hepatoma cells occurs through an endocytosis-independent mechanism.	GO: 0.125–16 µg/mL; CXYG: 0.25–32 µg/mL	[85]
BF2	GO in milli Q water (stock solution) + Eagle's medium	GO caused mitochondrial and lysosomal damage to BF-2 cells, oxidative stress, and morphological changes by GO through ROS, as indicated by the evaluated biomarkers LPO, GSH, SOD, CAT, and 8-OHdG.	0, 10, 20, 40, 60, 80 and 100 µg/mL for 24 h	[86]

Table 1. *Cont.*

Animal	Route of Graphene Exposure	Adverse Outcome	Dosage Concentration and Time	Ref.
PLHC-1 and CLC	GRMs – Carbon nanofibers (CNFs) and graphene oxide (GO)	GO sheets were present within vesicles as well as free in the cytoplasm of both cell types. CNFs toxicity was inversely related to the graphitization degree.	0–200 µg /mL of GRMs for 24 and 72 h	[87]
		Tested at embryonic or larvae stages of fish		
Danio rerio	Waterborne exposure	Hatching delay of zebrafish embryos at a high dosage of 50 mg/L. Embryos exposed to GO exhibited significant cellular apoptosis only in the forehead and eye region, and no aggravation of cellular apoptosis was observed with increasing concentration of GO.	0, 3.4, 7.6, 12.5, 25 and 50 mg/L 96 h post fertilization	[95]
Danio rerio	Waterborne exposure	GO impaired DNA modification, protein carbonylation, ROS generation (also superoxide radical)	1–100 µg/L 2.5 hpf-7 dpf	[60]
Danio rerio (adult and embryo)	Waterborne exposure	GO translocated from the water to the brains of parental and offspring fish with a significant loss of *claudin5a.* GO did not trigger obvious neurotoxicity in parental zebrafish, whereas remarkable neurotoxicity occurred in the offspring, which exhibited a loss of dopaminergic neurons and reductions in acetylcholinesterase activity.	GO exposed to parental zebrafish 24 h prior mating 0.01–1 µg/L	[97]
Danio rerio	Waterborne exposure	Regardless of the presence of HA, larvae exposed to GO for 5 days showed an increase in locomotor activity, reduction in the yolk sac size, and total length and inhibition of AChE activity, but there was no difference in enzyme expression. Results indicated that HA is associated with the toxicity risk modulation by GO.	GO-100 mg/L & HA 20 mg/L alone or together for 5–7 days	[99]
Danio rerio	Waterborne exposure	GO adhered to and enveloped the chorion of zebrafish embryos mainly via hydroxyl group interactions, blocked the pore canals of the chorionic membrane, and caused marked hypoxia and hatching delay. GO induced excessive generation of reactive oxygen species and increased oxidative stress, DNA damage, and apoptosis	0, 0.01, 0.1, 1, 100 mg/L for 24, 48 and 96 hpf	[101]

Table 1. *Cont.*

Animal	Route of Graphene Exposure	Adverse Outcome	Dosage Concentration and Time	Ref.
Danio rerio	Waterborne exposure of GO, Humic Acid (HA) and GO-HA	GO induced significant cardiac edema and hatching delay. HA decreased the interaction between GO and chorion, mitigated chorion damage by regulating morphology, structures, and surface negative charges of GO	GO 0–100 mg/L HA 0–100 mg/L 2.5 hpf-72 hpf	[100]
Danio rerio (larvae and adult)	Injections at ventral end of larvae	GO induced hepatic dysfunction through the ROS and PPAR-α mediated innate immune signaling in zebrafish	0, 0.25, 0.5, and 1 mg/L for 72 h	[98]
Danio rerio	Waterborne exposure of GO and reduced graphene (rGO)	GO had significant effects on the heart rate, while rGO affected the embryos hatching and the length of larvae in a dose-dependent manner	1, 5, 10, 50, 100 mg/L for 96 h	[96]
Danio rerio	Waterborne exposure	GO induced cardiac and dopaminergic alterations, as well as neuronal gene expression and morphology modifications. Altered locomotion in terms of increase of turn angle suggesting parkinsonian-like motor symptoms (at low concentrations).	5, 10, 50 or 100 mg/L for 6 days	[102]
Danio rerio	Waterborne exposure	GOs induced oxidative stress and apoptosis. In particular, the immune cell number, pro-inflammatory iNOS activity, and AChE activity (a neural development indicator) were found to be induced to some extent after GO exposure, suggesting the presence of both immunomodulatory and neurotoxic effects in zebrafish larvae. The waterborne-GO exposure on zebrafish during early development was not merely dependent on GO concentration but also the associated GO sizes.	GO particles (50–200 nm, <500 nm, and >500 nm) at 0.1, 1, 10, and 100 mg/L for 4–124 h post-fertilization	[103]
Danio rerio	Microinjection (4 nL/embryo)	Graphene induced no significant locomotion alterations, sleep behavior, and gene expression patterns.	Graphene at 1, 10, 50 μg/mL	[60]
		Tested at adult stage of fish		
Danio rerio	Waterborne exposure	GO caused toxicity-Oxidative stress and tissue damage induced in fish by GO through ROS, indicated by the biomarkers of MDA, GSH, SOD, and CAT; GO caused immunotoxicity in fish indicated by increased expression of inflammatory cytokines, TNF-, IL-1, and IL-6.	0, 1, 5, 10 or 50 mg/L GO for 14 days	[104]

Table 1. *Cont.*

Animal	Route of Graphene Exposure	Adverse Outcome	Dosage Concentration and Time	Ref.
Danio rerio	Carbon 14 labeled few-layered graphene (FLG)	At 48 h larger FLG (L-FLG) at 250 µg/L the amount of graphene was close to 48 mg/kg fish dry mass, 170-fold greater than body burden of the same concentration of smaller FLG (S-FLG). L-FLG accumulated in gut and S-FLG accumulated in gut and liver. L-FLG and S-FLG had significantly different impact on intestinal microbial community structure.	L-FLG- 300–700 nm S-FLG-30–70 nm 50 µg/L, 75 µg/L and 250 µg/L 4, 12, 24, 48, 72 h	[105]
Danio rerio	Graphene family materials (GFMs), Monolayer graphene powder (GR), graphene oxide nanosheet (GO), reduced graphene oxide powder (rGO)	GFMs led to different inflammatory responses and significantly altered the relative composition of the gut bacterial species. GFMs altered the intestinal morphology and antioxidant enzyme activities.	1 µg in fish diet for 21 days	[106]
Danio rerio	Waterborne exposure	GO caused increase in oxidative stress, increase in lipid peroxidation, changes in SOD, CAT, GPx. After 168 h: GO toxic effects decreased, but homeostasis not fully recovered.	2, 10, and 20 mg/L 48 h, recovery period 168 h	[107]
Anabas testudineus	Injection at base of caudal fin	GO induced oxidative stress in cell and mitochondria in fish	200 µL from 1 g/L 100 mg/L, 10 mg/L of GO in aqueous solution 24 h	[108]

7. Current Understanding of Graphene and Graphene Oxide (GO) Toxicity and Knowledge Gaps along with Other Carbon Nanomaterials

The unique properties of graphene and GO along with other carbon nanomaterials such as carbon nanotubes and fullerenes have been used for various applications and can be released in environment at significant amounts, posing threat to aquatic species as well as humans. Once released in the bodies of water, graphene and GO can also interact with existing inorganic ions and natural organic matter (NOM), posing threat for significant adverse effects on the ecosystem. However, intentional exposure of graphene in biomedical applications is of interest. The literature cites approximately 60% graphene-related materials applications in biomedical engineering as stated by Mao et al. [110]. This signifies scientific community is focused on developing various forms of therapy with graphene-based nanomaterials, which may yield commercialized products in the market soon [111]. Moreover, GO could be modified to have cell surface receptors that act like a net to reduce endocytosis and starve cells to death. This modification of GO with an anti-cancer drug might provide additive effects to cancer cell killing in BEA-2B and KB cervix tumor cells after 48 h via WST-8 [112]. Hence, it becomes important to analyze the toxicity criteria of graphene-related nanomaterials to help understand the specific mechanism of their working with various modifications, dose, physiochemical properties, and model organisms. The information regarding overall concentration of graphene and GO being released in aquatic environment is unknown [65]. However, the concentration of engineered nanomaterials based on probabilistic material free computer model ranges from ng/L to µg/L [113]. Consequently, the disposition of graphene and GO in aqueous environment is studied under this range. The published studies are still inadequate to establish guidelines for environmentally relevant concentration of graphene and GO to set limits for safety measurements of aquatic organisms.

Here in the present review, we have compiled, presented, and compared the current toxicological scenarios of graphene and GO in aquatic invertebrates and fish model organisms. We compared the paper published number (regarding aquatic toxicity induced by carbon-based nanomaterials) during the past 16 years (from 2004 to 2020). Results show the relative paper published number for graphene-based nanomaterial toxicity is around 50% less than their fullerene or carbon nanotube counterparts (Figure 3). In addition, during the compilation of this review paper, it has been observed that there exist plenty of knowledge gaps of carbon nanomaterials (graphene, carbon nanotubes, and fullerenes) specifically on organ toxicity of model organisms. Most of previous studies only address LC50 or whole-body enzyme activity alterations after carbon-based nanomaterial exposure. Although carbon-based nanomaterials toxicity studies in mentioned aquatic organisms have been evaluated in some limited dimensions, there exists a huge gap in understanding of organ toxicity of these organisms. However, the most prominent findings studies have reported are oxidative stress, lipid peroxidation, and cellular penetration; there is lack of existing studies on whole organism level like behavioral, transcriptomic, and histopathological analysis.

In case of continuous waterborne exposure, the developmental stages of the embryo and the duration of exposure are very critical. The embryos exposed in waterborne graphene and GO might agglomerate in the exposure media or on the chorion depleting embryo of oxygen supply and may cause developmental deformities or worst, mortality. The chorion has been reported as a major barrier to prevent nanomaterial uptake by fish embryos [114]. In this consideration, microinjection can be used to deliver nanomaterials to the developmental embryos [60,98]. However, in this particular treatment, the injected nanomaterials will be eventually diluted over time with the rapidly dividing embryonic cells. For adult fish, the most popular method for graphene delivery is waterborne exposure. However, the insoluble nature of graphene makes it difficult to measure the exact delivery dose. Other more precise delivery methods like oral delivery can be considered in the future [115]. Hence, to establish the toxicity criteria further, more studies are considered necessary to understand how graphene and GO can induce toxicity. As for the data available for analysis, it is difficult to set safety limits and differentiate in the effects caused by tested nanomaterials whether actual or in waterborne concentration on the organisms.

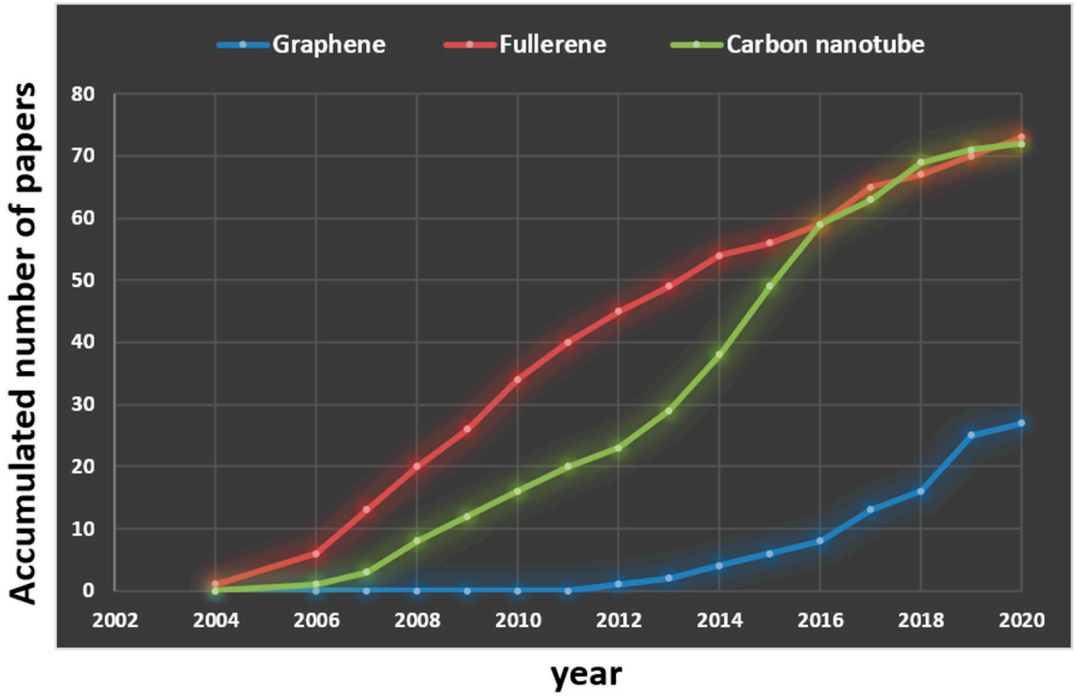

Figure 3. Comparison of paper publication number related to aquatic toxicity induced by three carbon-based nanomaterials during the past 16 years (from 2004 to 2020). Papers relevant to graphene-based nanomaterials are highlighted with blue color. Papers relevant to fullerene-based nanomaterials are highlighted with red color. Papers relevant to carbon nanotube are highlighted with green color.

8. Summary

In this review paper, we hereby summarize that research of graphene and GO toxicity specifically on aquatic organisms is relatively limited. The research on graphene-based nanomaterials toxicity has started taking place progressively in the last decade. Thus, a comprehensive understanding of interaction of graphene and GO with environment, aquatic organisms, and other living systems in vitro and in vivo is essential for their safe usage and further development. The large part of available current literature indicates that graphene-based nanomaterials are cytotoxic. Although the particular mechanism for their toxicity has not yet been established, ROS elevation, lipid peroxidation, nutrient/oxygen depletion, and inflammation have been most widely recognized mechanisms for graphene-based nanomaterials toxicity in aquatic organisms.

The applications and uses of graphene and GO are rising evidently in fields of biomedical sciences, supercapacitors, sensors, and construction materials. The release of waste material from these industries can prove to be harmful for environment, aquatic organisms, and humans. Graphene-based nanomaterials interact with natural organic material (NOM), aggregates, adsorbs, and colloids, which in turn can cause toxicity to aquatic organisms through many different body mechanisms. Furthermore, the physiochemical properties of graphene and GO such as particle size, surface functional groups, and oxygen content/surface charges may affect the toxicity upon interaction with aquatic organisms. The data we accumulated demonstrated a lot of information gaps that does not allow establishing a concrete statement regarding the toxicity criteria guidelines. It is also difficult to compare the toxicological effects of graphene and GO between different studies due to diversity in size, shape, surface modification, synthetization techniques, and model organisms. It is, hence, important to understand the toxicity caused by graphene nanomaterials for aquatic organisms in order to facilitate the practical applications of these promising new graphene-based nanomaterials.

Author Contributions: Conceptualization, N.M. and C.-D.H.; funding acquisition, T.-R.G. and C.-D.H.; investigation, T.-R.G and C.-D.H.; project administration, and C.-D.H.; resources, O.B.V., G.A., and P.S.; supervision, T.-R.G. and C.-D.H.; visualization, N.M. and C.-D.H.; writing—original draft, N.M., T.-R.G., J.-S.L., and C.-D.H. All authors have read and agreed to the published version of the manuscript.

Funding: This study was funded by the grants sponsored by the Ministry of Science and Technology MOST 105-2313-B-033-001-MY3 and MOST 107-2622-B-033-001-CC2 to C.-D.H. and MOST108-2221-E033-017-MY3 to T.-R.G.

Acknowledgments: We appreciate the anonymous reviewers and editors for their professional comments, which improved the quality of this paper.

Conflicts of Interest: The authors declare no conflicts of interest.

References

1. Ema, M.; Gamo, M.; Honda, K. A review of toxicity studies on graphene-based nanomaterials in laboratory animals. *Regul. Toxicol. Pharmacol.* **2017**, *85*, 7–24. [CrossRef]
2. Huang, X.; Qi, X.; Boey, F.; Zhang, H. Graphene-based composites. *Chem. Soc. Rev.* **2012**, *41*, 666–686. [CrossRef] [PubMed]
3. Chen, B.; Liu, M.; Zhang, L.; Huang, J.; Yao, J.; Zhang, Z. Polyethylenimine-functionalized graphene oxide as an efficient gene delivery vector. *J. Mater. Chem.* **2011**, *21*, 7736–7741. [CrossRef]
4. Munz, M.; Giusca, C.E.; Myers-Ward, R.L.; Gaskill, D.K.; Kazakova, O. Thickness-dependent hydrophobicity of epitaxial graphene. *Acs Nano* **2015**, *9*, 8401–8411. [CrossRef]
5. Bianco, A.; Cheng, H.-M.; Enoki, T.; Gogotsi, Y.; Hurt, R.H.; Koratkar, N.; Kyotani, T.; Monthioux, M.; Park, C.R.; Tascon, J.M. *All in the Graphene Family—A Recommended Nomenclature for Two-Dimensional Carbon Materials*; Elsevier: Amsterdam, The Netherlands, 2013.
6. Zhao, J.; Wang, Z.; White, J.C.; Xing, B. Graphene in the aquatic environment: Adsorption, dispersion, toxicity and transformation. *Environ. Sci. Technol.* **2014**, *48*, 9995–10009. [CrossRef] [PubMed]
7. Geim, A.K. Graphene: Status and prospects. *science* **2009**, *324*, 1530–1534. [CrossRef]
8. Balandin, A.A.; Ghosh, S.; Bao, W.; Calizo, I.; Teweldebrhan, D.; Miao, F.; Lau, C.N. Superior thermal conductivity of single-layer graphene. *Nano Lett.* **2008**, *8*, 902–907. [CrossRef]
9. Lee, C.; Wei, X.; Kysar, J.W.; Hone, J. Measurement of the elastic properties and intrinsic strength of monolayer graphene. *Science* **2008**, *321*, 385–388. [CrossRef]
10. Nair, R.R.; Blake, P.; Grigorenko, A.N.; Novoselov, K.S.; Booth, T.J.; Stauber, T.; Peres, N.M.; Geim, A.K. Fine structure constant defines visual transparency of graphene. *Science* **2008**, *320*, 1308. [CrossRef]
11. Novoselov, K.S.; Geim, A.K.; Morozov, S.V.; Jiang, D.; Zhang, Y.; Dubonos, S.V.; Grigorieva, I.V.; Firsov, A.A. Electric field effect in atomically thin carbon films. *Science* **2004**, *306*, 666–669. [CrossRef] [PubMed]
12. Jastrzębska, A.M.; Kurtycz, P.; Olszyna, A.R. Recent advances in graphene family materials toxicity investigations. *J. Nanoparticle Res.* **2012**, *14*, 1320. [CrossRef] [PubMed]
13. Kang, X.; Wang, J.; Wu, H.; Aksay, I.A.; Liu, J.; Lin, Y. Glucose oxidase–graphene–chitosan modified electrode for direct electrochemistry and glucose sensing. *Biosens. Bioelectron.* **2009**, *25*, 901–905. [CrossRef] [PubMed]
14. Razmi, H.; Mohammad-Rezaei, R. Graphene quantum dots as a new substrate for immobilization and direct electrochemistry of glucose oxidase: Application to sensitive glucose determination. *Biosens. Bioelectron.* **2013**, *41*, 498–504. [CrossRef]
15. Das, S.R.; Nian, Q.; Cargill, A.A.; Hondred, J.A.; Ding, S.; Saei, M.; Cheng, G.J.; Claussen, J.C. 3d nanostructured inkjet printed graphene via uv-pulsed laser irradiation enables paper-based electronics and electrochemical devices. *Nanoscale* **2016**, *8*, 15870–15879. [CrossRef] [PubMed]
16. Chen, K.; Chen, L.; Chen, Y.; Bai, H.; Li, L. Three-dimensional porous graphene-based composite materials: Electrochemical synthesis and application. *J. Mater. Chem.* **2012**, *22*, 20968–20976. [CrossRef]
17. Zhang, L.; Li, R.; Tang, B.; Wang, P. Solar-thermal conversion and thermal energy storage of graphene foam-based composites. *Nanoscale* **2016**, *8*, 14600–14607. [CrossRef]
18. Pumera, M. Graphene-based nanomaterials for energy storage. *Energy Environ. Sci.* **2011**, *4*, 668–674. [CrossRef]
19. Xu, C.; Wang, J.; Xu, Y.; Shang, G.; Wang, R.; Lin, Y. Review of and perspectives on the toxicology of graphene-based materials. *Curr. Drug Metab.* **2013**, *14*, 863–871. [CrossRef]
20. Chang, H.; Tang, L.; Wang, Y.; Jiang, J.; Li, J. Graphene fluorescence resonance energy transfer aptasensor for the thrombin detection. *Anal. Chem.* **2010**, *82*, 2341–2346. [CrossRef]

21. Lu, C.H.; Yang, H.H.; Zhu, C.L.; Chen, X.; Chen, G.N. A graphene platform for sensing biomolecules. *Angew. Chem. Int. Ed.* **2009**, *48*, 4785–4787. [CrossRef] [PubMed]
22. Li, X.; Zhu, H.; Wang, K.; Cao, A.; Wei, J.; Li, C.; Jia, Y.; Li, Z.; Li, X.; Wu, D. Graphene-on-silicon schottky junction solar cells. *Adv. Mater.* **2010**, *22*, 2743–2748. [CrossRef] [PubMed]
23. Yin, Z.; Sun, S.; Salim, T.; Wu, S.; Huang, X.; He, Q.; Lam, Y.M.; Zhang, H. Organic photovoltaic devices using highly flexible reduced graphene oxide films as transparent electrodes. *Acs Nano* **2011**, *4*, 5263–5268. [CrossRef] [PubMed]
24. Shi, W.; Zhu, J.; Sim, D.H.; Tay, Y.Y.; Lu, Z.; Zhang, X.; Sharma, Y.; Srinivasan, M.; Zhang, H.; Hng, H.H. Achieving high specific charge capacitances in fe 3 o 4/reduced graphene oxide nanocomposites. *J. Mater. Chem.* **2011**, *21*, 3422–3427. [CrossRef]
25. Li, F.; Song, J.; Yang, H.; Gan, S.; Zhang, Q.; Han, D.; Ivaska, A.; Niu, L. One-step synthesis of graphene/sno2 nanocomposites and its application in electrochemical supercapacitors. *Nanotechnology* **2009**, *20*, 455602. [CrossRef]
26. Zhang, H.; Lv, X.; Li, Y.; Wang, Y.; Li, J. P25-graphene composite as a high performance photocatalyst. *Acs Nano* **2010**, *4*, 380–386. [CrossRef]
27. Liu, J.; Liu, L.; Bai, H.; Wang, Y.; Sun, D.D. Gram-scale production of graphene oxide–tio2 nanorod composites: Towards high-activity photocatalytic materials. *Appl. Catal. B Environ.* **2011**, *106*, 76–82. [CrossRef]
28. Dong, L.; Gari, R.R.S.; Li, Z.; Craig, M.M.; Hou, S. Graphene-supported platinum and platinum–ruthenium nanoparticles with high electrocatalytic activity for methanol and ethanol oxidation. *Carbon* **2010**, *48*, 781–787. [CrossRef]
29. Jafri, R.I.; Rajalakshmi, N.; Ramaprabhu, S. Nitrogen doped graphene nanoplatelets as catalyst support for oxygen reduction reaction in proton exchange membrane fuel cell. *J. Mater. Chem.* **2010**, *20*, 7114–7117. [CrossRef]
30. Wang, S.; Goh, B.M.; Manga, K.K.; Bao, Q.; Yang, P.; Loh, K.P. Graphene as atomic template and structural scaffold in the synthesis of graphene− organic hybrid wire with photovoltaic properties. *Acs Nano* **2010**, *4*, 6180–6186. [CrossRef]
31. Han, T.H.; Lee, W.J.; Lee, D.H.; Kim, J.E.; Choi, E.Y.; Kim, S.O. Peptide/graphene hybrid assembly into core/shell nanowires. *Adv. Mater.* **2010**, *22*, 2060–2064. [CrossRef] [PubMed]
32. Wu, S.; Yin, Z.; He, Q.; Huang, X.; Zhou, X.; Zhang, H. Electrochemical deposition of semiconductor oxides on reduced graphene oxide-based flexible, transparent, and conductive electrodes. *J. Phys. Chem. C* **2010**, *114*, 11816–11821. [CrossRef]
33. Zhou, X.; Huang, X.; Qi, X.; Wu, S.; Xue, C.; Boey, F.Y.; Yan, Q.; Chen, P.; Zhang, H. In situ synthesis of metal nanoparticles on single-layer graphene oxide and reduced graphene oxide surfaces. *J. Phys. Chem. C* **2009**, *113*, 10842–10846. [CrossRef]
34. Muszynski, R.; Seger, B.; Kamat, P.V. Decorating graphene sheets with gold nanoparticles. *J. Phys. Chem. C* **2008**, *112*, 5263–5266. [CrossRef]
35. Huang, X.; Li, S.; Huang, Y.; Wu, S.; Zhou, X.; Li, S.; Gan, C.L.; Boey, F.; Mirkin, C.A.; Zhang, H. Synthesis of hexagonal close-packed gold nanostructures. *Nat. Commun.* **2011**, *2*, 1–6. [CrossRef]
36. Wang, Y.; Li, Z.; Hu, D.; Lin, C.-T.; Li, J.; Lin, Y. Aptamer/graphene oxide nanocomplex for in situ molecular probing in living cells. *J. Am. Chem. Soc.* **2010**, *132*, 9274–9276. [CrossRef]
37. Qi, X.; Pu, K.Y.; Li, H.; Zhou, X.; Wu, S.; Fan, Q.L.; Liu, B.; Boey, F.; Huang, W.; Zhang, H. Amphiphilic graphene composites. *Angew. Chem. Int. Ed.* **2010**, *49*, 9426–9429. [CrossRef]
38. Yang, H.; Zhang, Q.; Shan, C.; Li, F.; Han, D.; Niu, L. Stable, conductive supramolecular composite of graphene sheets with conjugated polyelectrolyte. *Langmuir* **2010**, *26*, 6708–6712. [CrossRef]
39. Qi, X.; Pu, K.Y.; Zhou, X.; Li, H.; Liu, B.; Boey, F.; Huang, W.; Zhang, H. Conjugated-polyelectrolyte-functionalized reduced graphene oxide with excellent solubility and stability in polar solvents. *Small* **2010**, *6*, 663–669. [CrossRef]
40. Dong, X.; Li, B.; Wei, A.; Cao, X.; Chan-Park, M.B.; Zhang, H.; Li, L.-J.; Huang, W.; Chen, P. One-step growth of graphene–carbon nanotube hybrid materials by chemical vapor deposition. *Carbon* **2011**, *49*, 2944–2949. [CrossRef]
41. Fan, Z.; Yan, J.; Zhi, L.; Zhang, Q.; Wei, T.; Feng, J.; Zhang, M.; Qian, W.; Wei, F. A three-dimensional carbon nanotube/graphene sandwich and its application as electrode in supercapacitors. *Adv. Mater.* **2010**, *22*, 3723–3728. [CrossRef] [PubMed]

42. Yoo, E.; Kim, J.; Hosono, E.; Zhou, H.-s.; Kudo, T.; Honma, I. Large reversible li storage of graphene nanosheet families for use in rechargeable lithium ion batteries. *Nano Lett.* **2008**, *8*, 2277–2282. [CrossRef] [PubMed]
43. Chen, D.; Feng, H.; Li, J. Graphene oxide: Preparation, functionalization, and electrochemical applications. *Chem. Rev.* **2012**, *112*, 6027–6053. [CrossRef]
44. Dreyer, D.R.; Park, S.; Bielawski, C.W.; Ruoff, R.S. The chemistry of graphene oxide. *Chem. Soc. Rev.* **2010**, *39*, 228–240. [CrossRef] [PubMed]
45. Loh, K.P.; Bao, Q.; Ang, P.K.; Yang, J. The chemistry of graphene. *J. Mater. Chem.* **2010**, *20*, 2277–2289. [CrossRef]
46. Stankovich, S.; Dikin, D.A.; Piner, R.D.; Kohlhaas, K.A.; Kleinhammes, A.; Jia, Y.; Wu, Y.; Nguyen, S.T.; Ruoff, R.S. Synthesis of graphene-based nanosheets via chemical reduction of exfoliated graphite oxide. *Carbon* **2007**, *45*, 1558–1565. [CrossRef]
47. Park, S.; Ruoff, R.S. Chemical methods for the production of graphenes. *Nat. Nanotechnol.* **2009**, *4*, 217. [CrossRef]
48. Wu, S.-Y.; An, S.S.A.; Hulme, J. Current applications of graphene oxide in nanomedicine. *Int. J. Nanomed.* **2015**, *10*, 9.
49. Chung, C.; Kim, Y.-K.; Shin, D.; Ryoo, S.-R.; Hong, B.H.; Min, D.-H. Biomedical applications of graphene and graphene oxide. *Acc. Chem. Res.* **2013**, *46*, 2211–2224. [CrossRef]
50. Segal, M. Selling graphene by the ton. *Nat. Nanotechnol.* **2009**, *4*, 612. [CrossRef]
51. Arvidsson, R.; Molander, S.; Sandén, B.A. Review of potential environmental and health risks of the nanomaterial graphene. *Hum. Ecol. Risk Assess. Int. J.* **2013**, *19*, 873–887. [CrossRef]
52. Volkov, Y.; McIntyre, J.; Prina-Mello, A. Graphene toxicity as a double-edged sword of risks and exploitable opportunities: A critical analysis of the most recent trends and developments. *2d Mater.* **2017**, *4*, 022001. [CrossRef]
53. Kotchey, G.P.; Allen, B.L.; Vedala, H.; Yanamala, N.; Kapralov, A.A.; Tyurina, Y.Y.; Klein-Seetharaman, J.; Kagan, V.E.; Star, A. The enzymatic oxidation of graphene oxide. *Acs Nano* **2011**, *5*, 2098–2108. [CrossRef] [PubMed]
54. Chowdhury, I.; Duch, M.C.; Mansukhani, N.D.; Hersam, M.C.; Bouchard, D. Colloidal properties and stability of graphene oxide nanomaterials in the aquatic environment. *Environ. Sci. Technol.* **2013**, *47*, 6288–6296. [CrossRef]
55. Zhao, Y.; Zhi, L.; Wu, Q.; Yu, Y.; Sun, Q.; Wang, D. P38 mapk-skn-1/nrf signaling cascade is required for intestinal barrier against graphene oxide toxicity in caenorhabditis elegans. *Nanotoxicology* **2016**, *10*, 1469–1479. [CrossRef]
56. Ouyang, S.; Hu, X.; Zhou, Q. Envelopment–internalization synergistic effects and metabolic mechanisms of graphene oxide on single-cell chlorella vulgaris are dependent on the nanomaterial particle size. *Acs Appl. Mater. Interfaces* **2015**, *7*, 18104–18112. [CrossRef]
57. Hu, X.; Zhou, Q. Health and ecosystem risks of graphene. *Chem. Rev.* **2013**, *113*, 3815–3835. [CrossRef]
58. Wu, Q.; Zhao, Y.; Fang, J.; Wang, D. Immune response is required for the control of in vivo translocation and chronic toxicity of graphene oxide. *Nanoscale* **2014**, *6*, 5894–5906. [CrossRef]
59. Hazeem, L.J.; Bououdina, M.; Dewailly, E.; Slomianny, C.; Barras, A.; Coffinier, Y.; Szunerits, S.; Boukherroub, R. Toxicity effect of graphene oxide on growth and photosynthetic pigment of the marine alga picochlorum sp. During different growth stages. *Environ. Sci. Pollut. Res.* **2017**, *24*, 4144–4152. [CrossRef]
60. Zhang, X.; Zhou, Q.; Zou, W.; Hu, X. Molecular mechanisms of developmental toxicity induced by graphene oxide at predicted environmental concentrations. *Environ. Sci. Technol.* **2017**, *51*, 7861–7871. [CrossRef]
61. Clemente, Z.; Castro, V.; Moura, M.; Jonsson, C.; Fraceto, L. Toxicity assessment of tio2 nanoparticles in zebrafish embryos under different exposure conditions. *Aquat. Toxicol.* **2014**, *147*, 129–139. [CrossRef] [PubMed]
62. Zhu, X.; Wang, J.; Zhang, X.; Chang, Y.; Chen, Y. The impact of zno nanoparticle aggregates on the embryonic development of zebrafish (danio rerio). *Nanotechnology* **2009**, *20*, 195103. [CrossRef] [PubMed]
63. Zhu, X.; Wang, J.; Zhang, X.; Chang, Y.; Chen, Y. Trophic transfer of tio2 nanoparticles from daphnia to zebrafish in a simplified freshwater food chain. *Chemosphere* **2010**, *79*, 928–933. [CrossRef] [PubMed]
64. Ray, S. Levels of toxicity screening of environmental chemicals using aquatic invertebrates—A review. *Invertebr. Exp. Models Toxic. Screen. IntechCroat.* **2016**, 1–11.
65. Dasmahapatra, A.K.; Dasari, T.P.; Tchounwou, P.B. Graphene-based nanomaterials toxicity in fish. In *Reviews of Environmental Contamination and Toxicology Volume 247*; Springer: Berlin, Germany, 2018; pp. 1–58.

66. Elmore, S.A.; Boorman, G.A. Environmental toxicologic pathology and human health. In *Haschek and Rousseaux's Handbook of Toxicologic Pathology*; Elsevier: Amsterdam, The Netherlands, 2013; pp. 1029–1049.
67. Liao, L.; Peng, H.; Liu, Z. Chemistry makes graphene beyond graphene. *J. Am. Chem. Soc.* **2014**, *136*, 12194–12200. [CrossRef] [PubMed]
68. Li, D.; Müller, M.B.; Gilje, S.; Kaner, R.B.; Wallace, G.G. Processable aqueous dispersions of graphene nanosheets. *Nat. Nanotechnol.* **2008**, *3*, 101–105. [CrossRef] [PubMed]
69. Paredes, J.; Villar-Rodil, S.; Martínez-Alonso, A.; Tascon, J. Graphene oxide dispersions in organic solvents. *Langmuir* **2008**, *24*, 10560–10564. [CrossRef]
70. Stankovich, S.; Dikin, D.A.; Dommett, G.H.; Kohlhaas, K.M.; Zimney, E.J.; Stach, E.A.; Piner, R.D.; Nguyen, S.T.; Ruoff, R.S. Graphene-based composite materials. *Nature* **2006**, *442*, 282–286. [CrossRef]
71. Ramanathan, T.; Abdala, A.; Stankovich, S.; Dikin, D.; Herrera-Alonso, M.; Piner, R.; Adamson, D.; Schniepp, H.; Chen, X.; Ruoff, R. Functionalized graphene sheets for polymer nanocomposites. *Nat. Nanotechnol.* **2008**, *3*, 327–331. [CrossRef]
72. Liu, Z.-B.; Xu, Y.-F.; Zhang, X.-Y.; Zhang, X.-L.; Chen, Y.-S.; Tian, J.-G. Porphyrin and fullerene covalently functionalized graphene hybrid materials with large nonlinear optical properties. *J. Phys. Chem. B* **2009**, *113*, 9681–9686. [CrossRef]
73. Gourmelon, A.; Ahtiainen, J. Developing test guidelines on invertebrate development and reproduction for the assessment of chemicals, including potential endocrine active substances—the oecd perspective. *Ecotoxicology* **2007**, *16*, 161–167. [CrossRef] [PubMed]
74. Cattaneo, A.; Gornati, R.; Chiriva-Internati, M.; Bernardini, G. Ecotoxicology of nanomaterials: The role of invertebrate testing. *Invertebr. Surviv. J.* **2009**, *6*, 78–97.
75. Emerich, D.F.; Thanos, C.G. The pinpoint promise of nanoparticle-based drug delivery and molecular diagnosis. *Biomol. Eng.* **2006**, *23*, 171–184. [CrossRef] [PubMed]
76. Allen, N.S.; Edge, M.; Sandoval, G.; Verran, J.; Stratton, J.; Maltby, J. Photocatalytic coatings for environmental applications. *Photochem. Photobiol.* **2005**, *81*, 279–290. [CrossRef] [PubMed]
77. Khan, B.; Adeleye, A.S.; Burgess, R.M.; Smolowitz, R.; Russo, S.M.; Ho, K.T. A 72-h exposure study with eastern oysters (crassostrea virginica) and the nanomaterial graphene oxide. *Environ. Toxicol. Chem.* **2019**, *38*, 820–830. [CrossRef] [PubMed]
78. Khan, B.; Adeleye, A.S.; Burgess, R.M.; Russo, S.M.; Ho, K.T. Effects of graphene oxide nanomaterial exposures on the marine bivalve, crassostrea virginica. *Aquat. Toxicol.* **2019**, *216*, 105297. [CrossRef]
79. De Marchi, L.; Neto, V.; Pretti, C.; Figueira, E.; Brambilla, L.; Rodriguez-Douton, M.J.; Rossella, F.; Tommasini, M.; Furtado, C.; Soares, A.M. Physiological and biochemical impacts of graphene oxide in polychaetes: The case of diopatra neapolitana. *Comp. Biochem. Physiol. Part C Toxicol. Pharmacol.* **2017**, *193*, 50–60. [CrossRef]
80. Zhang, Y.; Meng, T.; Shi, L.; Guo, X.; Si, X.; Yang, R.; Quan, X. The effects of humic acid on the toxicity of graphene oxide to scenedesmus obliquus and daphnia magna. *Sci. Total Environ.* **2019**, *649*, 163–171. [CrossRef]
81. Guo, X.; Dong, S.; Petersen, E.J.; Gao, S.; Huang, Q.; Mao, L. Biological uptake and depuration of radio-labeled graphene by daphnia magna. *Environ. Sci. Technol.* **2013**, *47*, 12524–12531. [CrossRef]
82. Souza, J.P.; Venturini, F.P.; Santos, F.; Zucolotto, V. Chronic toxicity in ceriodaphnia dubia induced by graphene oxide. *Chemosphere* **2018**, *190*, 218–224. [CrossRef]
83. de Melo, C.B.; Côa, F.; Alves, O.L.; Martinez, D.S.T.; Barbieri, E. Co-exposure of graphene oxide with trace elements: Effects on acute ecotoxicity and routine metabolism in palaemon pandaliformis (shrimp). *Chemosphere* **2019**, *223*, 157–164. [CrossRef] [PubMed]
84. Lammel, T.; Boisseaux, P.; Navas, J.M. Potentiating effect of graphene nanomaterials on aromatic environmental pollutant-induced cytochrome p450 1a expression in the topminnow fish hepatoma cell line plhc-1. *Environ. Toxicol.* **2015**, *30*, 1192–1204. [CrossRef] [PubMed]
85. Lammel, T.; Navas, J.M. Graphene nanoplatelets spontaneously translocate into the cytosol and physically interact with cellular organelles in the fish cell line plhc-1. *Aquat. Toxicol.* **2014**, *150*, 55–65. [CrossRef] [PubMed]
86. Srikanth, K.; Sundar, L.S.; Pereira, E.; Duarte, A.C. Graphene oxide induces cytotoxicity and oxidative stress in bluegill sunfish cells. *J. Appl. Toxicol.* **2018**, *38*, 504–513. [CrossRef] [PubMed]

87. Kalman, J.; Merino, C.; Fernández-Cruz, M.L.; Navas, J.M. Usefulness of fish cell lines for the initial characterization of toxicity and cellular fate of graphene-related materials (carbon nanofibers and graphene oxide). *Chemosphere* **2019**, *218*, 347–358. [CrossRef]
88. Shah, B.R.; Mraz, J. Advances in nanotechnology for sustainable aquaculture and fisheries. *Rev. Aquac.* **2020**, *12*, 925–942. [CrossRef]
89. Fako, V.E.; Furgeson, D.Y. Zebrafish as a correlative and predictive model for assessing biomaterial nanotoxicity. *Adv. Drug Deliv. Rev.* **2009**, *61*, 478–486. [CrossRef]
90. d'Amora, M.; Camisasca, A.; Lettieri, S.; Giordani, S. Toxicity assessment of carbon nanomaterials in zebrafish during development. *Nanomaterials* **2017**, *7*, 414. [CrossRef]
91. Wang, Z.G.; Rong, Z.; Jiang, D.; Jing, E.S.; Qian, X.; Jing, S.; Chen, Y.P.; Xin, Z.; Lu, G.; Li, J.Z. Toxicity of graphene quantum dots in zebrafish embryo. *Biomed. Environ. Sci.* **2015**, *28*, 341–351.
92. Zhu, Z.; Qian, J.; Zhao, X.; Qin, W.; Hu, R.; Zhang, H.; Li, D.; Xu, Z.; Tang, B.Z.; He, S. Stable and size-tunable aggregation-induced emission nanoparticles encapsulated with nanographene oxide and applications in three-photon fluorescence bioimaging. *Acs Nano* **2016**, *10*, 588–597. [CrossRef]
93. Jeong, J.; Cho, H.-J.; Choi, M.; Lee, W.S.; Chung, B.H.; Lee, J.-S. In vivo toxicity assessment of angiogenesis and the live distribution of nano-graphene oxide and its pegylated derivatives using the developing zebrafish embryo. *Carbon* **2015**, *93*, 431–440. [CrossRef]
94. Mold, D.E.; Dinitz, A.E.; Sambandan, D.R. Regulation of zebrafish zona pellucida gene activity in developing oocytes. *Biol. Reprod.* **2009**, *81*, 101–110. [CrossRef] [PubMed]
95. Chen, L.; Hu, P.; Zhang, L.; Huang, S.; Luo, L.; Huang, C. Toxicity of graphene oxide and multi-walled carbon nanotubes against human cells and zebrafish. *Sci. China Chem.* **2012**, *55*, 2209–2216. [CrossRef]
96. Liu, X.T.; MU, X.Y.; WU, X.L.; Meng, L.X.; Guan, W.B.; Qiang, Y.; Hua, S.; Wang, C.J.; LI, X.F. Toxicity of multi-walled carbon nanotubes, graphene oxide, and reduced graphene oxide to zebrafish embryos. *Biomed. Environ. Sci.* **2014**, *27*, 676–683. [PubMed]
97. Hu, X.; Wei, Z.; Mu, L. Graphene oxide nanosheets at trace concentrations elicit neurotoxicity in the offspring of zebrafish. *Carbon* **2017**, *117*, 182–191. [CrossRef]
98. Xiong, G.; Deng, Y.; Liao, X.; Zhang, J.E.; Cheng, B.; Cao, Z.; Lu, H. Graphene oxide nanoparticles induce hepatic dysfunction through the regulation of innate immune signaling in zebrafish (danio rerio). *Nanotoxicology* **2020**, *14*, 667–682. [CrossRef] [PubMed]
99. Clemente, Z.; Silva, G.H.; de Souza Nunes, M.C.; Martinez, D.S.T.; Maurer-Morelli, C.V.; Thomaz, A.A.; Castro, V.L.S.S. Exploring the mechanisms of graphene oxide behavioral and morphological changes in zebrafish. *Environ. Sci. Pollut. Res.* **2019**, *26*, 30508–30523. [CrossRef]
100. Chen, Y.; Ren, C.; Ouyang, S.; Hu, X.; Zhou, Q. Mitigation in multiple effects of graphene oxide toxicity in zebrafish embryogenesis driven by humic acid. *Environ. Sci. Technol.* **2015**, *49*, 10147–10154. [CrossRef]
101. Chen, Y.; Hu, X.; Sun, J.; Zhou, Q. Specific nanotoxicity of graphene oxide during zebrafish embryogenesis. *Nanotoxicology* **2016**, *10*, 42–52. [CrossRef]
102. Soares, J.; Pereira, T.; Costa, K.; Maraschin, T.; Basso, N.; Bogo, M. Developmental neurotoxic effects of graphene oxide exposure in zebrafish larvae (danio rerio). *Colloids Surf. B: Biointerfaces* **2017**, *157*, 335–346. [CrossRef]
103. Chen, Z.; Yu, C.; Khan, I.A.; Tang, Y.; Liu, S.; Yang, M. Toxic effects of different-sized graphene oxide particles on zebrafish embryonic development. *Ecotoxicol. Environ. Saf.* **2020**, *197*, 110608. [CrossRef]
104. Chen, M.; Yin, J.; Liang, Y.; Yuan, S.; Wang, F.; Song, M.; Wang, H. Oxidative stress and immunotoxicity induced by graphene oxide in zebrafish. *Aquat. Toxicol.* **2016**, *174*, 54–60. [CrossRef] [PubMed]
105. Lu, K.; Dong, S.; Petersen, E.J.; Niu, J.; Chang, X.; Wang, P.; Lin, S.; Gao, S.; Mao, L. Biological uptake, distribution, and depuration of radio-labeled graphene in adult zebrafish: Effects of graphene size and natural organic matter. *Acs Nano* **2017**, *11*, 2872–2885. [CrossRef] [PubMed]
106. Zheng, M.; Lu, J.; Lin, G.; Su, H.; Sun, J.; Luan, T. Dysbiosis of gut microbiota by dietary exposure of three graphene-family materials in zebrafish (danio rerio). *Environ. Pollut.* **2019**, *254*, 112969. [CrossRef] [PubMed]
107. Souza, J.P.; Mansano, A.S.; Venturini, F.P.; Santos, F.; Zucolotto, V. Antioxidant metabolism of zebrafish after sub-lethal exposure to graphene oxide and recovery. *Fish Physiol. Biochem.* **2019**, *45*, 1289–1297. [CrossRef]
108. Paital, B.; Guru, D.; Mohapatra, P.; Panda, B.; Parida, N.; Rath, S.; Kumar, V.; Saxena, P.S.; Srivastava, A. Ecotoxic impact assessment of graphene oxide on lipid peroxidation at mitochondrial level and redox modulation in fresh water fish anabas testudineus. *Chemosphere* **2019**, *224*, 796–804. [CrossRef] [PubMed]

109. Al-Rudainy, A.J.; Hawar, A. Hematological effects of graphene nanoparticles exposed to common carp cyprinus carpio l. *Pak. J. Biotechnol.* **2018**, *15*, 867–870.
110. Mao, H.Y.; Laurent, S.; Chen, W.; Akhavan, O.; Imani, M.; Ashkarran, A.A.; Mahmoudi, M. Graphene: Promises, facts, opportunities, and challenges in nanomedicine. *Chem. Rev.* **2013**, *113*, 3407–3424. [CrossRef]
111. Tan, E.; Li, B.L.; Ariga, K.; Lim, C.-T.; Garaj, S.; Leong, D.T. Toxicity of two-dimensional layered materials and their heterostructures. *Bioconjugate Chem.* **2019**, *30*, 2287–2299. [CrossRef]
112. Bidram, E.; Sulistio, A.; Cho, H.-J.; Amini, A.; Harris, T.; Zarrabi, A.; Qiao, G.; Stewart, A.; Dunstan, D.E. Targeted graphene oxide networks: Cytotoxicity and synergy with anticancer agents. *Acs Appl. Mater. Interfaces* **2018**, *10*, 43523–43532. [CrossRef]
113. Sun, T.Y.; Bornhöft, N.A.; Hungerbühler, K.; Nowack, B. Dynamic probabilistic modeling of environmental emissions of engineered nanomaterials. *Environ. Sci. Technol.* **2016**, *50*, 4701–4711. [CrossRef] [PubMed]
114. Chen, Z.-Y.; Li, N.-J.; Cheng, F.-Y.; Hsueh, J.-F.; Huang, C.-C.; Lu, F.-I.; Fu, T.-F.; Yan, S.-J.; Lee, Y.-H.; Wang, Y.-J. The effect of the chorion on size-dependent acute toxicity and underlying mechanisms of amine-modified silver nanoparticles in zebrafish embryos. *Int. J. Mol. Sci.* **2020**, *21*, 2864. [CrossRef] [PubMed]
115. Dayal, N.; Thakur, M.; Soparkar, A.; Doctor, M.; Patil, P.; Joshi, D. Effective method to deliver test substance in adult zebrafish. *Int. J. Adv. Res.* **2016**, *4*, 543–551. [CrossRef]

HHS Public Access

Author manuscript

Adv Drug Deliv Rev. Author manuscript; available in PMC 2017 October 01.

Published in final edited form as:

Adv Drug Deliv Rev. 2016 October 1; 105(Pt B): 109–144. doi:10.1016/j.addr.2016.04.028.

Toxicology of Graphene-Based Nanomaterials

Gaurav Lalwani[1,2,*], **Michael D'Agati**[2], **Amit Mahmud Khan**[2], and **Balaji Sitharaman**[1,2,**]

[1]Theragnostic Technologies Inc., Long Island High Technology Incubator Suite 123, Stony Brook, NY 11790

[2]Department of Biomedical Engineering, Stony Brook University, Stony Brook, NY 11794-5281

Abstract

Graphene based nanomaterials possess remarkable physiochemical properties suitable for diverse applications in electronics, telecommunications, energy and healthcare. The human and environmental exposure to graphene-based nanomaterials is increasing due to advancements in the synthesis, characterization and large-scale production of graphene and the subsequent development of graphene based biomedical and consumer products. A large number of *in vitro* and *in vivo* toxicological studies have evaluated the interactions of graphene-based nanomaterials with various living systems such as microbes, mammalian cells, and animal models. A significant number of studies have examined the short- and long-term *in vivo* toxicity and biodistribution of graphene synthesized by variety of methods and starting materials. A key focus of these examinations is to properly associate the biological responses with chemical and morphological properties of graphene. Several studies also report the environmental and genotoxicity response of pristine and functionalized graphene. This review summarizes these *in vitro* and *in vivo* studies and critically examines the methodologies used to perform these evaluations. Our overarching goal is to provide a comprehensive overview of the complex interplay of biological responses of graphene as a function of their physio-chemical properties.

Graphical abstract

[*]**Correspondence:** Gaurav Lalwani, Ph.D., Theragnostic Technologies Inc., Long Island High Technology Incubator Suite 123, Stony Brook, NY 11790, Tel: 631-512-3980, gauravlalwani06@gmail.com. [**]Balaji Sitharaman, Ph.D., Department of Biomedical Engineering, Bioengineering Building Room 115, Stony Brook University, Stony Brook, NY 11794-5281, Tel: 631-632-1810, balaji.sitharaman@stonybrook.edu.

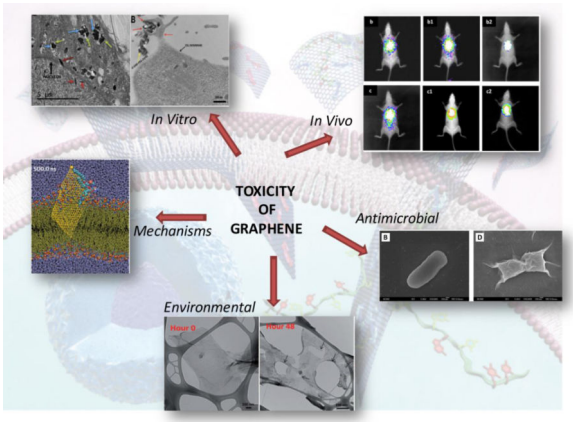

Keywords

Graphene; toxicity; *in vitro*; *in vivo*; antimicrobial; environmental; biodistribution

2. Introduction

Carbon nanomaterials such as fullerenes, carbon nanotubes and graphene are the most widely researched class of materials and hold immense potential to impact several scientific disciplines [1–3]. Their transformative potential has been recognized with multiple honors including the Kavli and Nobel Prize [4, 5]. Owing to the distinct arrangement of sp^2 bonded carbon atoms, each carbon nanomaterial can exhibit significantly different physical, morphological and chemical properties.

Graphene, a two-dimensional (2D) sheet of carbon atoms packed in a honeycomb lattice is widely regarded as a basic building block of graphitic allotropes (Figure 1)[6]. The theoretical existence of graphene was discussed over 55 years ago by Slonczewski and Weiss [7]. Landau, Peierls and Mermin reported that existence of atomically thin 2D crystals (such as graphene) was practically impossible due to thermodynamic instabilities, a theory that was supported by several independent experimental observations [8–11]. However, in 2004, Novoselov and Geim isolated single sheets of graphene by micromechanical cleavage of graphite or the “scotch-tape method” [12] and characterized their quantum electrodynamics [13, 14]. Since then research on graphene has exploded. The number of research papers published on graphene has been increasing exponentially (Figure 2) attracting scientists from all areas of science and technology towards the graphene “gold-rush”. In 2013, the European Union announced the graphene flagship project – a $1.3 billion 10 year investment in graphene research and development to translate graphene-based technologies from academic labs to the marketplace [15]. The Korean Graphene Project, also announced in 2013, is a $44 million 5 year investment for graphene research [16]. In 2011, United Kingdom committed £50 million investment for graphene research [17]. Recently, in October 2015, Chinese company Huawei Technologies has announced a $1 billion 5 year investment towards the development of information and communications technologies focused on graphene [18].

Graphene has interesting optical, thermal, mechanical and electrical properties. The sp^2 hybridization of 2D graphene plane results in delocalized out of plane π bonds that provide an exceptionally high carrier mobility (~ 200,000 $cm^2\ V^{-1}\ s^{-1}$ for suspended graphene [19, 20] and ~500,000 $cm^2\ V^{-1}\ s^{-1}$ for graphene-based field effect transistors) [21, 22]. Graphene exhibits room temperature quantum hall effect for electrons and holes [13, 23]. Graphene sheets also exhibit high surface area (2630 $m^2\ g^{-1}$) [21], thermal conductivity (~5000 $Wm\ K^{-1}$) [24], mechanical property (Young's modulus of ~ 1 TPa) [25] and optical transparency (single layer graphene absorbs ~2.3% of visible light) [26].

Graphene can be synthesized using various physical (such as mechanical cleavage ("scotch tape method") [27] or arc discharge [28]) and chemical methods (chemical vapor deposition [29], Hummer's method (chemical oxidation of graphite followed by mechanical exfoliation) [30] or longitudinal unzipping of carbon nanotubes [31]). Depending on the method of synthesis, graphene can exist in various morphologies such as sheets, platelets, ribbons, onions and quantum dots (Figure 3). Pristine graphene is apolar and very hydrophobic. It needs to be oxidized to improve its dispersibility in aqueous media.

Oxidized graphene is typically synthesized via chemical oxidation. Depending on the synthesis or morphology of the graphene, oxidized graphene are referred by various terminologies. For example, oxidized graphene prepared by Hummer's method is typically referred as graphene oxide (GO) or graphene nanoplatelet. Oxidized graphene prepared by longitudinal unzipping are referred as graphene oxide nanoribbons. The pristine sp^2 characteristic of graphene can to large extend (but not completely) be restored by treating oxidized graphene nanoparticles with reducing agents such as hydrazine, hydrogen iodide, etc. [32]. Although the presence of hydrogen bonds between the polar oxidative functional groups (such as oxide, acid, alcohol, epoxide etc.) of oxidized graphene imparts colloidal stability, the dispersibility of oxidized graphene in aqueous and biological media is inadequate for several biomedical applications. Functionalization strategies have been employed to further improve graphene's aqueous dispersibility. Graphene can be covalently or non-covalently functionalized with several chemical moieties (for instance amine) or biological molecules (such as nucleic acids and proteins). Oxidized graphene nanoparticle-based formulations has been extensively explored for several biomedical applications such as bioimaging [33–35], drug and gene delivery [36–38], photothermal therapy [39, 40], tissue engineering [41–43], and stem cell technology [44, 45]. Pristine or nearly pristine (oxidized graphene treated with reducing agents) graphene have also been investigated for several biomedical applications [27, 35, 46, 47].

The evaluation of *in vitro* cytotoxicity and *in vivo* biocompatibility is critical to develop nanoparticle-based formulations for biomedical applications. The potential widespread use of graphene-based nanomaterials for commercial materials science applications will increase their interactions with biological and environmental constituents. Furthermore, a thorough analysis of the biocompatibility of graphene is an essential prerequisite before their use for *in-vivo* biomedical applications. Consequently, several studies have been performed to assess the *in vitro* and *in vivo* cyto- and bio- compatibility of graphene-based nanomaterials [48–56]. These studies indicate that the toxicity of graphene is dependent on the complex interplay of several physiochemical properties such as shape, size, oxidative state, functional

groups, dispersion state, synthesis methods, route and dose of administration, and exposure times [48–57]. Post synthesis processing steps could lead to disruption of graphene structure and production of smaller carbonaceous debris or methods to synthesize graphene could lead to the incorporation of several metallic impurities in the final product. These confounding factors may elicit variable toxicity responses [58–60].

In this article, we provide a comprehensive review of recent *in vitro* and *in vivo* toxicity studies using graphene-based nanomaterials and examine the methodologies used to perform these evaluations. We also review studies investigating the effects of graphene on antimicrobial biota (eg. bacteria and fungi) and environmental constituents (e.g. crops, waste water, etc.). Finally we summarize the current understanding of the toxicity mechanisms of graphene-based nanomaterials. The goal of this article is to provide the readers with an overview on graphene toxicity and its dependence on the various physiochemical properties of graphene. Such an understanding could lead to development of strategies to mitigate potential adverse effects for successful development of graphene–based consumer and healthcare products.

3. *In vitro* toxicity

The assessment of *in vitro* cytotoxicity is the initial first step towards significantly expensive and elaborate *in vivo* studies. Table 1 summarizes the *in vitro* cytotoxicity of graphene and graphene oxide (GO) assessed using several representative cell lines at various treatment concentrations.

3.1 Dose, time, and morphology dependent cytotoxicity

Zhang et. al. investigated the interactions of graphene (diameter 100–110 nm, thickness 3–5 nm) with rat pheochromocytoma PC12 cells using 3-(4,5-dimethylthiazol-2-yl)-2,5-diphenyltetrazolium bromide (MTT) and Lactate Dehydrogenase (LDH) assays and compared the results with single-walled carbon nanotubes (SWCNTs) [61]. More than 70% cell death was observed for 100 μg/ml treatment concentration of SWCNTs whereas no cell death was observed for 0.01–10 μg/ml concentrations of graphene (Figure 4A). Nearly 15–20% cell death was observed for graphene treatment at 100 μg/ml. The observed cytotoxicity was attributed to the agglomeration of graphene, generation of reactive oxygen species (Figure 4B) and an increased caspase-3 activation (Figure 4C) resulting in apoptosis. These results show a dose dependent cytotoxicity trend that is dependent on the morphology (shape and composition) of the nanomaterial, with graphene exhibiting an overall lower toxicity compared to single-walled carbon nanotubes (SWCNTs). Vallabani et. al. investigated the toxicity of graphene oxide using normal human lung cells (BEAS-2B) after 24 and 48 hours of exposure at concentrations between 10–100 μg/ml. A significant dose- and time-dependent decrease in cell viability and an increase of early and late apoptotic cells was observed using MTT assay [62].

Yuan et. al. evaluated the cytotoxicity of graphene oxide on human hepatoma HepG2 cells using MTT assay, DFDA fluorescence analysis and 2D LC-MS proteome analysis [63]. After 48 hours of exposure to GO at 1 μg/ml concentration, HepG2 cells showed 6% mitochondrial damage, 8% increase in ROS generation and no significant changes in

apoptotic cell population, cell cycle, and expression of metabolic and cytoskeletal proteins. Cells treated with oxidized-SWCNTs (ox-SWCNTs) showed ~20% mitochondrial damage, >100% increase in ROS generation, ~26% increase in apoptotic cell population, and ~30 differentially expressed proteins involved in metabolic pathway, redox regulation, cytoskeleton formation, and cell growth. These results suggest that GO may be less cytotoxic compared to ox-SWCNTs. In another study, Lv et. al. show that GO does not elicit cytotoxic or apoptotic effects in human neuroblastoma SH-SY5Y cells at low concentrations (<80 μg/ml) [64]. Interestingly, GO enhances the retinoic acid induced differentiation of SH-SY5Y cells, improving neurite length and expression of MAP2 (neuronal marker), suggesting that GO may be suitable for applications in neurodegenerative diseases.

Talukdar et. al. have investigated the effects of graphene nanostructures of various morphologies (such as oxidized-nanoribbons (GONRs), oxidized-nanoplatelets (GONPs), and nanoonions (GNOs)) on the toxicity and stem cell differentiation potential of human mesenchymal stem cells (hMSCs) [65]. hMSCs (derived from bone marrow and adipose tissue) were treated with various concentrations (5–300 μg/ml) of GONRs, GONPs and GNOs for 24 or 72 hours and cytotoxicity was evaluated using Alamar blue and CalceinAM assays. Results show a dose –dependent (no time-dependent) cytotoxicity of various 2D graphene nanostructures with concentrations >50 μg/ml showing no cytotoxicity. TEM imaging shows cellular and nuclear uptake of GNOs and GONPs (Figure 5 A–D). Furthermore, results show that all graphene nanostructures did not induce any changes in the adipogenic and osteogenic differentiation of hMSCs (Figure 5 E–J) suggesting the used of graphene as labels for stem cell imaging and therapy.

Chng et. al. have reported a comparative study on the cytotoxicity of GONRs and GONPs [66]. GONRs were synthesized from the longitudinal unzipping of CNTs and GONPs were synthesized from stacked graphene nanofibers. *In vitro* cytotoxicity evaluated using MTT and WST-8 assays using human epithelial (A549 cells) show that GONRs exhibit a significantly higher cytotoxic response than GONPs over all concentrations (3–400 μg/ml). The increased cytotoxicity of GONRs was attributed to the presence of a greater amount of carbonyl groups (28.22% on GONRs vs. 11.06% on GONPs) and the high aspect ratio (width × length of GONRs ~310 × 5000 nm and GONPs ~ 100 × 100 nm) of GONRs.

Akhavan et. al. have reported the cyto- and geno-toxicity of reduced GONRs and reduced graphene oxide sheets (rGOS) using human MSCs derived from umbilical cord blood [67]. Cell viability measured by fluorescein diacetate (FDA) test shows that rGONRs are toxic, significant cytotoxicity was observed after 1 hour of exposure with rGONRs at 10 μg/ml, while the same cytotoxicity was observed upon incubation with 100 μg/ml of rGOS after 96 hours. The cytotoxicity of rGOS was attributed to the generation of oxidative stress whereas the cytotoxicity of rGONRs was attributed to DNA fragmentation and chromosomal aberrations (observed even at low concentrations of ~ 1 μg/ml after 1 hour) due to penetration of rGONRs inside the cells. These results suggest that the cytotoxicity and genotoxicity of graphene is dependent on the dose and shape of the nanomaterial (sheets vs. nanoribbons).

Jaworski et. al. have reported the interactions of graphene platelets with human glioblastoma U87 and U118 cells [68]. After 24 hours of incubation with 100 μg/ml graphene, 42% and 52% cell mortality was observed for U87 and U118 cells, respectively. However, graphene activated apoptosis only in U118 cells not in U87 cells where apoptosis and necrosis both were activated. These results suggest the potential application of graphene in anticancer therapy.

3.2 Functionalization dependent cytotoxicity

Sasidharan et. al. investigated the cytotoxicity of pristine graphene and carboxylated GO (GO-COOH) using monkey renal cells at concentrations between 10–300 μg/ml treatment concentrations to assess the differences between cellular interactions of hydrophobic and hydrophilic graphene derivatives [69]. Pristine graphene accumulated on the cell membrane leading to the destabilization of F-actin alignment whereas GO-COOH was internalized by cells and accumulated in the perinuclear region without any membrane destabilization even at 300 μg/ml doses. These results suggest that hydrophilic (more oxidized) graphene nanoparticles may be more cytocompatible and efficient intracellular delivery systems. In another study, Matesanz et. al. observed internalization and localization of poly(ethylene glycol amine)-functionalized GO sheets on F-actin filaments resulting in cell-cycle alterations, oxidative stress and apoptosis in MC3T3-E1 murine pre-osteoblasts, Saos-2 osteoblasts and RAW-264.7 macrophage cells [70].

Yuan et. al have investigated the cytotoxicity and distribution of three kinds of GQD (NH_2, COOH and CO-N$(CH_3)_2$ functionalized) in human neural glioma C6 and A549 lung carcinoma cells using MTT and Trypan blue assay [71]. Results show the absence of mortality and apoptosis or necrosis at all treatment concentrations (10–200 μg/ml) after 24 hours for all three GQD groups. Furthermore, Raman spectroscopic analysis showed the intracellular accumulation of all three GQDs; nuclear translocation was absent.

Horváth et. al. have evaluated the toxicity of GO and rGO in A549 human lung epithelial cells and RAW 264.7 mouse peritoneal macrophages using MTT assay, fluorometric DNA assay and fluorometric microculture cytotoxicity assay (FMCA) [72]. Cells treated with 0.0125–12.5 μg/cm^2 of GO or rGO for 5 days showed a dose dependent cytotoxicity. Significant differences in cell death between control and GO or rGO treated cells were observed from day 2 in A549 cells and day 3 in RAW 264.7 macrophages for two higher concentrations of 1.25–12.5 μg/cm^2. Cells treated with lower concentrations of GO (0.0125–0.125 μg/cm^2) did not lead to increases in ROS production. Cellular internalization of GO was observed in phagoendosomes without signs of any intracellular damage.

Aggregation of pristine graphene in biological buffers could result in greater cytotoxicity in comparison to oxidized graphene derivatives that can be readily dispersed without aggregation during the duration of cytotoxicity studies. Das et. al. have reported higher cytotoxicity of GO sheets compared to reduced graphene oxide sheets of similar dimensions, an effect attributed to the presence of high density of oxidative functional groups on the surface of GO which lead to the generation of reactive oxygen species [73]. HUVEC cells treated with 1, 5 or 10 μg/ml concentration of GO and rGO showed a dose and functionalization state dependent cytotoxicity. Furthermore, a size dependent cytotoxicity

was also observed for both GO and rGO. Upon a 10 fold reduction in sizes of oxidized and reduced graphene sheets, smaller graphene nanosheets showed a higher toxicity compared to non-sonicated larger GO or rGO sheets which was attributed to an increased intracellular interaction and uptake of small sized graphene. However, chong et. al. have reported the low cytotoxicity of PEG dispersed graphene quantum dots (>30nm diameter stacks of 1–10 graphene layers) upto 160 μg/ml for HeLa cells and 320μg/ml for A549 cells (Figure 6) [74].

Teo et. al. have investigated the cytotoxicity of halogenated graphene sheets [75]. GO sheets prepared by oxidation of graphite were thermally reduced with chlorine, bromine, and iodine vapor to form chlorine-, bromine-, and iodine-doped graphene, respectively (TRGO-Cl, TRGO-Br, and TRGO-I). A549 cells were treated with 0–200 μg/ml concentration of halogenated graphene for 24 hours and cell viability was analyzed using MTT and WST-8 assays. Results show that all halogenated graphene nanoparticles exhibit a dose-dependent cytotoxicity between 3.125–200 μg/ml with TRGO-Cl exhibiting highest cytotoxicity (~25.7% cell viability at maximum treatment concentration of 200 μg/ml). The levels of observed cytotoxicity follows the trend: TRGO-Cl > TRGO-Br > TRGO-I and is dependent on the amount of halogen functionalization. In another study, Teo et. al. have reported the cytotoxicity of fluorinated graphene (FG) [76]. Three types of graphene derivatives with varying amount of fluorine content were prepared (1.5%, 42.6%, and 50.7%). A549 cells were treated with 0–400 μg/ml of fluorinated graphene and cytotoxicity was analyzed using MTT and WST-8 assays. Results show a dose-dependent cytotoxicity response with greater cytotoxicity observed for graphene with higher mono-fluoro substituted carbon atoms. In a similar study, Chng et. al. synthesized highly hydrogenated graphene (HHG) and evaluated their *in vitro* cytotoxicity profile against A548 cells [77]. After 24 hours of exposure, MTT and WST-8 assay results show a dose-dependent cytotoxicity of HHG compared to GO controls at all treatment concentrations (0–400 μg/ml). The increased cytotoxicity of HHG was hypothetically attributed to the preferential adsorption of essential micronutrients on the hydrophobic surfaces of HHG compared to hydrophilic surfaces of GO sheets, thereby limiting nutrient availability.

Sawosz et. al. have investigated the cytotoxicity of arginine (Arg) and proline (Pro) functionalized rGO using U87 glioblastoma multiforme (GBM) cells and tumors *in vitro* [78]. Cells were treated with 50 μg/ml of rGO, rGO+Arg and rGO+Pro for 24 hours and cell viability was evaluated using Trypan blue and XTT assay. Results show ~40% cell death for rGO group and ~15% cell death for rGO+Arg and rGO+Pro groups greater than the controls. GBM tumors cultured on chorioallantoic membrane of chicken embryo were injected with rGO, rGO+Arg and rGO+Pro for 3 days. A greater reduction in tumor volume was observed for rGO compared to rGO+Arg and rGO+Pro groups, which also reduced the tumor volume albeit lower than rGO. Histological analysis of tumors showed the presence of white gaps and rupture sites indicating necrosis and endothelial proliferation. rGO+Arg were observed close to microglial cells and small blood vessels whereas rGO+Pro were aligned outside the cells in the tissue rather than inside the cells. Tumor cells require arginine for aggressive growth, therefore rGO+Arg were present in the outer layers of tumor – site for active angiogenesis. Gene expression analysis suggests that rGO+Arg, leads to the down regulation of MDM2 expression and increased expression of NQO1. Furthermore, no change in the

expression of COX6 and CASP3 mRNA expression were observed. These results suggest that rGO+Arg is anti-angiogenic and pro-apoptotic and has potential for GBM therapy.

3.3 Cell dependent cytotoxicity

Cytotoxicity of graphene nanoparticles is dependent on cell type. Mullick-Chowdhury et. al. reported the cytotoxicity screening of graphene oxide nanoribbons (GONRs) dispersed in DSPE-PEG (1,2-distearoyl-sn-glycero-3-phosphoethanolamine-N-[amino(polyethylene glycol)]) using six different assays and four representative cell lines: NIH-3T3 mouse fibroblast cells (NIH-3T3), Henrietta Lacks cells (HeLa) derived from cervical cancer tissue, Michigan cancer foundation-7 breast cancer cells (MCF7), and Sloan Kettering breast cancer cells (SKBR3)[36]. All cell lines exhibit a dose dependent (10–400 μg/ml) and time dependent (12–48 hours) decrease in cell viability. HeLa cells showed the least cell viability (5–25%), compared to other cell types (78–100%), depending on the treatment concentration and exposure time. An increased cellular uptake of GONRs was observed and attributed to an increased cytotoxic response in HeLa cells. TEM imaging (Figure 7) shows the formation of cytoplasmic vesicles to facilitate intracellular uptake. Swollen and ruptured plasma membrane was observed suggesting necrotic cell death.

3.4 Size dependent cytotoxicity

Akhavan et. al. investigated the cytotoxicity of reduced graphene oxide nanoplatelets (rGONPs) of various sizes (11±4 nm, 91±37 nm and 418±56 nm) and as prepared GO (3.8±0.4 μm) using human mesenchymal stem cells (hMSCs) [79]. The cytotoxicity and cell viability was assessed using fluorescein diacetate (FDA) assay, ROS assay, RNA efflux and Comet assay. Results showed a significant size-dependent cytotoxicity; a treatment concentration of 100 μg/ml rGONPs (11±4 nm) showed >95% cell death which reduced with increasing lateral size dimensions (Figure 8). As-prepared GO with largest lateral size dimensions (3.8±0.4 μm) showed lowest (~20%) cell death. Results show that rGONPs can also induce DNA fragmentation even at low concentration of 0.1 μg/ml.

Chang et. al. investigated the cytotoxicity of GO of various sizes (160±90 nm, 430±300 nm and 780±410 nm) using A549 (human lung adenocarcinoma) cells [80]. Cell viability was assessed using CCK-8 assay after 24–72 hours of incubation at GO concentrations 10–200 μg/ml. Small GO sheets (160±90 nm) showed lower cell viability of ~67% compared to large GO sheets (430±300 nm and 780±410 nm) that showed >80% cell viability. However, GO sheets of dimensions 780±410 nm show >50% higher ROS generation compared to GO of dimensions 160±90 nm and 430±300 nm. These results suggest that the cell viability and ROS generation potential of GO is dependent on the size of graphene sheets.

Dasgupta et. al. have reported the size dependent cytotoxicity of graphene oxide nanoribbons (GONRs) after post processing sonication steps that result in a size reduction of nanoparticles [60]. GONRs were dispersed in cell culture media by bath sonication (5 or 20 minutes) or probe sonication (1, 5 or 10 minutes) and MCF-7 and A549 cells were exposed to GONR containing media at 20 μg/ml concentrations. LDH assay, presto blue assay and ROS generation showed that GONR solutions prepared via probe sonication results in a decrease of metabolic stress of cells *in vitro*. No adverse effects were observed when cells

were exposed to non-sonicated and bath sonicated solutions of GONRs. TEM analysis showed presence of smaller GONR fragments and carbonaceous debris after probe sonication, which may be the cause of observed cytotoxicity.

Yue et. al. report that cellular internalization and regulation of cellular responses are directly dependent on the lateral dimension of GO [81]. In this study, six representative cell lines (peritoneal macrophage PMØ, murine macrophage J774A.1, murine Lewis lung carcinoma LLC, human breast cancer MCF-7, human hepatocarcinoma cells HepG2, and human umbilical vein endothelial cells HUVEC) were exposed to GO sheets of different sizes (350 nm and 2 μm) at a concentration of 20 μg/ml for cell viability analysis (LIVE/DEAD assay). After 48 hours of incubation, a significant cytotoxicity (~40–60% cell death) was detected for all six cell types. However, cell viability was restored upon the removal of manganese (Mn), an impurity present during the oxidative synthesis of GO. Cells upon treatment with Mn-free GO at 20 μg/ml showed ~80–100% cell viability. These results highlight the importance of purification steps involved during the synthesis of GO to eliminate false positive contributions from metal ions. PMØ and J774A.1 macrophage cells were treated with 2–6 μg/ml of nano- and micro-sized GO. Cellular uptake studies show that internalization of GO was independent of size and both nano- and micro-sized GO (350 nm and 2 μm) had similar intracellular accumulation. The analyses of uptake mechanisms showed that GO of size 350 nm was wrapped by filopodia of macrophages and internalized whereas GO of 2 μm was internalized via direct penetration. Post cellular internalization, the micron sized GO developed wrinkle formations and appeared to be sequestered into lysosomes. Furthermore, the micron sized GO induced a stronger inflammatory response and release of cytokines. These results suggest that cytokine release and inflammatory response are dependent on the size of GO sheets.

3.5 Immunotoxicity of graphene

Zhi et. al. have reported the immunotoxicity of GO with and without functionalization with poly(vinyl pyrrolidone) (PVP) against human immune cells such as T lymphocytes, dendritic cells and macrophages [82]. Results show that PVP-coated GO (PVP-GO) exhibit lower immunogenicity compared to pristine GO at concentrations between 25–100 μg/ml. The differentiation and maturation of dendritic cells was unaffected upon incubation with PVP-GO; the levels of secreted TNF- α and IL-1β showed no significant differences between GO and PVP-GO groups, yet the secretion of IL-6 was maintained in PVP-GO group. Incubation with PVP-GO also delayed the apoptosis of T lymphocytes and stimulated and enhanced the physiological activity of macrophages.

Li et. al. investigated the interactions of pristine graphene with RAW 264.7 macrophage cells at concentrations between 5–100 μg/ml (dispersed in 1% pluronic F108 surfactant).[83] Pristine graphene shows dose-dependent cytotoxicity in RAW 264.7 cells; ~ 78% cell death was observed at 100 μg/ml treatment concentrations. Further investigation of the mechanisms of cytotoxicity showed that interaction of pristine graphene with macrophage cell membrane leads to depletion of mitochondrial membrane potential thereby increasing ROS leading to the activation of apoptotic cascade. MAPK and TGF- β signaling pathways were activated which in turn activated two pro-apoptotic proteins (Bim and Bax).

Consequently, caspase-3 and PARP proteins were activated triggering apoptosis. The identification of mechanisms of cytotoxicity is extremely important and provides information towards development of strategies to control graphene-induced apoptosis.

Chen et. al. showed that GO triggers autophagy (catabolic self-destruction of dysfunctional cellular components) in liver cancer cells (SNU-449 and mahlavu), lung cancer cells (A549), human embryonic kidney cell (HEK293), and RAW 264.7 macrophages by stimulating toll-like receptor signaling cascade (release of cytokines such as IL-2, IFN-γ, IL-10 and TNF-α) at treatment concentrations of 5 or 100 μg/ml [84]. Toll like receptors - TLR4 and TLR9 were activated resulting in GO-mediated inflammatory responses. The results of this study show that GO exposure to cells simultaneously triggers autophagy and TLR4/9 mediated inflammatory responses.

Tkach et. al. showed that treatment of dendritic cells (DCs) with GO at 6.25 μg/ml results in an impaired stimulatory potential of DCs (activation of T-cells); treatment with similar concentrations of fullerenes (C_{60} and C_{60}-tris) promotes the ability of DCs to activate T-cells [85]. Further analysis showed that GO did not alter antigen uptake by DCs nor inhibit antigen peptide presenting abilities of DCs. However, exposure of DCs to GO resulted in suppression of an immunoproteosome subunit (LMP-7), which is a critical component of MHC-I antigen processing machinery (APM) illustrating the mechanism of inactivation of DCs by GO. These results suggest that GO may modulate antigen-specific T-cell response and emphasize the importance of elaborate assessment of immunomodulatory effects of graphene nanoparticles.

3.6 Hemolytic toxicity of Graphene

Hemolytic potential of graphene is dependent on the size and aggregation state of individual nanosheets. Liao et. al. investigated the cytotoxicity of graphene and GO using human erythrocytes (RBCs) [86]. Hemolysis was quantified by measuring the amount of hemoglobin released due to RBC membrane damage upon incubation with graphene and GO at 3–200 μg/ml for 3 hours. At 200 μg/ml, individually dispersed GO sheets showed ~60% hemolysis, significantly higher than graphene dispersions which showed ~20% hemolysis. The aggregation of graphene in DI water results in fewer cell-contractable ROS groups on the surface of graphene. However, cells interact with several ROS species present on the surface of individually dispersed GO, leading to greater hemolysis. Chitosan coated GO aggregate in DI water due to pH dependent conformational change of chitosan resulting in no hemolytic toxicity of GO.

Singh et. al. have reported the *in vitro* hemolytic toxicity of GO and rGO using human platelets [87]. Freshly isolated suspension of platelets exposed to GO (2 μg/ml) show aggregation and platelet activation at levels greater than induction by thrombin (1 U/ml, a strong platelet agonist). Exposure of platelets to GO resulted in the activation of Src kinases and release of calcium, leading to thrombus formation. In comparison, rGO at 2 μg/ml induced minor platelet aggregation, only 10% of aggregation induced by GO. In another study, Singh et. al. showed that amine functionalized GO does not induce lysis of erythrocytes and has no stimulatory effects on platelets highlighting their non-thrombotoxic

properties [88]. These results suggest that surface modifications of graphene nanoparticles play an important role towards defining their hemolytic activity.

Mullick Chowdhury et. al. show that graphene oxide nanoplatelets (GONPs) functionalized with biocompatible polymer dextran (GNP-Dex) exhibit no hematological toxicity [89]. RBL-2H3 mast cells and human platelets showed no histamine release, platelet activation or blood cell hemolysis upon treatment with GNP-Dex at concentrations ranging from 1–10 mg/ml. At concentrations >7 mg/ml, RBL-2H3 cells showed 12–20% increase in complement protein expression. However, cytokine TNF-Alpha and IL-10 levels remained within physiological levels. In another study, Mullick Chowdhury et. al. have investigated the interactions of DSPE-PEG functionalized graphene oxide nanoribbons (GONRs) with blood vascular system components [90]. No release of histamine, platelet PF4 activation and complement activation was observed from mast cells upto treatment concentrations of 80 μg/ml. TEM imaging shows significant uptake of GONRs into endothelial cells and exhibit a concentration dependent reduction of cell viability. Results show that DSPE-PEG functionalized GONRs are hemocompatible upto a concentration of 80 μg/ml.

3.7 Surfactant/coating dependent cytotoxicity

Wojtoniszak et. al. investigated the cytotoxicity of GO and rGO dispersed using three surfactants (polyethylene glycol (PEG), polyethylene glycol–polypropylene glycol–polyethylene glycol (Pluronic P123), and sodium deoxycholate (DOC)) at concentrations between 3.12–100 μg/ml using mice fibroblasts L929 cells [91]. Cytotoxicity analysis using WST-1 assay showed that the cell viability is dependent on the surfactant used to stabilize the suspension, chemical state of material (oxidized or reduced), and the treatment concentration. GO functionalized with PEG exhibits the lowest toxicity (cell viability ~ 36.3% at 100 μg/ml) whereas GO functionalized with DOC and Pluronic P123 shows 15.5% and 6.3% cell viability, respectively. L929 cells exposed to the PEG dispersed rGO between 3.125–25 μg/ml show ~95−60% cell viability. Similar results are observed for rGO functionalized with DOC, however rGO functionalized with Pluronic P123 showed least cell viability. Both, GO and rGO show good cytocompatibility between 3.125–12.5 μg/ml. GO dispersed in PEG shows the best cytocompatibility. These results suggest that GO and rGO exhibit a dose- and surfactant-dependent cytotoxicity.

Hu et. al. investigated the cytotoxic effects of fetal bovine serum (FBS) coated GO using A549 cells [92]. At 100 μg/ml exposure, FBS coated GO showed ~90% cell viability whereas GO without FBS coating showed only ~50% cell viability. TEM analysis showed irreversible cell membrane damage after 2 hours of exposure to GO. FBS coated GO did not induce any membrane damage. These results suggest that cytotoxicity of GO is a result of direct physical interactions with cell membrane that can be mitigated by coating GO with FBS.

Mu et. al. investigated the cellular uptake of bovine serum albumin (BSA) coated GO (flake size ~ 500 nm or ~1 μm) by mouse mesenchymal progenitor C2C12 cells [93]. Results show that small GO (~500 nm) are internalized by clathrin-mediated endocytosis whereas large GO (~1 μm) are internalized by phagocytosis. Large GO sheets translocate into the reticuloendothelial system and small GO sheets are accumulated in various organelles.

Mbeh et. al. have reported the cytotoxicity of albumin functionalized GONRs against A549 cells evaluated using Trypan blue and apoptosis (hoechst and propidium iodide staining) [94]. A dose-dependent cytotoxicity was observed wherein albumin functionalized GONRs at concentrations < 50 μg/ml did not exhibit significant cytotoxicity, whereas incubation of A549 cells with higher concentrations (100 μg/ml) resulted in loss of cell proliferation and induction of apoptosis.

4. *In vivo* toxicology

A crucial step in the toxicological assessment of graphene-based formulations is their dose- and/or time-dependent safety pharmacological assessment in small and large animal models under various modes of administration (e.g. intravenous. intraperitoneal, oral). Table 2 summarizes the cytotoxicity of graphene and graphene oxide (GO) assessed in animal models.

4.1 Intravenous administration

Intravenous (IV) administration is a widely employed method wherein a needle is inserted into the vein and formulation is administered through that needle. It is the preferred mode of systemically introducing pharmaceutical formulations for imaging, drug delivery or therapy. Singh et. al have investigated the *in vivo* platelet aggregation of GO and rGO nanosheets. GO and rGO sheets were administered intravenously via tail vein injection to Swiss male mice (8–12 weeks old) at 250 μg/kg dose for 15 minutes [87]. A collagen-epinephrine mixture was administered as positive control whereas saline was used as the negative control. After 15 minutes post injection, the mice were euthanized and lungs were harvested for histological analysis. Hematoxylin and eosin (H&E) staining showed ~48% thromboembolism whereas the collagen – epinephrine control solution resulted in ~64% occlusion of blood vessels. rGO was not as effective as GO towards platelet activation; rGO administration resulted in ~ 8% blood vessel blockage, significantly less than GO. These results show that GO induces severe pulmonary thromboembolism that may be attributed to the greater surface charge density of graphene surface upon oxidation. In a follow-up study, Singh et. al. investigated the *in vivo* thrombogenic properties of amine-modified GO (NH_2-GO) [95]. Compared to GO which induces platelet aggregation, NH_2-GO does not elicit any stimulatory effects on platelets or pulmonary thromboembolism. H&E staining revealed that GO resulted in ~46% blockage of pulmonary blood vessels while NH_2-GO showed no signs of obstruction.

Sasidharan et. al. have reported the long term *in vivo* toxicology of pristine and functionalized few layered graphene (FLG), FLG-COOH and FLG-PEG (Figure 9A) administered intravenously to Swiss albino mice at 20 mg/kg for 1, 8, 30, and 90 days [96]. Sterile physiological saline was administered to control animals. All animals survived over the course of 90 days, however, the body weight of FLG, FLG-COOH and FLG-PEG treated mice was lower on days 60–90 compared to control mice. To dynamically track the *in vivo* biodistribution, ^{99m}Tc labeled FLG-COOH and FLG-PEG were injected and whole body images were captured at 0.1, 1, 3, 12, and 24 hours (Figure 9B). ^{99m}Tc-FLG-COOH showed accumulation and retention in lungs over 24 hours. However, after 12 hours, ^{99m}Tc-FLG-

PEG was redistributed to RES system such as spleen and liver. FLG-COOH accumulated in the lungs resulting in thicker alveolar walls. Injection of FLG and FLG-COOH resulted in extensive spleen damage including the loss of dividing line between red pulp and marginal zone, abundance of megakaryocytes in the red pulp 90 days post injection, and lack of lymphocytes in the white pulp. On the contrary, FLG-PEG did not result in any injury to the marginal zone and only several black spots in the red pulp were observed. Liver tissue analysis revealed that FLG and FLG-COOH induced liver tissue degeneration while FLG-PEG did not and was observed as black spots. However, kidney necrosis was observed upon administration of both FLG and FLG-COOH as early as the first day of administration. FLG-PEG was present as black spots on the tissue but did not exhibit any signs of necrosis. FLG, FLG-COOH, and FLG-PEG did not damage brain, heart, or testis suggesting that graphene cannot pass through the blood-brain barrier.

Zhang et. al. have reported the toxicity of dextran functionalized graphene oxide (GO-Dex) intravenously administered via tail vein injection to female Balb/c mice at 20mg/kg dose for 1, 3, and 7 days [97]. H&E staining of liver sections showed a significant increase in black spots – areas of GO aggregation - after 7 days indicating clearance of GO-Dex from mouse liver. For biodistribution and pharmacokinetic studies, ^{125}I labeled GO-Dex (^{125}I-GO-Dex) was injected via tail vein at 4 mg/kg concentration and blood was collected after 4, 24, 72, and 168 hours. After 4 hours of administration, ^{125}I-GO-Dex was found in liver, spleen, stomach, lungs, kidney, and intestine. At later time points, ^{125}I-GO-Dex was predominantly found in the liver and spleen. Histological sections of liver and kidney confirm the presence of ^{125}I-GO-Dex as black dots that were abundant at day 1 and decreased at later time points suggesting the excretion of ^{125}I-GO-Dex via renal and fecal pathways. Since GO-Dex has a wide size distribution, small GO-Dex sheets could pass through glomerulus for renal excretion and large GO-Dex sheets accumulated in RES organs could be excreted out in feces via biliary pathway.

Zhang et. al. have reported the distribution and biocompatibility of GO after intravenous administration to male Sprague Dawley rats at 1 and 10 mg/kg dose [98]. Histopathological analysis of lung, liver, spleen and kidneys performed 14 days post injection shows no pathological changes for all organs examined for 1 mg/kg dose. For 10 mg/kg treatment, all organs except lung showed normal pathophysiology. However, due to high accumulation and slow clearance, GO accumulated in lungs resulted in pulmonary edema, granulomatous lesions, inflammatory cell infiltration, and fibrosis. These results suggest that GO is biocompatible, however, accumulation in lungs at higher concentration may lead to safety concerns. Biodistribution of GO was assessed by tracking intravenously administered ^{188}Re labeled GO (^{188}Re-GO) after 1, 3, 6, 12, 24, and 48 hours. It was observed that GO cleared from blood, accumulated in lungs, liver and spleen and was up taken by mononuclear phagocytes in the reticuloendothelial system.

Wang et. al. have reported the biocompatibility of GO administered via tail vein injections to 4–5 week old female kunming mice (Sprague Dawley rats) at 0, 0.1 mg (low), 0.25 mg (medium), and 0.4 mg (high) doses [99]. No toxicity was observed for low and medium doses. However, for high dose, 4 out of 9 mice died after 1 week due to airway blockage caused by accumulation of GO. Histology analysis after 1, 7, and 30 days shows long-term

accumulation of graphene in liver, kidney and spleen. Granuloma formation along with the presence of neutrophils and foamy alveolar macrophages was observed in lungs suggesting a foreign body immune response. No accumulation was observed in brain suggesting that GO cannot pass the blood brain barrier. These results suggest that GO is non-toxic at low concentrations and results in irreversible airway damage and chronic pulmonary toxicity at high concentrations.

Liu et. al. have reported the dose- and size- dependent toxicity and biodistribution of GO sheets [100]. Male ICR mice were intravenously injected with small and large GO sheets (s-GO and l-GO) labeled with ^{125}I to enable radioactive tracking of tissue biodistribution, organ accumulation and blood clearance of GO after 2–180 min post injection at 1–10 mg/kg doses. It was observed that s-GO mainly accumulated in the liver with some aggregates present in lungs and spleen, however, after 180 minutes, clearance of s-GO was observed with a residual accumulation of ~11% in liver and <1% in lungs. On the contrary, in comparison to s-GO, l-GO showed higher accumulation in lungs with a residual accumulation of ~19% after 180 minutes. TEM analysis of lung sections show intracellular accumulation of s-GO in phagocytic cells while l-GO particles (bigger than 1 μm) was lodged in cell gaps of lungs. The size-regulated biodistribution of s-GO and l-GO was attributed to the different aggregation states of the nanoparticles. The less dispersed GO resulted in the formation of larger GO-protein complexes, which were filtered by the pulmonary blood vessels. At higher doses, s-GO aggregated to large particulates resulting in the entrapment in lungs. The blood half-life of s-GO was 2.2 minutes ($T_{1/2}$ alpha) and 170 minutes ($T_{1/2}$ beta). For l-GO, $T_{1/2}$ alpha was 1.8 minutes and $T_{1/2}$ beta was 102 minutes. These results suggest that s-GO possesses longer blood retention time than l-GO.

Yang et. al. have reported *in vivo* biodistribution and photothermal activity of PEG functionalized nano graphene sheets (NGS-PEG) [101]. Cy7 dye labeled NGS-PEG was intravenously injected into tumor bearing Balb/C mice at a dose of 20 mg/kg and organs were harvested after 1, 6, and 24 hours. Significant accumulation of NGS-PEG was observed in tumors due to leaky vasculature along with low accumulation in RES organs. After 24 hours post injection, the kidneys showed strong fluorescence (Figure 10) attributed to the renal excretion of small sized NGS particles. NGS-PEG showed no toxicity - neither death nor significant weight loss was observed in all animals. After NGS-PEG administration, the tumors on the right shoulder of 4T1 Balb/c mice were exposed to 808 nm laser until the surface temperature reached ~50°C. The tumors disappeared 1-day post laser treatment leaving a black scar that disappeared after one week. No tumor regrowth was observed after 40 days. These results suggest that PEG functionalized graphene can be suitable for *in vivo* photothermal therapy applications. In another study, Yang et. al. have reported the long term *in vivo* biodistribution and pharmacokinetics of ^{125}I-labled NGS-PEG intravenously administered in Balb/c mice at 4 mg/kg dose [102]. For pharmacokinetics study, blood was drawn after 0–25 hours and measured by a gamma counter. To examine the biodistribution of ^{125}I-NGS-PEG, 4 mg/kg was administered intravenously and organs were harvested at various time points: 1 hour −60 days post injection. NGS-PEG initially accumulated in several organs, however accumulation at later time points was observed in liver and spleen. H&E staining of liver and spleen sections showed a reducing number of NGS-PEG aggregates over time suggesting removal of NGS-PEG from RES system. Renal

pathway cleared out smaller sized NGS-PEG (10 nm diameter) while larger NGS-PEG aggregates were excreted through biliary pathway into the feces. Blood biochemistry and hematology analysis showed normal levels of urea, blood cells, hemoglobin and other factors suggesting that there were no toxic effects of NGS-PEG to liver and kidneys. These results suggest that NGS-PEG does not exhibit long-term *in vivo* toxicity in mice.

Kanakia et. al. have reported the sub acute toxicity of dextran functionalized graphene nanoplatelets (GNP-Dex) administered via intravenous injections to Wistar rats at 1, 50, and 100 mg/kg doses 3 times a week for three weeks [103]. No signs of toxicity were observed for 1 mg/kg and 50 mg/kg doses. All vital parameters such as body weight, blood pressure, breathing and heart rate were normal. However, for 100 mg/kg dose, 2 out of 8 animals died after 2 weeks. A complete blood count analysis showed physiological levels of blood urea nitrogen and creatinine indicating normal kidney function. ALT and ALP levels were elevated, however, blood glucose was normal. Histology analysis after 3 weeks showed the presence of GNP-Dex in hepatic kuppfer cells and pulmonary alveolar macrophages, which increased with increasing dose of GNP-Dex (Figure 11). No adverse effects or inflammation were observed in brain, heart, spleen and kidney.

Mullick Chowdhury et. al. have reported the *in vivo* vasoactivity of GNP-Dex using male hamsters cheek pouch model [89]. GNP-Dex was administered at doses ranging from 1–50 mg/ml to the excised left cheek pouch tissue of hamsters using a micropipette. The arcade-terminal arteriolar network junction was the microvascular observation site. The baseline diameters of arcade and terminal arterioles were 23 μm and 8 μm, respectively. The administration of 0.1 mg/ml and 0.5 mg/ml GNP-Dex had no significant effect on the arteriole diameters. No significant differences in the dilation of arterioles were observed at higher doses of 10 mg/ml and 50 mg/ml. However, the administration of FDA-approved natural biopolymer dextran at 35 mg/ml resulted in ~23% dilation of arcade arterioles and ~ 63% dilation of terminal arterioles. The lack of dilation post GNP-Dex administration and an increased dilation due to dextran suggests that the observed minor vasoactive effects of GNP-Dex could be due to the dextran coating of GNPs.

In another study, Kanakia et. al. have evaluated the histopathology and biodistribution of GNP-Dex administered via intravenous injections in male Wistar rats at doses between 1–500 mg/kg after 1 and 30 days [104]. The results show that the maximum tolerable dose (MTD) of GNP-Dex is between 50–125 mg/kg. Blood half-life of GNP-Dex is ~30 minutes. Maximum accumulation of GNP-Dex after day 1 was found in liver and kidney, which reduced (at least 2–4 folds) after 30 days of administration suggesting a clearance of GNP-Dex via RES system (Figure 12 A&B). ICP analysis showed that GNP-Dex administered at 50 mg/kg had a higher blood concentration than 500 mg/kg doses 30 minutes post-administration (Figure 12C). Majority of GNP-Dex nanoparticles were excreted via feces (~60–90%) within 24 hours (Figure 12D), small amounts were excreted via urine (Figure 12E). Histopathological changes (Figure 12 F–J) were observed in heart, lung, liver, kidney and spleen at high treatment concentrations (250 μg/ml). No adverse effects were observed in brain. Hematological factors and cardiovascular parameters remained at physiological levels upto 125 mg/ml treatment doses. These results suggest that GNP-Dex is non-toxic with a MTD of 125 mg/kg.

Jasim et. al. have reported the *in vivo* biodistribution of chemically functionalized graphene (GO-DOTA) labeled with ^{111}In after intravenous injections in C57BL/6 mice at 200 μl dosage [105]. Post 1, 2, and 24 hours of administration, ^{111}In-DOTA-GO was accumulated in bladder and excreted via urine. No fecal elimination was observed. Maximum accumulation was observed in liver and spleen. Furthermore, at later time points, translocation of GO from liver to spleen was also observed. No organ damage was observed at all time points. These results show that chemically functionalized GO sheets are non-toxic and possess distinctly different physiological behavior (biodistribution and excretion characteristics) than pristine or non-covalently functionalized graphene sheets.

4.2 Intraperitoneal administration

Intraperitoneal (IP) administration is the injection of the formulation into the peritoneum (or body cavity). Yang et. al. have reported the *in vivo* toxicity of PEG functionalized GO administered intraperitoneally and orally in female balb/c mice [106]. PEG functionalized and ^{125}I labeled nano-graphene oxide (nGO-PEG), reduced graphene oxide (rGO – PEG), and nano reduced graphene oxide (nrGO – PEG) of diameters 25, 50, and 27 nm, respectively, were administered intraperitoneally at 50 mg/kg dose and orally at 100mg/kg. Animals were euthanized post 1, 7, 30 and 90 days post intraperitoneal administration and 1, 7, and 30 days post oral injections. All major organs were collected for histology and biodistribution analysis and blood was collected from the orbital for complete blood panel and serum biochemistry analysis. The radioactivity of GO formulations after oral administration was undetectable after 1 week suggesting negligible uptake of PEGylated GO administered orally. However, after intraperitoneal administration, PEGylated GO showed high accumulation in RES organs (black colored liver and spleen) after 1 and 7 days. Larger sized RGO-PEG showed higher uptake (> 2 fold, determined by radioactivity measurements) than smaller nGO-PEG and nrGO-PEG formulation. No animal death, body weight loss, inflammation, or significant changes in bloody panel or serum biochemistry were observed after 90 days post intraperitoneal administration indicating no signs of toxicity. These results suggest that PEGylated GO do not elicit any adverse effects under the above conditions in rodents, and the biodistribution and clearance profiles depend on the size, surface coating and route of administration.

Ali-Boucetta et. al. have investigated the *in vivo* pathogenicity of highly pure, colloidally stable dispersions of GO [107]. Conventional GO (cGO, size > 0.10 μm^2) prepared using Hummer's method was subjected to several purification steps to obtain highly pure GO (pGO, size 0.01 μm^2 to 0.02 μm^2). Both, cGO and pGO had similar chemical functional groups (carbonyls, hydroxyls and epoxides). pGO sheets were administered intraperitoneally at a dose of 50 μg/animal for 1 and 7 days. CNTs were used as positive controls. The inflammatory response was investigated by observing the change in protein levels and the change in the number of polymorphonuclear leucocytes 1 and 7 days post administration. After 1 day, pGO did not show a change in polymorphonuclear leucocyte (PMN) and protein levels whereas CNT controls induced at least 2-fold increase in total PMN count. After 7 days, there was accumulation of macrophages and giant cells with a deposition of collagen on the mesothelial membrane for CNT controls; pGO groups did not show any such effects.

These results show that highly pure single layered GO sheets show no signs of inflammation or granuloma formation upto 50 μg/animal dose administered intraperitoneally.

Sahu et. al. have investigated the *in vivo* biocompatibility of GO dispersed pluronic gels administered intraperitoneally via implantation in subcutaneous pockets in 6–7 weeks old balb/c mice [108]. Mild inflammation was observed 3 weeks post implantation. After 8 weeks, the number of macrophages reduced and no chronic inflammation, tissue necrosis or hemorrhaging was observed. Furthermore, no gel degradation or degradation products were observed in the surrounding tissues.

Strojny et. al. have reported the intraperitoneal toxicity of GO, graphite and nanodiamonds administered to 6 weeks old female Wistar rats [109]. Nanoparticle suspensions were injected at a dose of 4 mg/kg for 4 or 12 weeks at three-day intervals. After 4 or 12 weeks, rats were euthanized and liver and blood were collected. Results show the presence of nanoparticle aggregates in the peritoneal cavity close to the injection site. Smaller aggregates were observed in the mesentery and liver serosa suggesting transportation and accumulation of nanoparticles in liver. No adverse health effects were observed for all nanoparticles (GO, graphite or nanodiamonds) at all time points (4 or 12 weeks). Blood analysis and liver enzyme levels were normal suggesting good liver biocompatibility.

4.3 Oral administration

In oral administration a formulation/substance is administered via mouth in cases where a systemic effect is desired. Fu et. al. have investigated the development of mice offsprings after oral administration of graphene oxide at 0.5 and 0.05 mg/ml to maternal mice [110]. GO suspension in drinking water was administered to female ICR mice (8–9 weeks old) from 1–38 postnatal days (PND). Filial mice were administered GO water during the suckling period from 1–21 PND and normal water during the weaning period from 22–38 PND. After 21 and 38 days, pups were weighed and euthanized. Compared to the control groups that received normal water, significant decrease in body weight, body length and tail length of filial mice were observed for 0.5 mg/ml treatment group. Blood biochemistry analysis showed no significant differences in the levels of alanine aminotransferase (ALT), aspartate aminotransferase (AST), blood urea nitrogen (BUN) and creatinine (CREA) for both the GO groups. Pathological examination of heart, lung, spleen, kidney and liver of filial mice administered with 0.5 mg/ml GO suspension showed severe atrophy (Figure 13 A). H&E staining of duodenum, ileum, jejunum (parts of small intestine) showed increase in villi length and duodenum width post GO administration (Figure 13 B). These results show that GO can have significant negative effects on the development of filial mice during the lactation period.

Zhang et. al. have investigated the short-term and long-term effects of reduced GO (rGO) on general locomotor activity, neuromuscular coordination, balance, anxiety, learning and memory of male C57b/6 mice (6–8 weeks old) using rotarod, open field and Morris water maze tests [111]. HEPES Buffer dispersed rGO were administered via oral gavage every 24 hours for 5 days at 60mg/kg dose. rGO treated mice maintained normal body weight, organ weight, and instinctive behaviors (eating etc.) compared to control mice administered with chow and HEPES buffer. However, initial 3–4 days post treatment, mice showed decreased

neuromuscular coordination and locomotor activity failing the rotarod and open field tests. At later time points (15 and 60 days post administration), all these parameters returned to their normal state. No significant differences in blood biochemistry, liver function and kidney function and aging parameters were observed. The morphologies of neurons in the hippocampus and neuroglia cells as well as choline acetyl transferase and hippocampal acetylcholine esterase (enzymes involved in memory and learning) levels also remained normal post rGO administration. These results show that exposure to high concentration of rGO sheets via oral administration results in a short term decrease in neuromuscular coordination and locomotor activity which return to normalcy a few days post exposure; it does not affect learning, memory, anxiety, spatial and exploratory behaviors.

Wu et. al. have investigated the toxicity of graphene oxide at doses between 0.1–100 mg/L administered orally on nematode *Caenorhabditis elegans* after acute (24 hours) and prolonged exposure (larva to adult) [112]. GO was mixed with nematode food (K medium) and lethality, growth, reproduction and locomotion were analyzed. Results show that prolonged exposure at concentrations 0.5 mg/L and greater lead to significant primary (intestine) and secondary (neurons and reproductive) organ damage. Additionally, GO induces loss of villi and trans locates into the intestinal walls. Other adverse events noted were increased defecation cycle and hyper permeable intestinal barrier. These results show that GO upon exposure to environment would come into contact with nematodes, worms and other environmental organisms and may induce long-term adverse effects in the environmental flora.

4.4 Pulmonary administration

Schinwald et. al. have reported the *in vivo* toxicity of pristine GNPs after intrapleural and pharyngeal administration in 9 weeks old female C57BL/6 mice at 5 μg and 50 μg per mouse doses, respectively [113]. After 24 hours and 1 week of administration, a differential cell count of lavage fluid showed that mice exposed to GP had elevated levels (2× of physiological levels) of eosinophils and neutrophils. The chemokine and cytokine protein levels (MIP-1α, MCP-1, MIP-2, IL-8 and IL-1β) were also elevated. Microscopy imaging showed that pleural macrophages were not able to fully phagocytize GNPs due to their size and shape; multiple macrophages surrounding a single GNP forming a rosette-like cell/particle aggregation suggested frustrated phagocytosis. Histological evaluation showed extended retention of GNPs in pleural space and the formation of ganulomatous lesions in bronchiolar lumen. The initial inflammatory response to GNPs reduced after 1-week post administration; reduction in the number of inflammatory cells in the parietal pleura was observed. Clearance of GNPs from the pleural space to cranial mediastinal lymph nodes was observed. 1-week post administration, numerous small sized GNP fragments were observed in lymph nodes. This study shows that the toxicity of GNPs is dependent on the nanomaterial shape and size. The 2D size of GNPs leads to frustrated phagocytosis in lungs.

Duch et. al. have reported the pulmonary toxicity of three types of graphene (aggregated pristine graphene in water, pristine graphene in 2% pluronic and graphene oxide) administered via intratracheal instillation to male C56BL/6 mice at 50 μg/mouse dose [114]. After 24 hours of administration, mice were euthanized and lungs were analyzed by

histology and electron microscopy. Results show that the pulmonary toxicity of graphene varies as a function of dispersion and oxidation state. Highly dispersed pristine graphene in pluronic co-polymer solution induces an acute non-fibrotic lung inflammation, which is significantly lower compared to the local fibrotic response induced by aggregated graphene. Pristine graphene in dispersed or aggregated form does not induce apoptosis or ROS generation in lung macrophages. However, GO formulations lead to persistent lung injury that lasts > 21 days (Figure 14). These results suggest that compared to GO, the use of pristine graphene may reduce potential health risks associated with pulmonary exposure.

Li et. al. have analyzed the *in vivo* biodistribution and pulmonary toxicity of GO after intratracheal instillation in kunming mice at a dose of 0, 1, 5 or 10 mg/kg to evaluate dose-dependent acute and chronic pulmonary toxicity for 24 hours [115]. The authors have also evaluated time-dependent pulmonary toxicity by administering 10 mg/kg GO for 0, 24, 48, 72 hours and 1 week and chronic pulmonary toxicity at 10 mg/kg dose evaluated 1 and 3 months post instillation. Biodistribution was evaluated using SPECT imaging and pulmonary toxicity was assessed using histology and assays for cell injury, lung edema and neutrophil infiltration. Results show that GO was localized in the lungs even after 3 months of administration. Furthermore, GO induced a dose-dependent acute lung injury and resulted in chronic pulmonary fibrosis. A dose-dependent increase in neutrophils was observed in bronchoalveolar lavage fluid. Lung histopathological analysis showed alveolar septa thickening, extensive hemorrhage, changes in alveolar architecture and moderate interstitial edema. Furthermore, increases in the levels of superoxide dismutase and glutathione peroxidase were observed suggesting oxidative stress post 48 hours of GO administration. SPECT imaging showed that GO was mainly localized in the lungs with minor presence in other organs such as liver and intestines suggesting that GO can pass through the air-blood barrier. These results show that GO possesses severe pulmonary toxicity and appropriate steps must be taken to minimize human exposure to GO sources, especially during large-scale production.

4.5 Intravitreal administration

In intravitreal administration, a substance/formulation is administered directly into the eye using a needle. Yan et. al. have evaluated the ocular toxicity of GO after intravitreal administration in Japanese white rabbits at 0.1, 0.2, or 0.3 mg doses [116]. Eyes were reviewed for the effects of GO using a slit-lamp biomicroscopy and fundoscopy. Results show that GO did not have any effect on the corneas, interior media, posterior media, and the retina compared to the control group. The intraocular pressure showed no difference between the control and the experimental eye. Electroretinography (ERG) was performed to assess changes in the electrical impulse conduction in the eye. Compared to the controls, GO administration did not result in any significant changes in ERG amplitudes after 2, 7, 28 or 49 days of administration. H&E staining of eyes harvested 49 days post administration showed small amounts of GO residue, however, no retinal abnormality was observed.

5. Antimicrobial toxicity

Table 3 summarizes the studies assessing antimicrobial toxicity of graphene. Sawangphruk et. al. have investigated the antifungal activity of reduced graphene oxide (rGO) against *A. niger, A. oryzae,* and *F. oxysporum* between 0–500 μg/ml treatment concentrations [117]. Antifungal effects of rGO were assessed by quantifying mycelial growth inhibition. It was found that the rGO was effective against all three fungi with IC_{50} value between 50–100 μg/ml indicating a good antifungal activity of rGO (Figure 15). *A. niger* and *F. oxysporum* are pathogenic strains of fungi whereas *A. oryzae* is non-pathogenic, therefore; antifungal activity of rGO against *A. oryzae* could be a concern towards the development of graphene based broad spectrum antifungal agents. Akhavan et. al. have reported the antibacterial activity of graphene oxide nanowalls (GONWs) and reduced graphene oxide nanowalls (rGONWs) against E. *coli* and S. *aureus* [118]. Results show that bacterial cells are damaged by the direct contact of the cell membrane with extremely sharp edges of GO. Gram positive *S. aureus* without cell membrane showed greater cell death compared to gram positive *E. coli which* was more resistant due to the presence of outer membrane. Additionally, rGONWs were more toxic to bacterial cells than GONWs due to effective charge transfer between bacteria and edges of nanowalls during bacterial cell contact.

Cai et. al. have investigated the antibacterial activity of polyethyleneimine-modified reduced graphene oxide (PEI-rGO) and sliver nanoparticles functionalized PEI-rGO (PEI-rGO-AgNPs) against *E. coli* and *S. aureus* between 0–958 mg/L treatment concentration [119]. The results show that PEI-rGO-AgNPs are extremely effective in killing bacteria, >90% reduction in cell viability was observed for both *E. Coli* and *S. aureus* colonies at 958 mg/L concentration. The long term antibacterial activity of PEI-rGO-AgNPs was attributed to the damage of bacterial cell due to interactions with sharp blade like edges of GO which may facilitate effective interactions of Ag^+ ions with the intracellular contents, eventually killing bacteria. Chen et. al. have reported the dose-dependent antibacterial activity of GO and rGO against a rod shaped, gram negative phytopathogenic bacterium *Xanthomonas oryzae pv. Orzae* (*Xoo*) [120]. GO exhibited a greater antibacterial effect with ~94.5 and 86.4% cell mortality in DI water and 0.9% NaCl dispersions at 250μg/ml treatment concentration. rGO at 250μg/ml concentration resulted in 36.1 and 22.3% cell mortality Furthermore, an increased incubation time from 1 hour to 4 hours resulted in significant increases in the antibacterial activity of GO (from 19.4% to 66.1%) and rGO (13.8% to 30.5%). Further analysis by TEM and thiol quantification assay showed that GO resulted in physical damage and increased oxidative stress to bacterial cells. These results suggest that GO has a significantly greater dose- and time-dependent antibacterial activity compared to rGO.

Santos et. al. have investigated the antibacterial activity of poly(*N*-vinylcarbazole) graphene (PVK-G) solutions and thin films against *E. coli* and *B. subtilis* at concentrations between 0.01–1 mg/ml [121]. Results show a dose-dependent antibacterial effect of PVK-G solutions with~ 80% reduction in the percentage of metabolically active cells at 1 mg/ml treatment concentration. AFM imaging showed less bacterial coverage on PVK-G films compared to PVK and ITO (control) surfaces after 24 hours of incubation with *E coli*. Furthermore, PVK-G solutions at 1 mg/ml concentration showed ~ 80% cell viability of NIH3T3 fibroblast cells. These results show good antibacterial activity of PVK-G composites and thin films

and suggest a potential use of PVK-G nanocomposites for a wide variety of antibacterial applications where bactericidal properties along with good biocompatibility are desired. In another study, Carpio, Santos et. al. have investigated the antibacterial properties of PVK-graphene oxide (PVK-GO) nanocomposites between 10–1000 μg/ml treatment concentrations against *E coli, C metallidurans, B subtilis*, and *R opacus* [122]. The results of this study show a similar effect wherein addition of GO to PVK enhances the antimicrobial properties of the nanocomposite. PVK-GO nanocomposites in solution appear to effectively encapsulate the bacterial cells leading to reduction in microbial metabolic potential and eventual cell death. AFM imaging shows significant reduction in *E. coli* biomass after 48 hours of culture on PVK-GO films in comparison to PVK and ITO (controls) surfaces. Additionally, similar to PVK-G nanocomposites, PVK-GO nanocomposites are also cytocompatible (~90% cell viability of NIH3T3 cells was observed after 48 hours of exposure to PVK-GO solutions at 1000 μg/ml concentration).

Hu et. al. have investigated the antibacterial activity of GO and rGO nanosheets against *E. coli* cells at concentrations of 0, 20, and 85 μg/ml [123]. After 2 hours of incubation with GO at 20 and 85 μg/ml, the metabolic activity of *E. coli* cells (measured by luciferase-based ATP assay) decreased to ~70% and ~13%, respectively (Figure 16A). rGO exhibited antibacterial activity, 2 hours of incubation of *E. coli* cells with rGO solutions at 85 μg/ml resulted in only ~24% cell viability (Figure 16B). TEM studies show loss of cell integrity via physical damages to the cell membrane upon exposure to GO and rGO (Figure 16 C–E). Furthermore, cells cultured on GO and rGO paper also showed damages to cell membrane of bacteria. However, Mangadlao et. al. [124], Hui et. al. [125], and Li et. al. [126] have reported that antibacterial effect of GO films is not due to cell membrane rupture by graphene edges. The antibacterial effect is observed due to charge transfer between basal plane of graphene and bacterial cell body leading to inactivation of bacteria.

Kurantowicz et. al. have investigated the interactions of pristine graphene, graphene oxide (GO) and reduced graphene oxide (rGO) against food borne bacterial pathogens – *Listeria monocytogenes* and *Salmonella enterica* [127]. Bacteria were incubated with high (250 μg/ml) and low (25 μg/ml) treatment concentrations of pristine graphene, GO and rGO for 18 hours. At 250 μg/ml concentration, all nanomaterials consistently inhibited 100% growth of S. enterica and L monocytogenes. However, at lower concentration (25 μg/ml), only GO showed 100% inhibition of both bacteria. Pristine graphene inhibited the growth of S. enterica by 96.5% and L. monocytogenes by 54.5% whereas rGO inhibited the growth of L. monocytogenes by 91% and S. enterica by 46%. TEM results showed a uniform distribution of bacterial cells over the surface of GO whereas on the surface of pristine graphene and rGO, bacterial cells adhered to the edges and wrinkles of the graphene sheets. The authors hypothesize that the presence of oxidative functional groups throughout the surface of GO and on the edges of pristine graphene and rGO act as bait for attracting bacteria. After attaching to the flakes, cell may be damaged via direct contact or destabilization of the phospholipid cell membrane. These results show a functionalization state dependent antibacterial effect of graphene and GO.

Liu et. al. have investigated the time- and dose-dependent antibacterial activity of four types of graphene-based materials (graphite (Gt), graphite oxide (GtO), graphene oxide (GO), and

reduced graphene oxide (rGO)) against *E. coli* [128]. At 40 μg/ml treatment concentration after 2 hours of incubation, Gt, GtO, GO and rGO showed ~ 26.1 ± 4.8%, 15.0 ± 3.7%, 69.3 ± 6.1% and 45.9 ± 4.8%, respectively. After 4 hours, GO and rGO dispersions lead to ~ 89.7 ± 3.1% and 74.9 ± 4.8% inhibition of *E coli*. GO and rGO exhibit a concentration dependent antibacterial activity, cell mortality increases from 10.5 ± 6.6% to 91.6 ± 3.2% by increasing the GO concentration from 5 μg/ml to 80 μg/ml. Similarly, increases in rGO concentration from 5 μg/ml to 80 μg/ml leads to increased *E. coli* mortality from 8.4 ± 7.3% to 76.8 ± 3.1%. The antibacterial activity of GO and rGO was primarily due to inactivation of cellular functions due to loss of cell integrity. SEM imaging showed that direct contact of *E coli* cells with GO and rGO disrupts cell membrane (Figure 17). Additionally, graphene-based materials also oxidize glutathione, which is a redox mediator in bacterial cells, leading to oxidative stress. In another study, Liu et. al. investigated the lateral-dimension dependent antibacterial activity of GO [129]. The sizes of GO sheets used in this study were 0.753, 0.127, 0.065, 0.035, 0.013, and 0.010 μm^2, respectively. Results show that large GO sheets exhibit significantly greater antibacterial activity compared to small GO sheets. The results of both these investigations taken together suggest that GO and rGO are effective antibacterial agents and physiochemical properties such as functional group density, size, and morphology play an important role in influencing the antibacterial potential of graphene-based materials.

6. Environmental toxicity

The use of graphene for various industrial and healthcare applications would lead to increased environmental exposure and its disposal into waste streams. Therefore, it is important to assess the short- and long-term environmental toxicity of graphene and graphene-based materials and develop effective strategies to minimize any potential deleterious impact to flora and fauna. Table 4 summarizes the studies assessing environmental toxicity of graphene. Begum et. al. have investigated the phytotoxicity of graphene and its effects on root and shoot growth and shape, cell death and biomass by incubating seedlings of cabbage, tomatoes, red spinach and lettuce with 500–2000 mg/L for 20 days [130]. The results of physiological and morphological analysis show that graphene significantly inhibited plant growth and biomass production (Figure 18) and led to a reduction in the number and size of leaves in a dose-dependent manner. At 2000 mg/L concentration, ~18–78% root growth inhibition was observed depending on the plant species. Furthermore, leaves show wilting, necrotic lesions and reduction in leaf area. Graphene at high treatment concentrations (>500 mg/L) led to the production of reactive oxygen species leading to necrosis, loss of plasma membrane, and eventual cell death. No toxic effects were observed on lettuce at similar treatment concentrations. These results show that the phytotoxicity of graphene depends on the concentration, exposure time and plant species.

Khodakovskaya et. al. have investigated the toxicity of various carbon nanomaterials (activated carbon, graphene, single- and multi-walled carbon nanotubes) on the germination of tomato seedlings [131]. All nanomaterials were mixed with Murashige and Skoog (MS) growth medium at 50 μg/mL used to grow surface sterilized tomato seedlings. Examination of leaves and roots show that graphene (out of all materials tested) induced lowest activation

of stress-related *LeAqp2* gene (tomato water-channel protein); highest activation was observed for CNT groups. Photothermal and photoacoustic imaging studies show that graphene did not affect the plant growth rate due to the inability to penetrate plant tissues.

Mullick Chowdhury et. al. have evaluated the post-processing effects of graphene oxide nanoribbons (GONRs) dispersed in biological buffers using various sonication steps (bath sonication for 5 or 20 minutes or probe sonication for 5 or 10 minutes) on Medaka embryos [60]. Results show precocious hatching of the embryos when exposed to GONR solutions prepared by bath sonication. However, significant mortality (~50% increase in cell death) of the embryos was observed for GONR solutions prepared by probe sonication. AFM imaging showed the presence of smaller GONR particles and carbonaceous debris after probe sonication. Probe sonicated GONR solutions lead to structural damage of the chorionic membrane of embryos. These results suggest that post-processing steps of graphene such as high-energy sonication may lead to variable environmental toxicity.

Ahmed et. al. have investigated the effects of graphene oxide on the microbial community present in wastewater [132]. Efficient biological wastewater treatment requires functioning of diverse microbial species. Active sludge samples were incubated with 10–300 mg/L concentration of GO for 5 hours at room temperature to observe short-term toxicity. Results show a dose-dependent toxicity with significant reduction in bacterial metabolic activity, viability, and their capacity to effectively remove nutrients such as organics, phosphorous and nitrogen from activated sludge in the presence of GO. A dose-dependent reduction in the conversion of ammonia to nitrate was observed suggesting a reduction in the concentration of nitrifying bacteria. It was also observed that the presence of GO in wastewater led to deterioration of the quality of final wastewater effluent (increased turbidity was observed). Results also show that interaction of GO with wastewater sludge induced production of reactive oxygen species. These results show that the presence of GO loads in wastewater treatment sludge disrupts the functioning of antimicrobial community, which may lead to compromised treatment performance.

Hydrogen Peroxide (H_2O_2) is a naturally occurring ubiquitous compound found in rain and surface water, and in biological systems at concentrations ranging between 1 μM to 10000 μM. Xing et. al. have investigated the effects of hydrogen peroxide on the biodegradation of graphene [133]. TEM and AFM imaging studies show the presence of randomly distributed holes on graphene sheets in the presence of physiologically and environmentally relevant concentrations of H_2O_2 (Figure 19). After 10 hours of incubation with H_2O_2, the diameter of holes was between 1– 15 nm. An increase in the concentration of H_2O_2 from 1 μM to 10000 μM induced the formation of holes with significantly greater diameters (10–30 nm) suggesting a concentration dependent biodegradation of graphene. AFM studies show the depth of holes between 9.4–13.5 nm; greater than the height of a single graphene sheet (~0.34 nm). Therefore, based on these results, it was concluded that H_2O_2 attacked the inner layers of graphene along with the outer surface layers. Raman spectroscopy results show a progressive time- and concentration-dependent decrease in the intensity for both D and G band for all H_2O_2 treatment groups. The biodegradation of graphene by H_2O_2 may further be accelerated by the presence of trace elements such as nickel or iron (used as catalysts during the synthesis of graphene) by catalyzing the conversion of hydrogen peroxide to

hydroxyl radicals via the Haber-Weiss reaction. The results of this study show that multilayered graphene can undergo effective biodegradation at environmental and physiological concentrations of H_2O_2.

Lalwani et. al. have investigated the oxidative biodegradation of graphene oxide nanoribbons (GONRs) and reduced graphene oxide nanoribbons (rGONRs) by lignin peroxidase (LiP), an enzyme released by white rot fungi (*Phanerochaete chrysosporium*) distributed worldwide in forests soils with dead and decaying organic matter [134]. LiP degrades lignin – a component of plant cell wall. TEM (Figure 20) and Raman spectroscopy analysis of GONRs and rGONRs treated with LiP for 4–96 hours show the formation of holes confirming the structural degradation of graphene sheets. It was observed that GONRs showed a higher rate of biodegradation compared to rGONRs; numerous holes (1–5 nm diameter) were detected on GONR sheets within 4 hours of treatment which increased to ~300–350 nm after 48 hours. The diameter of holed on rGONRs was between 5–30 nm after 48 hours of enzymatic treatment. After 96 hours, GONRs appeared to have completely degraded whereas numerous holes extending throughout the width of rGONRs were observed. These results suggest that oxidized and reduced graphene nanoribbons released in the environment may undergo oxidative biodegradation by lignin peroxidase.

7. Mechanisms of toxicity

The interactions of graphene with cells, proteins, and other biomolecules is influenced by its physiochemical properties such as shape, size, functional group density and charge transfer abilities. The main mechanism of graphene toxicity is associated with the generation of intracellular reactive oxygen species that cause damage to proteins and DNA leading to cell death via apoptotic or necrotic pathways [83, 135, 136]. Graphene can be internalized into cells via passive internalization (endocytosis)[137, 138] or active internalization (clathrin mediated energy dependent endocytosis[139] or actin-dependent macropinocytosis[36]). Studies have elucidated two mechanism of graphene mediated ROS damage: (1) Upon cellular internalization, GO interferes with the electron transport system, induces overproduction of H_2O_2 and hydroxyl radicals. This leads to the oxidization of cardiolipin and the release and translocation of hemoprotein from mitochondrial inner membrane to the cytoplasm. This triggers release of cytochrome c complex (*cyt c*) which induces calcium release from endoplasmic reticulum and activates caspase 9 which in turn activates caspase 3 and 7 leading to cell death (Figure 21) [136]. (2) GO induces the activation of MAPK (JNK, ERK, p38) and TGF- β signaling pathways that lead to activation of Bcl-2 proteins which in turn activate mitochondria-induced apoptosis (Figure 22) [83]. In addition to ROS induced cell death, GO may also lead to the activation of toll-like receptors and induce autophagy via inflammatory pathways (Figure 23) [84]. Post internalization; graphene may induce DNA cleavage due to interactions such as pi-pi stacking, hydrophobicity, and electrostatic interactions [140–142]. Singh et. al. have shown that surface charge distribution on graphene sheets plays an important role in the activation of *src* kinases and release of calcium eventually leading to platelet aggregation (Figure 24) [87, 95].

Several studies have reported that extremely sharp edges of graphene lead to membrane destabilization and loss of cell integrity by direct contact [67, 118]. Wang et. al. have shown

that adsorption of GO on RBCs leads to the loss of cell membrane resulting in hemolysis [137]. Long sheets of graphene have also been observed to wrap around bacterial cells thereby inhibiting their growth [122]. Single layered GONRs exhibit greater cyto- and geno-toxicity due to the interactions between cells and sharp edges of nanoribbons resulting in extensive chromosomal aberration and DNA fragmentation [67]. Li et. al. have shown that graphene micro sheets enter cells through spontaneous membrane penetration at corner sites and edge asperities [143]. Molecular dynamics simulation studies have shown that graphene has a strong affinity for phospholipids and can be localized into the hydrophobic interior of biological membranes [144]. Tu et. al. have shown that due to strong interactions between graphene and lipids, graphene penetrates into and extracts significantly large amounts of phospholipids from cell membrane leading to cytotoxicity (Figure 25) [145]. Graphene quantum dots affect cellular function by inserting into cell membrane [146]; pristine GO has been reported to form aggregates on cell membrane thereby affecting cellular morphology [69]. rGO sheets inhibit the growth of fungal mycelium due to their direct insertion into the membrane of fungal cells [117].

8. Conclusion and Future Perspective

The studies till date indicate that toxicity of graphene could be dependent on the shape, size, purity, post-production processing steps, oxidative state, functional groups, dispersion state, synthesis methods, route and dose of administration, and exposure times. The morphology, shape and size of graphene nanoparticles could influence their cellular uptake characteristics whereas presence of functional groups can alter their interactions with proteins, biomolecules and micronutrients. The initial starting materials and the methods used in the production of oxidized graphene can result in the presence of metallic impurities and oxidative debris in the final product, which could result in variable toxicity effects. The post synthesis processing steps employed to disperse the nanoparticles in aqueous media could also influence toxicity. Reactive oxidation species mediated cell damage has been postulated as a primary cytotoxicity mechanism of graphene. Graphene sheets with sharp edges could induce direct physical damage and interact with phospholipids leading to membrane destabilization. Surface coating of graphene with several biocompatible moieties (e.g. natural polymers) can mitigate these cytotoxicity effects.

The studies taken together provide information on dosaging, biodistribution and pharmacology of various graphene-based formulations. It must be noted that even though there are many types of graphene nanoparticles, GO have been the most widely used for biomedical applications and studies that employ GO dominate the review. While majority of published literature on toxicity of other members of the graphene family have been reviewed herein, more toxicological studies on formulations of other types of graphene nanoparticles are warranted. Additionally, for all types of graphene nanoparticles, it is important to investigate and critically evaluate the potential short- and long-term health risks and toxicity hazards after acute, sub-acute and chronic exposures using *in vitro* and *in vivo* (small and large animal) models. Towards clinical translation of any graphene-based biomedical application that requires its systemic administration, formulations with high purity, dispersibility in aqueous media, and controlled physiochemical properties are highly desirable. For each of these formulations, regulatory compliance would require mapping of

their chemistry, manufacturing and control (CMC) process and completing new drug (IND)-enabling preclinical studies. With advancements in the synthesis methods and establishment of several commercial ventures for large-scale industrial production of graphene, the widespread use of graphene for several consumer products is becoming a reality. This ubiquitous use would lead to an increased environmental exposure of graphene. Therefore, more studies assessing the long-term environmental impact of graphene are required. Recent efforts have also involved incorporation of graphene nanoparticles in polymer matrices or their assembly in coating, films and porous scaffolds for bio-sensing, localized drug delivery or tissue engineering applications [147, 148]. For these applications, additional *in vitro* and *in vivo* toxicological studies specific to biomedical devices and implants would be needed. Finally, advances in graphene-like inorganic nanoparticles for biomedical applications allow opportunities to compare the biological response of graphene and its inorganic analogues [41, 43, 149–152]. All these studies will further advance the knowledge required to develop safe graphene-based technologies and products suitable for healthcare applications and to minimize the risks to human health.

Acknowledgments

The authors acknowledge the financial supp ort of National Institutes of Health (grant no. 1DP2OD007394-01) and Wallace H. Coulter Foundation.

References

1. Dresselhaus, MS.; Dresselhaus, G.; Eklund, PC. Science of fullerenes and carbon nanotubes: their properties and applications. Academic press; 1996.
2. Geim AK. Graphene: status and prospects. science. 2009; 324(5934):1530–1534. [PubMed: 19541989]
3. Lalwani G, Sitharaman B. Multifunctional Fullerene- and Metallofullerene-Based Nanobiomaterials. Nano LIFE. 2013; 3(3):1342003-1–1342003-22.
4. The rise and rise of graphene. Nat Nano. 2010; 5(11):755–755.
5. The Kavli Prize. Kavli Prize Laureates. Nanoscience. 2008 http://www kavliprize.org/prizes-and-laureates/prizes/2008-kavli-prize-laureates-nanoscience.
6. Geim AK, Novoselov KS. The rise of graphene. Nature materials. 2007; 6(3):183–191. [PubMed: 17330084]
7. Slonczewski J, Weiss P. Band structure of graphite. Physical Review. 1958; 109(2):272.
8. Peierls R. Quelques propriétés typiques des corps solides. Annales de l'institut Henri Poincaré. 1935
9. Landau L. Zur Theorie der phasenumwandlungen II. Phys. Z. Sowjetunion. 1937; 11:26–35.
10. Landau LD, Lifshitz E. Statistical physics, part I. Course of theoretical physics. 1980; 5:468.
11. Mermin ND. Crystalline order in two dimensions. Physical Review. 1968; 176(1):250.
12. Novoselov KS, Geim AK, Morozov S, Jiang D, Zhang Y, Dubonos Sa, Grigorieva I, Firsov A. Electric field effect in atomically thin carbon films. science. 2004; 306(5696):666–669. [PubMed: 15499015]
13. Novoselov K, Geim AK, Morozov S, Jiang D, Katsnelson M, Grigorieva I, Dubonos S, Firsov A. Two-dimensional gas of massless Dirac fermions in graphene. nature. 2005; 438(7065):197–200. [PubMed: 16281030]
14. Novoselov K, Jiang D, Schedin F, Booth T, Khotkevich V, Morozov S, Geim A. Two-dimensional atomic crystals. Proceedings of the National Academy of Sciences of the United States of America. 2005; 102(30):10451–10453. [PubMed: 16027370]
15. Johnson D. Europe Invests €1 Billion to Become “Graphene Valley”. IEEE Spectrum. 2013

16. Spasenovic M. South Korea To Spend US$40 Million On Graphene Development. Graphene Tracker. 2013
17. Brown M. Government announces £50m funding hub for UK graphene research. WIRED. 2011
18. HUAWEI. Huawei announces partnership with The University of Manchester to develop graphene-based technologies. 2015
19. Bolotin KI, Sikes K, Jiang Z, Klima M, Fudenberg G, Hone J, Kim P, Stormer H. Ultrahigh electron mobility in suspended graphene. Solid State Communications. 2008; 146(9):351–355.
20. Du X, Skachko I, Barker A, Andrei EY. Approaching ballistic transport in suspended graphene. Nature nanotechnology. 2008; 3(8):491–495.
21. Stoller MD, Park S, Zhu Y, An J, Ruoff RS. Graphene-based ultracapacitors. Nano letters. 2008; 8(10):3498–3502. [PubMed: 18788793]
22. Ponomarenko L, Geim A, Zhukov A, Jalil R, Morozov S, Novoselov K, Grigorieva I, Hill E, Cheianov V, Fal'Ko V. Tunable metal-insulator transition in double-layer graphene heterostructures. Nature Physics. 2011; 7(12):958–961.
23. Zhang Y, Tan Y-W, Stormer HL, Kim P. Experimental observation of the quantum Hall effect and Berry's phase in graphene. Nature. 2005; 438(7065):201–204. [PubMed: 16281031]
24. Balandin AA, Ghosh S, Bao W, Calizo I, Teweldebrhan D, Miao F, Lau CN. Superior thermal conductivity of single-layer graphene. Nano letters. 2008; 8(3):902–907. [PubMed: 18284217]
25. Lee C, Wei X, Kysar JW, Hone J. Measurement of the elastic properties and intrinsic strength of monolayer graphene. science. 2008; 321(5887):385–388. [PubMed: 18635798]
26. Nair R, Blake P, Grigorenko A, Novoselov K, Booth T, Stauber T, Peres N, Geim A. Fine structure constant defines visual transparency of graphene. Science. 2008; 320(5881):1308–1308. [PubMed: 18388259]
27. Avouris P, Dimitrakopoulos C. Graphene: synthesis and applications. Materials today. 2012; 15(3): 86–97.
28. Subrahmanyam K, Panchakarla L, Govindaraj A, Rao C. Simple method of preparing graphene flakes by an arc-discharge method. The Journal of Physical Chemistry C. 2009; 113(11):4257–4259.
29. Kim KS, Zhao Y, Jang H, Lee SY, Kim JM, Kim KS, Ahn J-H, Kim P, Choi J-Y, Hong BH. Large-scale pattern growth of graphene films for stretchable transparent electrodes. Nature. 2009; 457(7230):706–710. [PubMed: 19145232]
30. Stankovich S, Dikin DA, Piner RD, Kohlhaas KA, Kleinhammes A, Jia Y, Wu Y, Nguyen ST, Ruoff RS. Synthesis of graphene-based nanosheets via chemical reduction of exfoliated graphite oxide. Carbon. 2007; 45(7):1558–1565.
31. Kosynkin DV, Higginbotham AL, Sinitskii A, Lomeda JR, Dimiev A, Price BK, Tour JM. Longitudinal unzipping of carbon nanotubes to form graphene nanoribbons. Nature. 2009; 458(7240):872–876. [PubMed: 19370030]
32. Pei S, Cheng H-M. The reduction of graphene oxide. Carbon. 2012; 50(9):3210–3228.
33. Kanakia S, Toussaint JD, Chowdhury SM, Lalwani G, Tembulkar T, Button T, Shroyer KR, Moore W, Sitharaman B. Physicochemical characterization of a novel graphene-based magnetic resonance imaging contrast agent. International journal of nanomedicine. 2013; 8:2821. [PubMed: 23946653]
34. Lalwani G, Cai X, Nie L, Wang LV, Sitharaman B. Graphene-based contrast agents for photoacoustic and thermoacoustic tomography. Photoacoustics. 2013; 1(3):62–67. [PubMed: 24490141]
35. Lalwani G, Sundararaj JL, Schaefer K, Button T, Sitharaman B. Synthesis, characterization, in vitro phantom imaging, and cytotoxicity of a novel graphene-based multimodal magnetic resonance imaging-X-ray computed tomography contrast agent. Journal of Materials Chemistry B. 2014; 2(22):3519–3530.
36. Mullick Chowdhury S, Lalwani G, Zhang K, Yang JY, Neville K, Sitharaman B. Cell specific cytotoxicity and uptake of graphene nanoribbons. Biomaterials. 2013; 34(1):283–293. [PubMed: 23072942]
37. Chowdhury SM, Surhland C, Sanchez Z, Chaudhary P, Kumar MS, Lee S, Peña LA, Waring M, Sitharaman B, Naidu M. Graphene nanoribbons as a drug delivery agent for lucanthone mediated

therapy of glioblastoma multiforme. Nanomedicine: Nanotechnology, Biology and Medicine. 2015; 11(1):109–118.

38. Feng L, Zhang S, Liu Z. Graphene based gene transfection. Nanoscale. 2011; 3(3):1252–1257. [PubMed: 21270989]
39. Tian B, Wang C, Zhang S, Feng L, Liu Z. Photothermally enhanced photodynamic therapy delivered by nano-graphene oxide. ACS nano. 2011; 5(9):7000–7009. [PubMed: 21815655]
40. Huang P, Xu C, Lin J, Wang C, Wang X, Zhang C, Zhou X, Guo S, Cui D. Folic acid-conjugated graphene oxide loaded with photosensitizers for targeting photodynamic therapy. Theranostics. 2011; 1:240. [PubMed: 21562631]
41. Lalwani G, Henslee AM, Farshid B, Lin L, Kasper FK, Qin Y-X, Mikos AG, Sitharaman B. Two-Dimensional Nanostructure-Reinforced Biodegradable Polymeric Nanocomposites for Bone Tissue Engineering. Biomacromolecules. 2013; 14(3):900–909. [PubMed: 23405887]
42. Patel SC, Lalwani G, Grover K, Qin Y-X, Sitharaman B. Fabrication and cytocompatibility of in situ crosslinked carbon nanomaterial films. Scientific Reports. 2015; 5
43. Farshid B, Lalwani G, Sitharaman B. In vitro cytocompatibility of one-dimensional and two - dimensional nanostructure - reinforced biodegradable polymeric nanocomposites. Journal of Biomedical Materials Research Part A. 2015; 103(7):2309–2321. [PubMed: 25367032]
44. Talukdar Y, Rashkow JT, Lalwani G, Kanakia S, Sitharaman B. The effects of graphene nanostructures on mesenchymal stem cells. Biomaterials. 2014; 35(18):4863–4877. [PubMed: 24674462]
45. Nayak TR, Andersen H, Makam VS, Khaw C, Bae S, Xu X, Ee P-LR, Ahn J-H, Hong BH, Pastorin G. Graphene for controlled and accelerated osteogenic differentiation of human mesenchymal stem cells. ACS nano. 2011; 5(6):4670–4678. [PubMed: 21528849]
46. Yang Y, Asiri AM, Tang Z, Du D, Lin Y. Graphene based materials for biomedical applications. Materials today. 2013; 16(10):365–373.
47. Yang K, Feng L, Shi X, Liu Z. Nano-graphene in biomedicine: theranostic applications. Chemical Society Reviews. 2013; 42(2):530–547. [PubMed: 23059655]
48. Hu X, Zhou Q. Health and ecosystem risks of graphene. Chemical reviews. 2013; 113(5):3815–3835. [PubMed: 23327673]
49. Seabra AB, Paula AJ, de Lima R, Alves OL, Durán N. Nanotoxicity of graphene and graphene oxide. Chemical research in toxicology. 2014; 27(2):159–168. [PubMed: 24422439]
50. Zhao J, Wang Z, White JC, Xing B. Graphene in the aquatic environment: adsorption, dispersion, toxicity and transformation. Environmental science & technology. 2014; 48(17):9995–10009. [PubMed: 25122195]
51. Tonelli FM, Goulart VA, Gomes KN, Ladeira MS, Santos AK, Lorençon E, Ladeira LO, Resende RR. Graphene-based nanomaterials: biological and medical applications and toxicity. Nanomedicine. 2015; 10(15):2423–2450. [PubMed: 26244905]
52. Bitounis D, Ali-Boucetta H, Hong BH, Min DH, Kostarelos K. Prospects and challenges of graphene in biomedical applications. Advanced Materials. 2013; 25(16):2258–2268. [PubMed: 23494834]
53. Bianco A. Graphene: safe or toxic? The two faces of the medal. Angewandte Chemie International Edition. 2013; 52(19):4986–4997.
54. Yang K, Li Y, Tan X, Peng R, Liu Z. Behavior and toxicity of graphene and its functionalized derivatives in biological systems. Small. 2013; 9(9 – 10):1492–1503. [PubMed: 22987582]
55. Sanchez VC, Jachak A, Hurt RH, Kane AB. Biological interactions of graphene-family nanomaterials: an interdisciplinary review. Chemical research in toxicology. 2011; 25(1):15–34. [PubMed: 21954945]
56. Jastrzębska AM, Kurtycz P, Olszyna AR. Recent advances in graphene family materials toxicity investigations. Journal of Nanoparticle Research. 2012; 14(12):1–21. [PubMed: 22448125]
57. Zhang B, Wang Y, Zhai G. Biomedical applications of the graphene-based materials. Materials Science and Engineering: C. 2015
58. Wong CHA, Sofer Z, Kubešová M, Kučera J, Matějková S, Pumera M. Synthetic routes contaminate graphene materials with a whole spectrum of unanticipated metallic elements. Proceedings of the National Academy of Sciences. 2014; 111(38):13774–13779.

59. Ambrosi A, Chua CK, Khezri B, Sofer Z, Webster RD, Pumera M. Chemically reduced graphene contains inherent metallic impurities present in parent natural and synthetic graphite. Proceedings of the National Academy of Sciences. 2012; 109(32):12899–12904.
60. Mullick Chowdhury S, Dasgupta S, McElroy AE, Sitharaman B. Structural disruption increases toxicity of graphene nanoribbons. Journal of Applied Toxicology. 2014; 34(11):1235–1246. [PubMed: 25224919]
61. Zhang Y, Ali SF, Dervishi E, Xu Y, Li Z, Casciano D, Biris AS. Cytotoxicity effects of graphene and single-wall carbon nanotubes in neural phaeochromocytoma-derived PC12 cells. ACS Nano. 2010; 4(6):3181–3186. [PubMed: 20481456]
62. Vallabani NV, Mittal S, Shukla RK, Pandey AK, Dhakate SR, Pasricha R, Dhawan A. Toxicity of graphene in normal human lung cells (BEAS-2B). J Biomed Nanotechnol. 2011; 7(1):106–107. [PubMed: 21485826]
63. Yuan J, Gao H, Sui J, Duan H, Chen WN, Ching CB. Cytotoxicity evaluation of oxidized single-walled carbon nanotubes and graphene oxide on human hepatoma HepG2 cells: an iTRAQ-coupled 2D LC-MS/MS proteome analysis. Toxicol Sci. 2012; 126(1):149–161. [PubMed: 22157353]
64. Lv M, Zhang Y, Liang L, Wei M, Hu W, Li X, Huang Q. Effect of graphene oxide on undifferentiated and retinoic acid-differentiated SH-SY5Y cells line. Nanoscale. 2012; 4(13): 3861–3866. [PubMed: 22653613]
65. Talukdar Y, Rashkow JT, Lalwani G, Kanakia S, Sitharaman B. The effects of graphene nanostructures on mesenchymal stem cells. Biomaterials. 2014; 35(18):4863–4877. [PubMed: 24674462]
66. Chng ELK, Chua CK, Pumera M. Graphene oxide nanoribbons exhibit significantly greater toxicity than graphene oxide nanoplatelets. Nanoscale. 2014; 6(18):10792–10797. [PubMed: 25104246]
67. Akhavan O, Ghaderi E, Emamy H, Akhavan F. Genotoxicity of graphene nanoribbons in human mesenchymal stem cells. Carbon. 2013; 54:419–431.
68. Jaworski S, Sawosz E, Grodzik M, Winnicka A, Prasek M, Wierzbicki M, Chwalibog A. In vitro evaluation of the effects of graphene platelets on glioblastoma multiforme cells. Int J Nanomedicine. 2013; 8:413–420. [PubMed: 23378763]
69. Sasidharan A, Panchakarla LS, Chandran P, Menon D, Nair S, Rao CN, Koyakutty M. Differential nano-bio interactions and toxicity effects of pristine versus functionalized graphene. Nanoscale. 2011; 3(6):2461–2464. [PubMed: 21562671]
70. Matesanz MC, Vila M, Feito MJ, Linares J, Goncalves G, Vallet-Regi M, Marques PA, Portoles MT. The effects of graphene oxide nanosheets localized on F-actin filaments on cell-cycle alterations. Biomaterials. 2013; 34(5):1562–1569. [PubMed: 23177613]
71. Yuan X, Liu Z, Guo Z, Ji Y, Jin M, Wang X. Cellular distribution and cytotoxicity of graphene quantum dots with different functional groups. Nanoscale research letters. 2014; 9(1):1–9. [PubMed: 24380376]
72. Horváth L, Magrez A, Burghard M, Kern K, Forró L, Schwaller B. Evaluation of the toxicity of graphene derivatives on cells of the lung luminal surface. Carbon. 2013; 64:45–60.
73. Das S, Singh S, Singh V, Joung D, Dowding JM, Reid D, Anderson J, Zhai L, Khondaker SI, Self WT. Oxygenated functional group density on graphene oxide: its effect on cell toxicity. Particle & Particle Systems Characterization. 2013; 30(2):148–157.
74. Chong Y, Ma Y, Shen H, Tu X, Zhou X, Xu J, Dai J, Fan S, Zhang Z. The in vitro and in vivo toxicity of graphene quantum dots. Biomaterials. 2014; 35(19):5041–5048. [PubMed: 24685264]
75. Teo WZ, Chng ELK, Sofer Z, Pumera M. Cytotoxicity of halogenated graphenes. Nanoscale. 2014; 6(2):1173–1180. [PubMed: 24296830]
76. Teo WZ, Sofer Z, Šembera F, Janoušek Z, Pumera M. Cytotoxicity of fluorographene. RSC Advances. 2015; 5(129):107158–107165.
77. Chng ELK, Sofer Z, Pumera M. Cytotoxicity profile of highly hydrogenated graphene. Chemistry–A European Journal. 2014; 20(21):6366–6373.
78. Sawosz E, Jaworski S, Kutwin M, Vadalasetty KP, Grodzik M, Wierzbicki M, Kurantowicz N, Strojny B, Hotowy A, Lipińska L. Graphene Functionalized with Arginine Decreases the

Development of Glioblastoma Multiforme Tumor in a Gene-Dependent Manner. International journal of molecular sciences. 2015; 16(10):25214–25233. [PubMed: 26512645]

79. Akhavan O, Ghaderi E, Akhavan A. Size-dependent genotoxicity of graphene nanoplatelets in human stem cells. Biomaterials. 2012; 33(32):8017–8025. [PubMed: 22863381]
80. Chang Y, Yang ST, Liu JH, Dong E, Wang Y, Cao A, Liu Y, Wang H. In vitro toxicity evaluation of graphene oxide on A549 cells. Toxicol Lett. 2011; 200(3):201–210. [PubMed: 21130147]
81. Yue H, Wei W, Yue Z, Wang B, Luo N, Gao Y, Ma D, Ma G, Su Z. The role of the lateral dimension of graphene oxide in the regulation of cellular responses. Biomaterials. 2012; 33(16): 4013–4021. [PubMed: 22381473]
82. Zhi X, Fang H, Bao C, Shen G, Zhang J, Wang K, Guo S, Wan T, Cui D. The immunotoxicity of graphene oxides and the effect of PVP-coating. Biomaterials. 2013; 34(21):5254–5261. [PubMed: 23566800]
83. Li Y, Liu Y, Fu Y, Wei T, Le Guyader L, Gao G, Liu RS, Chang YZ, Chen C. The triggering of apoptosis in macrophages by pristine graphene through the MAPK and TGF-beta signaling pathways. Biomaterials. 2012; 33(2):402–411. [PubMed: 22019121]
84. Chen GY, Yang HJ, Lu CH, Chao YC, Hwang SM, Chen CL, Lo KW, Sung LY, Luo WY, Tuan HY, Hu YC. Simultaneous induction of autophagy and toll-like receptor signaling pathways by graphene oxide. Biomaterials. 2012; 33(27):6559–6569. [PubMed: 22704844]
85. Tkach AV, Yanamala N, Stanley S, Shurin MR, Shurin GV, Kisin ER, Murray AR, Pareso S, Khaliullin T, Kotchey GP, Castranova V, Mathur S, Fadeel B, Star A, Kagan VE, Shvedova AA. Graphene oxide, but not fullerenes, targets immunoproteasomes and suppresses antigen presentation by dendritic cells. Small. 2013; 9(9–10):1686–1690. [PubMed: 22887961]
86. Liao KH, Lin YS, Macosko CW, Haynes CL. Cytotoxicity of graphene oxide and graphene in human erythrocytes and skin fibroblasts. ACS Appl Mater Interfaces. 2011; 3(7):2607–2615. [PubMed: 21650218]
87. Singh SK, Singh MK, Nayak MK, Kumari S, Shrivastava S, Gracio JJ, Dash D. Thrombus inducing property of atomically thin graphene oxide sheets. ACS Nano. 2011; 5(6):4987–4996. [PubMed: 21574593]
88. Singh SK, Singh MK, Kulkarni PP, Sonkar VK, Gracio JJ, Dash D. Amine-modified graphene: thrombo-protective safer alternative to graphene oxide for biomedical applications. ACS Nano. 2012; 6(3):2731–2740. [PubMed: 22376049]
89. Chowdhury SM, Kanakia S, Toussaint JD, Frame MD, Dewar AM, Shroyer KR, Moore W, Sitharaman B. In vitro hematological and in vivo vasoactivity assessment of dextran functionalized graphene. Scientific reports. 2013; 3
90. Chowdhury SM, Fang J, Sitharaman B. Interaction of graphene nanoribbons with components of the blood vascular system. Future Science OA. 2015; 1(3)
91. Wojtoniszak M, Chen X, Kalenczuk RJ, Wajda A, Lapczuk J, Kurzewski M, Drozdzik M, Chu PK, Borowiak-Palen E. Synthesis, dispersion, and cytocompatibility of graphene oxide and reduced graphene oxide. Colloids Surf B Biointerfaces. 2012; 89:79–85. [PubMed: 21962852]
92. Hu W, Peng C, Lv M, Li X, Zhang Y, Chen N, Fan C, Huang Q. Protein corona-mediated mitigation of cytotoxicity of graphene oxide. ACS Nano. 2011; 5(5):3693–3700. [PubMed: 21500856]
93. Mu Q, Su G, Li L, Gilbertson BO, Yu LH, Zhang Q, Sun YP, Yan B. Size-dependent cell uptake of protein-coated graphene oxide nanosheets. ACS Appl Mater Interfaces. 2012; 4(4):2259–2266. [PubMed: 22409495]
94. Mbeh DA, Akhavan O, Javanbakht T, Mahmoudi M, Yahia LH. Cytotoxicity of protein corona-graphene oxide nanoribbons on human epithelial cells. Applied Surface Science. 2014; 320:596–601.
95. Singh SK, Singh MK, Kulkarni PP, Sonkar VK, Grácio JJ, Dash D. Amine-modified graphene: thrombo-protective safer alternative to graphene oxide for biomedical applications. Acs Nano. 2012; 6(3):2731–2740. [PubMed: 22376049]
96. Sasidharan A, Swaroop S, Koduri CK, Girish CM, Chandran P, Panchakarla L, Somasundaram VH, Gowd GS, Nair S, Koyakutty M. Comparative in vivo toxicity, organ biodistribution and

immune response of pristine, carboxylated and PEGylated few-layer graphene sheets in Swiss albino mice: A three month study. Carbon. 2015; 95:511–524.

97. Zhang S, Yang K, Feng L, Liu Z. In vitro and in vivo behaviors of dextran functionalized graphene. Carbon. 2011; 49(12):4040–4049.
98. Zhang X, Yin J, Peng C, Hu W, Zhu Z, Li W, Fan C, Huang Q. Distribution and biocompatibility studies of graphene oxide in mice after intravenous administration. Carbon. 2011; 49(3):986–995.
99. Wang K, Ruan J, Song H, Zhang J, Wo Y, Guo S, Cui D. Biocompatibility of graphene oxide. Nanoscale Res Lett. 2011; 6(8):1–8.
100. Liu J-H, Yang S-T, Wang H, Chang Y, Cao A, Liu Y. Effect of size and dose on the biodistribution of graphene oxide in mice. Nanomedicine. 2012; 7(12):1801–1812. [PubMed: 22830500]
101. Yang K, Zhang S, Zhang G, Sun X, Lee S-T, Liu Z. Graphene in mice: ultrahigh in vivo tumor uptake and efficient photothermal therapy. Nano letters. 2010; 10(9):3318–3323. [PubMed: 20684528]
102. Yang K, Wan J, Zhang S, Zhang Y, Lee S-T, Liu Z. In vivo pharmacokinetics, long-term biodistribution, and toxicology of PEGylated graphene in mice. ACS nano. 2010; 5(1):516–522. [PubMed: 21162527]
103. Kanakia S, Toussaint J, Hoang DM, Mullick Chowdhury S, Lee S, Shroyer KR, Moore W, Wadghiri YZ, Sitharaman B. Towards An Advanced Graphene-Based Magnetic Resonance Imaging Contrast Agent: Sub-acute Toxicity and Efficacy Studies in Small Animals. Scientific Reports. 2015; 5:17182. [PubMed: 26625867]
104. Kanakia S, Toussaint JD, Chowdhury SM, Tembulkar T, Lee S, Jiang Y-P, Lin RZ, Shroyer KR, Moore W, Sitharaman B. Dose ranging, expanded acute toxicity and safety pharmacology studies for intravenously administered functionalized graphene nanoparticle formulations. Biomaterials. 2014; 35(25):7022–7031. [PubMed: 24854092]
105. Jasim DA, Ménard-Moyon C, Bégin D, Bianco A, Kostarelos K. Tissue distribution and urinary excretion of intravenously administered chemically functionalized graphene oxide sheets. Chemical Science. 2015
106. Yang K, Gong H, Shi X, Wan J, Zhang Y, Liu Z. In vivo biodistribution and toxicology of functionalized nano-graphene oxide in mice after oral and intraperitoneal administration. Biomaterials. 2013; 34(11):2787–2795. [PubMed: 23340196]
107. Ali-Boucetta H, Bitounis D, Raveendran-Nair R, Servant A, Van den Bossche J, Kostarelos K. Purified graphene oxide dispersions lack in vitro cytotoxicity and in vivo pathogenicity. Advanced healthcare materials. 2013; 2(3):433–441. [PubMed: 23184580]
108. Sahu A, Choi WI, Tae G. A stimuli-sensitive injectable graphene oxide composite hydrogel. Chemical Communications. 2012; 48(47):5820–5822. [PubMed: 22549512]
109. Strojny B, Kurantowicz N, Sawosz E, Grodzik M, Jaworski S, Kutwin M, Wierzbicki M, Hotowy A, Lipińska L, Chwalibog A. Long Term Influence of Carbon Nanoparticles on Health and Liver Status in Rats. PloS one. 2015; 10(12):e0144821. [PubMed: 26657282]
110. Fu C, Liu T, Li L, Liu H, Liang Q, Meng X. Effects of graphene oxide on the development of offspring mice in lactation period. Biomaterials. 2015; 40:23–31. [PubMed: 25498802]
111. Zhang D, Zhang Z, Liu Y, Chu M, Yang C, Li W, Shao Y, Yue Y, Xu R. The short- and long-term effects of orally administered high-dose reduced graphene oxide nanosheets on mouse behaviors. Biomaterials. 2015; 68:100–113. [PubMed: 26276695]
112. Wu Q, Yin L, Li X, Tang M, Zhang T, Wang D. Contributions of altered permeability of intestinal barrier and defecation behavior to toxicity formation from graphene oxide in nematode Caenorhabditis elegans. Nanoscale. 2013; 5(20):9934–9943. [PubMed: 23986404]
113. Schinwald A, Murphy FA, Jones A, MacNee W, Donaldson K. Graphene-based nanoplatelets: a new risk to the respiratory system as a consequence of their unusual aerodynamic properties. ACS nano. 2012; 6(1):736–746. [PubMed: 22195731]
114. Duch MC, Budinger GS, Liang YT, Soberanes S, Urich D, Chiarella SE, Campochiaro LA, Gonzalez A, Chandel NS, Hersam MC. Minimizing oxidation and stable nanoscale dispersion improves the biocompatibility of graphene in the lung. Nano letters. 2011; 11(12):5201–5207. [PubMed: 22023654]

115. Li B, Yang J, Huang Q, Zhang Y, Peng C, Zhang Y, He Y, Shi J, Li W, Hu J. Biodistribution and pulmonary toxicity of intratracheally instilled graphene oxide in mice. NPG Asia Materials. 2013; 5(4):e44.
116. Yan L, Wang Y, Xu X, Zeng C, Hou J, Lin M, Xu J, Sun F, Huang X, Dai L. Can graphene oxide cause damage to eyesight? Chemical research in toxicology. 2012; 25(6):1265–1270. [PubMed: 22587431]
117. Sawangphruk M, Srimuk P, Chiochan P, Sangsri T, Siwayaprahm P. Synthesis and antifungal activity of reduced graphene oxide nanosheets. Carbon. 2012; 50(14):5156–5161.
118. Akhavan O, Ghaderi E. Toxicity of graphene and graphene oxide nanowalls against bacteria. ACS nano. 2010; 4(10):5731–5736. [PubMed: 20925398]
119. Cai X, Lin M, Tan S, Mai W, Zhang Y, Liang Z, Lin Z, Zhang X. The use of polyethyleneimine-modified reduced graphene oxide as a substrate for silver nanoparticles to produce a material with lower cytotoxicity and long-term antibacterial activity. Carbon. 2012; 50(10):3407–3415.
120. Chen J, Wang X, Han H. A new function of graphene oxide emerges: inactivating phytopathogenic bacterium Xanthomonas oryzae pv. Oryzae. Journal of nanoparticle research. 2013; 15(5):1–14.
121. Santos CM, Mangadlao J, Ahmed F, Leon A, Advincula RC, Rodrigues DF. Graphene nanocomposite for biomedical applications: fabrication, antimicrobial and cytotoxic investigations. Nanotechnology. 2012; 23(39):395101. [PubMed: 22962260]
122. Carpio IEM, Santos CM, Wei X, Rodrigues DF. Toxicity of a polymer–graphene oxide composite against bacterial planktonic cells, biofilms, and mammalian cells. Nanoscale. 2012; 4(15):4746–4756. [PubMed: 22751735]
123. Hu W, Peng C, Luo W, Lv M, Li X, Li D, Huang Q, Fan C. Graphene-based antibacterial paper. Acs Nano. 2010; 4(7):4317–4323. [PubMed: 20593851]
124. áde Leon A. On the antibacterial mechanism of graphene oxide (GO) Langmuir– Blodgett films. Chemical Communications. 2015; 51(14):2886–2889. [PubMed: 25582092]
125. Hui L, Piao JG, Auletta J, Hu K, Zhu Y, Meyer T, Liu H, Yang L. Availability of the basal planes of graphene oxide determines whether it is antibacterial. ACS Appl Mater Interfaces. 2014; 6(15):13183–13190. [PubMed: 25026597]
126. Li J, Wang G, Zhu H, Zhang M, Zheng X, Di Z, Liu X, Wang X. Antibacterial activity of large-area monolayer graphene film manipulated by charge transfer. Sci Rep. 2014; 4:4359. [PubMed: 24619247]
127. Kurantowicz N, Sawosz E, Jaworski S, Kutwin M, Strojny B, Wierzbicki M, Szeliga J, Hotowy A, Lipińska L, Koziński R. Interaction of graphene family materials with Listeria monocytogenes and Salmonella enterica. Nanoscale research letters. 2015; 10(1):1–12. [PubMed: 25977644]
128. Liu S, Zeng TH, Hofmann M, Burcombe E, Wei J, Jiang R, Kong J, Chen Y. Antibacterial activity of graphite, graphite oxide, graphene oxide, and reduced graphene oxide: membrane and oxidative stress. Acs Nano. 2011; 5(9):6971–6980. [PubMed: 21851105]
129. Liu S, Hu M, Zeng TH, Wu R, Jiang R, Wei J, Wang L, Kong J, Chen Y. Lateral dimension-dependent antibacterial activity of graphene oxide sheets. Langmuir. 2012; 28(33):12364–12372. [PubMed: 22827339]
130. Begum P, Ikhtiari R, Fugetsu B. Graphene phytotoxicity in the seedling stage of cabbage, tomato, red spinach, and lettuce. Carbon. 2011; 49(12):3907–3919.
131. Khodakovskaya MV, de Silva K, Nedosekin DA, Dervishi E, Biris AS, Shashkov EV, Galanzha EI, Zharov VP. Complex genetic, photothermal, and photoacoustic analysis of nanoparticle-plant interactions. Proceedings of the National Academy of Sciences. 2011; 108(3):1028–1033.
132. Ahmed F, Rodrigues DF. Investigation of acute effects of graphene oxide on wastewater microbial community: a case study. Journal of hazardous materials. 2013; 256:33–39. [PubMed: 23669788]
133. Xing W, Lalwani G, Rusakova I, Sitharaman B. Degradation of Graphene by Hydrogen Peroxide. Particle & Particle Systems Characterization. 2014; 31(7):745–750.
134. Lalwani G, Xing W, Sitharaman B. Enzymatic degradation of oxidized and reduced graphene nanoribbons by lignin peroxidase. Journal of Materials Chemistry B. 2014; 2(37):6354–6362.
135. Ma Y, Shen H, Tu X, Zhang Z. Assessing in vivo toxicity of graphene materials: current methods and future outlook. Nanomedicine. 2014; 9(10):1565–1580. [PubMed: 25253502]

136. Zhang W, Wang C, Li Z, Lu Z, Li Y, Yin JJ, Zhou YT, Gao X, Fang Y, Nie G. Unraveling Stress-Induced Toxicity Properties of Graphene Oxide and the Underlying Mechanism. Advanced Materials. 2012; 24(39):5391–5397. [PubMed: 22927326]

137. Wang T, Zhu S, Jiang X. Toxicity mechanism of graphene oxide and nitrogen-doped graphene quantum dots in RBCs revealed by surface-enhanced infrared absorption spectroscopy. Toxicology Research. 2015

138. Liu K, Zhang J-J, Cheng F-F, Zheng T-T, Wang C, Zhu J-J. Green and facile synthesis of highly biocompatible graphene nanosheets and its application for cellular imaging and drug delivery. Journal of Materials Chemistry. 2011; 21(32):12034–12040.

139. Huang J, Zong C, Shen H, Liu M, Chen B, Ren B, Zhang Z. Mechanism of Cellular Uptake of Graphene Oxide Studied by Surface - Enhanced Raman Spectroscopy. Small. 2012; 8(16):2577–2584. [PubMed: 22641430]

140. Ren H, Wang C, Zhang J, Zhou X, Xu D, Zheng J, Guo S, Zhang J. DNA cleavage system of nanosized graphene oxide sheets and copper ions. ACS nano. 2010; 4(12):7169–7174. [PubMed: 21082807]

141. Zhang L, Wang Z, Lu Z, Shen H, Huang J, Zhao Q, Liu M, He N, Zhang Z. PEGylated reduced graphene oxide as a superior ssRNA delivery system. Journal of Materials Chemistry B. 2013; 1(6):749–755.

142. Wu M, Kempaiah R, Huang P-JJ, Maheshwari V, Liu J. Adsorption and desorption of DNA on graphene oxide studied by fluorescently labeled oligonucleotides. Langmuir. 2011; 27(6):2731–2738. [PubMed: 21302946]

143. Li Y, Yuan H, von dem Bussche A, Creighton M, Hurt RH, Kane AB, Gao H. Graphene microsheets enter cells through spontaneous membrane penetration at edge asperities and corner sites. Proceedings of the National Academy of Sciences. 2013; 110(30):12295–12300.

144. Titov AV, Král P, Pearson R. Sandwiched graphene– membrane superstructures. ACS nano. 2009; 4(1):229–234. [PubMed: 20025267]

145. Tu Y, Lv M, Xiu P, Huynh T, Zhang M, Castelli M, Liu Z, Huang Q, Fan C, Fang H. Destructive extraction of phospholipids from Escherichia coli membranes by graphene nanosheets. Nature nanotechnology. 2013; 8(8):594–601.

146. Nurunnabi M, Khatun Z, Huh KM, Park SY, Lee DY, Cho KJ, Lee Y-k. In vivo biodistribution and toxicology of carboxylated graphene quantum dots. ACS nano. 2013; 7(8):6858–6867. [PubMed: 23829293]

147. Lalwani G, Patel SC, Sitharaman B. Two- and Three-Dimensional All-Carbon Nanomaterial Assemblies for Tissue Engineering and Regenerative Medicine. Annals of Biomedical Engineering - Accepted Manuscript. 2016

148. Lalwani G, D'Agati M, Gopalan A, Rao M, Schneller J, Sitharaman B. Three-Dimensional Macroporous Graphene Scaffolds for Tissue Engineering. Journal of Biomedical Materials Research Part A - Accepted Manuscript. 2016

149. Farshid B, Lalwani G, Shir Mohammadi M, Simonsen J, Sitharaman B. Boron nitride nanotubes and nanoplatelets as reinforcing agents of polymeric matrices for bone tissue engineering. Journal of Biomedical Materials Research Part B: Applied Biomaterials. 2015

150. Rashkow JT, Talukdar Y, Lalwani G, Sitharaman B. Interactions of 1D-and 2D-layered inorganic nanoparticles with fibroblasts and human mesenchymal stem cells. Nanomedicine. 2015; 10(11): 1693–1706. [PubMed: 26080694]

151. Teo WZ, Chng ELK, Sofer Z, Pumera M. Cytotoxicity of Exfoliated Transition - Metal Dichalcogenides (MoS2, WS2, and WSe2) is Lower Than That of Graphene and its Analogues. Chemistry–A European Journal. 2014; 20(31):9627–9632.

152. Chng ELK, Sofer Z, Pumera M. MoS 2 exhibits stronger toxicity with increased exfoliation. Nanoscale. 2014; 6(23):14412–14418. [PubMed: 25341082]

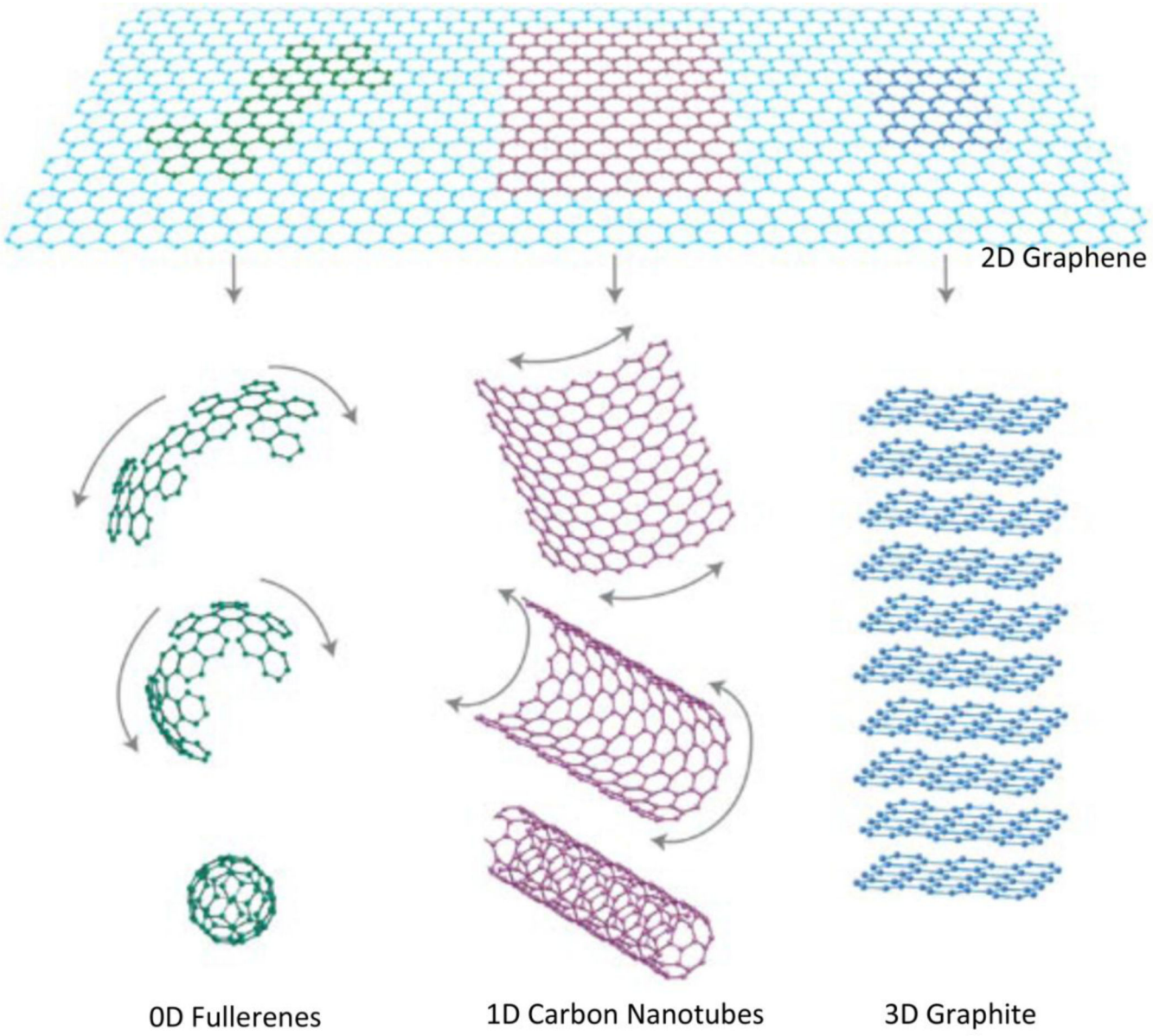

Figure 1.

Graphene is the building material for 0D fullerenes, 1D carbon nanotubes and 3D graphite. Schematic adapted from Reference [6] with permission, copyright © Macmillan Publishers Limited, 2007.

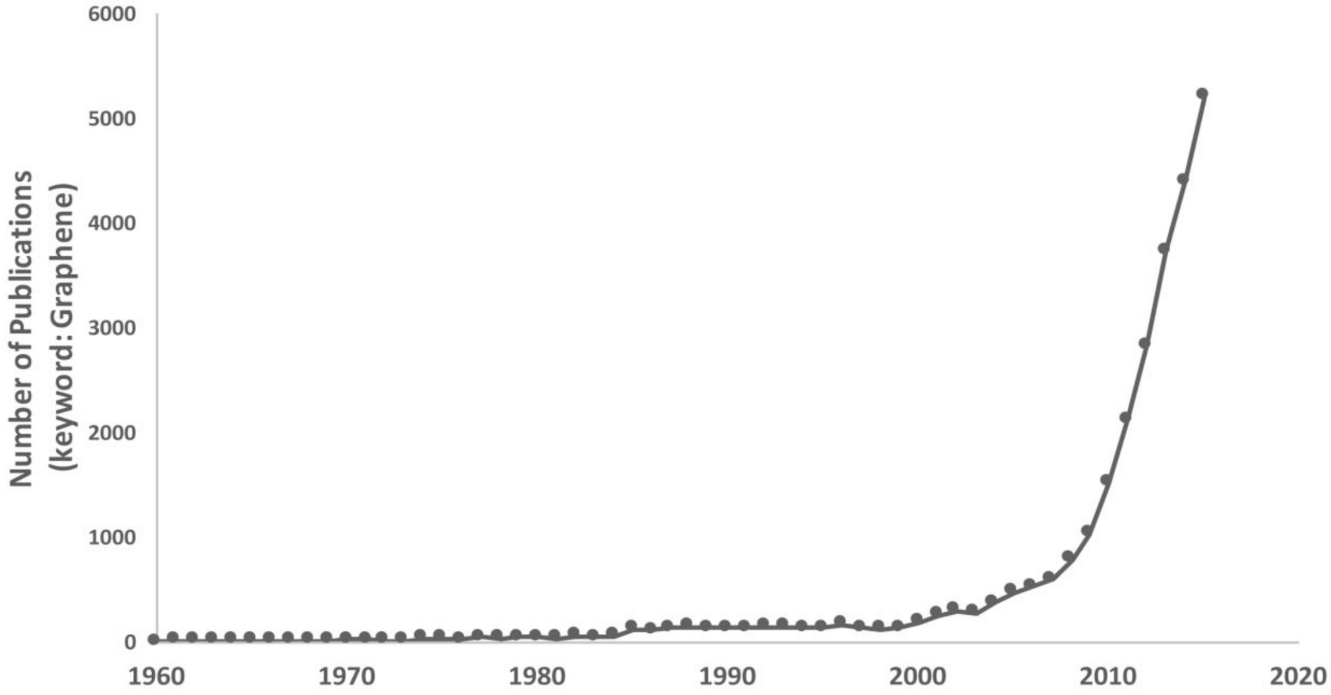

Figure 2.
Number of publications with the keyword ‘graphene’ from 1960–2015. Data retrieved from PubMed (www ncbi.nlm nih.gov).

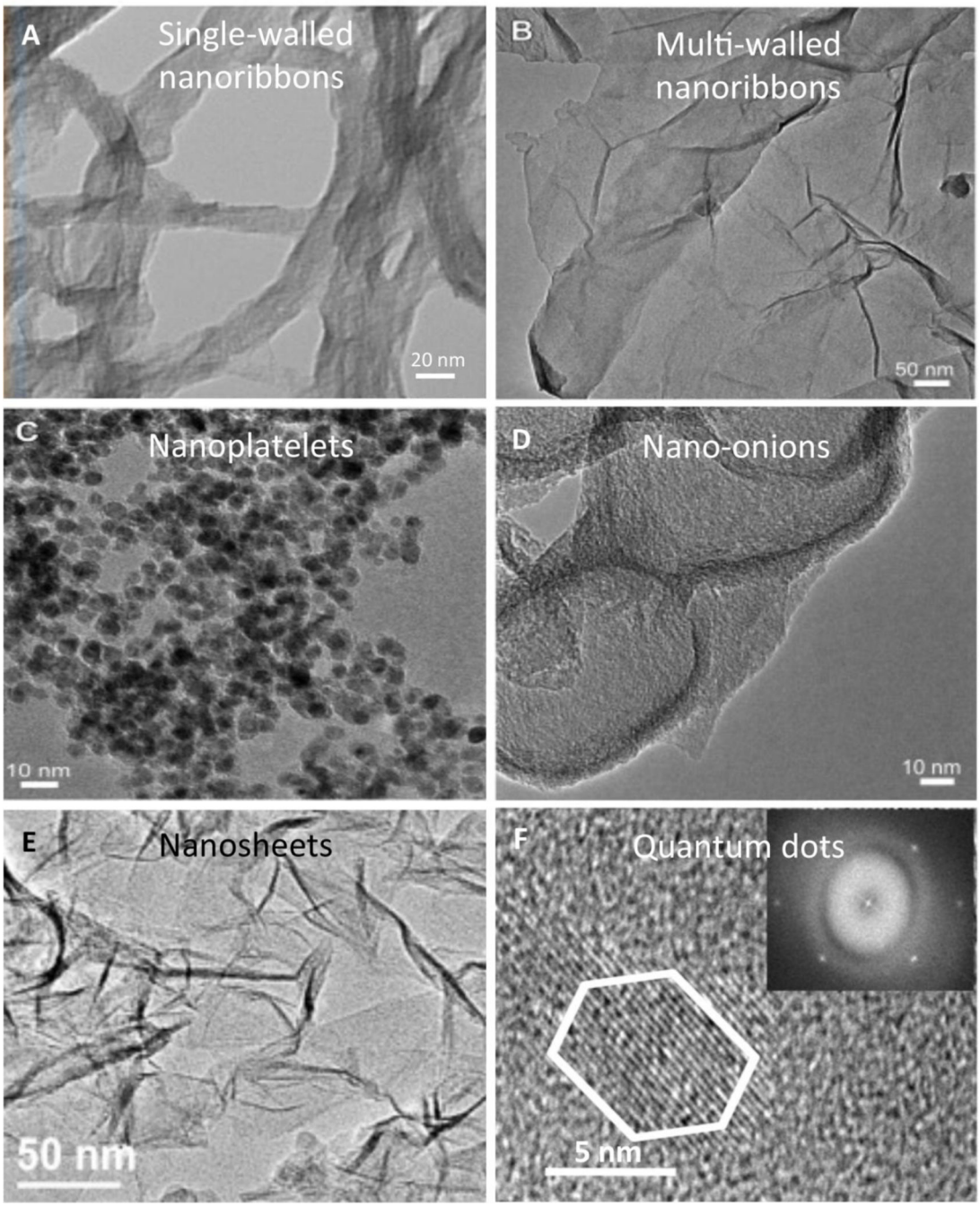

Figure 3.

Representative transmission electron microscopy images of (A and B) graphene nanoribbons, (C) graphene nanoplatelets, (D) graphene nanoonions, (E) graphene nanosheets and (F) graphene quantum dots. Image (A) adapted from Reference [41], (B–D) adapted from Reference [44], (E) adapted from Reference [96] and (F) adapted from Reference [146], with permissions. (A) copyright © American Chemical Society 2013, (B–D) copyright © Elsevier 2014, (E) copyright © Elsevier 2015, and (F) copyright © American Chemical Society, 2013.

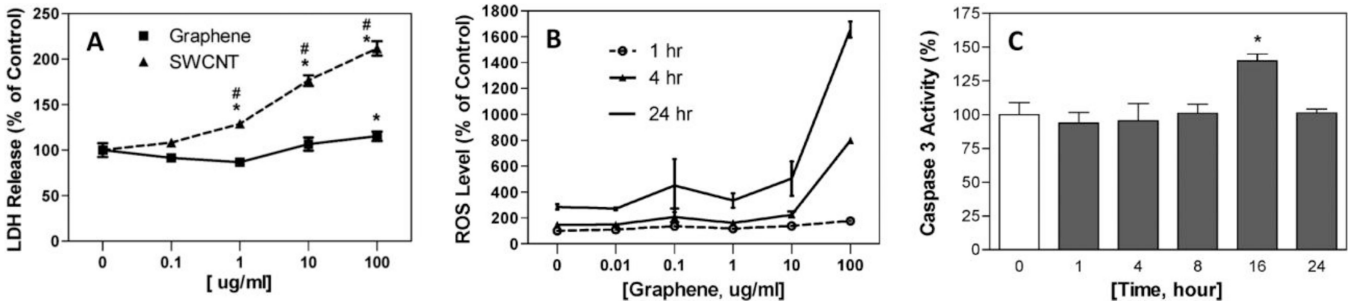

Figure 4.

Effects on (A) lactate dehydrogenase release, (B) reactive oxygen species generation and (C) caspase-3 activity (apoptosis marker) of PC12 cells treated with 0.1–100 μg/ml of graphene and single-walled carbon nanotubes. Adapted from Reference [61] with permission, copyright © American Chemical Society, 2010.

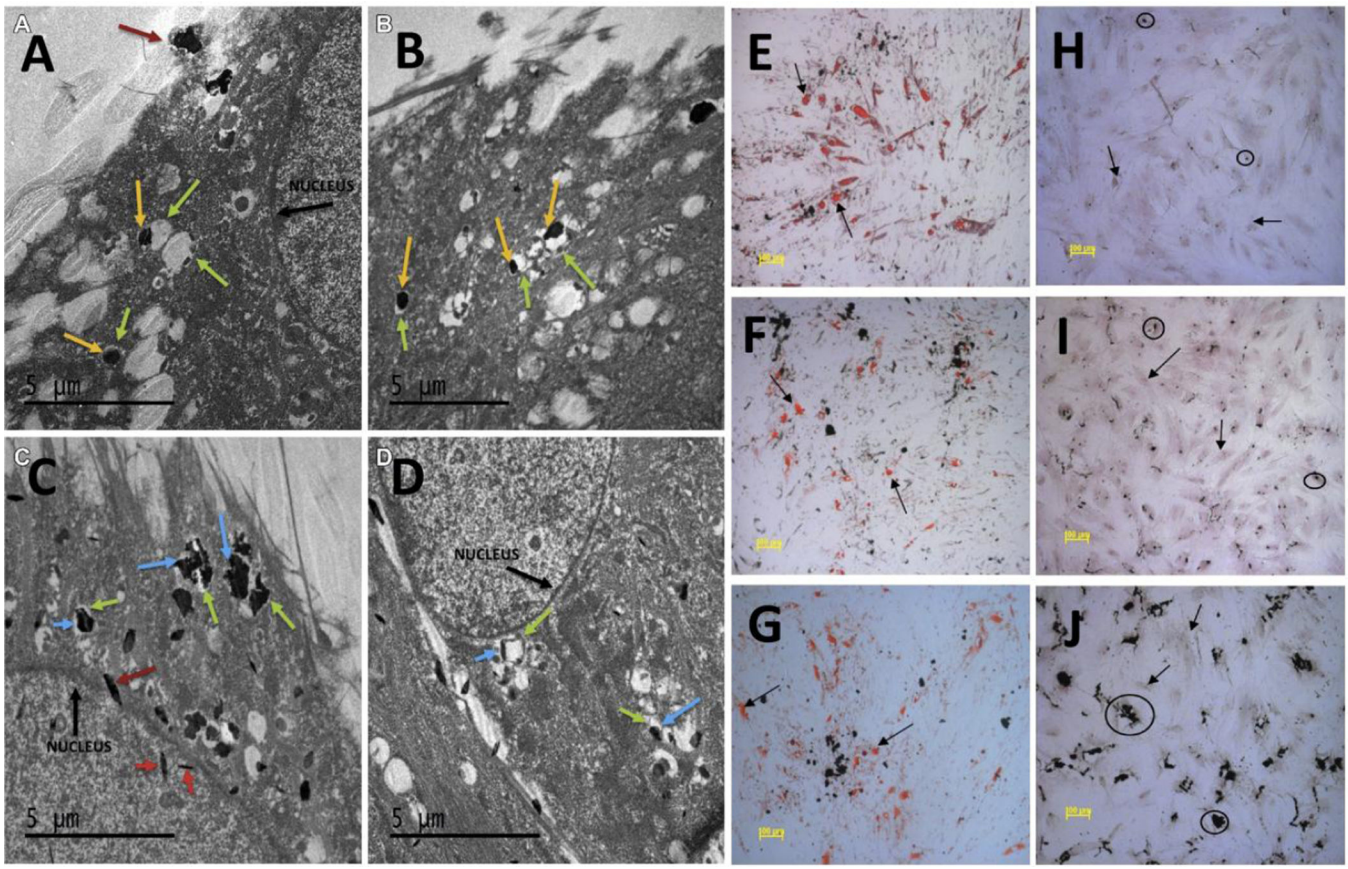

Figure 5.

Representative transmission electron microscopy images of mesenchymal stem cells (MSC) treated with graphene nanoonions (GNOs, A&B) and oxidized-graphene nanoplatelets (GONPs, C&D) at 50 μg/ml for 24 hours. Yellow arrows correspond to aggregates of GNO visualized in vacuoles (green arrows). No nuclear uptake of GNOs was observed. Blue arrows correspond to aggregates of GONPs. GONPs were observed inside the nucleus (red arrows). Oil red O staining after adipogenic differentiation of MSC treated with 50 μg/ml of (E) GNO, (F) GONR and (G) GONP. Alizarin Red staining after osteogenic differentiation of MSC treated with 50 μg/ml of (H) GNO, (I) GONR and (J) GONP. No changes in the adipogenic and osteogenic differentiation of MSCs were observed. Adapted from Reference [44] with permission, copyright © Elsevier, 2014.

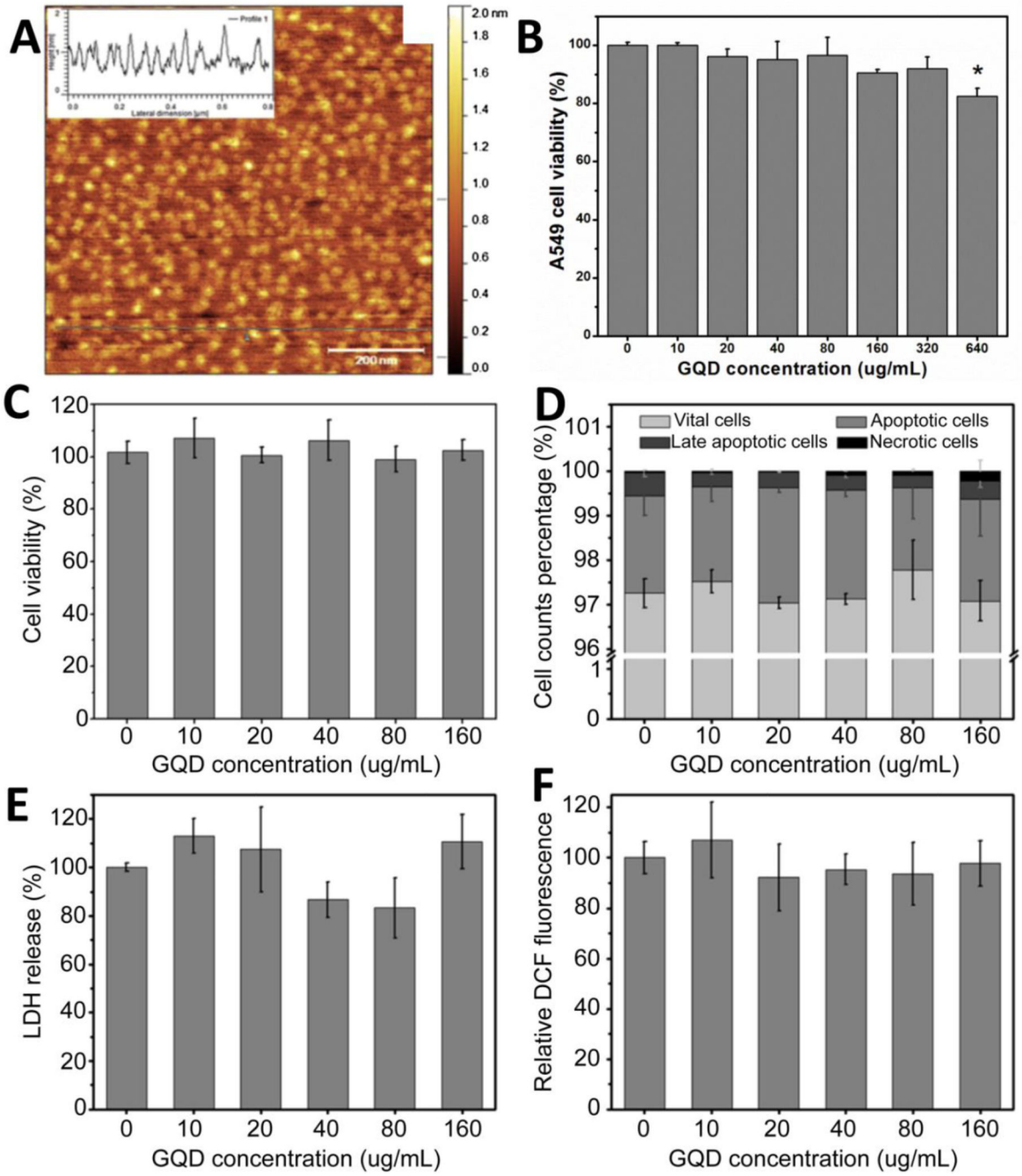

Figure 6.

(A) Representative atomic force microscopy (AFM) image of graphene quantum dots (GQDs). Inset in image A depicts AFM height profile. (B) Cell viability of A549 cells assessed by WST-1 assay. Data reported as means ± SE. No significant differences in cell viability were observed upto a treatment concentration of 320 μg/ml. (C) Cell viability assessed by WST-1 assay, (D) cell apoptosis and necrosis (E) LDH assay and (F) ROS generation by HeLa cells upon treatment with 0–160 μg/ml of GQDs. No toxicity upto 160

μg/ml concentration was observed. Adapted from Reference [74] with permission, copyright © Elsevier, 2014.

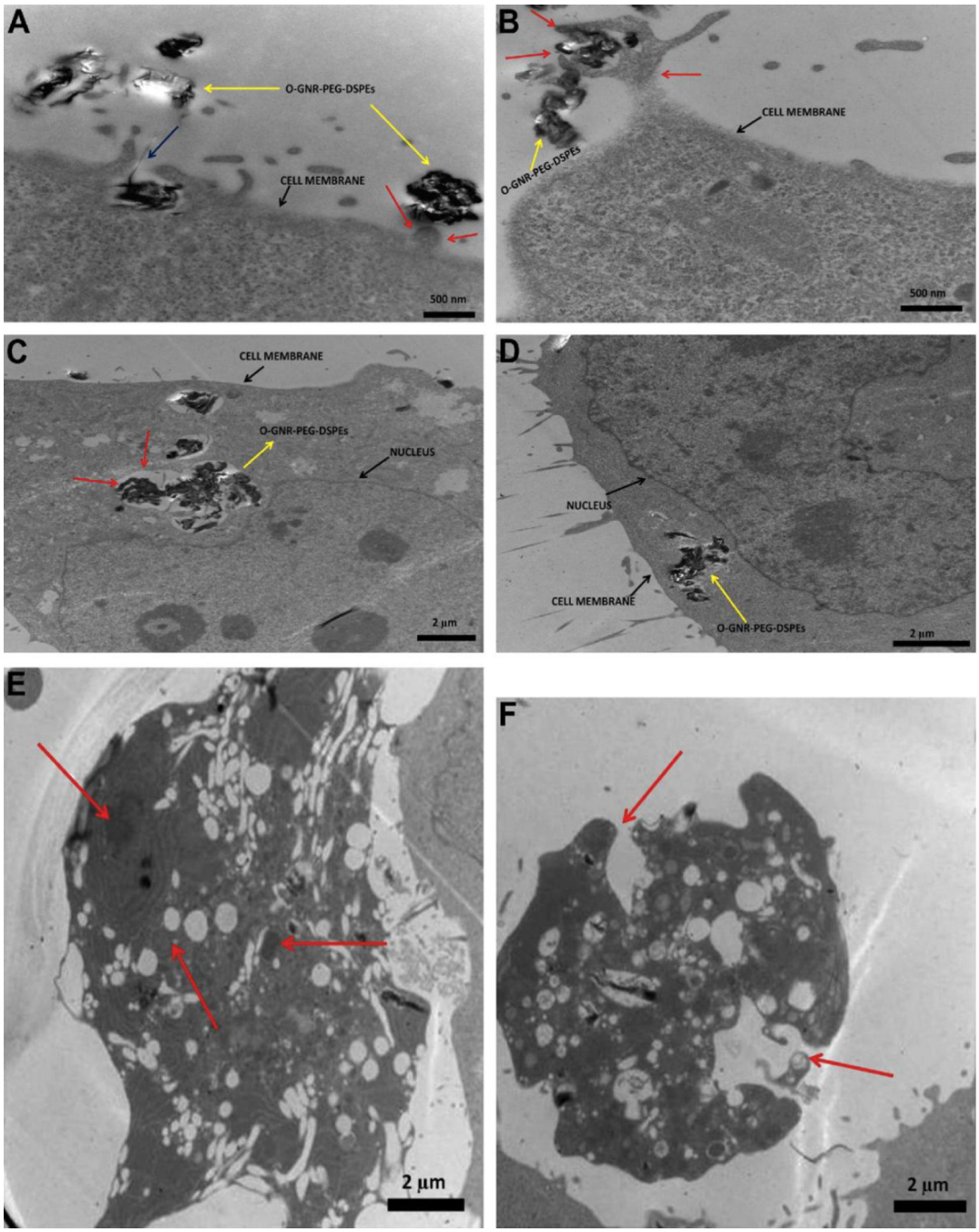

Figure 7.

Representative transmission electron microscopy images of HeLa cells treated with 20 µg/ml of PEG-DSPE dispersed graphene oxide nanoribbons for 3 hours. (A) Presence of GONR aggregates towards cell periphery (blue arrows), (B) cell membrane protrusion and internalization of GONRs (red arrows), (C & D) GONR aggregates enclosed in large cytoplasmic vesicles or endosomes (red arrows), (E and F) HeLa cells showing ruptured plasma membrane and swollen vesicles suggesting necrotic cell death after 24 hours of

exposure to 20 μg/ml DSPE-PEG dispersed GONRs. Adapted from Reference [36] with permission, copyright © Elsevier, 2013.

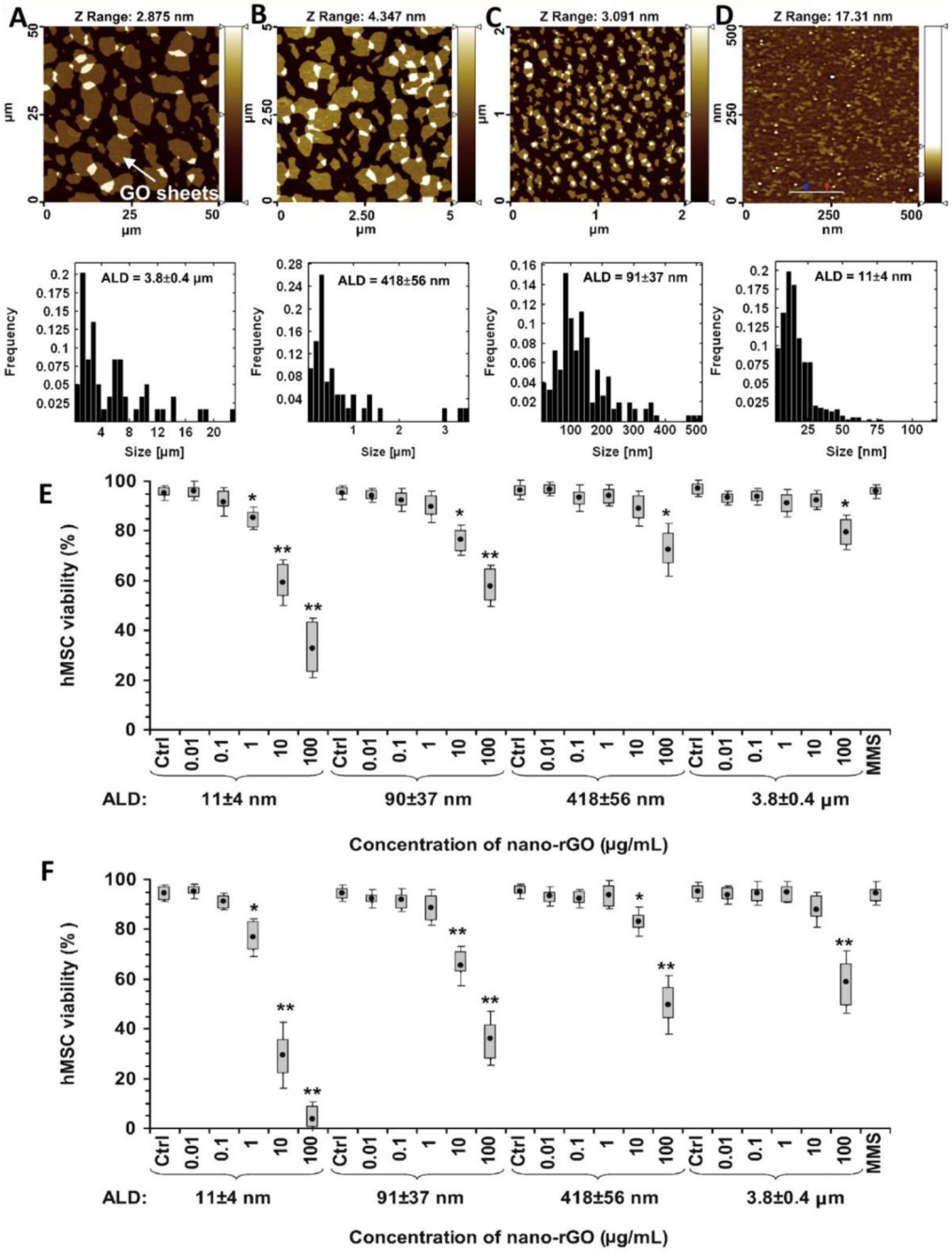

Figure 8.

Representative atomic force microscopy (AFM) images of (A) as-prepared rGO (3.8±0.4 μm), (B) sonicated rGO (418±56 nm), (C) large rGONPs (91±37 nm) and (D) small rGONPs (11±4 nm). Corresponding lateral size distributions are shown below. Images (E and F) show human mesenchymal stem cell viability after treatment with 0.01–100 μg/ml concentration of rGONPs for 1 and 24 hours, respectively. Adapted from Reference [79] with permission, copyright © Elsevier, 2012.

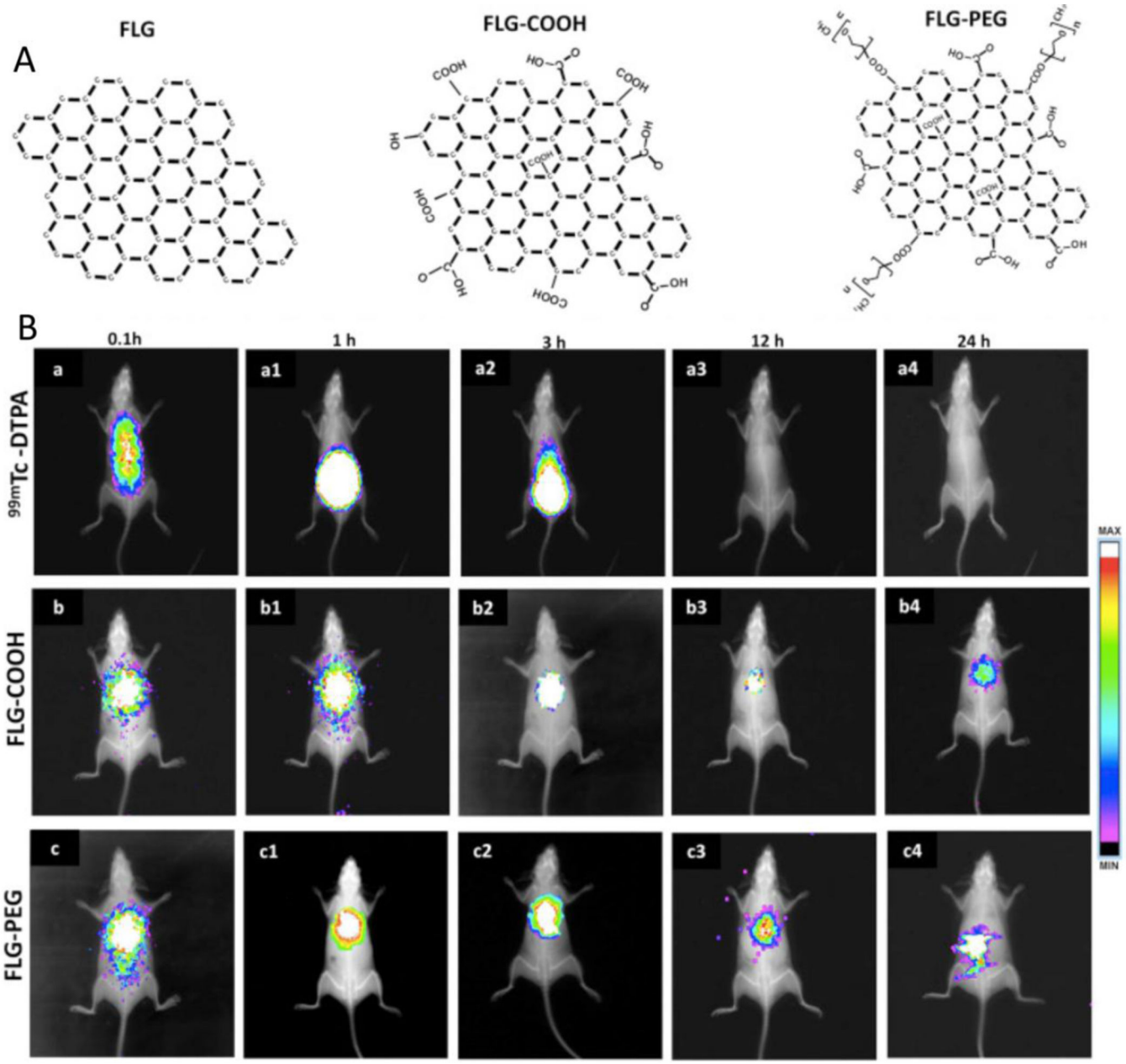

Figure 9.

(A) Schematic illustrating structural depiction of few layered graphene (FLG), FLG-COOH and FLG-PEG. (B) Real time *in vivo* biodistribution of ^{99}Tc labeled FLG, FLG-COOH, FLG-PEG, signal accrued for 24 hours. Adapted from Reference [96] with permission, copyright © Elsevier, 2015.

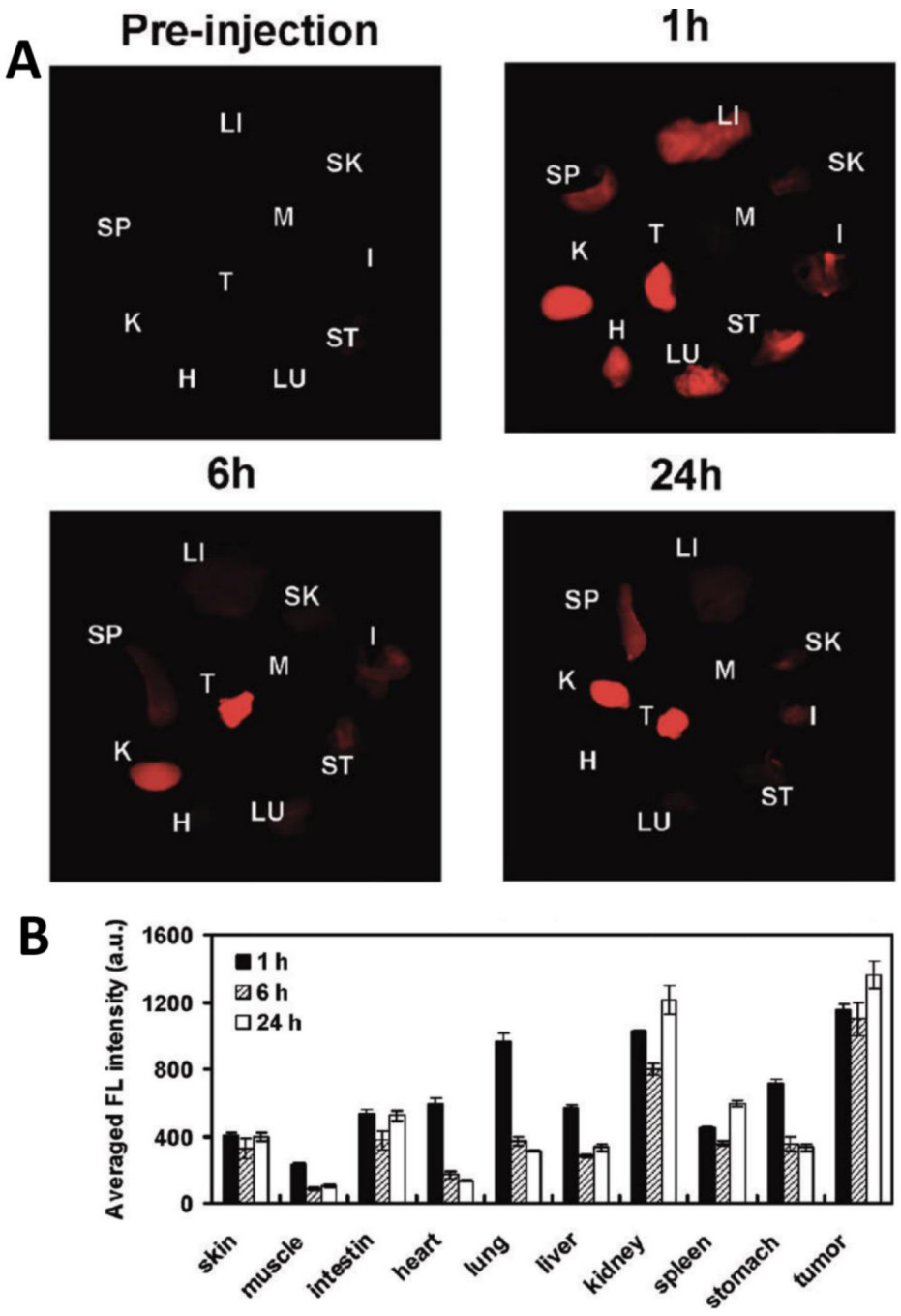

Figure 10.

Biodistribution analysis of Cy7 labeled PEG functionalized nano graphene sheets (NGS-PEG-Cy7). Tumor bearing 4T1 mice were sacrificed after 1, 6, and 24 hours of NGS-PEG-Cy7 administration. (A) Spectrally resolved *ex vivo* fluorescence images of SK-skin, M-muscle, I-intestine, H-heart, LU-lung, LI-liver, K-kidney, SP-spleen, ST-stomach, and T-tumor. (B) Chart depicting semi quantitative biodistribution of each organ for n=3 mice per group. Adapted from Reference [101] with permission, copyright © American Chemical Society, 2010.

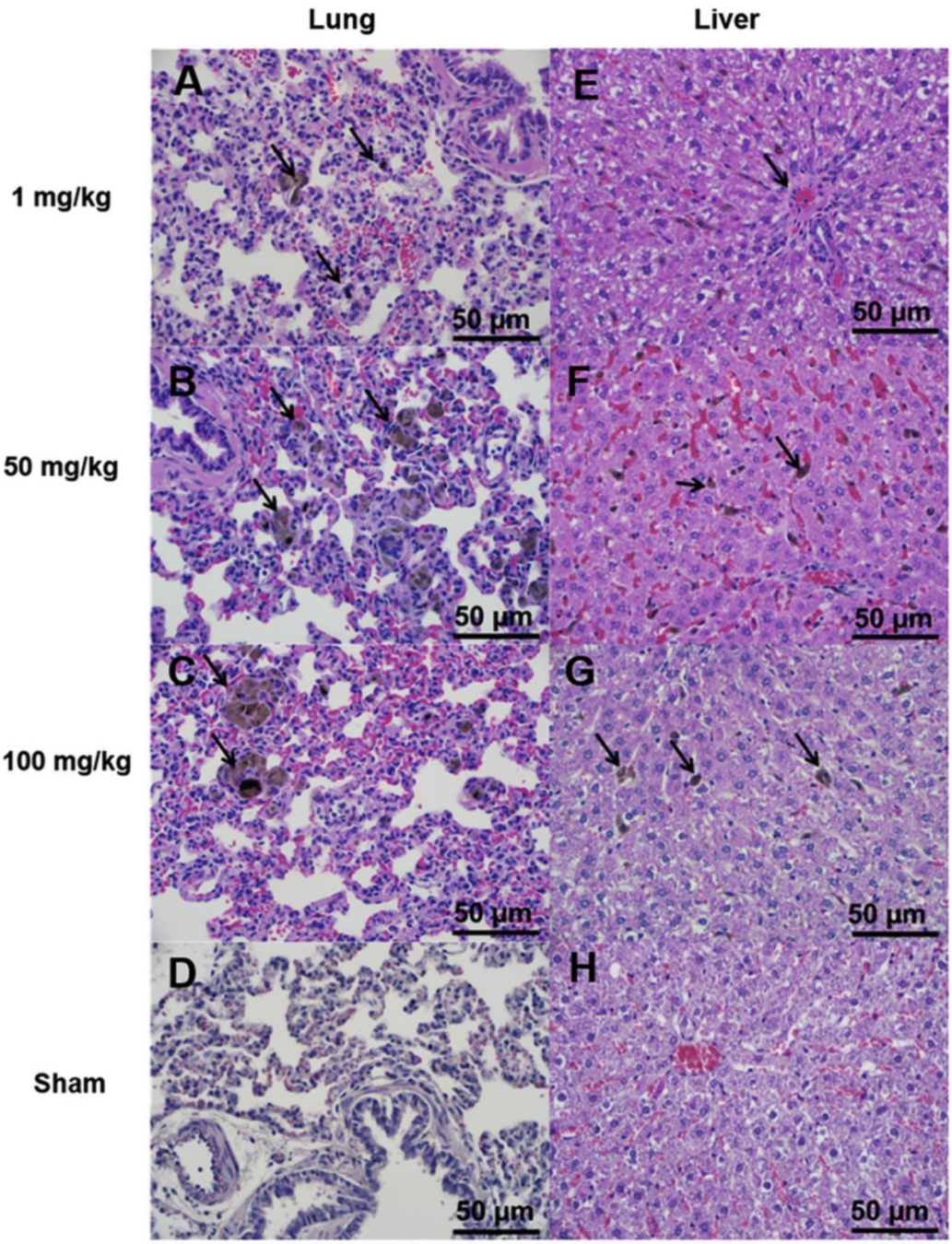

Figure 11.

Representative H&E staining of lung and liver sections post GNP-Dex administration at 1, 50, and 100 mg/kg in Wistar rats. Pigmentation (arrows, A–C) was observed within alveolar macrophages in lungs at all GNP-Dex administration concentrations indicating the presence of graphene nanoparticles. (D) Sham lungs showed no diagnostic abnormalities. Liver sections at 1 mg/kg (E) showed minimal at liver steatosis, at 50 mg/kg (F) showed pigmented macrophages in Kupffer cells indicating the presence of graphene. No signs of inflammation were observed. At 100 mg/kg dose (G), an increase in pigmentation was

observed. (H) Sham liver sections showed no diagnostic abnormality. Adapted from Reference [103] with permission, copyright © Kanakia et. al. (open access, Nature Scientific Reports), 2015.

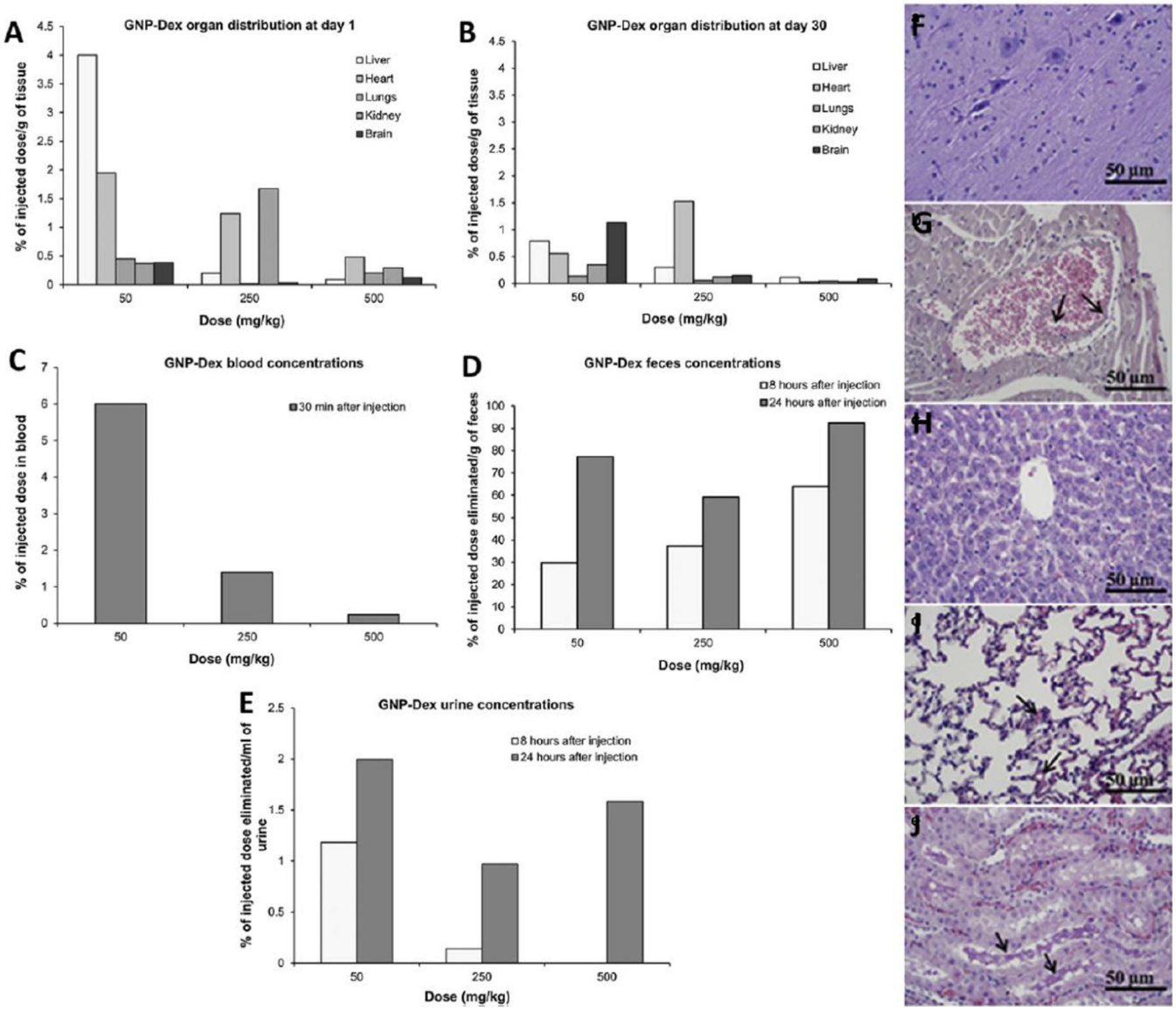

Figure 12.

(A&B) Tissue biodistribution, (C) blood half life, (D) elimination via feces and (E) urine after GNP-Dex administration at doses 50–500 mg/kg to Wistar rats analyzed via ICP-MS. Liver and kidney showed maximum uptake after 24 hours of administration. Majority of GNP-Dex was excreted via feces; small amounts were cleared via urine. Histological sections of (F) cerebral cortex, (G) myocardium, (H) liver, (I) pulmonary parenchyma and (J) renal cortex after 24 hours of GNP-Dex administration at 250 mg/kg dose. No diagnostic abnormalities were observed in cerebral cortex and liver. Vascular congestion of myocardium was observed. Arrows in (G) show dilated vein containing debris of GNP-Dex. Mild focal congestion was observed in the alveolar capillaries of pulmonary parenchyma. Vascular congestion and proteinaceous casts were observed in renal tubules of renal cortex. Adapted from Reference [104] with permission, copyright © Elsevier, 2014.

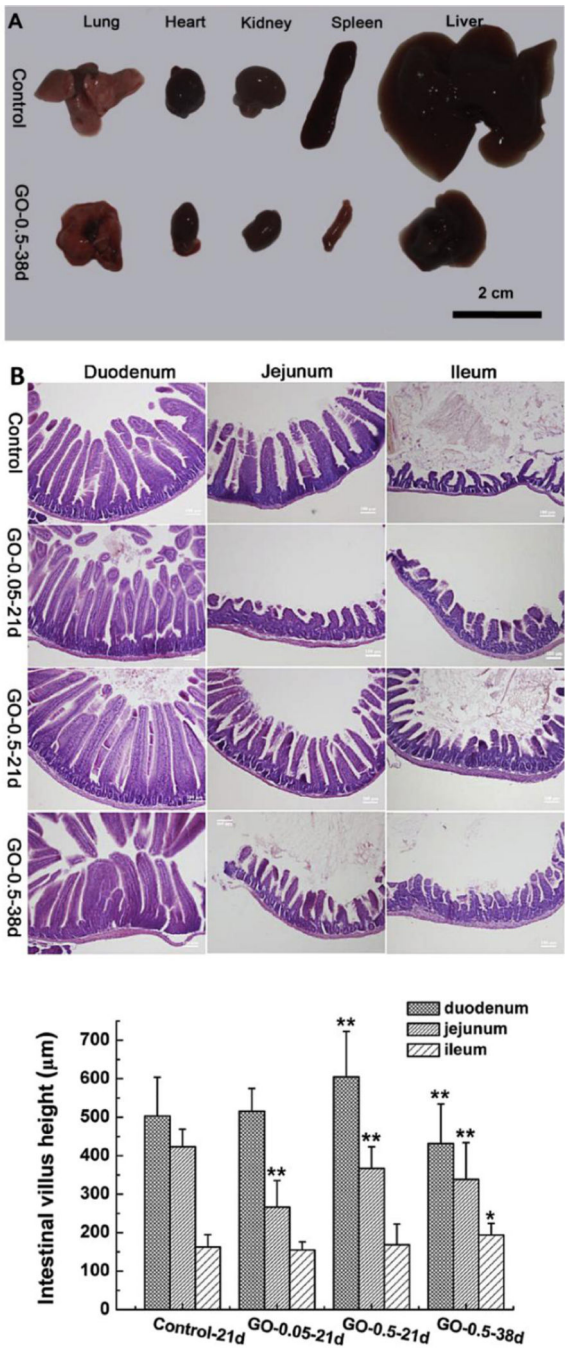

Figure 13.

(A) Pathological examination of lungs, heart, kidney, spleen and liver collected from control and GO administered mice (0.5 mg/ml) after 38 days showing severe atrophy of all major organs. (B) H&E staining of duodenum, jejunum and ileum of GO treated filial mice at 0.05 mg/ml for 21 days and 0.5 mg/ml for 21 and 38 days. The length, width and height of villi of GO administered groups were longer than control groups. Scale bars represent 100 μm. Adapted from Reference [110] with permission, copyright © Elsevier, 2015.

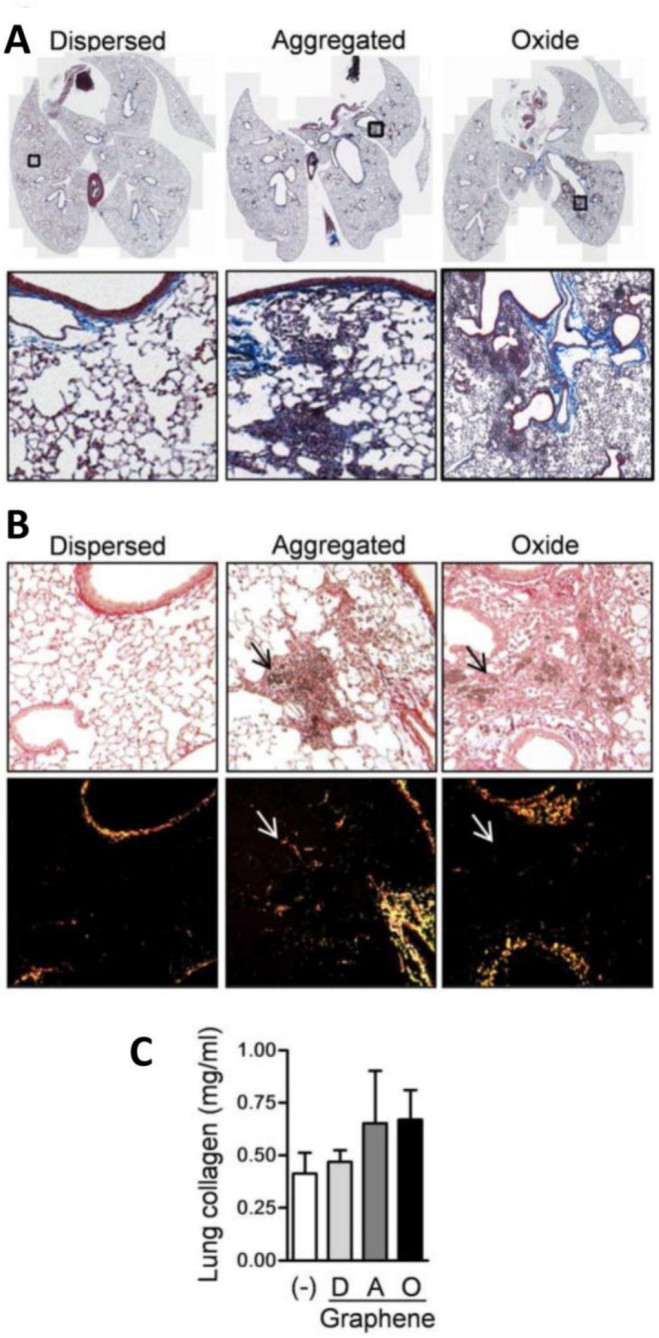

Figure 14.

Aggregated graphene induces patchy fibrosis in mice. Mice were treated with highly purified and dispersed preparations of graphene in 2% Pluronic (Dispersed), aggregates of graphene in water (Aggregated) or GO in water (Oxide) by intratracheal instillation and 21 days later, the lungs were examined for markers of fibrosis. (a) Trichrome stained lung sections. (b) Sirius Red stained lung sections. (c) Total lung collagen determined by picrosirius red precipitation of whole lung homogenates (GD; dispersed graphene, GA; aggregated

graphene, GO; graphene oxide). Adapted from Reference [114] with permission, copyright © American Chemical Society, 2011.

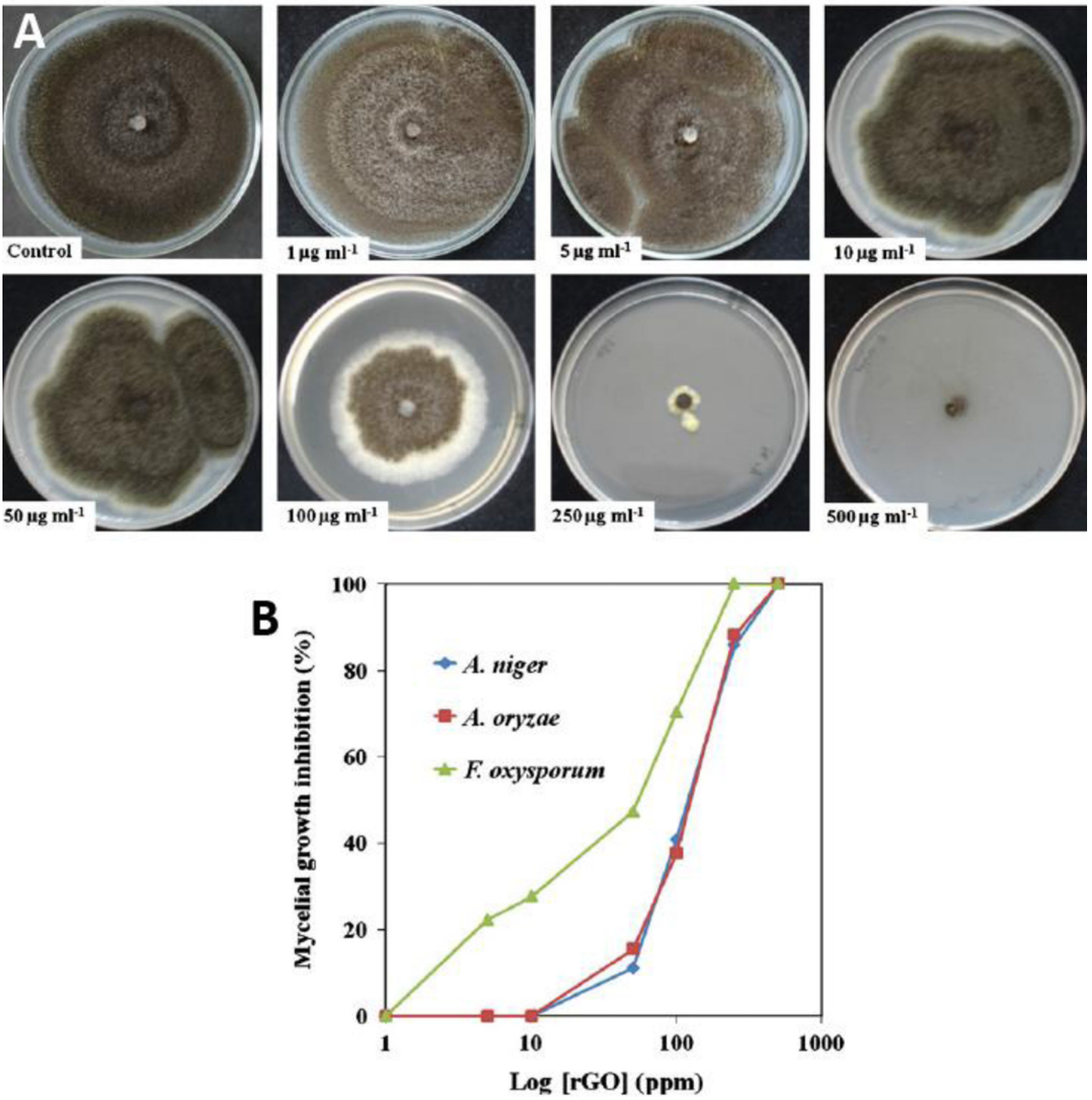

Figure 15.

(A) Mycelial growth inhibition of *A. niger* on media containing 0–500 µg/ml of rGO. (B) Plot of rGO concentration (µg/ml) vs. mycelial growth inhibitory activity (%) of *A. niger, A. oryzae* and *F. oxysporum*. Adapted from Reference [117] with permission, copyright © Elsevier, 2012.

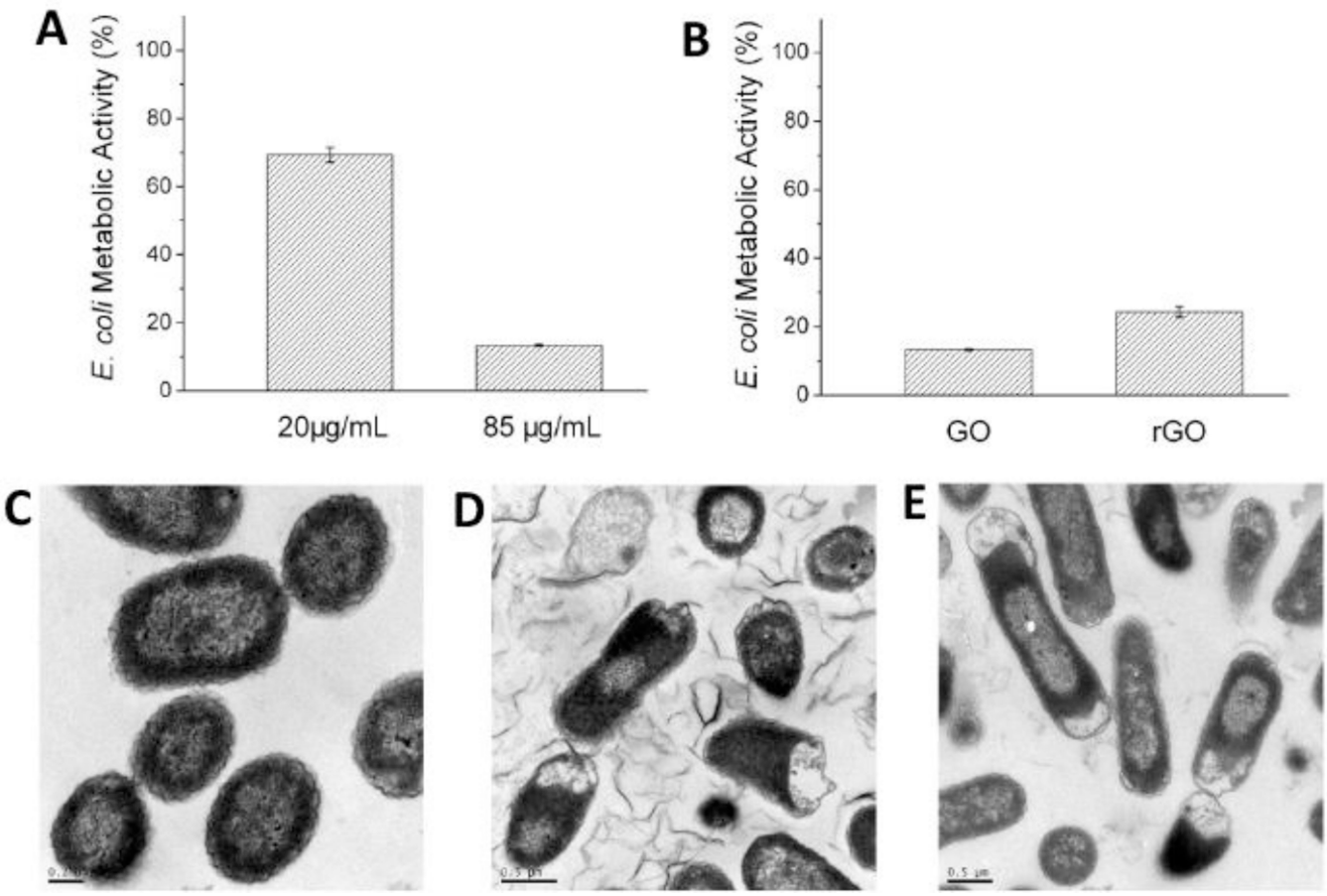

Figure 16.

(A) Metabolic activity of *E. coli* cells upon exposure to GO at 20 and 85 μg/ml concentration for 2 hours. (B) Comparative metabolic activity of GO and rGO at 85 μg/ml concentration for 2 hours. GO shows greater antibacterial activity than rGO. Transmission electron microscopy images of *E. coli* cells - (C) control (D) after exposure to GO and (E) rGO at 85 μg/ml. Loss of membrane integrity are observed. Adapted from Reference [123] with permission, copyright © American Chemical Society, 2010.

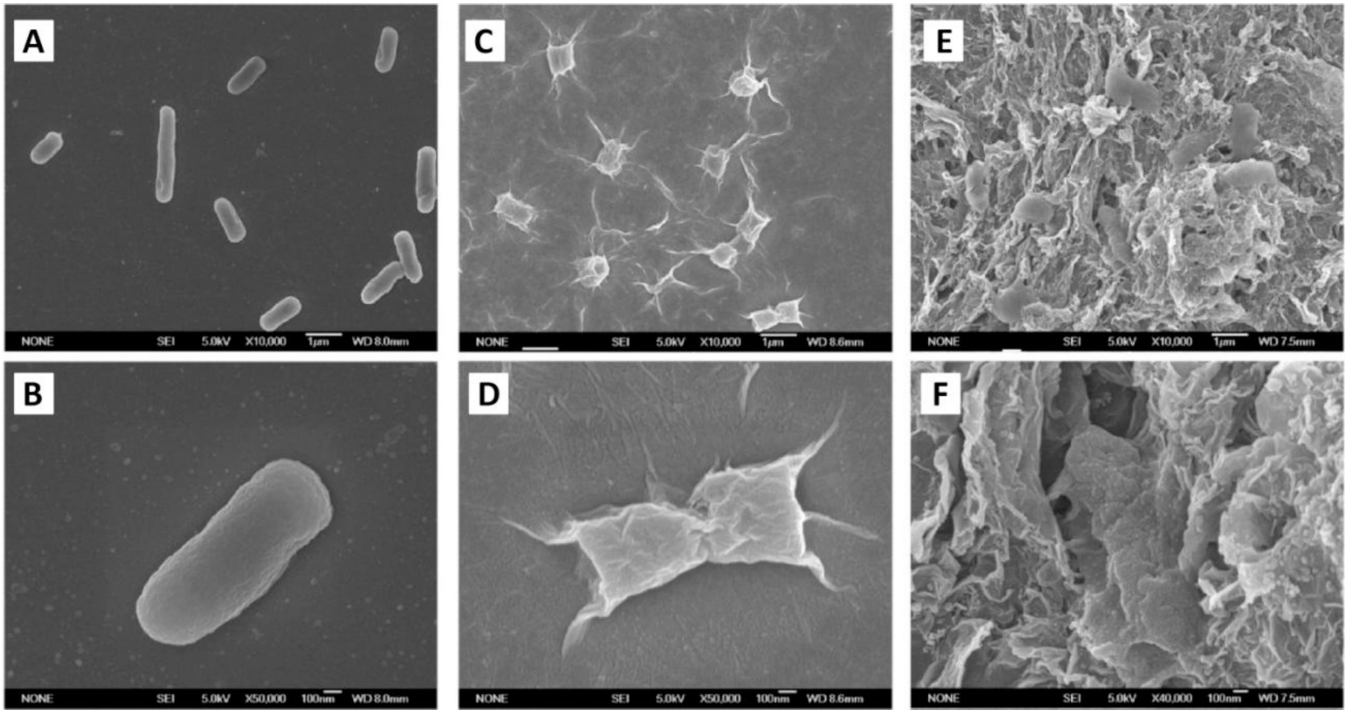

Figure 17.

Scanning electron microscopy images of *E. coli* after 2 hours of incubation with (A, B) saline solution, (C, D) GO dispersions 40 μg/ml, (E, F) rGO dispersions at 40 μg/ml. Loss of membrane integrity is clearly observed. Adapted from Reference [128] with permission, copyright © American Chemical Society, 2011.

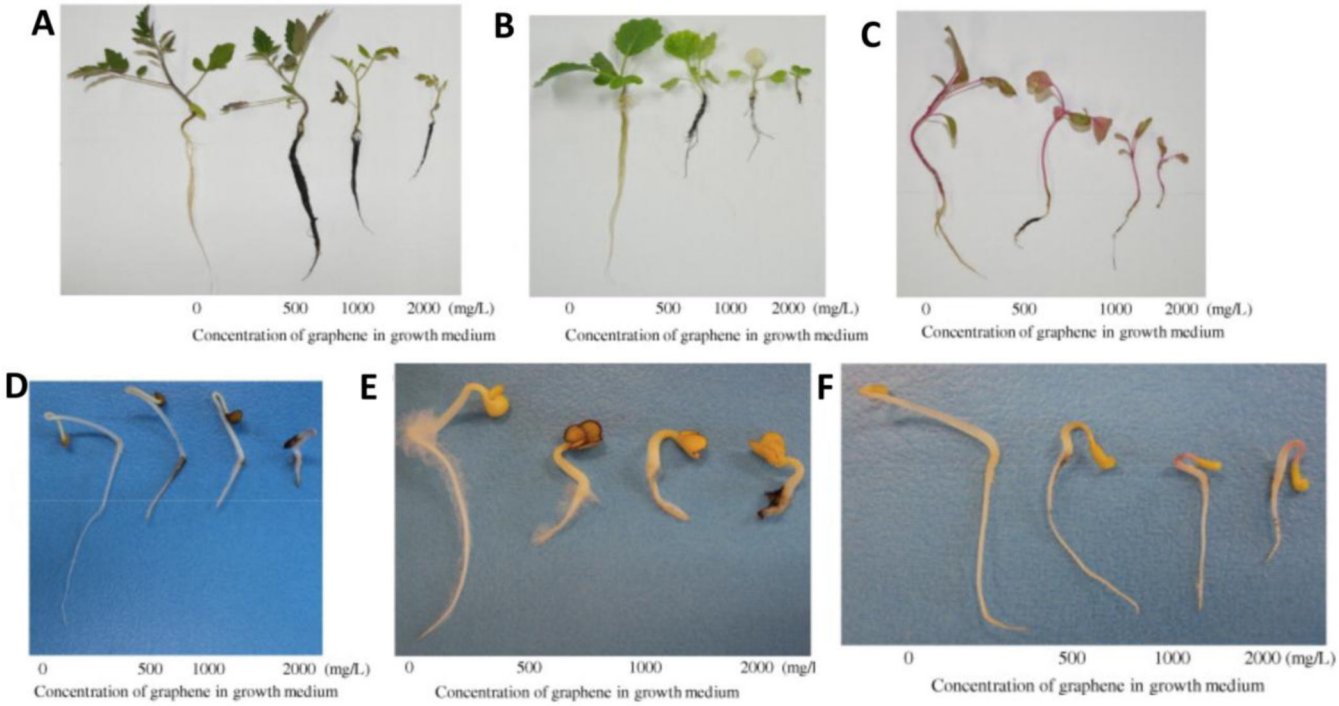

Figure 18.

Effect of graphene on growth and development of (A–C) seedling and (D–F) cotyledons and root systems of cabbage, tomato and red spinach after exposure to 500–2000 mg/L concentration for 20 and 4 days, respectively. A dose-dependent reduction in the plant growth and biomass production is observed. Adapted from Reference [130] with permission, copyright © Elsevier, 2011.

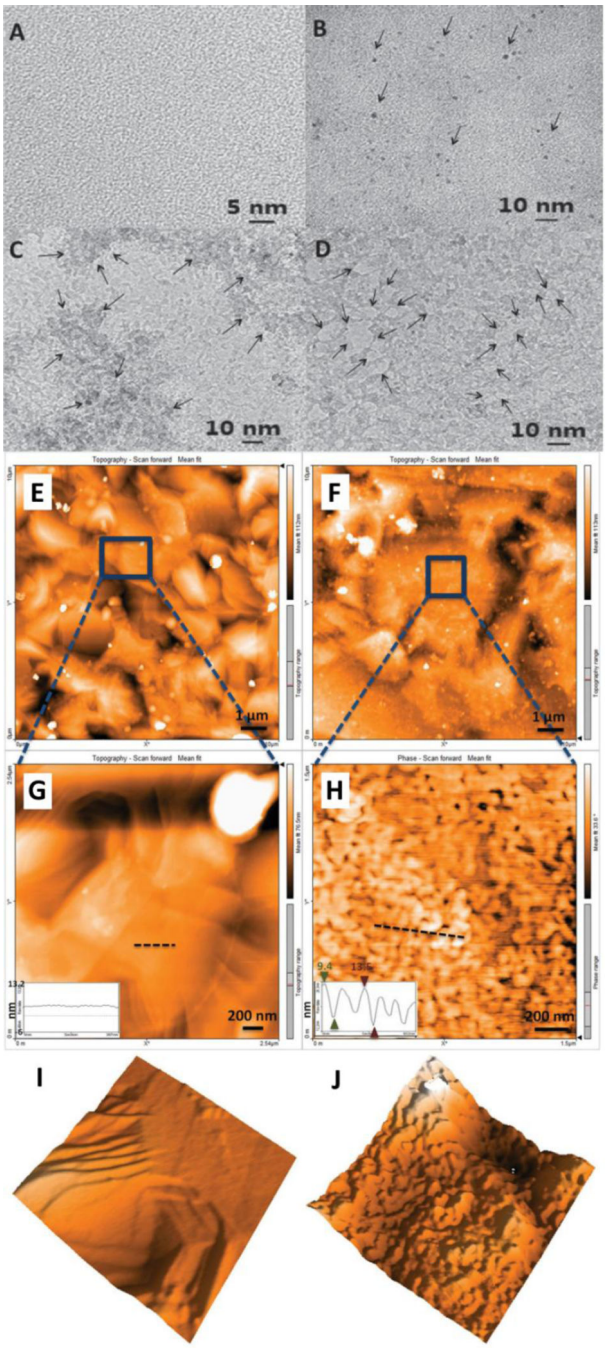

Figure 19.

(A–D) Representative transmission electron microscopy images of multilayered graphene treated with (A) DI water, (B) 1 μM H_2O_2, (C) 100 μM H_2O_2 and (D) 10000 μM H_2O_2 for 10 hours. Arrows in (B) indicate the formation of holes on graphene sheets and in (C) indicate the formation of lighter (few graphene layers) and darker regions (multiple graphene layers) suggesting the degradation of multilayered graphene. (E–J) Representative atomic force microscopy images of multilayered graphene on Ni wafer. (E and G) are topographical scans of graphene incubated with DI water for 25 hours. (G and H) show

graphene after 25 hours of incubation with 10000 μM H_2O_2. Inset in images (G and H) are corresponding height profiles. (I and J) are 3D representations of images G and H. Adapted from Reference [133] with permission, copyright © John Wiley and Sons Inc., 2014.

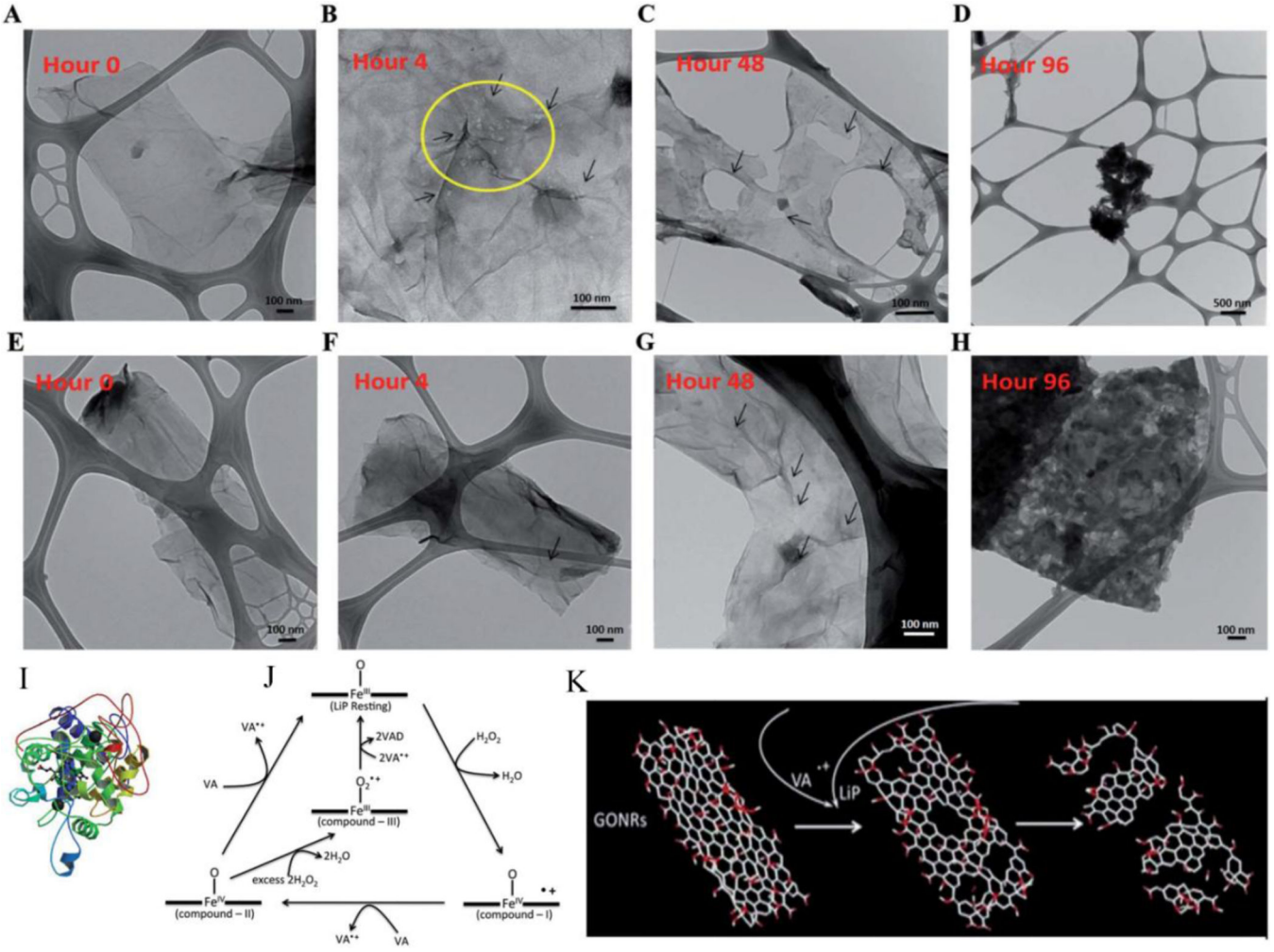

Figure 20.

Representative transmission electron microscopy images of oxidized and reduced graphene oxide nanoribbons (GONRs – A–D) and (rGONRs – E–H) after 0, 4, 48, and 96 hours of treatment with lignin peroxidase. Arrows in B, D and G indicate the formation of holes on graphene sheets. Extensive biodegradation of GONRs whereas the formation of holey rGONRs is observed after 96 hours of incubation. (I) Ribbon diagram of lignin peroxidase, (J) Enzymatic cycle of lignin peroxidase and (K) Schematic representation of degradation of graphene in the presence of lignin peroxidase. Adapted from Reference [134] with permission, copyright © Royal Society of Chemistry, 2014.

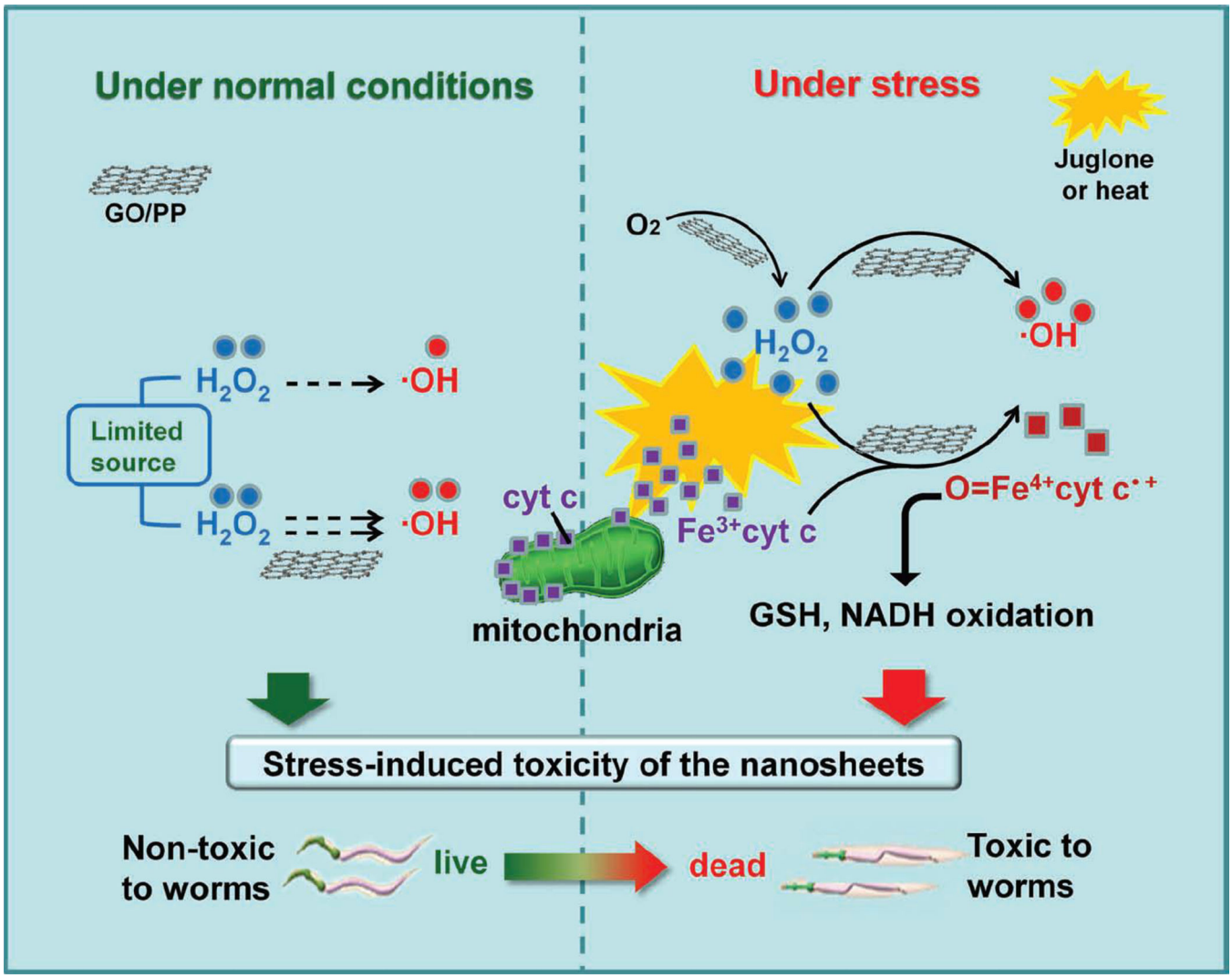

Figure 21.

Schematic representation of the proposed mechanism of oxidative stress induced toxicity by graphene oxide. Adapted from Reference [136] with permission, copyright © John Wiley & Sons Inc., 2012.

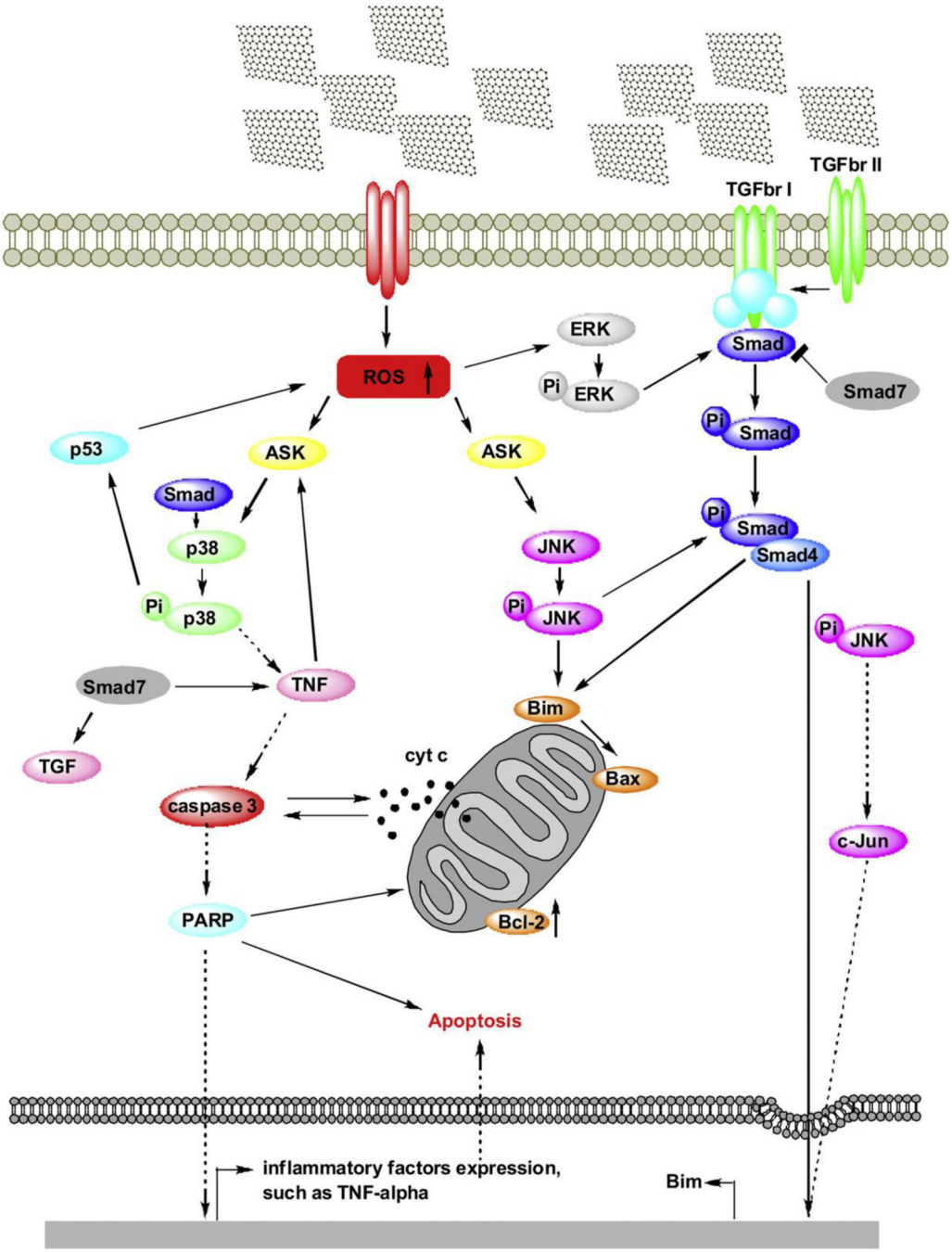

Figure 22.

Schematic illustrating the signaling pathways involved in pristine-graphene induced cell apoptosis via ROS mediated MAPK and TGF-beta pathways (mitochondria dependent apoptotic cascades). Adapted from Reference [83] with permission, copyright © Elsevier, 2012.

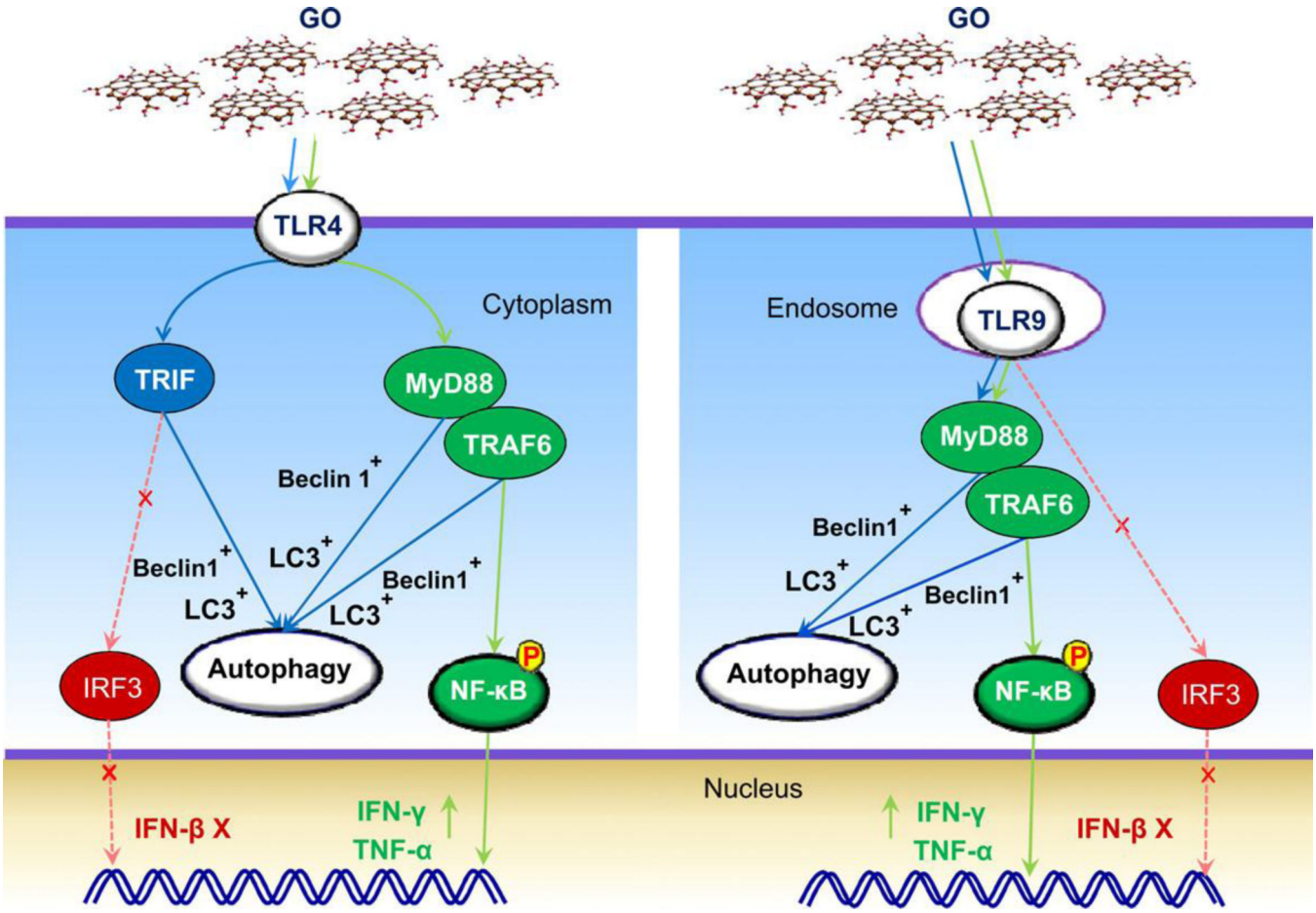

Figure 23.

Overview of the GO-induced cytokine response and autophagy mediated by the TLR4/TLR9 signaling pathway. GO treatment led to the activation of TLR4 and TLR9, which relayed signals through MyD88-TRAF6-NF-kB and ultimately gave rise to cytokine expression. However, GO-induced TLRs signaling neither elicited IFN-b expression nor activated IRF3, suggesting that TRIF and IRF3 were dispensable in the inflammatory response. Conversely, GO-induced TLR4-MyD88-TRAF6 and TLR4-TRIF signaling cascades signaled through Beclin 1 to initiate autophagy. GO engagement of TLR9 also activated MyD88 and TRAF6, leading to Beclin 1 and LC3 activation and subsequent autophagy. Adapted from Reference [84] with permission, copyright © Elsevier, 2012.

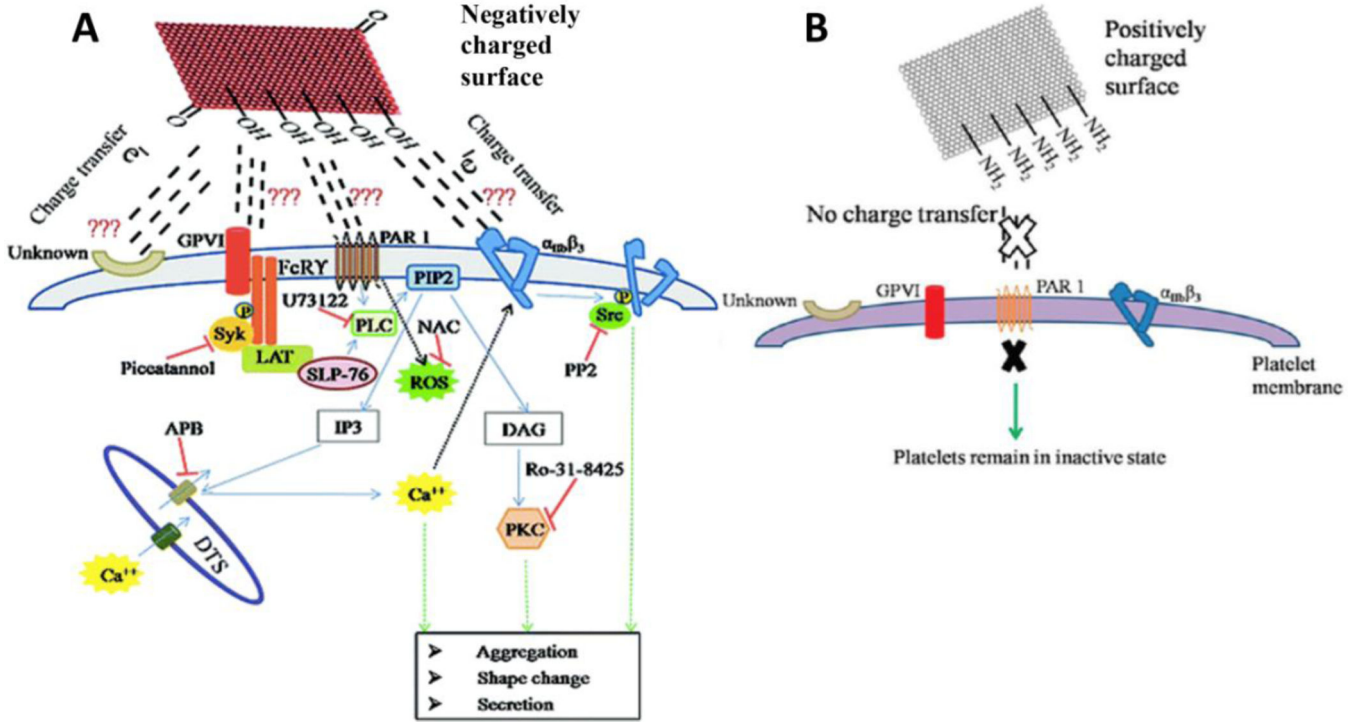

Figure 24.

Schematic illustrating the interaction of (A) graphene oxide (negative surface charge) and (B) amine-modified graphene (positive surface charge) on platelet function. Surface charge distribution determines the interactions of graphene with different agonist receptors on platelet membrane. (A) Adapted from Reference [87] and (B) adapted from Reference [88] with permissions, copyright © American Chemical Society, 2011 and 2012.

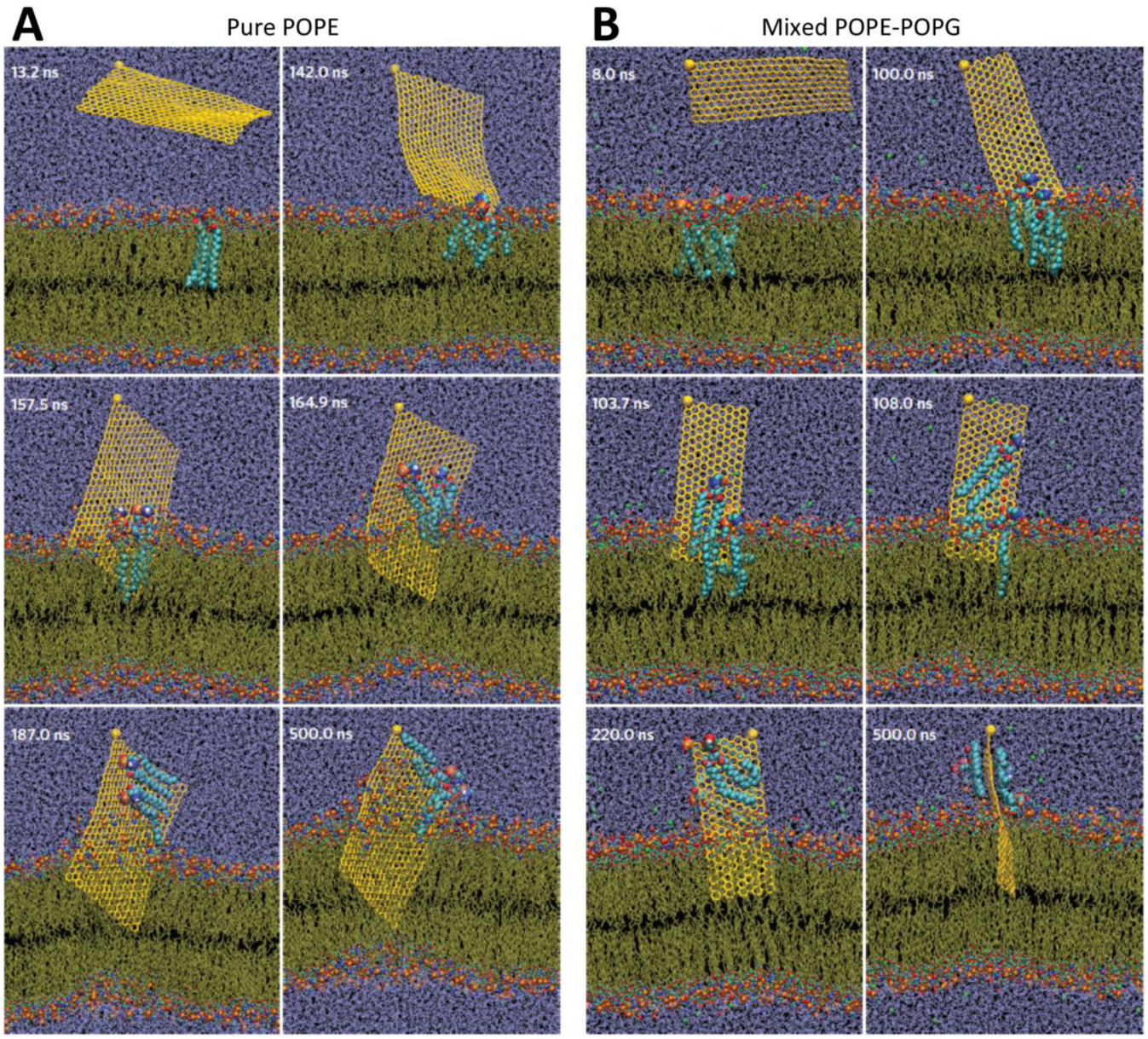

Figure 25.

Representative simulated trajectories of graphene nanosheets insertion and lipid extraction in the outer membrane (pure palmitoyloleoylphosphatidylethanolamine, POPE) and inner membrane (mixed POPE-POPG) of E. coli. Water is represented in violet and phospholipids in tan lines with hydrophilic charged atoms as colored spheres (hydrogen – white, oxygen – red, nitrogen – dark blue, carbon – cyan and phosphorus – orange). Graphene is shown as yellow sheet with a large sphere marked at one corner representing restrained atom in simulations. Extracted phospholipids are shown as large spheres. Adapted from Reference [145] with permission, copyright © Macmillan Publishers Limited, 2013.

Adv Drug Deliv Rev. Author manuscript; available in PMC 2017 October 01.

Table 1

In vitro cytotoxicity of graphene

Material	Characterization	Properties	Treatment Concentration	Cell line	Assays	Conclusions	References
Graphene, SWCNT	TEM, SEM, AFM, microscopy, spectroscopy, X-ray diffraction	G: Thickness = 3–5nm	0.01–100 μg/ml	PC12 cells	MTT, LDH, ROS, Caspase 3/7	Dose and shape dependent cytotoxicity was observed for graphene and SWCNT.	Zhang et al. [61]
GO, ox-SWCNT	AFM, FTIR, EDS	GO: Length = 100nm; Height = 1nm	1 μg/ml	HepG2 cells	MTT, ROS, FITC, DFDA Fluorescence analysis, 2D LC-MS Proteome Analysis	GO shows less mitochondrial damage, ROS generation, apoptotic cell population compared to cells treated with ox-SWCNTs.	Yuan et. al. [63]
GO	AFM, DLS, FTIR, Uv-Vis	GO: Thickness = 1nm; Size = 100–600nm	10–100 μg/ml	SH-SY5Y cells	MTT, Caspase-3	Viability of cells are dose and time dependent. No apoptosis induced by GO. MAP2 expression and neurite length improved.	Lv et. al. [64]
GNO, GONP, GONR (PEG-DSPE dispersed)	TEM, Raman, TGA, Zeta potential, Hydrodynamic diameter	GNO: Diameter = 50–300 nm; I_D/I_G = 0.92; ζ-potential = −32.3 ±1.35; Hydrodynamic radius = 460.76 ±53.58	5–300 μg/ml	Human adMSCs and bmMSCs	Alamar blue, Calcein AM, Adipogenic differentiation (oil red O) and Osteogenic differentiation (alizarin red, ALP, calcium deposition)	Dose dependent cytotoxicity (not time dependent; Graphene does not affect differentiation potential of human stem cells	Talukdar et. al. [44]
		GONR: Width = 60–90 nm, Length = 500–1500 nm; I_D/I_G = 1.28; ζ-potential = −26.3 ±0.75; Hydrodynamic radius = 457.5 ± 35.70					
		GONP: Diameter					

Material	Characterization	Properties	Treatment Concentration	Cell line	Assays	Conclusions	References
		= 20–40 nm, Thickness = 3–5 nm; I_D/I_G = 1.09; ζ-potential = −12.47 ± 0.12; Hydrodynamic radius = 296.4 ± 20.32					
GONR and GONP	Raman, XPS	GONR: I_D/I_G = 1.09; Lattice Size = 22.2 nm; C/O ratio = 1.9; Percentage of C=O groups = 28.22	3–400 μg/ml	A549 cells	MTT, WST-8	Size and functional group dependent toxicity; GONR exhibit greater toxicity than GONP due to presence of greater number of carbonyl groups and greater length	Chng et. al. [66]
		GONP: I_D/I_G = 0.88; Lattice size = 19.1 nm; C/O ratio = 1.9; Percentage of C=O groups = 11.06					
GONR, rGONR, GOS and rGOS	TEM, SEM, AFM, XPS, Raman spectroscopy	GONR and rGONR: Length = 10μm, width = 50–200 nm; Thickness = 1 nm; O/C ratio = 54% for GONR and 19% for rGONR; Increase in I_D/I_G ratio upon reduction	0.01–100 μg/ml	Human MSCs	ROS assay, RNA efflux, cell viability (FDA) assay, Comet assay, Giemsa staining	Dose and shape dependent cytotoxicity with GONRs more cytotoxic than GOS. GONRs and rGONRs induce DNA fragmentation and chromosomal aberrations at 1 μg/ml.	Akhavan et. al. [67]
		GOS and rGOS: Thickness = 1.2 nm; Lateral size = 2μm; Reduction in oxygen content and increase in I_D/I_G ratio upon reduction					
GP	TEM, z-potential	GP: Diameter = 450nm−1.5μm; z-potential = −9.61	5–100μg/ml	U87, U118	Trypan blue, XXT-based proliferation, LDH, apoptosis kit	Activated apoptosis and necrosis in U87 cells whereas only apoptosis was activated in U118	Jaworski et. al. [68]

Material	Characterization	Properties	Treatment Concentration	Cell line	Assays	Conclusions	References
						cells.	
Pristine-G, COOH-GO	TEM, AFM, Raman, XPS	Thickness = 0.5μm	0–300μg/ml	Vero cells	Alamar Blue, LDH, Apoptosis, ROS,	Surface functionalization of graphene is critical for pacifying strong hydrophobic interaction associated with toxicity effects.	Sasidharan et. al. [69]
GQD-NH_2, GQD-COOH, GQD-CO-$N(CH_3)_2$	UV-Vis, TEM, FTIR	GQD-NH_2: Diameter = 7.5 nm; UV-Vis peak = 230 nm; Ex/Em = 420/500 nm; FTIR peaks at 1627 cm^{-1} (C=O), 1417 cm^{-1} (N-H), 1328 cm^{-1} (C-N),	0–200μg/ml	A549 and C6 glioma cells	MTT, Trypan blue, Fluorescence imaging,	No cytotoxic effects upto 200μg/ml treatment for all GQDs. Intracellular accumulation of GQDs was observed, nuclear translocation was absent.	Yuan et. al. [71]
		GQD-COOH: Diameter = 15 nm; UV-Vis peak = 362 nm; Ex/Em = 400/440 nm; FTIR peaks at 1388 and 1571 cm^{-1} (COO-),					
		GQD-CO-N(CH3)2: Diameter = 3–10 nm; UV-Vis peak = 300 nm; Ex/Em = 400/500 nm; FTIR peaks at 1400 and 1304 cm^{-1} (C-N)					
GO and rGO	AFM, EDX, Aerodynamic diameter (d_{ae})	Lateral dimension = 100nm – 5μm; Height = 1.1–15nm; d_{ae} = 20–200nm; Oxygen content = 40% in GO and 10% in rGO	0.0125–12.5 μg/cm^2	A549 and RAW 264.7 cells	MTT, DNA assay, FMCA assay, apoptosis, ROS, cell TEM	Dose dependent cytotoxicity. Cellular internalization of GO inside phagoendosomes was observed	Horváth et. al. [72]

Material	Characterization	Properties	Treatment Concentration	Cell line	Assays	Conclusions	References
PEG-amine functionalized GO	TEM, AFM, FTIR, DLS	Thickness = 1.8nm; Hydrodynamic size = 10–120nm;	75μg/ml	Saos-2 osteoblasts, MC3t 3-E1 preosteoblast, RAW-264.7 macrophages	ROS, Hoechst 33258, Gen-Probe Diaclone kit	After internalization, nanosheets are localized on F-actin filaments inducing cell-cycle alterations, apoptosis, and oxidative stress.	Matesanz et. al. [70]
GO, rGO	AFM, TEM, XPS, Raman spectroscopy	Flake size = 0.4–0.8μm; Thickness = 1 nm,	1–10μg/ml	HUVEC	MTT, LDH, ROS, FACS, RT-PCR, Comet assay	Oxidation state, dose and size dependent cytotoxicity. GO exhibits higher toxicity than rGO due to ROS generation. Small flake size graphene exhibit greater cytotoxicity compared to larger sheets due to intracellular accumulation of graphene.	Das et. al. [73]
GQD-PEG	AFM, TEM, FTIR, TGA, XPS, Elemental analysis	Diameter = 3–5 nm; Height = 0.5–1 nm; 1–2 graphene layers; Oxygen content 36%	10–640 μg/ml	HeLa, A549	WST-1, annexin V and PI, LDH, ROS,	No cytotoxicity; (HeLa cells treated with 160 μg/ml and A549 cells with 320 μg/ml doses show no cytotoxicity)	Chong et. al. [74]
TRGO-Cl, TRGO-Br, TRGO-I	Raman Spectroscopy, Elemental analysis, XPS	TRGO-Cl: Crystallite size/nm = 14.4, Amt. of halogen = 2.1, C/O = 16.77; TRGO-Br: Crystallite size/nm = 15.4, Amt. of halogen = 1.6, C/O = 20.37; TRGO-I: Crystallite size/nm = 22.3, Amt. of halogen = 0.2, C/O = 11.75.	0–200 μg/ml	A549	MTT, WST-8	Dose-dependent cytotoxicity between 3.125–200 μg/ml. Cytotoxicity depends on the amount of halogen content and follows the trend: TRGO-Cl > TRGOO-Br > TRGO-I.	Teo et. al. [75]

Material	Characterization	Properties	Treatment Concentration	Cell line	Assays	Conclusions	References
Fluorinated Graphene (F-G)	SEM, Elemental analysis, XPS, FTIR, XRD	Three different formulations with varying F content – 1.5%, 42.6%, 50.7%, C=C (284.5 eV), C-F (289 eV), C-F_2 (284.5 eV), C-CF (286.1 eV), C-CF_2 (287.3 eV), CF-CF_2 (290.5 eV), C-F_3 (293 5 eV); FTIR peaks at 1150 cm^{-1} (C-F)	0–400 μg/ml	A549	MTT, WST-8	Dose-dependent cytotoxicity of fluorinated graphene with greater cytotoxicity for graphene containing higher mono-fluoro substituted carbon atoms.	Teo et. al. [76]
Highly hydrogenated graphene (HHG) and GO	XPS, Elemental analysis	HHG: C/O ratio (8.79), H (37.42%), O (10.41%); GO: C/O ratio (2.78), H (25.72%), O (37.65%)	0–400 μg/ml	A549	MTT, WST-8	Greater cytotoxicity was observed due to increased adsorption of micronutrients on hydrophobic surface of HHG sheets limiting their availability.	Chng et. al. [77]
rGO, rGO+Arg, rGO+Pro	TEM, FTIR, Zeta ζ potential	Size: 100 nm – 1.5 μm. ζ = 19.5 (rGO), 32.5 (rGO+Arg), 39.8 (rGO+Pro) FTIR: rGO: 1769 cm^{-1} (C=O), 1602 cm^{-1} (C=C) and 1289 cm^{-1} (C-O); rGO+Arg and rGO+Pro: 3500–3140 cm^{-1} (O-H, N-H), 1570 cm^{-1} (C-O, C-N), 890-810 cm^{-1} (N-H), 1725 cm^{-1} (C=O)	50 μg/ml	U87	Trypan blue, XTT, gene expression	Reduction in GBM tumor volume was observed. rGO+Arg shows anti-angiogenic and pro-apoptotic characteristics and has potential for GBM therapy.	Sawosz et. al. [78]
GONR (PEG-DSPE dispersed)	TEM, Raman	Width = 125–220 nm, Length = 500–2500 nm; I_D/I_G = 1.3	10–400 μg/ml	HeLa, MCF-7, SKBR3, NIH3T3	Alamar blue, Neutral red, Trypan blue, LDH, ROS	Cell type dose, and time dependent cytotoxicity. Significant cell death observed for HeLa cells.	Mullick Chowdhury et. al. [36]

Material	Characterization	Properties	Treatment Concentration	Cell line	Assays	Conclusions	References
rGONP, GONP	AFM, XPS, Raman,	GONP: Length = 3.8±0.4μm; Thickness = 0.7nm;	0.01–100 μg/ml	hMSCs	FDA, ROS, RNA efflux, comet,	Size dependent cytotoxic response with smaller particles eliciting lower cytotoxicity compared to larger particles. Oxidative stress and direct contact interaction of extremely sharp edges of graphene were determined as most likely mechanisms for cytotoxicity of sheets and nanoplatelets.	Akhavan, et. al. [79]
		rGONP: Length = 418±56nm; Thickness = 1.1–2.3nm					
GO	TEM, AFM, FTIR, Raman spectroscopy, XPS, Particle-size distribution and ζ-potential	Large (l-GO): Size = 780±410 nm, Thickness = 0.9 nm, Hydrodynamic diameter = 556 nm, FTIR peaks at 1720cm^{-1} and band at 3400cm^{-1}, Oxygen content = 33.1%, I_D/I_G = 1.27, ζ-potential = −72.9	10–200 μg/ml	A549 cells	CCK-8, Trypan Blue, LDH, FITC-annexin V apoptosis, ROS	Cell viability and ROS generation is dependent on the size of GO sheets. Smaller GO sheet exhibit greater cell viability and less ROS generation.	Chang et. al. [80]
		Small (s-GO):Size = 160±90 nm, Thickness = 0.9 nm, Hydrodynamic diameter = 148 nm, FTIR peaks at 1720cm^{-1} and band at 3400cm^{-1}, Oxygen content = 37%, I_D/I_G = 1.26, ζ-potential = −51.9					
		Mixture (m-GO): Size = 430±300 nm, Thickness =					

Material	Characterization	Properties	Treatment Concentration	Cell line	Assays	Conclusions	References
		0.9 nm, Hydrodynamic diameter = 588 nm, FTIR peaks at 1720cm^{-1} and band at 3400cm^{-1}, Oxygen content = 35.8%, I_D/I_G = 1.25, ζ-potential = −59.2					
GO	AFM, stability and dispersion capacity, carboxyl group assay, TEM	GO: Length = 350nm and 2μm; Height = 3.9 and 4.05nm; Thickness = 1nm;	0–20μg/ml	PMØ, J774A.1, LLC, MCF-7, HepG2, HUVEC	LIVE/DEAD, CCK8, Coomassie Blue, CLSM, Cytokine assay	Cellular internalization independent of graphene size due to differential uptake mechanisms. Removal of Mn from Graphene sheets resulted in reduction of toxicity. Micron sized graphene induced stronger inflammatory response and release of cytokines.	Yue et. al. [81]
GO, PVP-GO	AFM, UV-Vis, FTIR	GO: Thickness = 1.7 nm; UV absorption peaks at 230 nm and 300 nm; FTIR peaks at 3395 cm^{-1}, 1726 cm^{-1}, 1620 cm^{-1}, 1410 cm^{-1}, 1226cm^{-1}, 1052cm^{-1}	25–100μg/ml	Dendritic cells, Macrophages, T lymphocytes	MTT assay, Phenotype assessment, Apoptosis assay	PVP functionalized GO sheets are immunocompatible and may be used as adjuvants to improve vaccine therapy	Zhi et. al. [82]
		PVP-GO: Thickness = 2.5 nm; UV absorption peak at 265 nm; FTIR peaks at 3395 cm^{-1}, 1726 cm^{-1}, 1620 cm^{-1}					
Pristine Graphene in 1% F108 pluronic	SEM, XRD, Raman	GO: I_D/I_G = 1.23; Thickness = 2–3nm; Size = 500–1000nm;	0–100μg/ml	RAW 264.7 macrophages	ROS, MMP, Apoptosis, TEM, Western-blotting, PCR,	Pristine Graphene can induce cytotoxicity through the depletion of mitochondrial membrane potential resulting in the	Li et. al. [83]

Material	Characterization	Properties	Treatment Concentration	Cell line	Assays	Conclusions	References
						increase of ROS leading to the activation of MAPK and TGF-β that in turn activate caspase-3 and PARP proteins resulting in apoptosis.	
GO	AFM, HRXPS, ATR-FTIR, DLS	GO: Thickness = 1–1.2nm; Hydrodynamic diameter = 2.4μm and 350nm;	5 or 100μg/ml	SNY-449, Mahlavu, A549, HEK293, RAW 264.7	TEM, Immunofluorescence, Western-blotting, RT-PCR, Flow Cytometry, siRNA	GO simultaneously triggers autophagy and activates toll-like receptors TLR4/TLR9 resulting in inflammatory responses.	Chen et. al. [84]
GO, C_{60}, C_{60}-tris	TEM, SEM, AFM, microscopy, spectroscopy, X-ray diffraction	GO: z-potential = −32.4mV; C60-Fullerenes: z-potential = −13.6; Sizes = 45.2±25.3nm; C60-TRIS Fullerenes: z-potential = −26 1; Size = 45.6±18.8nm	1.0, 6.25, 25.0μg/ml	B3Z T cells	LAL, FITC/Lucifer Yellow,	Both C60 and graphene capable of modulating antigen-specific T cell responses due to ability to directly affect functional activity of dendritic cells. GO suppresses antigen processing machinery of DCs.	Tkach et. al. [85]
GO, GS	X-ray diffraction, AFM, XPS, DLS, Z-potential	GO: Diameter = 765nm; z-potential = −40.6; GS: Diameter = 3018nm; z-potential = −37.2mV	3–200μg/ml	Suspended human RBCs and adherent skin fibroblasts.	MTT, WST-8, Trypan blue, ROS	Individually dispersed GO leads to greater RBC membrane damage compared to aggregated graphene sheets. Chitosan coated GO show no hemolytic activity	Liao et. al. [86]
GO, rGO	HR-TEM, 2DFFT, FTIR	Size = 0.2–5μm	0–20μg/ml	Human platelets	FITC, immunoblotting, LDH, ROS, Electron Microscopy	GO can evoke strong aggregatory response in platelets comparable to that elicited by thrombin.	Singh et. al. [87]
G-NH_2	FTIR, HR-TEM, FFT, Raman, z-potential, FSC, SSC	Size = 2μm	0–10μg/ml	Human platelets	ROS, MTT	G-NH2 is not associated with any pro-thrombotic characteristics and does not induce platelet-stimulating response. Membrane integrity of RBCs is	Singh et. al. [95]

Material	Characterization	Properties	Treatment Concentration	Cell line	Assays	Conclusions	References
						maintained.	
GO, rGO	HR-TEM, Raman, UV/vis, XRD	Size = 100–350nm	3–100μg/ml	L929 mice fibroblast cells	WST-1	Dose and surfactant dependent cytotoxicity of GO and rGO. Good cytocompatibility observed for concentrations between 3.125 and 12 5 μg/ml of GO and rGO dispersed in PEG.	Wojtonis zak et. al. [91]
GNP-Dex	AFM	Diameter = 60–100 nm; Thickness = 2–4 nm	1–10 mg/ml	RBL-2H3 mast cells, human platelets	Histamine release, platelet activation, complement activation, cytokine release, blood cell hemolysis	Dextran coated graphene oxide nanoplatelets exhibit no hematological toxicity	Mullick Chowdhury et. al. [89]
FBS-GO	TEM, AFM	Thickness = 1nm	20 and 100μg/ml	A549 cells	MTT, Bradford Protein Assay	FBS coating of GO attenuates cytotoxicity	Hu et al. [92]
BSA-GO	FITC-BSA, Steady State fluorescence spectra, AFM, Z-potential, SEM, CLSM, Flow cytometry, TEM,	Flake size: 50 nm or 1μm; z-potential = −10mV; Thickness = 9.1±7.1nm	50μg/ml	C2C12 cells	TEM, SEM, confocal microscopy, WST-1	BSA coated GO sheets exhibit size-dependent internalization. Small GO sheets are internalized by clathrin-mediated endocytosis and large GO sheets are internalized by phagocytosis.	Mu et. al. [93]
FBS and human plasma serum functionalized GONRs	AFM, XPS, Raman spectroscopy, FTIR, Mass spectrometry	Width = 100 nm; Height = 1 nm; FTIR peaks at 3400 cm^{-1} (O-H), 1760 cm^{-1} (C=O), 1300 cm^{-1} (C-OH), 1080 cm^{-1} (C-O); O/C ratio = 0.54; I_D/I_G = 1.38	10–100μg/ml	A549 cells	Trypan blue and Apoptosis assay	Dose dependent cytotoxicity of protein-functionalized GONRs was observed. Concentrations below 50μg/ml did not exhibit cytotoxic effects.	Mbeh et. al. [94]

Adv Drug Deliv Rev. Author manuscript; available in PMC 2017 October 01.

Table 2

In vivo toxicity of graphene

Intravenous Administration						
Material	**Characterization**	**Properties**	**Animal Model**	**Dose, Route and Duration**	**Conclusion**	**References**
GO, rGO	HR-TEM, Zeta-potential, UV-Vis NIR Spectroscopy, flow cytometry and fluorescence spectroscopy	GO: Size = 0.2–5 μm, Bilayer GO sheets with intersheet distance of 0.40±0.02 nanometer. FFT diffraction pattern confirms single and bi-layer GO. FTIR peak at 1735 cm^{-1} confirming C=O groups. rGO : Size = 0.2–5 μm, UV Vis: Red shift to 260 nm. FTIR confirms removal of oxygenated functional groups.	Swiss male mice (8–12 weeks old)	**Intravenous administration.** 250μg/kg dose injected via tail vein. Lungs collected for histological analysis (H&E staining) after 15 minutes.	**GO:** Thrombotoxicity, pulmonary embolism and human platelet aggregation observed. Nearly 48 % lung vessels totally or partially obstructed by platelet thrombosis. **rGO:** Limited platelet aggression and reduced thromboembolism compared to GO. rGO induce ~ 8% total or partial obstruction of lung blood vessels.	Singh et. al. [87]
Amine Graphene Oxide (NH_2-GO)	HR-TEM, FTIR, Raman spectroscopy, Zeta-potential, UV-Vis NIR spectroscopy, Flow cytometry	Sheet size: 2 μm, FTIR peaks: 950 cm^{-1}, 1250 cm^{-1}, 1573 cm^{-1}; Raman spectroscopy: G band = 1580 cm^{-1}, D band = 1350 cm^{-1}. High absorbance in visible and NIR region. No detectable fluorescence properties.	Swiss male mice (8–12 weeks old)	**Intravenous administration.** 250μg/kg dose injected via tail vein. Lungs collected for histological analysis (H&E staining) after 15 minutes.	**NH_2-GO** No thrombotoxicity. Blood vessels appear normal with no indication of occlusive pathology	Singh et. al. [95]
FLG, FLG-COOH, FLG-PEG, ^{99m}Tc-FLG-COOH, ^{99m}Tc-FLG-PEG	HR-TEM, AFM, Raman spectroscopy, FTIR, BET	Graphene sheets with 2 – 4 layers; Size: 128 ± 37.6 nm; Thickness: 0.7 ± 0.31 nm; Raman peaks at 1325 cm^{-1}, 1575 cm^{-1}, and 2640 cm^{-1} corresponding to D, G, and 2D bands, respectively; BET surface area = 210 – 650 m^2/g. FTIR peaks at 3400	Swiss albino mice (4–5 weeks old)	**Intravenous administration.** A single dose of 20 mg/kg injected via tail vein. Brain, kidney, lungs, liver, spleen, intestine, heart and testis were collected after 1, 8, 30, and 90 days.	Mice survived after 90 days of graphene administration. Body Weight of mice on days 60, 70, 80, and 90 were significantly lower than untreated mice.	Sasidharan et. al. [96]

		cm^{-1}, 1715 cm^{-1}				
GO-Dex, ^{125}I-GO-Dex	AFM, FTIR, TGA, UV-Vis	Size: 50–100 nm; Thickness: 2.8 nm; UV-VIS absorbance peak at 230 – 240nm	Female Balb/c Mice	**Intravenous administration.** 20 mg/kg GO-Dex injected into tail vein. Major organs collected for histology after 1, 3 and 7 days post injection. ^{125}I-GO-Dex injected at a dose of 4mg/kg. Blood collected for pharmacokinetics and biodistribution study at 4, 24, 72, and 168 hours post injection.	No short-term toxicity, excretion via renal and fecal pathways.	Zhang et. al. [97]
GO, ^{188}Re-GO	AFM, Raman spectroscopy, zeta potential	Size: 100–800nm; Thickness: 1nm; Single layered sheets; Zeta potential = −29.87 (GO), −20.47 (^{188}Re-GO)	Kun Ming Mice (Sprague-Dawley Rats, 6–8 weeks old)	**Intravenous administration. GO:** 1 and 10 mg/kg dose. Histopathological analysis of lung, liver, spleen and kidneys performed after 14 days post injection. **^{188}Re-GO:** 200μl (50 μCi) dose. Biodistribution measured after 1, 3, 6, 12, 24, and 48 hours post injection.	Dose dependent toxicity. No significant pathological changes were observed after day 1 whereas inflammation, cell infiltration, pulmonary edema and granuloma formation were observed after 14 days. GO exhibits high blood half life (5.3 ± 1.2 hours) and low RES uptake. Maximum uptake was observed in lungs.	Zhang et. al. [98]
GO	AFM, TEM, FTIR	Monolayer sheet; Thickness: 1nm; FTIR peaks at 3395 cm^{-1} (O-H), 1726 cm^{-1} (C=O), 1426 cm^{-1} (O-H), 1226 cm^{-1} (C-O), 1052 cm^{-1} (C-O)	Female Kunming Mice (Sprague-Dawley Rats, 4–5 weeks old)	**Intravenous administration.** Doses: 0 mg, 0.1, mg, 0.25 mg and 0.4 mg per mouse injected via tail vein. Histology and biodistribution analysis performed after 1, 7, and 30 days post injection.	No toxicity observed upto 0.25 mg dose. Chronic toxicity observed for 0.4 mg dose with 4/9 mice death. Long-term accumulation observed in liver, kidneys and spleen along with granuloma formation in lungs. No accumulation in brain - GO cannot pass blood brain barrier.	Wang et. al. [99]

GO, ^{125}I-GO	AFM, TEM, Raman Spectroscopy, Infrared Spectroscopy, particle size distribution, zeta potential, DLS	Size: Large GO = 1–5μm, Small GO = 110–500nm; Thickness: 0.9 nm (single layer); D_h for large GO = 914nm, D_h for small GO = 243nm.	Male ICR Mice	**Intravenous administration.** Single dose of 1–10 mg/kg administered via tail vein injection for biodistribution and pharmacokinetics studies. Tissue samples collected after 2–180 min post injection. For ultrastructural observation, 10 mg/kg dose was administered and lungs and liver collected 10 min post injection.	GO elimination from blood was observed. Large GO sheets accumulated in lungs and small GO accumulated in liver. Small GO has a longer blood half-life than large GO.	Liu et. al. [100]
NanoGraphene Sheets functionalized with polyethylene glycol (NGS-PEG)	AFM, FTIR, UV-Vis, NIR fluorescence	Size: 10–50 nm; Single or bi-layered sheets; FTIR peaks at 2800 cm^{-1} (C-H) and 1100–1500 cm^{-1} (C-O)	Tumor bearing Balb/c Mice	**Intravenous administration.** Single dose of 20 mg/kg. Organs harvested after 1, 6, and 24 hours post injection.	High tumor build up, no sign of abnormalities on the kidney, spleen, heart, liver and lung. Gradual elimination. Low uptake by RES. Photothermal therapy resulted in disappearance of tumor after 1-day treatment and an increase in the longevity of mouse by at least 24 days.	Yang et. al. [101]
NanoGraphene Sheets functionalized with polyethylene glycol (NGS-PEG), ^{125}I-NGS-PEG	AFM, FTIR, XPS	Size: 10–30 nm; Single or bi-layered GO sheets; FTIR peaks at 2800 cm^{-1} (C-H) and 1100–1500 cm^{-1} (C-O)	Balb/c Mice	**Intravenous administration.** Pharmacokinetics study: Mice injected with 4-mg/kg doses of ^{125}I-NGS-PEG and blood drawn between 0 – 25 hours. Biodistribution study: 4mg/kg dose injected then sacrificed at 1 h, 6 h, 1 d, 3 d, 7 d, 15 d, 30 d, 60 d. Blood biochemistry/Hematology study: injected	NGS-PEG mainly accumulates in the reticuloendothelial system and can be gradually cleared by renal and fecal excretion.	Yang et. al. [102]

				intravenously 20 mg/kg sacrificed at 3, 7, 20, 40, and 90 days.		
GNP-Dex	TEM, AFM	Disc Shaped; Diameter: 100 nm; Thickness: 3 nm	Wistar Rats	**Intravenous administration.** Dose: 1, 50, and 100 mg/kg 3 times a week for 3 weeks. Heart, liver, kidney and brain harvested for histology.	1 mg/kg and 50 mg/kg doses show no sign of toxicity. All vital parameters such as body weight, blood pressure, breathing and heart rate were normal. Two out of 8 animals died for 100mg/kg dose after 2 weeks.	Kanakia et. al. [103]
GNP-Dex	AFM	Diameter range: 60 – 100 nm. Thickness: 2 – 4 nm. Soluble in water up to 100 mg/ml	Male hamsters	Hamsters' left cheek pouch was exteriorized, pinned across a Lucite pedestal, and cleared of connective tissue. GNP-Dex was micropipetted at dosages of 0, 0.1, 0.5, 2.6, 10, 50 mg/ml at 30 seconds exposure and 5-minute washout between dosages.	GNP-Dex showed no signs of arteriole dilation upto concentrations of 50mg/ml.	Chowdhury et. al. [89]
GNP-Dex	TEM, AFM	Disc Shaped; Diameter: 100 nm; Thickness: 3 nm	Wistar Male Rats	**Intravenous administration.** Single doses of 1, 25, 50, 125, 250 and 500 mg/kg were injected via tail vein. Organs were harvested 1 and 30 days post injection of GNP-Dex for biodistribution and histopathological analysis.	Maximum Tolerable dosage is between 50 mg/kg and 125 mg/kg. No changes in brain, neither cardiovascular, nor hematological factors at dosages less than 125 mg/kg.	Kanakia et. al. [104]
GO, GO-NH_2, GO-DOTA, ^{111}In-DOTA-GO	TEM, AFM, FTIR, XPS, TGA, Raman spectroscopy	Size: 50–2000 nm; Single or bilayered GO sheets, FTIR peaks at 3400 cm^{-1} (OH), 1729 cm^{-1} (C=O), 1624 cm^{-1} (H-O-H), 1374 cm^{-1} (O-H), 1225 cm^{-1}	C57BL/6 mice (6–8 weeks)	**Intravenous administration.** A dose of 200 μl of ^{111}In-GO-DOTA (5–6 MBq) was injected via tail vein (t = 1, 4, 24 hours) for SPECT/CT study.	Maximum accumulation was observed in liver and spleen, however, GO translocation from liver to spleen was also observed. No bilary excretion or metabolism by	Jasim et. al. [105]

			(C-O-C); I_D/I_G = 1.34 (GO-DOTA), 1.21 (GO), 0 31 (Graphite)		For biodistribution study, animals were injected with 1–2 MBq equivalent dose for 1, 4, and 24 hours.	hepatocytes was observed. GO was eliminated via urine. These results suggest that chemical functionalization of GO sheets can alter their biodistribution.	
Intraperitoneal Administration							
^{125}I labeled GO, nGO-PEG, RGO-PEG and nRGO-PEG	AFM	Size: Diameters of GO, nGO-PEG, RGO-PEG and nRGO-PEG are 450, 25, 50 and 27 nm, respectively. Average thickness of GO, GO-PEG, RGO-PEG, and nRGO-PEG are 0.94, 1.22, 4.43 and 5.66 nm, respectively.	Female Balb/c Mice	**Intraperitoneal administration:** 80 mice were intraperitoneally injected with GO, nGO-PEG, RGO-PEG, and nRGO-PEG at 50 mg/kg (20μCi) and euthanized 1, 7, 30, and 90 days post administration. **Oral administration:** 15 mice were orally injected with nGO-PEG at 100 mg/kg dose and euthanized at 1, 7, and 30 days post injection. Blood was collected for serum biochemistry and blood panel analysis. All major organs were collected for histology and biodistribution.	High accumulation in liver and spleen after intraperitoneal administration. No accumulation was observed after oral administration. PEG GO derivatives were phagocytized in the RES system in a size and surface coating dependent manner. Despite long-term retention, no toxicity was observed in blood analysis, serum biochemistry and histology analysis. Toxicity and biodistribution of graphene is dependent on size, surface coatings and route of administration.	Yang et. al. [106]
cGO and pGO (highly pure GO)	TEM, AFM, FTIR, Raman spectroscopy, UV-Vis	Size: cGO: > 0.1 μm^2, pGO; 0.01–0.02 μm^2; Thickness ~1 nm. UV absorbance peak at 230 nm. Raman spectroscopy: D Band = 1350 cm^{-1}, G Band = 1590 cm^{-1}	C57BL/6 Mice (6–8 weeks old)	**Intraperitoneal administration:** Dose 50 μg in 0.5 ml saline. Animals euthanized 24 hours and 7 days post administration and assessment of Inflammatory reactions, protein levels in peritoneal lavage and histology of diaphragm was performed.	Highly purified single layered GO sheets show no signs of inflammation or granuloma formation upto 50-μg/animal dose administered intraperitoneally.	Ali-Boucetta et. al. [107]
GO-pluronic hydrogel	TEM, SEM, Rheology	Size: 100–500 nm. Gelation at pH = 7, absorbs IR light	Female Balb/c mice (6–7 weeks old)	**Intraperitoneal administration.** Gel composition: 0.4% GO-0.25–1% pluronic. GO-pluronic gel implanted in subcutaneous cavity of mice. After 3 and 8 weeks post implantation, dermal tissue was analyzed by histology.	No toxicity was observed. Mild inflammation observed after 3 weeks of implantation. After 8 weeks, the number of macrophages reduced. No tissue necrosis, acute inflammation or tissue hemorrhaging was observed suggesting a good biocompatibility of GO-pluronic gels.	Sahu et. al. [108]

GO, graphite, nanodiamonds (ND)	TEM, Zeta potential	Size: 8–25 nm (GO), 3–4 nm (graphite and ND); Zeta potential: −83.8 ± 0.25 mV (GO), 12.5 ± 0.43 (graphite), −15.8 ± 0.55 mV (ND)	Female Wistar rats (6 weeks old)	**Intraperitoneal administration:** 40 mice were injected with a dose of 4 mg/kg administered for 4 or 12 weeks at 3-day intervals. Liver and blood collected post euthanasia for analysis of blood serum biochemical indices, blood morphology and liver physiology.	No toxicity was observed. Blood biochemical indices and liver enzymes were within physiological range. Large aggregates of nanomaterials were observed at the injection site, smaller aggregates were observed in liver serosa and mesentery.	Strojny et. al. [109]	
Oral Administration							
GO	TEM, AFM, XRD, FTIR, XPS, UV-Vis and Raman spectroscopy,	Size: 0.2 μm; Thickness = 1.8 nm; XRD peaks at 12 and 43 ; UV-Vis peaks at 232 nm and 280 nm; FTIR peaks at 1715 cm^{-1} (C=O), 1120 cm^{-1} (C-O-C), 3400 and 1620 cm^{-1} (O-H); XPS - C:O molar ratio 2:11, C1s peaks at 285 eV (C=C), 286.1 eV (C-O), 287.5 eV (C=O), 288.5 eV (C=O); Raman peaks at 1355 cm^{-1} (D band), 1588 cm^{-1} (G band) and 2680 cm^{-1} (2D band).	Female ICR mice (6–8 weeks old)	**Oral administration.** Dose: 0.5 and 0.05 mg/ml. GO mixed with drinking water. Days 1–38 for maternal mice and 1–21 for filial mice. After 21 and 38 days, blood was collected for biochemistry analysis and organs were harvested for H&E staining.	Decrease in body weight, body length and tail length for high concentration group. No significant differences in blood biochemistry. Pathological examination shows severe atrophy of all major organs. H&E staining of intestine showed increased villi and duodenum width. Results show that GO is toxic to developmental offsprings in mice.	Fu et. al. [110]	
^{125}I-rGO	TEM, Particle size distribution	Size: Small GO (~100nm), Large GO (~450nm)	Male C57b/6 mice (6–8 weeks old)	**Oral administration.** Dose 60mg/kg, administered via oral gavage every 24 hours for 5 days.	Initial decrease neuromuscular coordination and locomotor activity, which were restored to normal levels at later time points (15 and 60 days post administration). No significant differences in blood biochemistry, liver function, kidney function, blood enzyme levels, learning, memory, anxiety, and spatial and exploratory behaviors. rGO administered via oral administration is non-toxic.	Zhang et. al. [111]	

GO	TEM, AFM, FTIR, Raman spectroscopy and Particle size tracking	Size: 72 ± 11 nm; Thickness: 1 nm, FTIR peaks: 3425 cm^{-1} (O-H), 1749 cm^{-1} (C=O), 1630 cm^{-1} (C=O), 1130 cm^{-1} (C-O). Raman peaks at 1377 cm^{-1} (D band) and 1609 cm^{-1} (G band); Zeta potential = −20.2 mV.	*Caenorhabditis elegans*	**Oral administration.** GO mixed with food (K medium) at 0.1–100 mg/L.. Acute exposure (24 hours) and prolonged exposure (larvae to adult). Lethality, growth, reproduction and locomotion behavior was analyzed.	Prolonged exposure to 0.5–100 mg/L of GO caused damage in primary (intestine) and secondary (neurons and reproductive) organs. GO translocated into intestinal wall due to loss of villi and were distributed surrounding mitochondria. Additional observations were increased mean defecation cycle length and hyper-permeable state of intestinal barrier. Results suggest that GO exposure to environmental organisms is toxic.	Wu et. al. [112]
Pulmonary Administration							
GNPs	SEM, EPR, BET, density measurement, Aerodynamic diameter, ICP-MS	Size: Diameter = 5.64 ± 4.56 nm, Layers = 1–10; Surface area = ~100m^2/g; Density = ~2; EPR = 867.3± 77.5 a.u.	Female C57BL/6 mice (9 weeks old)	**Pharyngeal administration.** Dose - 50 μg/mouse. Mice sacrificed after 24 hours and 1-week post exposure. BAL fluid was extracted. **Intrapleural injection:** Dose - 5μg /mouse. Mice sacrificed after 24 hours and 7 days. Pleural space was lavaged and the surrounding tissue was excised for histology.	GNPs upto 25 μm are respirable and deposit beyond ciliary airways post inhalation. GNPs induced inflammation in lung and pleural space with an increase in the levels of MIP-1α, MCP-1, MIP-2, IL-8 and IL-1β. SEM images revealed signs of frustrated phagocytosis. Inflammatory response decreased one-week post exposure.	Schinwald et. al. [113]
Graphene (aggregated in water), Graphene (2% pluronic), GO	AFM, XPS, Raman spectroscopy, optical absorbance	Optical absorbance: 600nm; Size: 40,000 nm^2 (Graphene), 200,000 nm^2 (GO); Thickness: 1.2–5 nm (Graphene), 0.5–2 nm (GO)	Male C56BL/6 mice (8–12 weeks old)	**Pulmonary administration.** Dose - 50 μg/mouse administered via intratracheal instillation. GO is injected directly into the lungs. Lung assessment post 24 hours using histology and electron microscopy	Inflammation, apoptosis, increase of mitochondrial respiration and pulmonary inflammation were observed.	Duch et. al. [114]
^{125}I-GO	TEM, SEM, AFM, FTIR, Raman spectroscopy	Size: 10–800 nm; Thickness: 1 nm; FTIR peaks at 1731 cm^{-1} (O-H), 1628	Male Kunming mice (biodistribution) and male	**Pulmonary administration.** Dose: 1, 5, 10 mg/kg for dose dependent acute and chronic pulmonary toxicity assessed after 24 hours. 10mg/kg for time dependent toxicity assessed after 0, 24,	Acute lung injury, thickening of alveolar septa, increased neutrophil counts and oxidative damage were observed. GO can pass through air-blood	Li et. al. [115]

		cm^{-1} (C=C), 1078 cm^{-1} (C-O); Raman peaks: 1333 cm^{-1} (D band), 1594 cm^{-1} (G band).	C57BL/6 mice (pulmonary toxicity)	48, 72 hours and 1 week. 10 mg/kg for long-term chronic toxicity assessed after 1 and 3 months. Biodistribution evaluated by SPECT imaging, pulmonary toxicity by histology and cell injury, lung edema and neutrophil infiltration assays.	barrier albeit in smaller amounts and care must be taken to ensure minimal exposure by inhalation during large-scale production of GO.	
Intravitreal administration							
GO	AFM, FTIR, Raman spectroscopy	Size: 50–500 nm; Thickness: 1 nm; FTIR peaks at 3430 cm^{-1}, 1720 cm^{-1}, and 1000 cm^{-1}; Raman Spectroscopy: D band at 1370 cm^{-1}, G band at 1590 cm^{-1}. I_D/I_G = 0.75	Japanese White Rabbits (2–3 kgs)	**Intravitreal administration.** Dose: 0.1, 0.2, or 0.3 mg. Eye function was measured using electroretinography (ERG) after 2, 7, 28 and 49 days post injection. After 49 days, animals were euthanized and eyes were collected for histological examination. Balanced sale solution was used as the controls.	No significant differences in ERG amplitudes compared to controls. H&E staining showed small amounts of GO residue, however, no retinal abnormality was observed.	Yan et. al. [116]

Table 3

Antibacterial toxicity of graphene

Material	Characterization	Properties	Dose	Cell line	Assays	Conclusions	References
rGO	FTIR, Raman, TEM, SEM	Size: < 5μm; Raman peaks: 1342 cm^{-1} (D band), 1576 cm^{-1} (G band), I_G/I_D = 0.85; FTIR peaks at 3200–3400 cm^{-1} (O-H), 1718 cm^{-1} (C=O), 1579 cm^{-1} (C=C), 1226 cm^{-1} (C-OH), 1070 cm^{-1} (C-O)	0–500μg/ml	A. niger, F. oxysporum, A. oryzae	Antifungal Assay	IC_{50} value is between 50–100 μg/ml. rGO shows good antifungal activity.	Sawangphruk et. al. [117]
GONW, rGONW	SEM, XPS, Raman	XPS peaks at 285 eV (C-C, C=C, C-H), 285.8 eV (C-OH), 287.6 (C=O), 289.1 eV (O=C-OH); A_{COH}/A_{CC} = 1 35 (GONW) and 0.08 (rGONW). I_D/I_G: 1.78 (GONW) and 1.26 (rGONW)	1mg/ml	E. coli, S. aureus	Efflux of RNA	Sharp edges of the nanowalls resulted in efflux of RNA. S. aureus bacteria was further damaged as compared to E. coli.	Akhavan et. al. [118]
PEI-rGO, PEI-rGO-AgNPs	z-potential, XPS, TEM, UV/vis, AFM, FTIR, XRD	Thickness: 0.6nm, Size: 5–15nm, Zeta potential = −46.7 mV.	0–958 mg/L	E. coli, S. aureus	Antibacterial Test	PEI-rGO shows ~14–20% antibacterial activity which increases to ~90% for PEI-rGO-AgNPs. Blade like edges of PEI-rGO-AgNP causes cell disruption leading to long-term antibacterial effect	Cai et. al. [119]
rGO, GO	DLS, AFM, UV-Vis, TEM, Raman, FTIR	Size: 300–600 nm; Thickness: 0.76 nm (GO), 1.6 nm (rGO); Raman peaks at 1350 cm^{-1} 1590 cm^{-1}; UV-Vis peak: 230 nm (GO), 267 nm (rGO); FTIR peaks at 3423 cm^{-1} (O-H), 1750 cm^{-1} (C=O), 1200 cm^{-1}	50–250μg/ml	Xanthomonas oryzae pv. Oryzae, Xoo	Antibacterial Activity	GO has extremely prominent dose-dependent inhibitory effect on cell growth due to combination of membrane damage and oxidative stress.	Chen et. al. [120]

Material	Characterization	Properties	Dose	Cell line	Assays	Conclusions	References
		(C-OH), 1050 cm^{-1} (C-O) for GO and 3400 cm^{-1} and 1047 cm^{-1} for rGO.					
PVK-GNP thin films	TGA, AFM, UV-Vis	Thickness: 150nm; Roughness: 24.7nm, UV Vis peaks at 240, 250, 295, 331 and 344 nm	1, 0.5, 0.05, 0.01mg /ml	E. coli, B. subtilis	Metabolic Activity Assay, Bacterial Viability Assay	Antimicrobial property of PVK-GNP nanocomposite is dependent on the concentration of GNPs. PVK-GNP films do not show cytotoxicity to NIH3T3 fibroblasts.	Santos et. al. [121]
PVK-GO	SEM	Size: ~ 1μm; Thickness: 150nm; Roughness: 24.7nm, UV Vis peaks at 240, 250, 295, 331 and 344 nm	10–1000μg /ml	Escherichia coli, Cupriavidus metallidurans, Bacillus subtilis, Rhodococcus opacus	Metabolic Activity Assay	The addition of PVK to GO enhances antimicrobial properties of the nanocomposite in a dose-dependent manner. PVK-GO nanocomposite has low toxicity towards mammalian cells.	Carpio et. al. [122]
GO, rGO and GO or rGO antibacterial paper	SEM, AFM, TEM	Thickness: 1.1nm (GO), 1 nm (rGO); 1.5μm (GO paper), 4.6μm (rGO paper);	0, 20, 85 μg/ml	E. coli	ATP assay	GO and rGO demonstrate superior antibacterial effect with only mild cytotoxicity towards mammalian cells (A549). rGO showed slightly greater toxicity towards A549 cells than GO	Hu et. al. [123]
Pristine graphene, GO, rGO	TEM, SEM, Zeta potential, FTIR	**Pristine graphene:** Size = 1.86 ± 0.6 μm, Zeta potential = −17.7± 4.3 mV, C=C. **GO:** Size = 1.27 ± 0 1 μm, Zeta potential = −49.8± 1 mV, O-H, C=C, C=O, C-O, C-H. **rGO:** Size = 2.53 ± 0 2 μm,	25 and 250 μg/ml	*Listeria monocytogenes* and *Salmonella enterica*	Bacterial growth inhibition	GO inhibits (~100% cell death) both bacterial strains at high and low treatment concentration. Pristine graphene and rGO exhibit variable antibacterial response. Presence of oxidative functional groups is important for bacterial cell attachment to graphene	Kurantowicz et. al. [127]

Material	Characterization	Properties	Dose	Cell line	Assays	Conclusions	References
		Zeta potential = −25.1± 2.6 mV, C=C, C-O, C=O.					
GO	AFM, SEM, XPS	Size: 0.753, 0.127 0.065 0.035 0.013 0.010 μm^2, Thickness: 1nm; XPS peaks at 283.17 eV (C=C), 285.21 eV (C-O), 286.9 eV (C=O).	0–80 μg/ml	E. coli	Antibacterial Activity	Size dependent antibacterial activity of GO sheets. Larger sheets exhibit greater antibacterial activity	Liu et. al. [129]
GO, rGO	AFM, SEM, FTIR, XPS	Size: 300 nm (GO), 2.71 μm (rGO); Thickness: 1nm (GO) and few microns (rGO, aggregated); FTIR peaks at 3430 cm^{-1} (O-H), 1720 cm^{-1} (C=O), 1215 cm^{-1} (C-OH), 1050 cm−1 (C-O), for rGO no peaks at 1720 cm^{-1}, 1050 cm^{-1} and 1215 cm^{-1}	5–80μg/ml	E. coli	Bacterial Membrane, Oxidative Stress	GO has a higher antibacterial activity than other materials including reduced graphene oxide, graphite oxide and reduced graphite oxide that can be attributed to membrane and oxidative stresses.	Liu et. al. [128]

Table 4

Environmental toxicity of graphene

Material	Characterization	Properties	Conclusion	References
Graphene	AFM, SEM, TEM	Height: 1 nanometer. TEM reveals typical wrinkled structure. Range of length × breadth: 0.5 × 0.6 – 1.5 × 6 5 μm	Cotyledons and root system growth were slowed down with increasing concentration on tomatoes, cabbage, and red spinach; had no effect on lettuce. Primary roots were shorter and disappeared root hairs compared to the control. Graphene caused decreased root and shoot weight. Decreased number of leaves.	Begum et. al. [130]
Few Layer Graphene	TEM, AFM	Thickness: 2–5 nm; Diameter: 100–200 nm	No Significant effect on growth of tomato plants.	Khodakovskaya et. al. [131]
GONRs	AFM, FTIR, Raman spectroscopy	Bath sonication: 700–900 nm (20 mins) Probe sonication: 300–400 nm (1 min), <300 nm (5 mins), <200 nm (10 mins) I_D/I_G ratio: 1.30 (bath sonication) – 2.30 (probe sonication)	Post processing high energy sonication leads to reduction in size of GONRs. Probe sonicated solutions of GONRs show greater medaka embryo mortality compared to non sonicated or bath sonicated solutions.	Mullick Chowdhury et. al. [60]
GO	AFM, XPS, SEM	Interlayer Spacing: 1 nm.	Inhibition of metabolic activity at all concentrations. GO is biodegraded by at least 50% after 5h. Inhibition of nitrifying bacteria.	Ahmed et. al. [132]
Graphene	TEM, AFM, Raman spectroscopy	No Holes or Defects, Basic Hexagonal Lattice. Height: 0.34 nm	Post Hydrogen Peroxide Treatment: Randomly distributed holes in Graphene. Diameter of holes increase with higher concentration of H2O2.	Xing et. al. [133]
GONRs and rGONRs	TEM, Raman Spectroscopy, UV-Vis	Flat, Smooth, and uniform multi-layered sheets.	Lignin peroxidase Activity: GONR: Structure completely degraded by 96 hours. rGONR: Holes from outer to inner layers in the sheets. Both materials eventually degrade, but there is a delay in degradation for rGONR compared to GONR	Lalwani et. al. [134]

Éric Bédard

De: Marie-Pascale Sassine
Envoyé: 30 mars 2021 07:45
À: Patricia Hudson
Cc: Marième Pelletier; Stéphane Caron; Stéphane Perron
Objet: Masque Graphene: Avis de Santé Canada

Bonjour Patricia, lorsque tu parleras avec Richard Massé. S'il y a des suites à ce dossier, est-ce possible de demander si des démarches avec santé Canada ont été entreprises pour en savoir davantage?

Merci

Marie-Pascale Sassine

Chef d'unité scientifique

Santé au travail, DRBST

marie-pascale.sassine@inspq.qc.ca

INSPQ Centre d'expertise et de référence en santé publique

190 rue Crémazie est Montréal (Québec) H2P 1E2

From: Patricia Hudson <patricia.hudson@inspq.qc.ca>
Sent: Friday, March 26, 2021 11:38:43 AM
To: Marie-Pascale Sassine <marie-pascale.sassine@inspq.qc.ca>; Stéphane Caron <stephane.caron@inspq.qc.ca>; Marième Pelletier <marieve.pelletier@inspq.qc.ca>
Subject: TR: Avis de Santé Canada

Merci de donner suite en répondant directement à Richard et me mettant en copie. SVP me revenir avec un échéancier de réponse.

Patricia Hudson, M.D., FRCPC
Directrice scientifique
Institut national de santé publique du Québec
Direction des risques biologiques et de la santé au travail
courriel : patricia.hudson@inspq.qc.ca

Adresse physique : 190, boulevard Crémazie, 2.36, Montréal (Québec) H2P 1E2
Téléphone : 514 864-1600, poste 3201

Adresse postale : 945, rue Wolfe, C5-21, Québec (Québec) G1V 5B3
Adjointe de direction : 418 650-5115, poste 5200

De :	Roberts, Jessica (HC/SC)
A :	Vladisavljevic, Djordje (HC/SC); Jean-Bernard Gamache
Cc :	Marie-Pascale Sassine; Bell, Mary-Jane (HC/SC); Ashby, Deborah (HC/SC); Schmidt, Chris (HC/SC); Fisher, Brad (HC/SC)
Objet :	RE: Graphene nanoparticles masks
Date :	1 avril 2021 16:06:34

Thank you for responding, Djordje;

CHPSD agrees with your direction to Mr. Gamache to consult the Medical Devices Directorate, seeing that we (CHPSD- Risk Assessment Bureau) have not previously been involved in the assessment of graphene.

Kind regards,

Jess
~~~~~~~~~~~~~~~~~

Jessica Roberts
(she / her | elle)
Unit Head, Toxicology
Risk Assessment Bureau
Consumer and Hazardous Products Safety Directorate
Health Canada,

jessica.roberts@canada.ca

Chef d'unité, toxicologie
Bureau de l'évaluation du risque
Direction de la Sécurité des produits de consommation et des produits dangereux
Santé Canada

From: Vladisavljevic, Djordje (HC/SC) <djordje.vladisavljevic@canada.ca>
Sent: 2021-04-01 2:04 PM
To: Jean-Bernard Gamache <Jean-Bernard.Gamache@inspq.qc.ca>; Roberts, Jessica (HC/SC) <jessica.roberts@canada.ca>
Cc: Marie-Pascale Sassine <marie-pascale.sassine@inspq.qc.ca>; Bell, Mary-Jane (HC/SC) <mary-jane.bell@canada.ca>; Ashby, Deborah (HC/SC) <deborah.ashby@canada.ca>; Schmidt, Chris (HC/SC) <chris.schmidt@canada.ca>
Subject: RE: Graphene nanoparticles masks

Hello Dr. Gamache,
~~~~~~~~~~~~~~~~~

I would refer you to the Medical Devices Directorate of Health Canada who are currently leading HC's response to the issue of face masks containing graphene. Chris Schmidt and Mary-Jane Bell have been directly involved in the risk assessment and provision of policy advice, I have CC'd them here.

My team has been involved in a secondary role consulting with the Medical Devices Directorate and reaching out to one of the companies who are manufacturing graphene in Canada to bring them into compliance with the New Substances Notification Regulations (NSNR) under the Canadian Environmental Protection Act (in addition to their obligations under the Food and Drugs Act, as the masks in question are considered Class I medical devices).

In the summer of 2020 my Section conducted a risk assessment of graphene under the NSNR and issued a notice for additional information under specific use scenarios for graphene (CAS RN 1034343-98-0). The chemists and biologists on my team are experts in risk assessment of nanomaterials and we would be happy to help INSPQ in responding to any requests you have received.

Please let us know when you would like to arrange a meeting and we will do our best to accommodate you.

Regards,

Djordje Vladisavljevic
(pronouns: he, him | pronoms: il, lui)

Head, Nanotechnology Section
New Substances Assessment and Control Bureau
Healthy Environments and Consumer Safety Branch
Health Canada / Government of Canada
djordje.vladisavljevic@canada.ca / [redacted]

Chef de section, Section de la nanotechnologie
Bureau de l'évaluation et du contrôle des substances nouvelles
Direction générale de la santé environnementale et de la sécurité des consommateurs
Santé Canada / Gouvernement du Canada
djordje.vladisavljevic@canada.ca / [redacted]

From: Jean-Bernard Gamache <Jean-Bernard.Gamache@inspq.qc.ca>
Sent: 2021-04-01 1:23 PM
To: Vladisavljevic, Djordje (HC/SC) <djordje.vladisavljevic@canada.ca>; Roberts, Jessica (HC/SC) <jessica.roberts@canada.ca>
Cc: Marie-Pascale Sassine <marie-pascale.sassine@inspq.qc.ca>
Subject: Graphene nanoparticles masks

Mr Vladisavljevic,
Mrs Roberts

Our organization has received a request regarding the health risks of masks that contain graphene nanoparticles. Are you currently working on similar requests? Would you have some exerts among your teams that we could contact concerning this specific subject?

I would welcome an opportunity to meet you in the coming weeks.

Best regards,

Jean-Bernard Gamache, PharmD, MBA
Chef d'unité scientifique - Évaluation et soutien à la gestion des risques
Direction de la santé environnementale et de la toxicologie
Institut national en santé publique du Québec
190 boulevard Crémazie E, Montréal (Québec) H2P 1E2
jean-bernard.gamache@inspq.qc.ca
INSPQ Centre d'expertise et de référence en santé publique
www.inspq.qc.ca

Éric Bédard

De: Marie-Josée Archetto
Envoyé: 6 avril 2021 08:10
À: Caroline Huot; Stéphanie Potvin; Mariève Pelletier; Stéphane Caron; Stéphane Perron
Cc: Christiane Thibault; Marie-Pascale Sassine; Jean-Bernard Gamache
Objet: TR : PVI - Avis de Santé Canada - Les masques contenant du graphène peuvent présenter des risques pour la santé

PVI

Marie-Josée Archetto, B.Sc.inf, att.SP

Conseillère à la direction
Direction des risques biologiques et santé au travail
Institut national de santé publique du Québec
190, boulevard Crémazie Est, Montréal (Québec) H2P 1E2
Tél. : 514-864-1600
Courriel : marie-josee.archetto@inspq.gouv.qc.ca

INSPQ Centre d'expertise et de référence en santé publique
www.inspq.qc.ca

De : Josée Dubuque <Josee.Dubuque@msss.gouv.qc.ca>
Envoyé : 6 avril 2021 07:47
Objet : TR: PVI - Avis de Santé Canada - Les masques contenant du graphène peuvent présenter des risques pour la santé

Destinataires
Coordonnateurs en MI
cc : INSPQ/DRBST, Équipe Intervention du MSSS

Bonjour,

Je vous fais suivre pour information le courriel ci-dessous de Santé Canada concernant les masques contenant du graphène.

Bonne journée
Josée

Santé et Services sociaux Québec

Josée Dubuque, M.Sc.
Directrice de la prévention et du contrôle des maladies infectieuses
Direction générale adjointe de la protection de la santé publique
Ministère de la Santé et des Services sociaux
201, Crémazie Est, bureau 2.01
Montréal (Québec) H2M 1L2
Téléphone : **(438) 985-6529**
Télécopieur : (514) 864-2778
Courriel : josee.dubuque@msss.gouv.qc.ca

Bonjour,

Simplement vous aviser, considérant l'étendue de la couverture médiatique à ce sujet au Québec, que Santé Canada a émis l'avis suivant destiné au grand public, aux professionnels de la santé, et aux hôpitaux **le vendredi 2 avril**.

Les masques contenant du graphène peuvent présenter des risques pour la santé
Face masks that contain graphene may pose health risks

Salutations, et Joyeuses Pâques!
Maganga

_____

Maganga Lumbu
Directrice régionale /
Regional Director
Direction des affaires publiques et des communications /
Communications and Public Affairs Directorate
Santé Canada et Agence de la santé publique du Canada - Région du Québec /
Health Canada and the Public Health Agency of Canada - Quebec Region
Tel : (514) 770-6645
www.santecanada.gc.ca / www.healthcanada.gc.ca

Votre santé et votre sécurité… notre priorité / Your health and safety… our priority

Éric Bédard

De: Che, Melinda (HC/SC) <melinda.che@canada.ca>
Envoyé: 8 avril 2021 09:09
À: Jean-Bernard Gamache
Cc: Medical Devices Directorate / Direction des instruments méd (HC/SC); Marie-Pascale Sassine
Objet: FW: Graphene nanoparticles masks

Indicateur de suivi: Assurer un suivi
État de l'indicateur: Terminé

Dear Mr. Gamache:

Thank you for your email. I am writing from the Science Advisor Office of the Medical Devices Directorate (MDD). We are responsible for regulating the importation and sale of medical devices. Our team has been reviewing the information on the Biomass graphene mask.

We would certainly like to meet with you to further discuss the request. I could arrange for a meeting with our team next week. Please let me know if you have any preferred date/time.

Sincerely,

Melinda

Melinda Ché
Health Canada | Santé Canada
Medical Devices Directorate | Direction des instruments médicaux
Director General's Office | Bureau du directeur général
Email |Courriel melinda.che@canada.ca
Telephone | Téléphone 613-941-1143 / Facsimile | Télécopieur 613-957-9969
[redacted]
Government of Canada | Gouvernement du Canada

From: Jean-Bernard Gamache <Jean-Bernard.Gamache@inspq.qc.ca>
Sent: 2021-04-01 1:23 PM
To: Vladisavljevic, Djordje (HC/SC) <djordje.vladisavljevic@canada.ca>; Roberts, Jessica (HC/SC) <jessica.roberts@canada.ca>
Cc: Marie-Pascale Sassine <marie-pascale.sassine@inspq.qc.ca>
Subject: Graphene nanoparticles masks

Mr Vladisavljevic,
Mrs Roberts

Our organization has received a request regarding the health risks of masks that contain graphene nanoparticles. Are you currently working on similar requests? Would you have some exerts among your teams that we could contact concerning this specific subject?

I would welcome an opportunity to meet you in the coming weeks.

Best regards,

Jean-Bernard Gamache, PharmD, MBA
Chef d'unité scientifique - Évaluation et soutien à la gestion des risques
Direction de la santé environnementale et de la toxicologie
Institut national en santé publique du Québec
190 boulevard Crémazie E, Montréal (Québec) H2P 1E2
jean-bernard.gamache@inspq.qc.ca
INSPQ Centre d'expertise et de référence en santé publique
www.inspq.qc.ca

Éric Bédard

De: Jean-Bernard Gamache
Envoyé: 12 avril 2021 17:19
À: Vladisavljevic, Djordje (HC/SC); Marie-Pascale Sassine
Cc: Ashby, Deborah (HC/SC)
Objet: RE: Graphene nanoparticles masks

Hi Djordje,

Thank you for sharing all this information. It will definitely help to our teams of experts. We will contact you and your team if we have further questions.

It was our pleasure meeting you.

Cordially,

Jean-Bernard Gamache, PharmD, MBA
Chef d'unité scientifique - Évaluation et soutien à la gestion des risques
Direction de la santé environnementale et de la toxicologie
Institut national en santé publique du Québec
190 boulevard Crémazie E, Montréal (Québec) H2P 1E2
jean-bernard.gamache@inspq.qc.ca
INSPQ Centre d'expertise et de référence en santé publique
www.inspq.qc.ca

De : Vladisavljevic, Djordje (HC/SC) <djordje.vladisavljevic@canada.ca>
Envoyé : 9 avril 2021 16:40
À : Jean-Bernard Gamache <Jean-Bernard.Gamache@inspq.qc.ca>; Marie-Pascale Sassine <marie-pascale.sassine@inspq.qc.ca>
Cc : Ashby, Deborah (HC/SC) <deborah.ashby@canada.ca>
Objet : RE: Graphene nanoparticles masks

Great speaking with you both,

The format of this email is going to be a little strange, so I apologize, but if you have any questions please do not hesitate to contact me. Feel free to reach out to any of the people I have listed here, I have hyperlinked their email addresses to their names.

As discussed, our program operates under the Canadian Environmental Protection Act and uses the Health Canada Working Definition for Nanomaterials as a basis for determining whether a substance is a nanomaterial.

My section is responsible for the human health risk assessment of nanomaterials that are new to Canada and, more recently, those that are already listed on the Domestic Substances List. We have 3 exposure chemists and 2 biologists with extensive experience in nanomaterial toxicology. We represent Canada at the Working Party on Manufactured Nanomaterials (WPMN) at the Organisation for Economic Co-operation and Development (OECD) where we work to develop international guidance and approaches to the assessment and management of risks from nanomaterials. Two of our chemists also participate in the ISO TC229 Technical Committee on nanotechnologies.

Andrew Belknap and Kathy Nguyen were the evaluators who conducted the graphene risk assessment in 2020 and proposed the significant new activity notice (SNAc) published in November 2020. I have attached the risk assessment summary that has not yet been published. Andrew is a chemist with many years of chemical risk assessment experience and Kathy is our senior biologist with over a decade of nanotoxicology experience.
Yi Zhang is the senior chemist in our section.

Marie-Claude Sauve is the Section Head for the Nanotechnology group at Environment and Climate Change Canada. Please contact her if you would like to speak with experts on the ecotoxicology side of things.

We often work with the following research scientists from the Environmental Health Science & Research Bureau of Health Canada, who are all experts in the field of nanotoxicology or exposure to nanomaterials:

Sabina Halappanavar
Prem Kumarathasan
Dalibor Breznan
Azam Tayabali
Pat Rasmuussen

Finally, the following journal article may be a good place to start for familiarizing yourselves with graphene:
https://pubs.acs.org/doi/10.1021/acsnano.8b04758

Hope this is useful and please let me know if I can do anything else to help your organization meet its mandate.

Cheers,

Djordje Vladisavljevic
(pronouns: he, him | pronoms: il, lui)

Head, Nanotechnology Section
New Substances Assessment and Control Bureau
Healthy Environments and Consumer Safety Branch
Health Canada / Government of Canada
djordje.vladisavljevic@canada.ca / [redacted]

Chef de section, Section de la nanotechnologie
Bureau de l'évaluation et du contrôle des substances nouvelles
Direction générale de la santé environnementale et de la sécurité des consommateurs
Santé Canada / Gouvernement du Canada
djordje.vladisavljevic@canada.ca / [redacted]

Éric Bédard

De: Schmidt, Chris (HC/SC) <chris.schmidt@canada.ca>
Envoyé: 10 mai 2021 12:48
À: Jean-Bernard Gamache; Che, Melinda (HC/SC)
Cc: Marie-Pascale Sassine; Bell, Mary-Jane (HC/SC)
Objet: RE: Graphene nanoparticles masks

Good morning Jean-Bernard,
Thank you for your inquiry. As the risk assessment contains confidential business information (CBI) provided by the manufacturer, we are not in a position to share that. However, we can advise you when the outcome of that assessment along with salient details will be published.

Kind regards,

Chris Schmidt, MSc
Scientific Evaluator
Medical Devices Directorate/Direction des matériels médicaux
Health Canada/Santé Canada

From: Jean-Bernard Gamache <Jean-Bernard.Gamache@inspq.qc.ca>
Sent: 2021-05-10 12:38 PM
To: Che, Melinda (HC/SC) <melinda.che@canada.ca>; Schmidt, Chris (HC/SC) <chris.schmidt@canada.ca>
Cc: Marie-Pascale Sassine <marie-pascale.sassine@inspq.qc.ca>
Subject: Graphene nanoparticles masks

Hi,

Thank you very much once again for sharing some information regarding the risk assessment of masks that contain graphene nanoparticles.

Regarding that matter, would it be possible for you to share the report you are currently working on before it is available to the general public?

Cordially,

Jean-Bernard Gamache, PharmD, MBA
Chef d'unité scientifique - Évaluation et soutien à la gestion des risques
Direction de la santé environnementale et de la toxicologie
Institut national en santé publique du Québec
190 boulevard Crémazie E, Montréal (Québec) H2P 1E2
jean-bernard.gamache@inspq.qc.ca
INSPQ Centre d'expertise et de référence en santé publique
www.inspq.qc.ca

Nicolas Ribes Turgeon

De: Élisabeth Lajoie (CISSSMC16) <elisabeth.lajoie.med@ssss.gouv.qc.ca>
Envoyé: 4 juin 2021 16:06
À: Geoffroy Denis (CCSMTL); Ghislain Brodeur; Marie-Pascale Sassine; Marième Pelletier; Stéphane Caron; Stéphane Perron
Objet: Masques en graphène : analyse IRSST

Catégories: À lire car en destinataire

Bonjour,

Aviez-vous vu ce document :
https://www.irsst.qc.ca/covid-19/avis-irsst/id/2844/les-masques-jetables-gris-contenant-des-nanoparticules-de-graphene-sont-ils-dangereux-pour-la-sante

Les masques jetables gris contenant des nanoparticules de graphène sont-ils dangereux pour la santé? > IRSST : Institut de recherche Robert-Sauvé en santé et en sécurité du travail

Contexte. Le 2 avril 2021, Santé Canada a émis un avis de risque potentiel pour la santé lié au port de masques contenant du graphène. Santé Canada n'a pas reçu de preuves démontrant que ces masques étaient sécuritaires et efficaces contre le virus de la COVID-19, et considère qu'ils présentent un danger d'émission de particules de graphène qui pourraient être inhalées ...

www.irsst.qc.ca

Élisabeth Lajoie
Médecin spécialiste en santé publique et médecine préventive, et médecine du travail
Cheffe du service médical de santé environnementale et santé au travail
Direction de santé publique
CISSS de la Montérégie-Centre

1255, rue Beauregard
Longueuil (Québec) J4K 2M3
Téléphone : 450 928-6777, poste 14077

Télécopieur : 450 928-3783
Nouvelle adresse courriel : elisabeth.lajoie.med@ssss.gouv.qc.ca
www.santemc.quebec
Suivez-nous sur Facebook! https://www.facebook.com/DSPMonteregie/